Abstract

INVESTIGATION, DESIGN AND IMPLEMENTATION OF MIMO ANTENNAS FOR MOBILE PHONES

Simulation and Measurement of MIMO Antennas for Mobile Handsets and Investigations of Channel Capacity of the Radiating Elements Using Spatial and Polarisation Diversity Strategies

Muhammad Usman

Keywords

Multiple Input Multiple Output; Rayleigh Fading Channel; Power Azimuth Spectrum; Channel Capacity; Spatial Diversity; Polarisation Diversity

The objectives of this work were to investigate, design and implement Multiple-Input Multiple-Output (MIMO) antenna arrays for mobile phones. Several MIMO antennas were developed and tested over various wireless-communication frequency bands. The radiation performance and channel capacity of these antennas were computed and measured: the results are discussed in the context of the frequency bands of interest.

A comprehensive study of MIMO antenna configurations such as 2 × 1, 3 × 1, 2 × 2 and 3 × 3, using polarisation diversity as proposed for future mobile handsets, is presented. The channel capacity is investigated and discussed, as applying to Rayleigh fading channels with different power spectrum distributions with respect to azimuth and zenith angles. The channel capacity of 2 × 2 and 3 × 3 MIMO systems using spatial polarisation diversity is presented for different antenna designs. The presented results show that the maximum channel capacity for an antenna contained within a small volume can be reached with careful selection of the orthogonal spatial fields. The results are also compared against planar array MIMO antenna systems, in which the antenna size considered was much larger.

A 50% antenna size reduction method is explored by applying magnetic wall concept on the symmetry reference of the antenna structure. Using this method, a triple dual-band inverted-F antenna system is presented and considered for MIMO application. Means of achieving minimum coupling between the three antennas are investigated over the 2.45 GHz and 5.2 GHz bands.

A new 2 × 2 MIMO dual-band balanced antenna handset, intended to minimise the coupling with the handset and human body was proposed, developed and tested. The antenna coupling with the handset and human hand is reported in terms the radiation performance and the available channel capacity.

In addition, a dual-polarisation dipole antenna is proposed, intended for use as one of three collocated orthogonal antennas in a polarisation-diversity MIMO communication system. The antenna actually consists of two overlaid electric and magnetic dipoles, such that their radiation patterns are nominally identical but they are cross-polarised and hence only interact minimally.

Acknowledgements

In the name of Allah, the most merciful and beneficent. I am grateful to my Lord who has given me strength and wisdom to complete this work.

I would like to thank the following, who accompanied me during the time when I was working for this degree.

I wish to express my deepest gratitude to my supervisors***, Prof. Raed A. Abd-Alhameed*** and ***Prof. Peter S. Excell.*** I am most grateful to them for advice, assistance, support and their continuous encouragement during the difficult starting times, sharing with me the exciting times and for being consistently supportive throughout this work. I will never forget the many opportunities that they gave me in facilities, publications, teaching and travel during the years of my PhD study.

My thanks are also extended to ***Dr N J McEwan*** and ***Mr M Child*** for their great support and all the other people in the research laboratories, especially ***Dr. D.Zhou***, ***Dr. C.H. See*** whose co-operation in connection with the practical aspect of this work cannot be underestimated.

I am grateful to my parents ***Mr & Mrs Abdul Wahid*** and my family for supporting me all these years and for providing me with financial and moral support for the completion of this degree.

I am thankful to my parents in law ***Mr & Mrs Raja Waheed Abbassi*** for their moral support during all these years.

My greatest acknowledgements are for my dear wife ***Sarish*** for her continuous support during the hardest times of my study.

TABLE OF CONTENTS

List of Figures

List of Tables

List of Abbreviations

AOA	Angle of Arrival
BWr	Impedance Relative Band-Width
BTS	Base Transceiver Station
BLAST	Bell Labs Layered Space Time
BER	Bit Error Rate
CSI	Channel State Information
DRA	Dielectric Resonant Antennas
DSP	Digital Signal Processor
EDGE	Enhanced Data GSM Environment
FDD	Frequency Division Duplex
FDTD	Finite Difference Time Domain
FIR	Finite Impulse Response
HDTV	High Definition Television
HFSS	High Frequency Simulation Software
IFA	Inverted F Antenna
ILA	Inverted L Antenna
ISI	Inter Symbol Interference
LAN	Local Area Network
MIMO	Multiple Input Multiple Output
MISO	Multiple Input Single Output
MIB-DFE	Multi Independent Beam Decision Feed Back
OFDM	Orthogonal Frequency Division Multiplexing
PAS	Power Azimuth Spectrum

PIFA	Planner Inverted F Antenna
RF	Radio Frequency
RX	Receiver
SAR	Specific Absorption Rate
SNR	Signal to Noise Ratio
SIMO	Single Input Multiple Output
SISO	Single Input Single Output
TX	Transmitter
TDD	Time Division Duplex
TDMA	Time Division Multiple Access
UMTS	Universal Mobile Telecommunication System
VLSI	Very Large Scale Integration
WLAN	Wireless Local Area Network
WiMAX	Worldwide Interoperability for Microwave Access

CHAPTER 1

INTRODUCTION

1.1 BACKGROUND AND MOTIVATION

Smart antenna arrays, which may be understood conceptually as Multiple Input Multiple Output (MIMO) systems, are proving to be an important technological advance for the next generations of voice and/or data wireless communications networks. These technologies are now well positioned to replace some of the existing, more traditional engineering systems, whilst delivering greater bandwidth and spectral efficiencies [1-9]. This has in turn triggered significant activity in the field of digital beam-forming [10-15] which is rapidly making the transition from the research laboratory to real world applications. Digital beam-forming can be seen as a parallel development with advances in DSP and RF/VLSI technologies, in which the implementation of complex algorithms, channel coding and signal analysis can be performed within small low power consumption devices [16].

In classical information theory, Shannon's theorem shows (Eq1.1) that the channel capacity delivers the highest possible data rate that the channel can sustain. Basically, the channel capacity is a function of bandwidth and SNR and can be given as [17]:

$$C = \mathbb{E}\log_2\left|\left(\mathbb{I} + \frac{P_t}{n_t\sigma}\right)\boldsymbol{H}\boldsymbol{H}^{\dagger}\right| \tag{1.1}$$

Intuitively one may seek to improve channel capacity by raising the signal power and extending the channel bandwidth. However, both ideas are impractical. In any mobile terminal technology the power is constrained, and the channel spectrum is additionally constrained by regulatory specifications. Thus, in order to meet these requirements for higher spectral efficiencies many advanced digital modulation and channel coding schemes have been anticipated [18-27].

The use of spatial diversity through antenna arrays has emerged in the last few decades, and is now regarded as the strongest candidate for next generation wireless communications. The logical extension of having multiple antennas on both sides (i.e. MIMO) can tremendously enhance the system throughput, reliability and coverage, without the necessity of extra power and bandwidth [28-30]. In the last decade such MIMO systems have received extensive attention due to their potential benefits, and related research has become very dynamic in recent years, in both academia and industry [31]. Recent standardizations for many commercial radio applications may be seen as evidence for this trend. Table 1.1 below, describes the wireless standards that promote MIMO techniques to enhance their performance. It can be seen that with the exception of 3GPP Release 7, all of these standards utilize Orthogonal frequency Division Multiplexing (OFDM) schemes. This gives rise to the expectation that future system developments will combine MIMO and OFDM [32].

Table 1.1 MIMO Standards and Corresponding Air- Interface Technology

Standards	Air- Interfaces
WLAN 802.11n	OFDM
WiMAX 802.16 2004	OFDM/OFDMA
WiMAX 802.16e	OFDMA
3GPP Release 7	WCDMA
3GPP Release 8 (LTE)	OFDMA
802.20	OFDM
802.22	OFDM

1.2 OBJECTIVES AND GOALS OF THE PROPOSED RESEARCH

This research is principally concerned with the design fundamentals for MIMO based antenna systems for mobile phones. At the present MIMO technology has been successfully implemented in various wireless infrastructure sectors such as wireless LAN. The main inspiration for this research is to implement MIMO technology in mobiles phones in order to increase the channel capacity and bandwidth. In order to implement MIMO on mobiles the main design constraint is antenna size and mutual coupling between multiple antennas. Thus a major requirement for this MIMO implementation will be the objective reduction of antenna size within the set physical constraints of size and performance. The initial theoretical approach adopted in this research, supported by orthogonality modelling design concepts, gives positive results in support of the basic idea of small sized MIMO antenna systems [33, 34].

In this respect, both 2×2 and 3×3 MIMO antennas have been successfully designed, and the prototype has been tested for a generic mobile phone. Furthermore a comprehensive study of the enhanced channel capacity of these MIMO systems was investigated for use on the mobile. The goal is to employ spatial polarisation techniques to realize the goal of optimal 2×2 and 3×3 MIMO mobile systems performance. The rationale for using spatial polarization diversity is to reduce the antenna size and to preserve the maximum channel capacity. This maximum channel capacity can be achieved through optimum process of the orthogonal components of the spatial field distributions. This research has intensively investigated these goals using a variety of modelling and measurement techniques.

A new design concept for a compact 2×2 MIMO balanced handset antenna has been proposed and investigated vs. the requirements of improved channel capacity and working bandwidth.

The coupling between the antenna and handset chassis, and a hand model was also studied; in which the antennas realize a reduced coupling level, and 0.2 bps/Hz maximum degradation in the channel capacity.

In realizing compact MIMO antenna designs, the major issues are the coupling between the multiple antennas and the required coverage gain. For the designs presented in this thesis, the geometries have been carefully selected and presented in such a way as to achieve these goals using the polarization diversity concept. In addition, a dual-band MIMO system used for mobiles utilizing the IEEE 802.11b/g/a (WLAN) standard are also investigated.

A new design procedure is considered, in which a dual polarised dipole antenna is intended for use as one of the three collocated orthogonal antennas in a polarisation diverse MIMO system. This antenna consists of two overlaid dipoles, one electric and the other magnetic, such that their radiation patterns are nominally identical but they are cross-polarised.

A size reduction technique for the MIMO antenna is proposed using a magnetic wall concept [35] to accommodate further size reductions of the new transceiver board and chassis. The antenna miniaturisation is achieved by removing half of the antenna structure along the line of symmetry. The resulting performance targets of return loss, gain, and radiation pattern are compared for both the modified and full sized 3×3 MIMO antenna structures.

Each of the forthcoming chapters of this thesis builds up to a generic design approach for compact MIMO antennas and the calculation of channel capacity for mobile phones. These antenna structures are integrated onto a rectangular metal box, with dimensions 100mm×50mm×20mm, which emulate the size of a contemporary handset. The frequency response, coupling, and fields of each design have been presented and explained.

1.3 OVERVIEW OF PRESENT THESIS

This thesis principally addresses the channel capacity of simple 2×2 and 3×3 MIMO systems using spatial polarization diversity for different channel requirements. This study includes the determination of the channel capacity for orthogonal spatial polarizations arising from several antenna structures that can be suitably located on a

mobile handset. The research goal is to achieve the maximum channel capacity within the small volume space available and to carefully maintain the optimum operation of the radiating elements.

Chapter 2 presents the relevant history and the background of MIMO systems for mobile wireless applications. Different beam forming schemes are discussed in this chapter, and addresses the basic concept of MIMO, and the role potential for multiple antennas systems. The performance of MIMO system for Channel State Information (CSI) along with its role in TDMA and different systems is also discussed.

Chapter 3 starts with the basic concept of modelling MIMO systems. This chapter also covers the initial mathematical interpretation of MIMO systems with different numbers of antennas. This analysis establishes the necessary preliminaries for the use of spatial polarization within the MIMO antenna design. The detailed derivation of the channel capacity for 2×2 and 3×3 MIMO systems is addressed. The channel capacity is also calculated for different polarisation angles over a Rayleigh Fading Channel. These results have been computed using original Matlab source codes.

Chapter 4 presents the detailed designs for the 2×2 and 3×3 MIMO handset antennas. A new technique for reducing antenna size with respect to the limited available chassis volume is discussed and implemented for a test body. Furthermore, the effect of a human hand on the 3x3 MIMO system has been investigated in detail. The antennas are designed over a copper box which emulates the intended handset. Orthogonal antenna locations are selected to obtain a suitable gauge for the compact 2×2 and 3×3 MIMO

antennas. The channel capacity and radiation performance of the MIMO antennas are computed and measured in this chapter.

Chapter 5 describes a new design concept for the 2×2 balanced MIMO antenna system. The coupling and required input port matching of the 2×2 MIMO antenna handset are investigated with and without introducing hand model present. The variations of the channel capacity, radiation performance and induced surface current distribution on the antenna handset were computed and discussed. Measured scattering parameters are presented and compared with those for the theoretical models.

The idea of using a dual-polarised dipole antenna as one of three collocated orthogonal antennas in a polarisation-diversity Multiple-Input Multiple-Output (MIMO) communication system has been introduced in Chapter 6. This antenna actually consists of a new development of two overlaid dipoles, one electric and the other magnetic; such that their radiation patterns are nominally identical but they are cross-polarised and hence only interact minimally. The antenna modelling was performed using the High Frequency Structure Simulator (HFSS, Ansoft Corporation) and a FDTD code developed at Bradford University [36]. The actual antenna performance is broadly within expectations, but the engineering needed to create a suitable realisation would be challenging. The channel capacity and radiation pattern of the new proposed MIMO antenna are also investigated.

Conclusions and suggestions for future work on related topics are presented in Chapter 7.

1.4 REFERENCES

[1] Da-shan, Gerard J.Foschini, Michael J.Gans and Joseph M. Kahn, "Fading Correlation and Its Effect on the Capacity of Multi-element Antenna Systems", IEEE Transactions on Communications, Vol.48, No.3, March 2000.

[2] Ezio Biglirie, Robert Calderbank, Anthony Constantinides, "MIMO Wireless Communications", Chapter (1-3), ISBN-12:978052187.

[3] T. M. Cover and J. A, "Thomas, Elements of Information Theory", 2nd ed. Wiley–Interscience, 2006.

[4] J. Paulraj and C.B. Papadias, "Space-time processing for wireless communications", IEEE Signal Processing Mag, pp. 49-82, Nov. 1997.

[5] Lozano, F. R. Farrokhi, and R. A. Valenzuela, "Lifting the limits on high-speed wireless data access using antenna arrays", IEEE Commun. Mag., pp. 156-162, Sept. 2001.

[6] S. D Blostein and H. Leibs, "Multiple antennas systems: Their role and impact in future wireless access", IEEE Commun. Mag., pp. 94-101, July. 2003.

[7] D. Gesbert, M. Shafi, D.-S. Shiu, P. Smith and A. Naguib, "From theory to practice: An overview of MIMO time-space coded wireless systems", IEEE J. Select. Areas Commun. Vol.21, pp. 281-302, April. 2003.

[8] J. Paulraj, D. A, Gore, R. U. Nabar, and H. Bolcskei, "An overview of MIMO communications – a key to gigabit wireless", Proc. IEEE, vol. 92, no. 2, pp. 198-218, Feb. 2004.

[9] “Introduction to MIMO systems”, Application Note 1MA102, Rohde and Schwarz, June 2006.

[10] Jack Winters, “Optimum Combining in Digital Mobile Radio with Co-channel interference”, IEEE Journal on Selected Areas in Communications, vol. 2, no. 4, July 1984, pp. 528-539.

[11] Zetterberg, P and Ottersten, B, ”The Spectrum Efficiency of a Base Station Antenna Array for Spatially Selective Transmission”, IEEE Transactions on Vehicular Technology, vol. 44, August 1994, pp. 651-660.

[12] Gerlach, D, ”Transmit antenna beamforming for the Advanced Mobile Phone System”, Asilomar Conference on Signals, Systems and Computers, 1995 vol. 2, 30 Oct. - 2 Nov. 1995, pp. 1162 – 1166.

[13] Bores, T.; Raleigh, G.G.; Pollack, M.A, “Adaptive space-time equalization for rapidly fading communication channels”, Global Telecommunications Conference, 1996. GLOBECOM '96. 'Communications, The Key to Global Prosperity, vol. 2, 18-22 Nov. 1996, pp. 984 – 989.

[14] Raleigh, G.G.; Jones, V.K , “Adaptive antenna transmission for frequency duplex digital wireless communication”, IEEE International Conference on Communications, 1997. ICC 97 Montreal 'Towards the Knowledge Millennium', vol. 2, 8-12 June 1997, pp. 641 – 646.

[15] Raleigh, G.G.; Diggavi, S.N.; Jones, V.K.; Paulraj, A, “ A blind adaptive transmit antenna algorithm for wireless communication”, IEEE International Conference on Communications, 1995. ICC 95 Seattle Gateway to Globalization, vol. 3, 18-22 June 1995, pp. 1494 – 1499.

[16] Mu Xiao Ting, Zhou Ming Yu, Tao Yang Bing, Tao Xiao Feng , “DSP Design of Channel Estimation in MIMO-OFDM System”, Vehicular Technology Conference, 2007. VTC-2007 Sept. 30 -Oct. 3, pp. 1278-1282.

[17] Dietrich, C.B., Jr.; Dietze, K.; Nealy, J.R.; Stutzman, W.L , “Spatial, polarization, and pattern diversity for wireless handheld terminals”, Antennas and Propagation, IEEE Transactions on Volume 49, Issue 9, Sep 2001 Page(s):1271 – 1281

[18] G. L. Stuber, J. R. Barry, S. W. McLauhlin, Y. Li, M. A. Ingram, and T. G. Pratt, “Broadband MIMO-OFDM wireless communications”, Proc. IEEE, vol. 92, pp. 271-294, Feb 2004.

[19] G. L. Stuber, “Principles of Mobile Communications”, 2nd ed. Norwell, MA: Kluwer, 2002.

[20] Raleigh, G.G.; Cioffi, J.M, “Spatio-Temporal Coding for Wireless Communications”, Global Telecommunications Conference, 1996: GLOBECOM 96, The Key to Global Prosperity, vol. 3, 18-22 Nov. 1996, pp. 1809-1814.

[21] Foschini, G.J., “Layered Space-Time Architecture for Wireless Communication in a Fading Environment When Using Multi-Element Antennas”, Bell Labs Technical Journal, autumn 1996, pp. 41-59.

[22] Foschini, G.J. and Gans, M.J , “On the Limits of Wireless Communications in a Fading Environment When Using Multiple Antennas”, Wireless Personal Communication, vol. 6, March 1998, pp. 311-335.

[23] Raleigh, G.G.; Cioffi, J.M, “Spatio-Temporal Coding for Wireless Communications”, IEEE Transactions on Selected Areas of Communications, vol. 46, Issue 3, March 1998, pp. 357-366.

[24] Raleigh, G.G.; Jones, V.K , “Multivariate Modulation and Coding for Wireless Communication”, Global Telecommunications Conference, 1998: GLOBECOM 98 The Bridge to Global Integration, vol. 6, 8-12 Nov. 1998, pp. 3261-3269.

[25] Raleigh, G.G.; Jones, V.K , “Multivariate Modulation and Coding for Wireless Communication”, IEEE Transactions on Selected Areas of Communications, vol. 17, Issue 5, May 1999, pp. 851-866.

[26] Gesbert et al , “From Theory to Practice: An Overview of MIMO Space-Time Coded Wireless Systems”, IEEE Journal on Selected Areas in Communication, vol. 21, No 3, April 2003, pp. 281-302.

[27] Bangeter et al , “High-Throughput Wireless LAN Air Interface”, Intel Technical Journal, vol. 7, Issue 3, August 2003.

[28] “Prediction Algorithms Using Measurements”, Thomas Syantesson and Jonw. WallaceBrigham, Department of Electrical and Computer Engineering, Brigham Young University, Provo, UT 84602-4099.

[29] A.F. Naguib, N. Seshadri and A. R. Calderbank, “Increasing data rate over wireless channels”, IEEE Signal Processing Mag., pp. 76-92, May 2000.

[30] W. Mohr and W. Konhauser, “Access networks evolution beyond third generation mobile communications”, IEEE Commun. Mag., pp. 122-133, Dec 2000.

[31] L. M. Correia and R. Prasad, “An overview of wireless broadband communications”, IEEE Commun. Mag., pp. 28-33, Jan 1997.

[32] Sampath, H. Talwar, S. Tellado, J. Erceg, V. Paulraj, A, “A fourth-generation MIMO-OFDM broadband wireless system: design, performance, and field trial results”, IEEE Communication Magazine, Sep 2002, Vol No.40, Issue No.9, pp No. 143-149.

[33] Muhammad Usman, Raed A Abd-Alhameed and Peter S Excell, “Investigation of channel capacity of MIMO system on mobile phones”, Informatics Workshop, University of Bradford, 2007, United Kingdom, Paper No. 2.

[34] Muhammad Usman, Raed A Abd-Alhameed and Peter S Excell, “Channel Capacity of MIMO Systems for Mobile Phones Using Polarization Diversity for Different Power Azimuth Spectrums”, by published in URSI Symposium 2-3 July 2007, University of Portsmouth, United Kingdom, paper No 6.

[35] Antonchik, V, Vaughan, R, “Far field pattern for rectangular PIFA antenna from the cavity model”, Antennas and Propagation Society International Symposium, 2005 IEEE, Vol. 2B, pp. 226 – 229, 3-8 July 2005 .

[36] A.D.Tinniswood and P.S.Excell, “High Performance Computing and Networking”, pp No.60-65, ISBN 978-3-540-61142-4.

CHAPTER 2

BASIC CONCEPT OF MIMO

2.1 BASIC CONCEPT OF MIMO SYSTEM

MIMO concepts were first introduced into the field of personal and mobile communications through the work of Jack Winters and the AT&T Research Labs in 1987 [1,2]. Winters' technical background was in the phase modulation of adaptive arrays, and his aim was to extend such concepts to ad-hoc networking using multiple antennas at both ends. Winters described two basic scenarios. The first of these addressed communication between multiple mobile units (phones or terminals) and a base transceiver station (BTS) with multiple antenna elements. The second examined communication between two mobile units each with multiple antennas.

Subsequently, the papers of Foschini presented the analytical basis of MIMO systems and proposed two suitable architectures for their realization known as vertical BLAST (Bell Labs Layered Space Time), and diagonal BLAST [3-17]. The basic motive was to increase the data rate in a constrained spectrum. The initial application of MIMO was envisaged for indoor WLAN, fixed wireless access networks, wireless local loop, and building-to-building wireless communications. Later other applications were proposed such as metropolitan voice/data wireless networks (UMTS, EDGE, and 4th generation networks), very high speed fixed and mobile wireless (point to multipoint), and broadcast systems such as HDTV.

MIMO separates several different data streams which occupy a common bandwidth through de-correlating these signals in the presence of multi-path interference. This analysis assumes an independent flat Rayleigh fading channel model, and constrained total power. The data streams are transmitted in bursts such that each channel is quasi-stationary. The channel is known at the receiver (RX) through the transmission of a training sequence, but not necessarily at the transmitter (TX). In this way the receiver will have sufficient information of the channel coefficients to extract the required input data streams. To achieve the maximum transmission rate, it is necessary to choose the number of transmit antennas such that half the interval is used for training, and the other for data transmission.

Channel knowledge at the transmitter is beneficial in the sense that the transmitter can optimize its operation adaptively over the 'good' channels. For time division duplex (TDD) channels the channel is required to be stationary. This approach may not be practical in that the channel coefficient must be fed back to the transmitter at the same rate as the channel. Frequency division duplex (FDD) channels are not reciprocal, so the feedback approach may not be optimal. So, whilst adaptive MIMO can provide a higher channel capacity, its practical implementation requires a coherent time estimation of the channel. This is especially significant for the outdoor environment where high Doppler shifts are expected, e.g. 35Hz at 2GHz, even by a stationary user [18]. It is possible that this feedback constraint may be overcome through feeding back the spatial mean of the channel coefficients, instead of their instantaneous values.

In this coherent bandwidth 'flat fading' sense, MIMO can be considered as a narrowband concept; therefore the majority of the channel expressions are quoted for

the narrowband case. With the wideband case, the frequency selective channel provides diversity gain and hence a higher capacity.

2.2 MULTIPLE INPUT MULTIPLE OUTPUT (MIMO) SYSTEMS FOR WIRELESS COMMUNICATIONS

MIMO radio access network technologies are based on links involving multi-antenna TX and RX components. Spatial diversity may be exploited to improve the overall performance of the wireless channel. Performance metrics are typically quoted as average bit rates (bit s^{-1}), or as average bit error rates (BER). For a given MIMO channel, duplex method and transmission bandwidth, the system nay be categorized as: flat, or frequency fading with full, limited channel state information (CSI). Full CSI implies that the MIMO channel transfer function is fully specified. In a time division duplex (TDD) system where the duplex time is less than the coherence time of the channel, full CSI is available at the TX, and the channel is reciprocal. In a frequency division duplex (FDD) system, it is usual for a feedback channel to be present between RX and TX, providing the TX with partial CSI. In fact it is quite possible to define a robust wireless link with TX CSI through the use of TX diversity [19]. Diversity can be achieved through the use of so called space-time coding, such as the Alamouti code for two TX antennas, the high bit rates are achieved by spatial multiplexing, e.g. BLAST (Bell Labs).

For a broadband wireless connection, the symbol rate must be increased, leading to a frequency selective channel. Channel equalisation one possible approach, but there is an alternative method, which divides the channel into flat fading components, and doesn't require channel equalisation, e.g. OFDM [19]. It is always possible to convert a

frequency selective channel to many flat fading channels using OFDM, apply the developed flat fading MIMO signalling techniques to each of these sub-channels.

2.3 ALGORITHMS FOR COMBINED SPATIAL AND TEMPORAL EQUALISATION IN TDMA

The received baseband signals in a TDMA cellular network is corrupted by channel noise and inter symbol interference (ISI) due to multipath propagation, there is also some influence from co-channel interference from other others. If only a single element is available at the receiver it is possible to use temporal equalisation, in which the transmit sequence is estimated by filtering the received time series. When several antennas are available, the possibility of spatial filtering through beam forming in the direction of the desired signal. Noise, interference and delayed signals result in ISI, which may be suppressed if they arrive from other directions. Beam-forming can be combined with temporal equalisation – so called spatio-temporal equalisation; this makes a more effective use of the energy in the delayed signals from the multiple directions, whilst suppressing the signals of co-channel interferers [20, 21].

Spatio-temporal equalisation can be presented as a generalisation of single-input-single-output (SISO) digital feedback equalisation to a multiple-input-single-output (MISO) digital feedback equalisation. Alternatively, Viterbi detection could also be used (i.e. maximum likelihood sequence estimation). A MISO digital feedback equaliser contains, by definition, a larger number of tuneable parameters than for the SISO case. This leads to two potential problems. Firstly, the needs to adjust a large number of filtering parameters, the adjustments are based on noise sensitive short training sequences. The computational complexity of the algorithm also increases. These two key issues have

been investigated, for different filter structures and different adjustment schemes. The structure of one promising algorithm, the Multiple Independent Beam Decision Feedback Equaliser (MIB-DFE), is illustrated in figure 2.1 below.

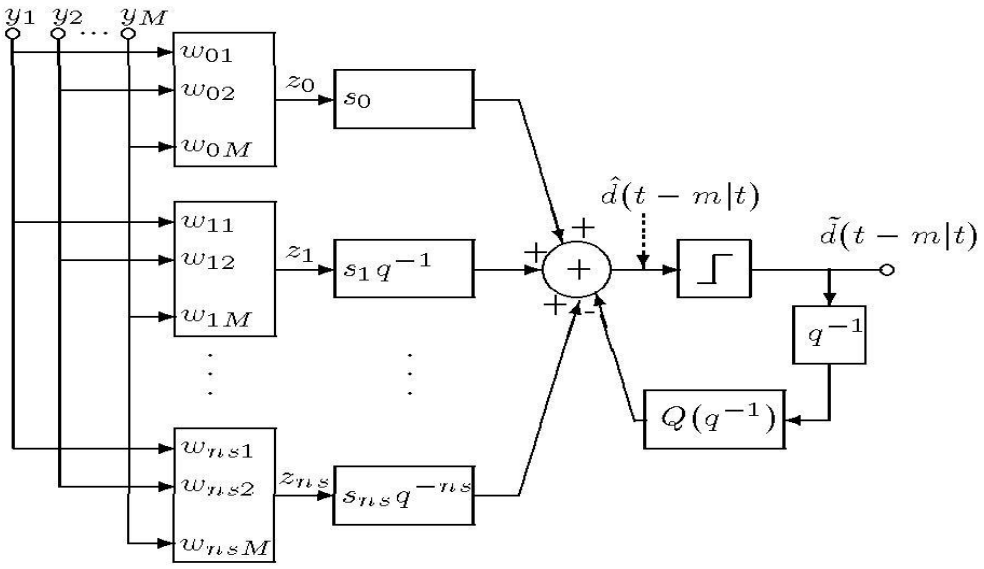

Figure 2.1: Multiple Independent Beam Decision Feedback equaliser [20].

When multiple antenna elements are present, we may investigate the still harder task of detecting several users simultaneously, on the same frequency band. The use of BTS (base transceiver station) antenna arrays is obviously practical, but there are many issues in extending array designs into terminal technologies. To date, therefore, most of the techniques which are in use or under investigation deal with transmission from the mobile units to the BTS.

2.4 MODELLING THE WIRELESS MIMO SYSTEM

To be able to analyze and improve a wireless communication system, working models are required for signals, hardware and the channels.

2.4.1 Signal models

Many digital signals are transmitted using a modulated carrier over a bandwidth constrained channel. If the signal and channel system bandwidths are small compared to the carrier frequency, then the system is said to be narrowband and band-pass [22]. When analyzing communication systems, it is often unnecessary to model the up- and down-conversion from the baseband to the carrier frequency, so one can choose to work with baseband models, or equivalent low pass signals and channels, which are complex valued, $x(t) = A(t)e^{j\phi(t)}$. In the following discussions of signal transmission only complex baseband form will be used, unless stated otherwise. Most signal models are assumed to vary in discrete time, i.e. they are sampled with a uniform sampling rate, and the continuous time signal $x(t)$ is replaced by $x(n)$, where n is a non negative integer. When simulating non-linear systems, the continuous time signals must be sampled at a rate much higher than the symbol rate. The choice of sampling frequency in non-linear simulation depends on the accuracy and the desired number of higher order harmonics in the output signal [18-22].

2.4.2 Channel models

Linear, discrete-time MIMO model may be used to describe a multi-element antenna transceiver system with n_t transmit (TX) antennas and n_r receive (RX) antennas. Due to multipath propagation from the transmitter to the receiver, the received signal at a certain antenna contains a weighted sum of early transmitted symbols. Thus, in the most general case, the MIMO channel model can be written as the infinite series given as [21]:

$$\boldsymbol{H}_{(q-1)} = \sum_{n=0}^{\infty} Hn[q-n] \tag{2.1}$$

where $\boldsymbol{H}_{(n)}$ are matrices with dimension $n_r \times n_t$ that contain complex valued elements that represent the attenuation and phase shift for the received signal with delay n. The (i,j)th element of $\boldsymbol{H}$ is the transfer function from transmitter j to receiver i. In practice, it is impossible to estimate the infinite number of channel matrices $\boldsymbol{H}_{\mathrm{n}}$ from a finite number of data, so often a linear model with finite number of parameters is used, described by a rational function or by limiting the number of terms in which results in a finite impulse response (FIR) channel model.

The discrete time complex low pass channel model must also incorporate the effect of the pulse shaping, and also incorporate the effect of RX and TX filtering. In the most common configuration the transmitters and receivers are connected to different antennas. Other possibilities include connections to different polarizations of a single antenna, different beams in a multi-beam antenna, a multimode antenna, a switched-beam antenna, or even combinations of these. Hence, there are many potential configurations that must all be described by the channel model. Degenerate cases of the MIMO channel model are the single-input multiple-output (SIMO), multiple-input, single-output (MISO) where $\boldsymbol{H}_{(q^{-1})}$ is a column or row vector respectively and the single-input, single-output (SISO) case where $\boldsymbol{H}_{(q^{-1})}$ is a sum of scalar terms. Assume that we would like to model the communication between a terminal and a base-station or vice versa and $N_I + 1$ multiple users are active and sharing the common radio space in all dimensions; time, frequency and space (see Figure 2.2)

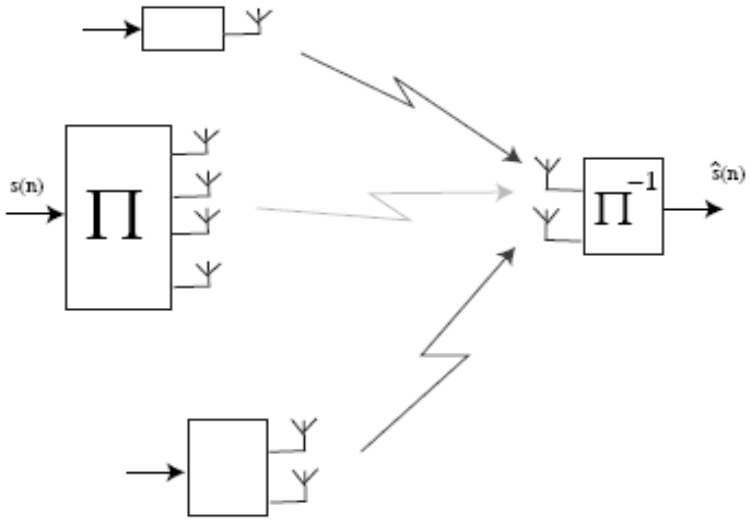

Figure 2.2: The communication model between a terminal and a base-station

Then N_I users are said to be interfering with the particular transmission under investigation (the desired user), these are termed co-channel interferers (CCI). Using the channel model (in equation 3.3), the MIMO communication system with co-channel interferers can be written as [21]:

$$\boldsymbol{y}[n] = \boldsymbol{H}_{(q-1)}\boldsymbol{c}[n] + N_I \sum_{i=1} \boldsymbol{H}_{i(q-1)}\boldsymbol{c}_i[n] + \mathcal{N}_T\boldsymbol{y}[n] \qquad (2.2)$$

where **y**[n] is the received signal vector of dimension $n_r \times 1$ and $\mathcal{N}_T$ is the thermal noise in the receivers. Furthermore, **c**[n] and $\mathbf{c}_i$[n] are the transmitted vector from our desired user and the interferers respectively, and $\mathbf{H}_{(q-1)}$ is the channel for the desired user. The matrices {**H**i(q−1)NΣIi=1} are the channels for the interfering users with row dimension n_r and a column dimension that matches the number of transmit antennas of the particular co-channel interferer, i.e. the row dimension of ci(n).

2.5 REFERENCES

[1] “MIMO Wireless Communications”, by Ezio Biglirie, Robert Calderbank, Anthony Constantinides, Chapter (1-3), ISBN-12:978052187.

[2] “Fundamentals of Wireless Communication”, by David Tse and Pramod Viswanath, Chapter (7-10), Cambridge University Press, 2005.

[3] D. Chizhik, G. Foschini, M. Gans, and R. Valenzuela, Keyholes, “Correlations, and Capacities of Multielement Transmit and Receive Antennas”, IEEE Transaction on Wireless Communications. Vol. 1, No. 2, April 2002, pp. 361-368.

[4] . J. Foschini, M. J. Gans, “Capacity when Using Multiple Antennas at Transmit and Receive Sites and Rayleigh-Faded Matrix Channel is Unknown to the Transmitter”, Advances in Wireless Communications, Ed. J. M Holtzman and M. Zorzi, Kulwer Academic Publishers, 1998.

[5] G. D. Golden, G. J. Foschini, R. A. Valenzuela, P. W. Wolniansky, “Detection Algorithm and Initial Laboratory Results using the V-BLAST Space-Time Communication Architecture” , Electronics Letters, Vol. 35, No. 1, Jan. 7, 1999, pp. 14-15.

[6] G. J. Foschini, G.D.Golden, R.A.Valenzuela, P.W.Wolniansky, “Simplified Processing for Wireless Communication at High Spectral Efficiency”, IEEE Journal on Select Areas in Coummunications, Vol. 17, No. 11, 1999.

[7] D-S. Shiu, G.J. Foschini, M.J. Gans, J.M.Kahn, “Fading Correlation, and its Effect on the Capacity of Multielement Antenna Systems”, IEEE Transactions on Communications, Vol. 48, No. 3, 2000.

[8] P. W. Wolniansky, G. J. Foschini, G. D. Golden, R. A. Valenzuela, V-BLAST, “An Architecture for Realizing Very High Data Rates Over the Rich-Scattering Wireless Channel”, invited paper, Proc. ISSSE-98, Pisa, Italy, Sept. 29, 1998.

[9] G. D. Golden, G. J. Foschini, P. W. Wolniansky, R. A. Valenzuela, V-BLAST, “A High Capacity Space-Time Architecture for the Rich-Scattering Wireless Channel” , Proc. Int'l Symposium on Advanced Radio Technologies, Boulder, CO, Sept. 10, 1998.

[10] G. D. Golden, G. J. Foschini, R. A. Valenzuela, P. W. Wolniansky, V-BLAST, “A High Capacity Space-Time Architecture for the Rich-Scattering Wireless Channel” , Fifth Workshop on Smart Antennas in Wireless Mobile Communications, Stanford Univ., July 23-24, 1998.

[11] G. J. Foschini and M. J. Gans, “On Limits of Wireless Communications in a Fading Environment When Using Multiple Antennas”, Wireless Personal Communications, Volume 6, No. 3, March 1998, p. 311.

[12] G. J. Foschini and R. A. Valenzuela, “Initial Estimation of Communications Efficiency of Indoor Wireless Channels” , Wireless Networks, 3 (1997) pp 141-154.

[13] G. J. Foschini, “Layered Space-Time Architecture for Wireless Communication in a Fading Environment When Using Multiple Antennas”, Bell Labs Technical Journal, Vol. 1, No. 2, Autumn 1996, pp 41-59.

[14] G. J. Foschini and M. J. Gans, “Capacity When Using Diversity at Transmit and Receive Sites and the Matrix Channel is Unknown at the Transmitter” , Proceedings of the 6-th WINLAB Workshop on 3rd Generation Wireless Information Networks, March 20-21, 1996, New Brunswick, New Jersey.

[15] M. Gans et. al., “Multielement Antenna Systems Capacity Measurements at 2.44GHz in Suburban Outdoor Environment”, IEEE Vehicular Technology Conference, Spring 2001.

[16] J. Ling, et. al., “ Multiple Transmit Multiple Receive (MTMR) Capacity Survey in Manhattan” , Electronic Letters, Vol. 37, No. 16, August 2001, pg. 1041.

[17] E.Biglirie, et al, “MIMO Wireless Communications”, Chapters 1 – 3, John Wiley, NY, ISBN-978052187.

[18] “MIMO Systems and Adaptive Arrays For Wireless Communication”, by Mattias Wennstrom, Uppsala University, 2002.

[19] “Channel Capacity of TDD, OFDM MIMO for Multiple Access Points in a Wireless Single Frequency Network”, by Y.Takatori, F.Fitzek, K.Tsunekawa, R.Parsad , MIMO MAP Springer 2005.

[20] “Predisction Algorithms Using Measurements”, by Thomas Syantesson and Jonw.WallaceBrigham, Department of Electrical and Computer Engineering, Brigham Young University, Provo, UT 84602-4099.

[21] Liang Dong,Hosung Choo, Robert W. Heath, Hao Ling, “Simulation of MIMO Channel Capacity With Antenna Polarization Diversity”, IEEE Transaction on Wireless Communication, Vol. 4, July 2005.

[22] Da-shan, Gerard J.Foschini, Michael J.Gans and Joseph M. Kahn, “Fading Correlation and Its Effect on the Capacity of Multi element Antenna Systems”, IEEE Transactions on Communications,Vol.48, NO.3, March 2000.

CHAPTER 3

MIMO MODELING WITH RAYLEIGH FADING CHANNEL

3.1 MODELING OF MIMO SYSTEM

In the previous Chapter it has been explained how MIMO systems are theoretically able to provide an increased throughput, with consequently improved error performance over traditional systems [1-4]. For antenna systems a particular area of interest is the practical utilisation of multi-path propagation [5, 7]. Multi-path propagation occurs when the radio signals sent from the transmitter reflected from intermediate objects before reaching the receiver; some of these reflected signals may travel along entirely separate paths, and reach the receiver at different times. These effects combined with digital beam-forming enhance the potential for greater system capability and bandwidth. In order to realize this potential it is necessary to understand how the use of spatial correlation based on polarization states impacts on the achievable volume of the radiating structures.

Here the spatial, polarization technique is used to improve the channel capacity of the system will be considered. The potential for integrating MIMO systems comprising both 2×2 and 3×3 elements into a mobile handset environment will be considered. The MIMO channels will be subject to Rayleigh fading, and the results are compared against

linear (or planar) arrays. In addition, different azimuthal spectra will be considered in evaluating the actual system performance [8-13].

3.2 MATHEMATICAL CAPACITY MODEL

For a system having *N* transmitters and *N* receivers the channel capacity is given by the well known formula [14],

$$C = \mathbb{E}\log_2\left|\left(\mathbb{I} + \frac{P_t}{n_t\sigma}\right)\boldsymbol{H}\boldsymbol{H}^{\dagger}\right| \tag{3.1}$$

which is an expectation value incorporating, the variance of the noise power (σ), the mean of the total transmitted power (P_t), and the channel transfer matrix, $\boldsymbol{H}$. The matrix size is $n_r \times n_r$, $\mathbb{I}$ is the identity, and '†' is the conjugate transpose operation. If the spatial matrices characterising the receiver ($\boldsymbol{W}_r$) and transmitter ($\boldsymbol{W}_t$) are also known, then $\boldsymbol{H}\boldsymbol{H}^{\dagger}$ may be obtained simply as follows:

$$\boldsymbol{H}\boldsymbol{H}^{\dagger} = \boldsymbol{W}_r\boldsymbol{G}_w\boldsymbol{W}_t^{\dagger} \tag{3.1}$$

The characteristic channel properties are encoded in the system matrix$\boldsymbol{G}_w$, so for a channel with Rayleigh fading these matrix elements are drawn from a complex Gaussian distribution [15-19]. A further simplification can be introduced into the modelling, where the spatial transmitter matrix for maximum channel capacity is given as the identity, this is justifiable on physical grounds: Its normalized version can be obtained as follows:

$$G_w\big|_n = \frac{G_w}{norm} \tag{3.3}$$

where

$$norm = \sqrt{\frac{1}{n_r n_t}\|G_w\|_F^2}$$

where $\|G_w\|_F$ denotes the Frobenius norm of the matrix G_w and is given by:

$$\|G_w\|_F = \sqrt{\sum diag(G_w.G_w^*)} \tag{3.4}$$

Now, since the space availability on the transmitter side, then the spatial matrix of the transmitter for maximum channel capacity can be given as an identity matrix. Therefore equation (3.2) can be reduced to the following:

$$\boldsymbol{HH}^{\dagger} = \boldsymbol{W}_r \boldsymbol{G}_w \tag{3.5}$$

The elements of the spatial receiver matrix $\boldsymbol{W}_r$ can be stated as follows:

$$W_{r_{ij}} = \sqrt{\frac{\oiint d\Omega(\boldsymbol{E}_{ai} \cdot \boldsymbol{E}_i)(\boldsymbol{E}_{ai} \cdot \boldsymbol{E}_i)^*}{\sigma_1 \sigma_2}} \tag{3.6}$$

where

$$\sigma_j = \oiint d\Omega\left(\boldsymbol{E}_{aj} \cdot \boldsymbol{E}_j\right)^2 \tag{3.7}$$

The spatial integrals used in the above equations are understood to be parameterised as $\oiint = \int_{\phi_1}^{\phi_2} \int_{\theta_1}^{\theta_2} (\cdot)$ with measure $d\Omega = \sin\theta \, d\theta d\phi$. The $\boldsymbol{E}_{ai}$ are the electric fields of the radiating elemnts, whilst the $\boldsymbol{E}_i$ are the electric fields incidents on the receiver side.

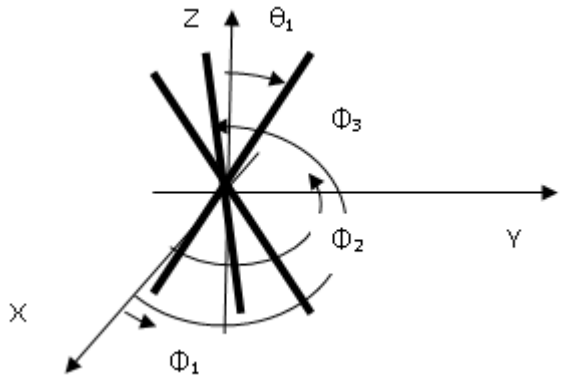

Figure 3.1: The basic antenna geometry.

The polarisation geometry assumes three dipoles collocated over the azimuthal axis and centred at the origin as shown in Figure 1.1 and Figure 1.2. This analysis is restricted to a maximum of three radiating elements; at this stage the mutual couplings are ignored. The elements are located with respect to the elevation angle (which is the polarization angle in this case). To reduce complexity, short dipoles are employed in which their radiating field can be easily stated (e.g. as a short dipole oriented in the azimuthal axis, the total field is $E_\theta = \sin\theta$, where θ and Φ are elevation and azimuth angles).

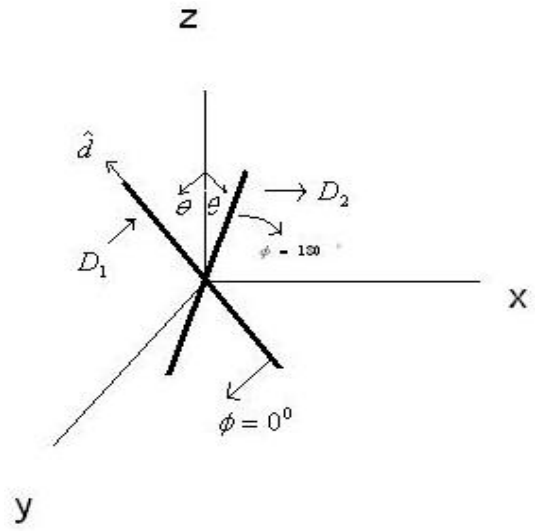

Figure 3.2: Geometry of a 2 × 2 MIMO Antenna system

However, for arbitrary dipole orientation in (θ_d, ϕ_d), the following unit vector, which defines the local axis of the dipole, can be expressed as follows:

$$\hat{\boldsymbol{d}} = \sin\theta_d \cos\phi_d \, \hat{\boldsymbol{e}}_x + \sin\theta_d \sin\phi_d \hat{\boldsymbol{e}}_y + \cos\theta_d \, \hat{\boldsymbol{e}}_z \tag{3.8}$$

where $\{\hat{\boldsymbol{e}}_i\}$ form an orthonormal right handed triad. The radiated dipole field can be given as follows:

$$\boldsymbol{E}_a = E_\theta(\theta, \phi)\hat{\boldsymbol{e}}_\theta + E_\phi(\theta, \phi)\hat{\boldsymbol{e}}_\phi \tag{3.9}$$

The components E_θ and E_ϕ are defined as the (spatially averaged) scalar products,

$$E_\theta(\theta, \phi) = \langle \hat{\boldsymbol{d}} \cdot \hat{\boldsymbol{u}}_\theta \rangle \tag{3.10}$$

$$E_\phi(\theta, \phi) = \langle \hat{\boldsymbol{d}} \cdot \hat{\boldsymbol{u}}_\phi \rangle \tag{3.11}$$

And

$$\hat{\boldsymbol{u}}_{\theta} = \cos\theta\cos\phi\hat{\boldsymbol{e}}_x + \cos\theta\sin\phi\,\hat{\boldsymbol{e}}_y + \sin\theta\,\hat{\boldsymbol{e}}_z \tag{3.12}$$

$$\hat{\boldsymbol{u}}_{\phi} = -\sin\phi\,\hat{\boldsymbol{e}}_x + \cos\phi\,\hat{\boldsymbol{e}}_y \tag{3.13}$$

3.3 POWER SPECTRUM DISTRIBUTION FUNCTIONS

In order to calculate the channel capacity of MIMO system, several power distribution functions have been used [20-23]. The well known uniform distributions – Gaussian, Laplacian and Secant Squared, are considered over the azimuthal angle. In addition raised cosine and nth order raised cosine distributions are considered along the zenith angle. These distributions are combined with one another to form the incident plane wave illuminating the receiver elements. The following analysis considers all possible combinations between these distributions in such a way as to predict the maximum degradations and/or improvements of the proposed MIMO system performance. In general, there are twelve combinations can be considered to compute the channel capacity of the MIMO system.

3.3.1 Gaussian distribution

The power spectrum over the azimuthal direction using a Gaussian distribution can be defined as follows:

$$P_{\phi}(\phi) = \sqrt{A}\exp\left\{-\frac{\left(\phi - m_{\phi}\right)^2}{2\sigma_{\phi}^2}\right\} \quad -\pi \le \phi \le \pi \tag{3.14}$$

where A is the normalization factor, this can be given by:

$$A = 2\sigma_\phi^2 \pi \left\{ -\operatorname{erf}\left(\frac{-\pi + m_\phi}{\sqrt{2}\sigma_\phi}\right) + \operatorname{erf}\left(\frac{\pi + m_\phi}{\sqrt{2}\sigma_\phi}\right)\right\}^2 \quad 3.15$$

m_ϕ and σ_ϕ are the mean and variance of the Gaussian function respectively. Several plots of this function for different values of m_ϕ and σ_ϕ are illustrated in Figure 3.3.

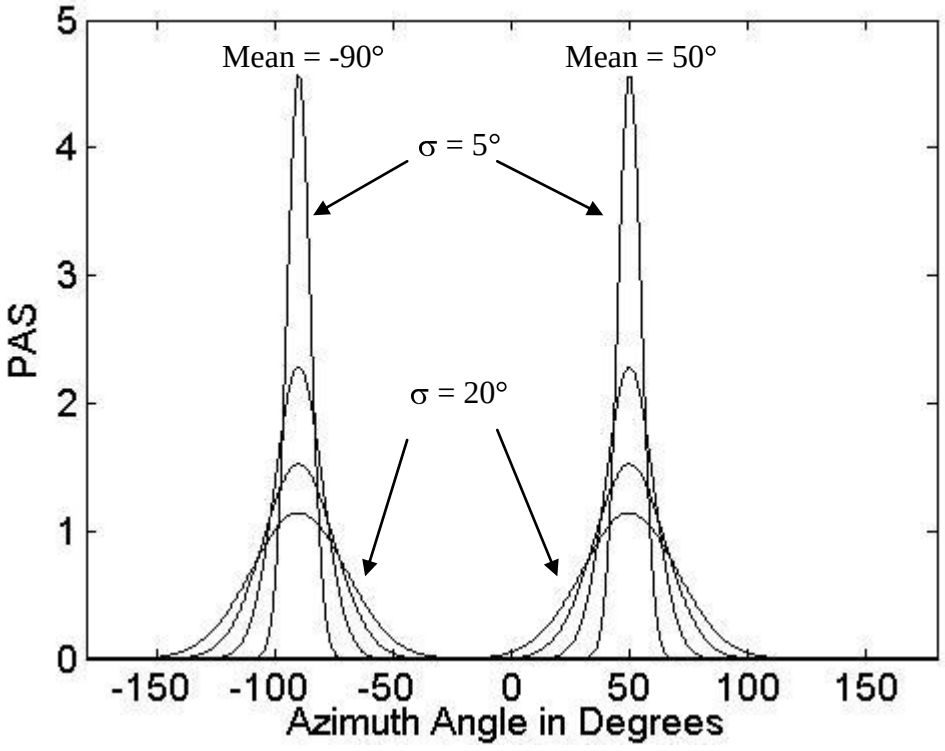

Figure 3.3: Gaussian distribution functions for different values of m_ϕ and σ_ϕ.

3.3.2 Laplacian distribution

A well known practical channel capacity approximation uses the Laplace power distribution along azimuthal direction [24, 25]. Laplacian distribution can be simply expressed as follows:

$$P_\phi(\phi) = \sqrt{A}\exp\left\{-\frac{|\phi - m_\phi|}{\sigma_\phi}\right\} \quad -\pi \le \phi \le \pi \tag{3.16}$$

Where

$$A^2 = -\frac{\sigma_\phi}{\sqrt{2}}e^{\left(\frac{\sqrt{2}(-\pi+m)}{\sigma_\phi}\right)} + \left[\frac{\sigma_\phi}{\sqrt{2}}e^{\left(\frac{\sqrt{2}(-\pi+m)}{\sigma_\phi}\right)} + \frac{\sigma_\phi}{\sqrt{2}}e^{\left(\frac{-\sqrt{2}(-\pi+m)}{\sigma_\phi}\right)} - \sqrt{2}\sigma_\phi\right] f_1$$

$$-\frac{\sigma_\phi}{\sqrt{2}}e^{\left(\frac{-\sqrt{2}(\pi+m)}{\sigma_\phi}\right)} + \left[\frac{\sigma_\phi}{\sqrt{2}}e^{\left(\frac{\sqrt{2}(\pi+m)}{\sigma_\phi}\right)} - \sqrt{2}\sigma_\phi e^{\left(\frac{-\sqrt{2}(\pi+m)}{\sigma_\phi}\right)} + \frac{\sigma_\phi}{\sqrt{2}}e^{\left(\frac{-\sqrt{2}(\pi+m)}{\sigma_\phi}\right)}\right] f_2$$

$$f_1 = \begin{cases} 0, -\pi + m < 0 \\ 1 \end{cases} \ \& \ f_2 = \begin{cases} 0, -\pi - m < 0 \\ 1 \end{cases} \tag{3.17}$$

The behaviour of this distribution for different values of m_ϕ and σ_ϕ are illustrated in Figure 3.4. Note that these distributions show narrower, and sharp variations, around the mean of the incident angle compared to that found in the Gaussian distributions.

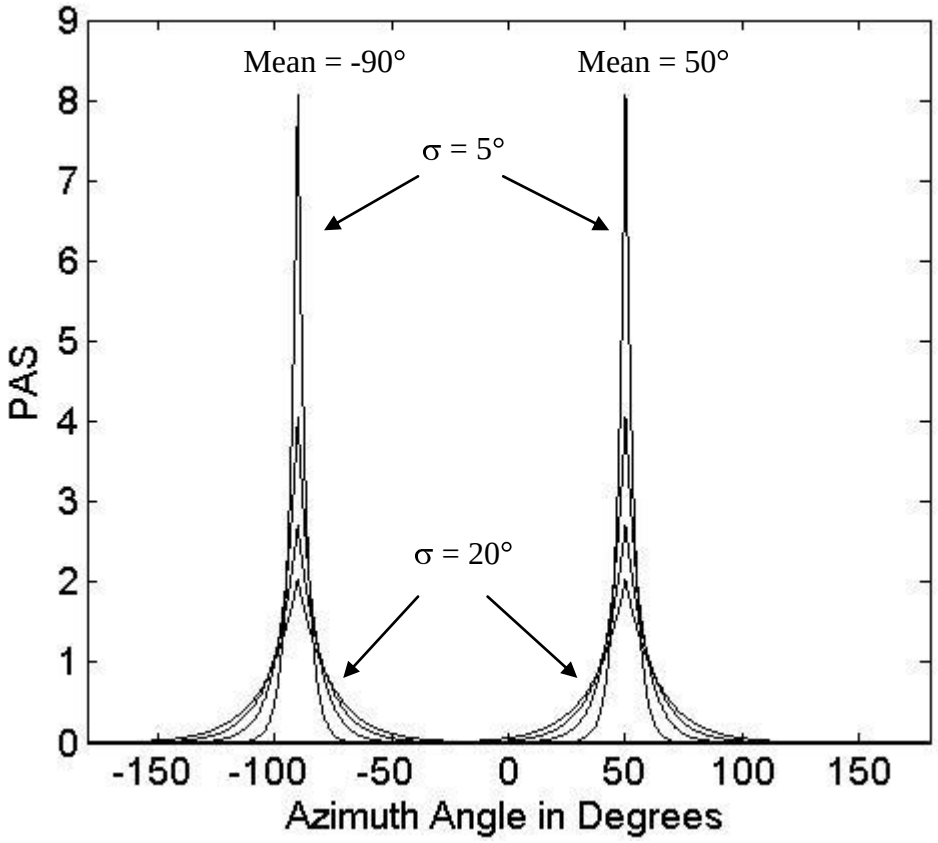

Figure 3.4: Laplacian distribution functions for different means and variances.

3.3.3 Secant Square Distribution

Raised (n^{th} order) cosine distributions applied along an angular direction are also used in some applications when calculating the channel capacity. This distribution function can be expressed as follows,

$$P_{\phi}(\phi) = \frac{0.5}{(\pi - \phi_0) + \tan\phi_0} \begin{cases} \sec(\phi_0 - |\pi - \phi_0|) \,, \left|\phi - m_{\phi}\right| \leq \phi_0 \\ 1 \,, \left|\phi - m_{\phi}\right| > \phi_0 \end{cases}, -\pi \leq \phi \leq \pi \qquad 3.18$$

where $2\phi_0$ is the width of the angle when the distribution is not constant, and m_ϕ is the mean angle in which the incident fields scattered on the antenna. Several distribution functions of this kind of PAS are shown in Figure 3.5.

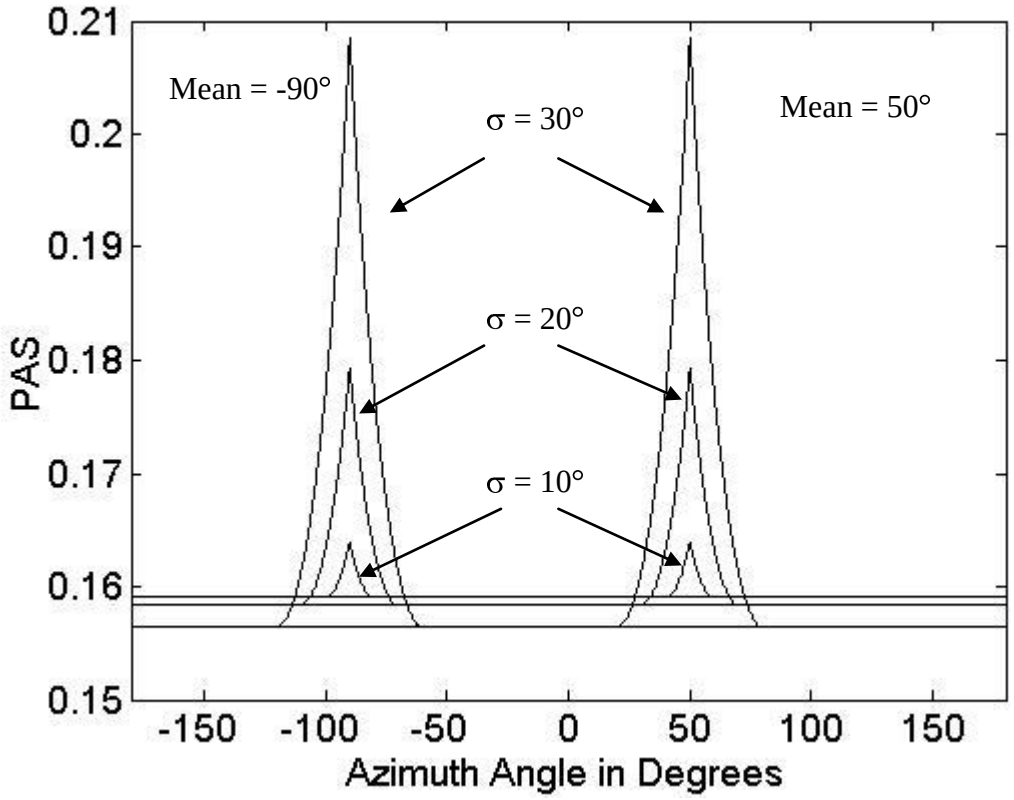

Figure 3.5: Secant square distribution functions for different m_ϕ and angular widths.

3.3.4 Raised cosine and Raised cosine-n distributions

Raised (nth order) cosine distributions applied along an angular direction are also sued in some applications when calculating the channel capacity. This distribution function can be expressed as follows,

$$P_\theta(\theta) = A\left(1 + \cos\left(\frac{2\pi(\theta - m_\theta)}{s}\right)\right)^n \quad \text{for } m_\theta - \frac{s}{2} \le \theta \le m_\theta + \frac{s}{2} \qquad 3.19$$

where m_θ is the mean angle, *s* is the total width angle and *A* is the normalization factor. The distribution functions for $n = 1$, $n = 2$ and $n = 4$ are shown in Figure 3.6 for different values of *s* and m_θ.

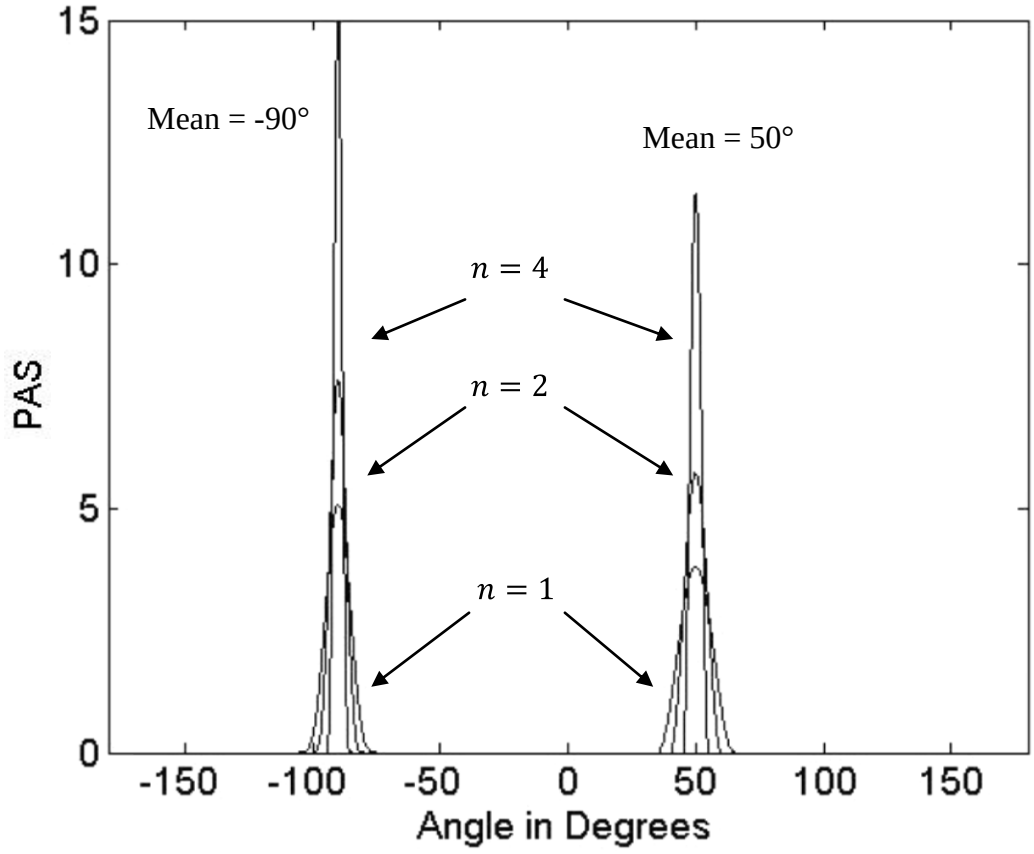

Figure 3.6: Raised Cosine distribution functions for different means and angle widths.

3.4 CHANNEL SIMULATION AND RESULTS

If the signal to noise ratio is high, then the channel capacity can be given by :

$$C = \sum_{i=1}^{n} \left(\mathbb{I} + \frac{P}{n_T \sigma} \lambda_i \right) \qquad (3.20)$$

where λ_i (for $i = 1,2,3$) are the eignvalues of the matrix given in equation 3.20. However, the channel capacity is also computed (Appendix A) for comparison using equation 3.1. The incident fields are assumed to have uniform distribution over the range $[0,2\pi]$ for azimuthal angle ϕ, and 30° over the elevation angle at the horizontal plane for an urban channel. For suburban channels the variation over elevation angle is similar to the urban channel model. The azimuth is taken at 5° intervals from 5° to 20°, and the corresponding Laplacian spectra are computed and compared.

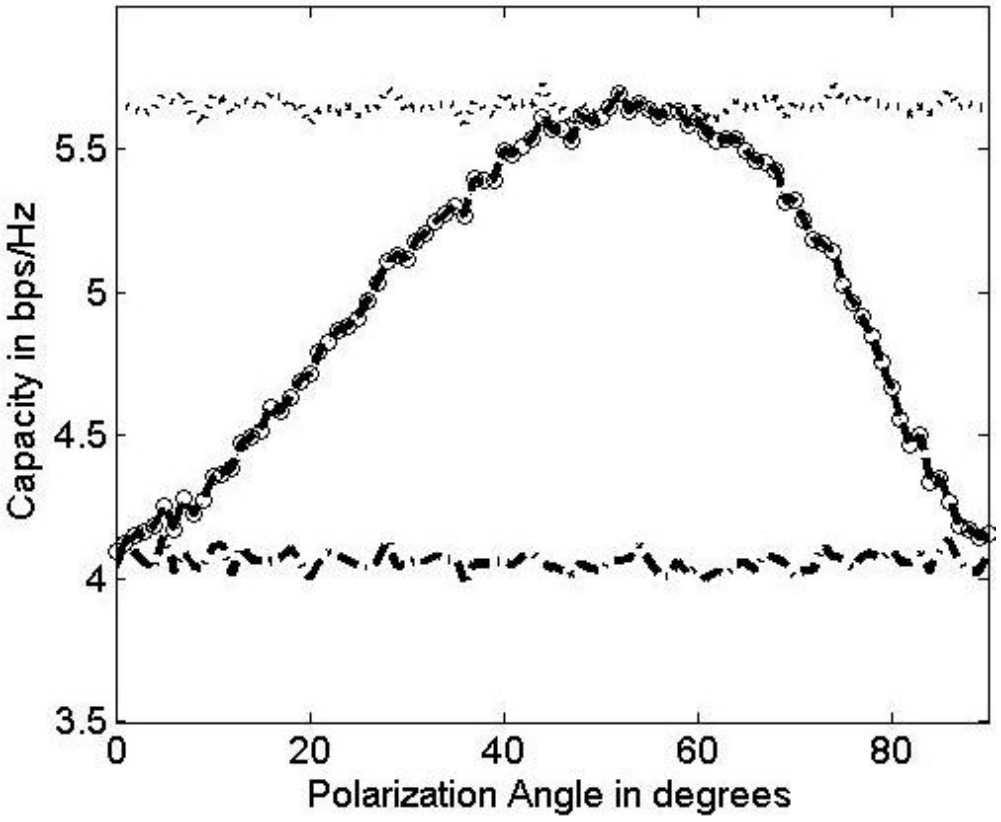

Figure 3.7: The channel capacity of 2 x 2 MIMO system as oriented in Figure 3.2 as a function of the polarization angle using Gaussian distributions. ('…..': upper limit of 2 x 2 MIMO fading channel, '.-.-.-': upper limit of 2 x 1 MIMO fading channel, Capacity using Equation 3.1: '_ _ _, Capacity using Equation 3.20: 'o o o').

The $\boldsymbol{E}_\theta$ and $\boldsymbol{E}_\phi$ of the incident fields were assumed to be independent over the angular range$[\theta, \phi]$, and their variations are uniform for the channel models under consideration. It was also assumed that the phase variations are uniform over $[0,2\pi]$.

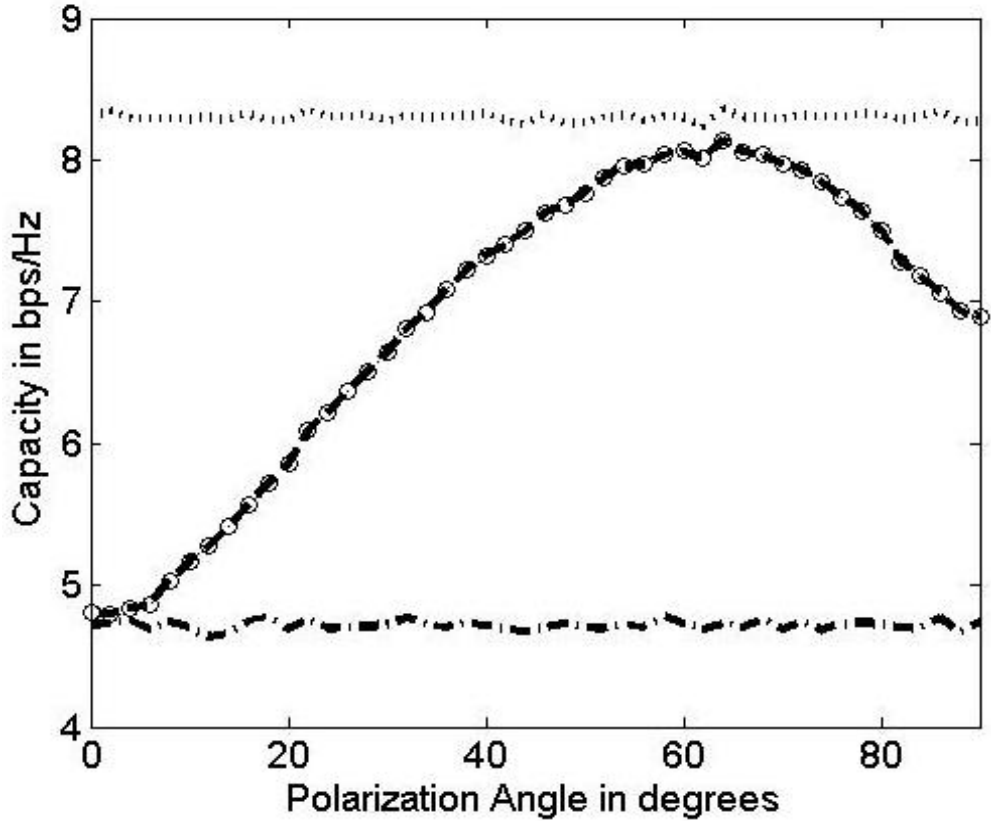

Figure 3.8: The channel capacity of 3 × 3 MIMO system as oriented in Figure 3.1 as a function of the polarization angle. ('…..': upper limit of 3 × 3 MIMO fading channel, '.-.-.-': upper limit of 3 × 1 MIMO fading channel, Capacity using equation 3.1: '_ _ _', Capacity using equation 3.20: 'ooo').

Channel capacities for an urban channel model are simulated for both the 2×2 and 3×3 MIMO systems, the results are shown in Figures 3.7 and 3.8. The antennas for the 2×2 system are located at $\phi = 0°$ and $180°$, whereas for the 3×3 system $\phi = \{0°, 120°, 240°\}$. The data used to generate these figures employs a closed form

solution for the elements of $\boldsymbol{W}_r$. The capacity was evaluated over a Rayleigh fading model, the average was taken over 1000 complex samples. The transfer function was normalized at each point to provide a good prediction of the maximum variation of the spatial matrices for these MIMO antennas. It should be noted that the maximum capacities for the 2×2 and 3×3 cases occur at 55° and 63° respectively. These angles should be selected for the required orthogonalisation of the spatial field distributions for the antenna geometry (in Figure 3.1).

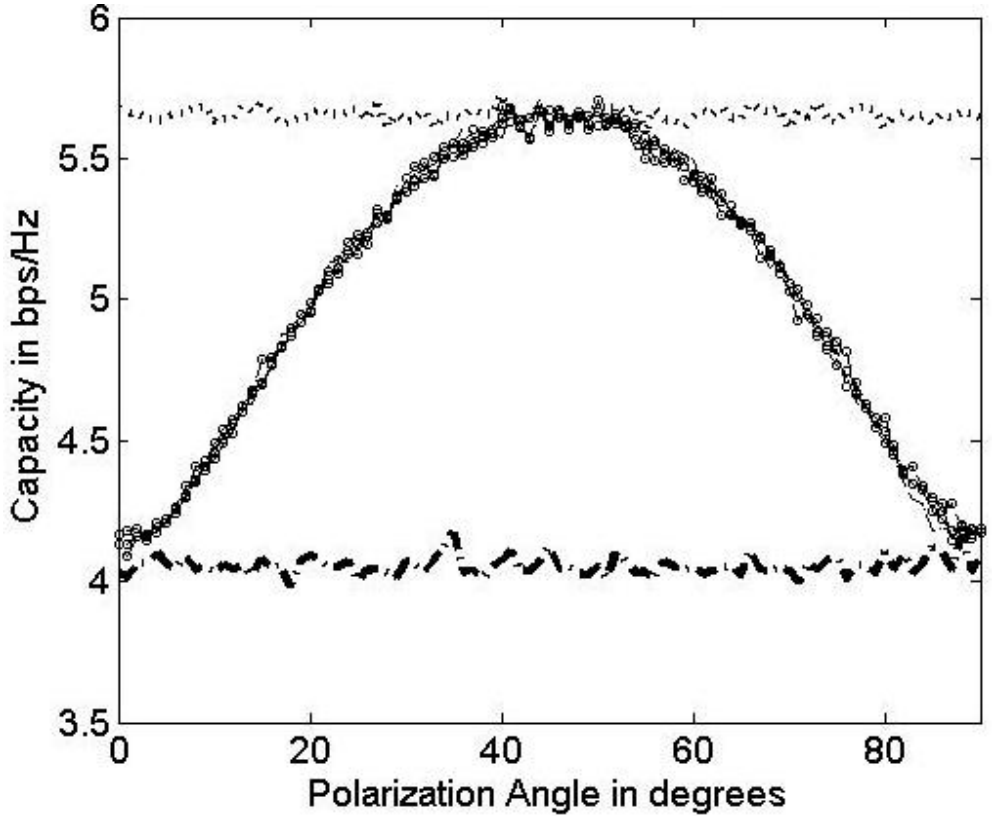

Figure 3.9: The channel capacity of 2 × 2 MIMO system as oriented in Figure 3.2 (the antennas are rotated by 90 degrees over azimuth angle) as a function of the polarization angle. ('…..': upper limit of 2 × 2 MIMO fading channel, '.-.-.-': upper limit of 2 × 1 MIMO fading channel, Capacity using equation 3.1: '_ _ _', Capacity using equation 3.20: 'ooo').

The same sequence of results is presented for the suburban channel model in Figures 3.9 and 3.10. for various values of σ_ϕ. Here the maximum capacity limits for the 2×2 MIMO case are reached for all the presented values of σ_ϕ; in the 3×3 case there is a slight, but detectable reduction, as σ_ϕ increases.

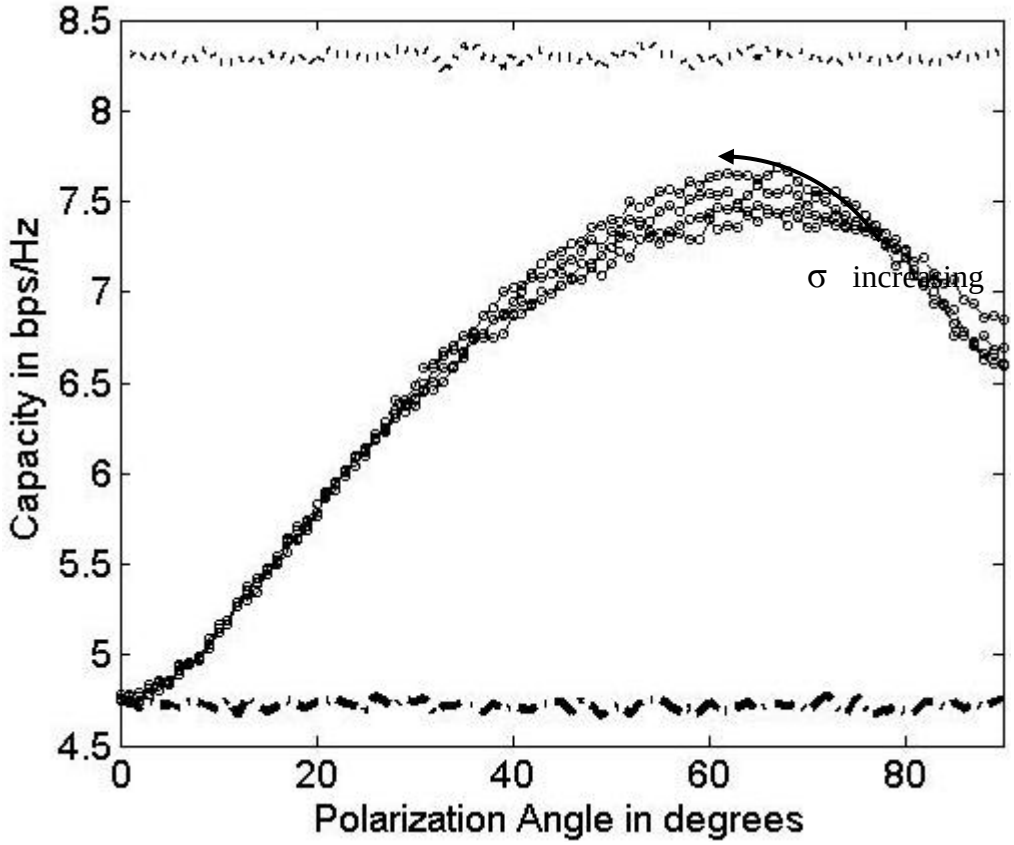

Figure 3.10: The channel capacity of 3 x 3 MIMO system as oriented in figure 3.1 (the antennas are located at 90, 210 and -30 azimuth angles) as a function of the polarization angle. ('…..': upper limit of 3 x 3 MIMO fading channel, '.-.-.-': upper limit of 3 x 1 MIMO fading channel, Capacity using equation 3.1: '_ _ _', Capacity using equation 3.20: 'ooo').

The elevation angle is varied uniformly over 30 degrees at the horizontal plane, whereas azimuth angle varied as Laplacian spectrum of different values of σ_ϕ (5, 10, 15, 20 degrees for the geometry presented in Figure 3.1) in which the azimuth direction randomly selected between 0 and 2π.

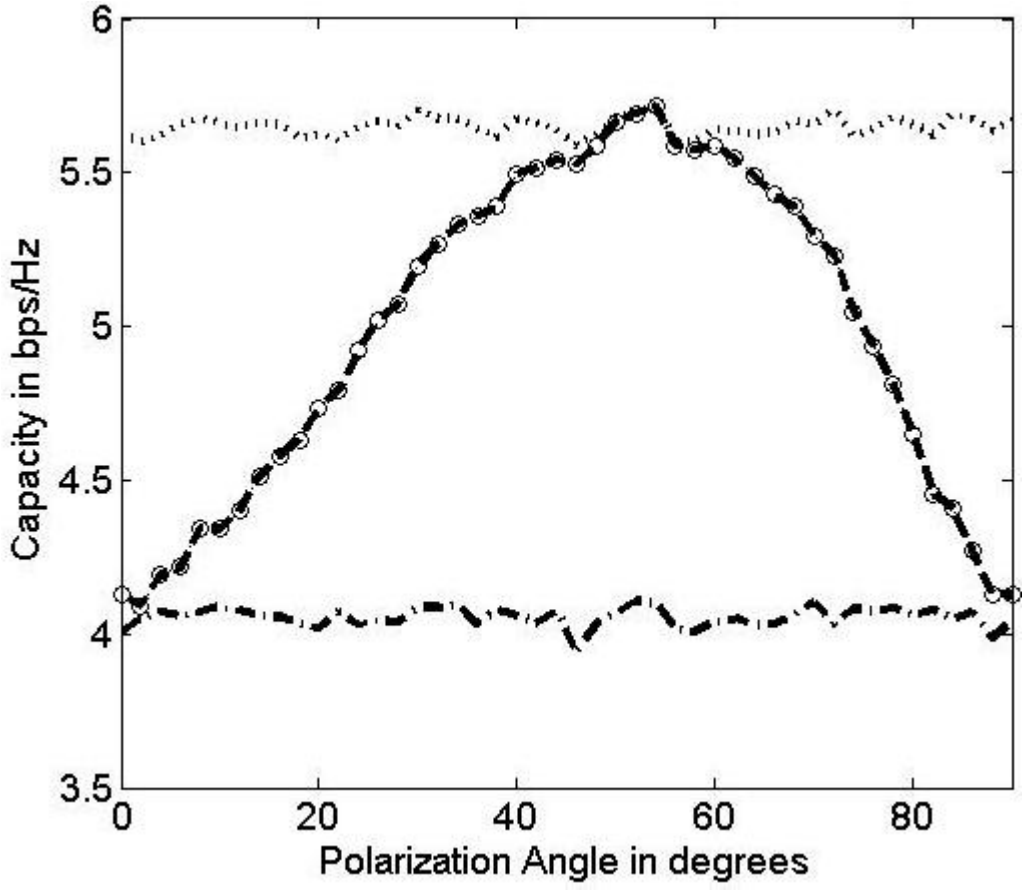

Figure 3.11: The channel capacity of 2 x 2 MIMO system as oriented in Figure 3.2 as a function of the polarization angle using secant square distributions. ('…..': upper limit of 2 x 2 MIMO fading channel, '.-.-.-': upper limit of 2 x 1 MIMO fading channel, Capacity using Equation 3.1: '_ _ _, Capacity using Equation 3.20: 'o o o').

Channel capacities for the 2×2 and 3×3 cases using the Secant square distribution along azimuth angle are shown in Figures 3.11 and 3.12. The antennas for the 2×2 case are located at $\phi = 0°$ and $180°$, whereas for the 3×3 case $\phi = \{0°, 120°, 240°\}$. For the 2×2

and 3×3 systems the maximum channel capacities have been observed at 55° and 62° respectively.

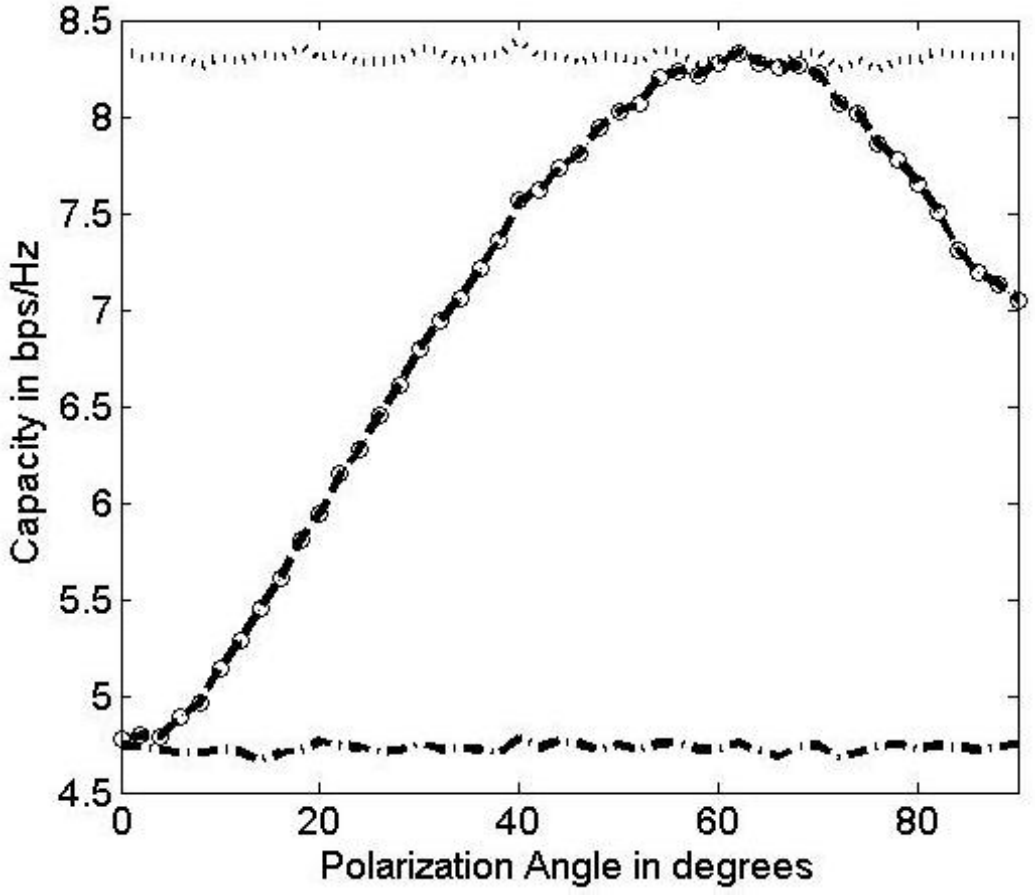

Figure 3.12: the channel capacity of 3 × 3 MIMO system as oriented in Figure 3.1 as a function of the polarization angle. ('…..': upper limit of 3 × 3 MIMO fading channel, '.-.-.-': upper limit of 3 × 1 MIMO fading channel, Capacity using equation 3.1: '_ _ _', Capacity using equation 3.20: 'ooo').

Figures 3.14 and 3.15 show the channel capacities of 2x2 and 3x3 systems as described in figures 3.1 and 3.2 respectively. The channel capacity has been calculated by assuming the Raised cosine distributions along the zenith angle whereas Gaussian distribution has been used along the azimuth. In both cases the calculated channel capacity is seen to approach the maximum limit.

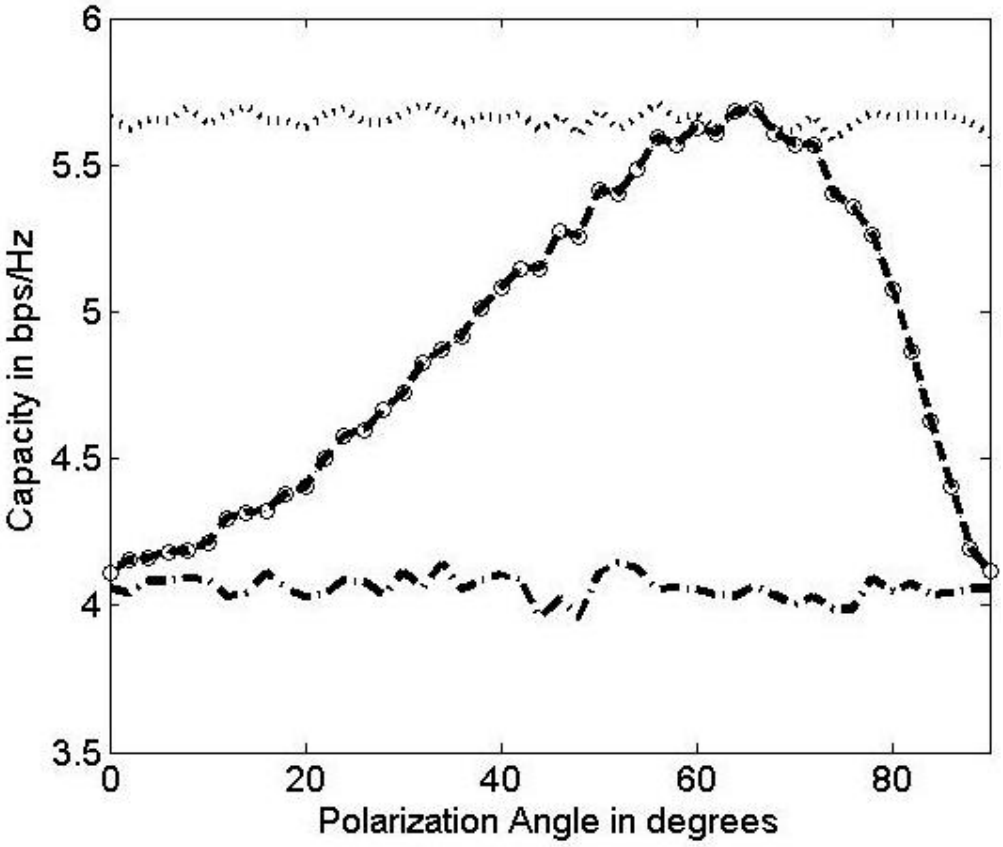

Figure 3.13: The channel capacity of 2 x 2 MIMO system as oriented in Figure 3.2 as a function of the polarization angle. ('…..': upper limit of 2 x 2 MIMO fading channel, '.-.-.-': upper limit of 2 x 1 MIMO fading channel, Capacity using Equation 3.1: '_ _ _, Capacity using Equation 3.20: 'o o o').

It should be noted that the channel capacity results shown in Figures 3.13 and 3.14 are approximately similar to the capacities calculated using Laplacian and Secant squared distributions. The maximum capacities for both 2×2 and 3×3 MIMO systems have been observed at the polarization angles of 64°.

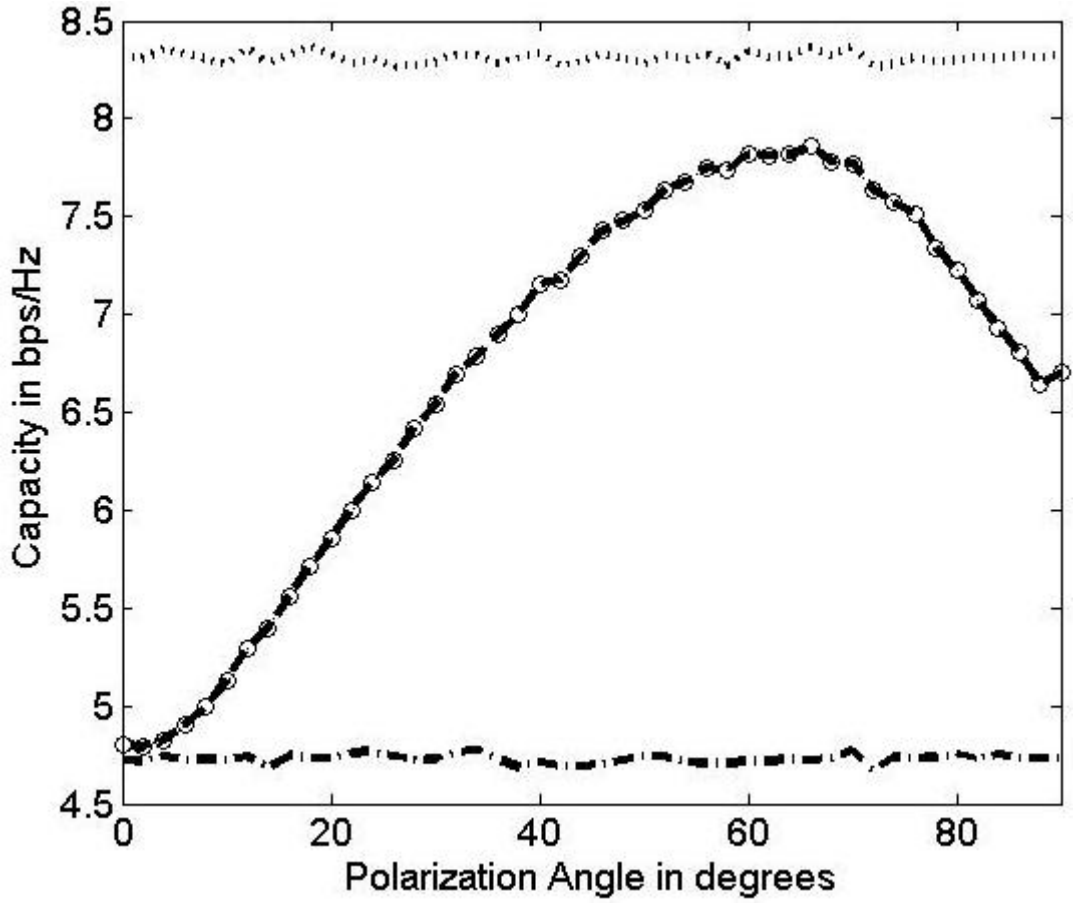

Figure 3.14: The channel capacity of 3 × 3 MIMO system as oriented in Figure 3.1 as a function of the polarization angle. ('…..': upper limit of 3 × 3 MIMO fading channel, '.-.-.-': upper limit of 3 × 1 MIMO fading channel, Capacity using equation 3.1: '_ _ _', Capacity using equation 3.20: 'ooo').

The channel capacities for different transmitted powers are shown in Figure 3.15, here the elevation angle varies uniformly over 180° from the centre (with zero crossings), but with the same azimuthal variations used for Figures 3.8 and 3.10. The channel capacities can be seen to increase with increasing SNR (this is in fact approximately linear); with the maxima located at an elevation angle of 63°.

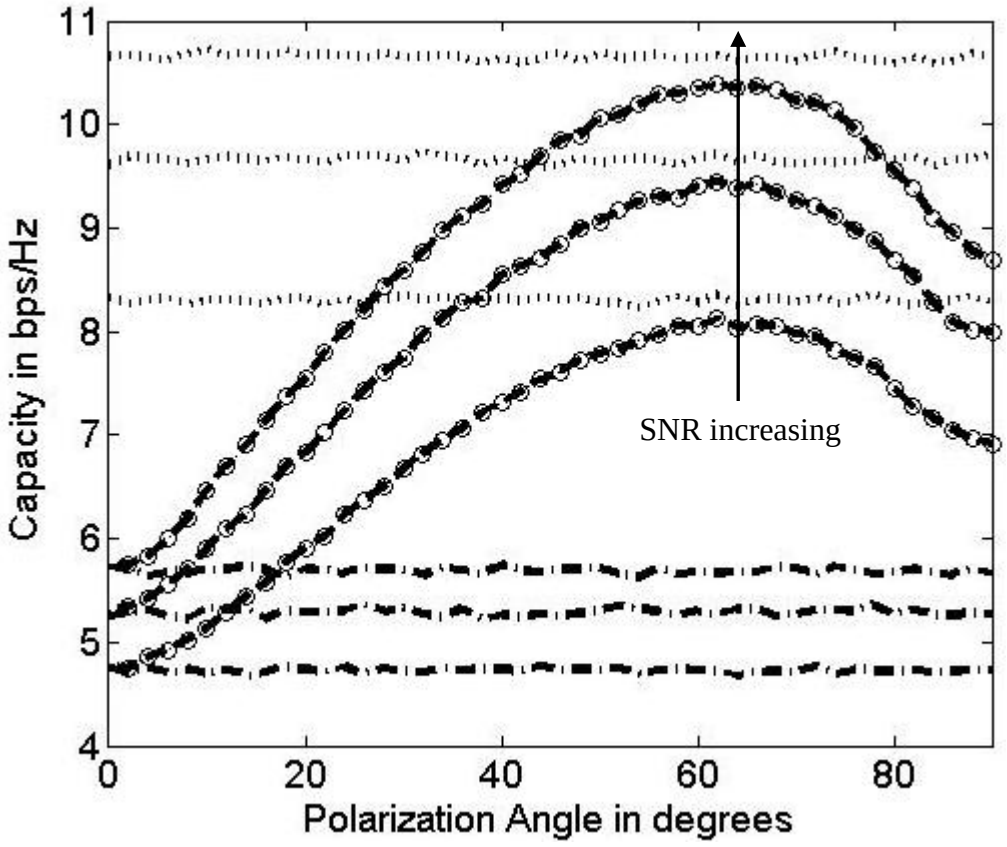

Figure 3.15: The channel capacity of 3 × 3 MIMO system as oriented in Figure 3.1 as a function of the polarization angle for different SNR as 10dB, 15dB and 20dBs; ('…..': upper limit of 3 × 3 MIMO fading channel, '.-.-.-': upper limit of 3 × 1 MIMO fading channel, Capacity using equation 3.1: '_ _ _', Capacity using equation 3.20: 'ooo').

Figures 3.16 and 3.17 show a comparison, using the urban channel model, of the channel capacity for the MIMO antenna geometry vs. a simple planar ring array. The channel capacity of the planar ring is at a maximum when the ring radius is approximately $\lambda/4$ (i.e. the distance of separation between the elements is $\lambda/2$). These results clearly indicate the possible benefits for volume reduction using the MIMO antenna geometry proposed in Figure 3.1.

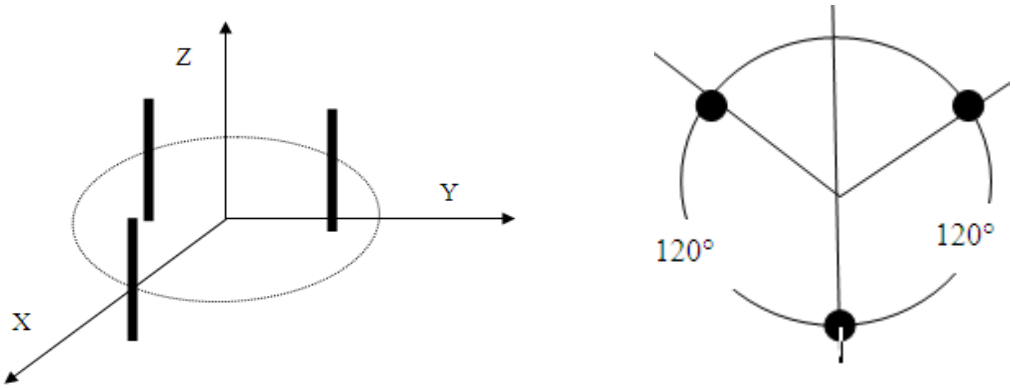

(a) (b)

Figure 3.16: 3×3 MIMO ring antenna array system;
(a) 3D geometry, (b) top view

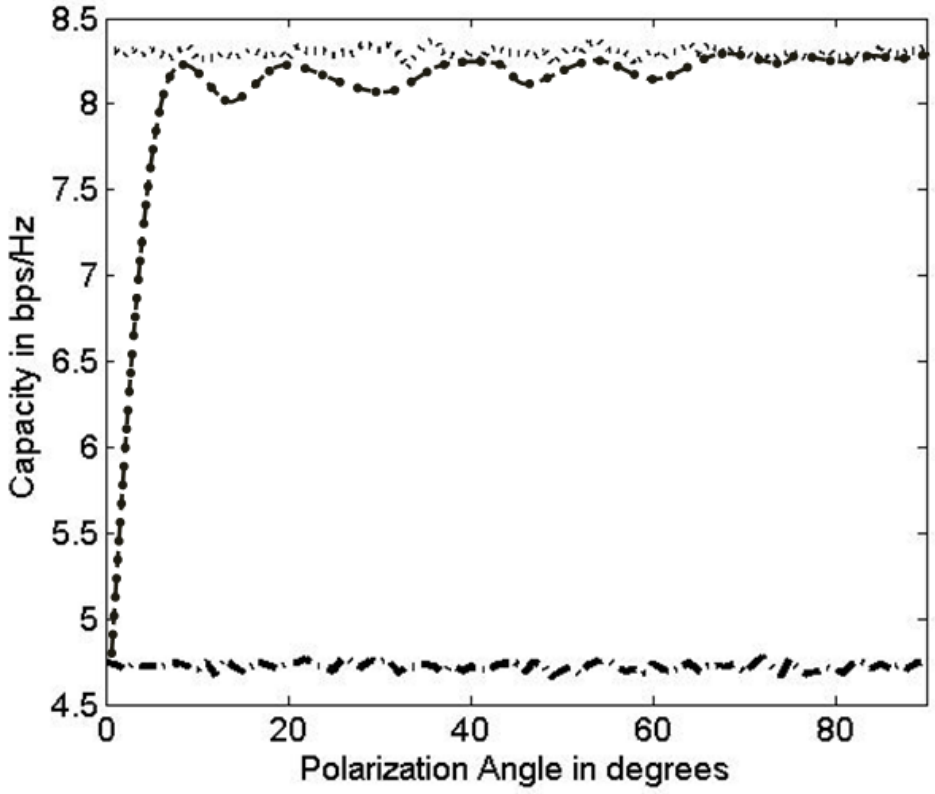

Figure 3.17: The channel capacity of 3 × 3 MIMO system as oriented in Figure 3.16 (the antennas are located at 0°, 120° and -120° azimuth angles) as a function of the radius distance in wavelength; ('…..': upper limit of 3 × 3 MIMO fading channel, '.-.-.-': upper limit of 3 × 1 MIMO fading channel, Capacity using equation 3.1: '_ _ _', capacity using equation 3.20: 'o o o').

3.5 CONCLUSION

In this chapter the channel capacity of 2×2 and 3×3 MIMO systems using spatial polarization diversity for a variety of channel models has been discussed; the simulated results have been compared and verified using the dominant eigenvalues of the channel matrix. The results show that the maximum channel capacity within a small volume can be reached by careful selection of the intrinsic orthogonalities of the spatial field distribution. The results are also compared with a planar array in which the antenna volume was much larger to that of the MIMO system described here.

3.6 REFERENCES

[1] Da-Shan, G.J. Foschini, M.J. Gans and J.M. Kahn, "Fading Correlation and Its Effect on the Capacity of Multi-element Antenna Systems", IEEE Transactions on Communications,Vol.48, NO.3, March 2000.

[2] T. Syantesson and J.W. Brigham, "Prediction Algorithms Using Measurements", Department of Electrical and Computer Engineering, Brigham Young University, Provo, UT 84602-4099.

[3] E. Biglirie, et al, "MIMO Wireless Communications", Chapters 1 – 3, John Wiley, NY, ISBN-978052187.

[4] D. Tse and P. Viswanath, "Fundamentals of Wireless Communication", Chapters 7 – 10, Cambridge University Press, 2005.

[5] L. Dong, H. Choo, R.W. Heath, and H. Ling, "Simulation of MIMO Channel Capacity With Antenna Polarization Diversity", IEEE Transaction on Wireless Communication, Vol. 4, July 2005.

[6] Y. Takatori, F. Fitzek, K. Tsunekawa, R. Prasad, “Channel Capacity of TDD, OFDM MIMO for Multiple Access Points in a Wireless Single Frequency Network”, MIMO MAP Springer 2005.

[7] G. J. Foschini and M. J. Gans, “On limits of wireless communication in a fading environment when using multiple antennas”, Wireless Personal Commun., vol. 6, no. 3, pp. 311–335, Mar. 1998.

[8] G. J. Foschini and R. A. Valenzuela, “Initial estimation of communication efficiency of indoor wireless channel”, Wireless Networks, vol. 3, pp. 141–154, 1997.

[9] J. W. Wallace and M. A. Jensen, “Modelling the indoor MIMO wireless channel”, IEEE Trans. Antennas Propag., vol. 50, no. 5, pp. 591–599,May 2002.

[10] J.W. Wallace, M.A. Jensen, A.L. Swindlehurst, and B.D. Jeffs, “Experimental characterization of the MIMO wireless channel: Data acquisition and analysis”, IEEE Trans. Wireless Commun., vol. 2, no. 2, pp. 335–343,Mar. 2003.

[11] D. Gesbert, H. Bölcskei, D.A. Gore, and A. Paulraj, “Outdoor MIMO wireless channels: Model and performance prediction”, IEEE Trans. Commun., vol. 50, no. 12, pp. 1926–1934, Dec. 2002.

[12] L. Dong, H. Choo, R.W Heath and H. Ling, “Simulation of MIMO Channel Capacity with Antenna Polarization Diversity”, IEEE Transactions on wireless communications, vol. 4, no. 4, July 2005, pp. 1869-1873.

[13] C.E. Shannon, "A Mathematical Theory of Communication", Bell System Technical Journal, vol. 27, pp. 379-423, 623-656, July, October, 1948

[14] J.H. Winters, J. Salz, and R.D. Gitlin, “The impact of antenna diversity on the capacity of wireless communication systems”, IEEE Trans. Commun., vol. 42, pp. 1740–1751, Feb. 1994.

[15] M.R. Andrews, P.P. Mitra, and R.de Carvalho, “Tripling the capacity of wireless communications using electromagnetic polarization”, Nature, vol. 409, no. 6818, pp. 316–318, Jan. 2001.

[16] T. Svantesson, “On capacity and correlation of multi-antenna systems employing multiple polarizations”, in IEEE Int. Antennas Propagation Symp. Digest, San Antonio, TX, Jun. 2002, pp. 202–205.

[17] D.D. Stancil, A. Berson, J.P. Van’t Hof, R. Negi, S. Sheth, and P. Patel, “Doubling wireless channel capacity using co-polarised, co-located electric and magnetic dipoles”, Electron. Lett., vol. 38, no. 14, pp. 746–747, Jul. 2002.

[18] H.D. Tuan, D. Pham, B. Vo, T.Q. Nguyen, “Entropy of General Gaussian Distributions and MIMO Channel Capacity Maximizing Precoder and Decoder”, Acoustics, Speech and Signal Processing, 2007. ICASSP 2007. IEEE International Conference on Volume 3, Issue , 15-20 April 2007 Page(s):III-325 - III-328.

[19] G. Turin, F. Clapp, T. Johnston, S. Fine, and D. Lavry, “A statistical model of urban multipath propagation”, IEEE Trans. Veh. Technol., vol.21, pp. 1–9, Feb. 1972.

[20] H. Suzuki, “A statistical model for urban radio propagation”, IEEE Trans. Commun., vol. 25, pp. 673–680, July 1977.

[21] S.A. Zekavat and C.R. Nassar, “Power-azimuth-spectrum modelling for antenna array systems: a geometric-based approach”, Antennas and Propagation, IEEE Transactions on Antennas and Propagation, Volume 51, Issue 12, Page(s):3292 – 3294, December 2003.

[22] K.I. Pedersen, P.E. Mogensen, and B.H. Fleury, “A Stochastic Model of the Temporal and Azimuthal Dispersion Seen at the Base Station in Outdoor Propagation Environments”, IEEE Transactions on vehicular Technology, Vol .49,No.2, March 2000.

[23] P.C. Hsieh and F.C. Chen, “ A new MIMO spatial correlation approximation of large angular spread”, Antennas and Propagation Society International Symposium, 2007 IEEE Volume , Issue , 9-15 June 2007 Page(s):1909 – 1912.

[24] L.J. Dong, J. Ma, J. Zhou, and H. Kikuchi, “ Performance of MIMO with UCA and Laplacian Angular Distribution Using Correlation Matrix”, Wireless Communications, Networking and Mobile Computing, 2007. WiCom 2007. International Conference on Volume , Issue , 21-25 Sept. 2007 Page(s):53 – 56.

CHAPTER 4

PRACTICAL IMPLEMENTATION OF MIMO SYSTEM

4.1 INTRODUCTION

Mobile MIMO communications provides an improved transmission capacity and error performance over traditional digital transmission systems. This is because MIMO can positively utilise the multi-path environment, whereby a multiplicity of reflected signals may travel along entirely separate paths, and even reach the receiver at different times. Traditional systems cannot use these multi-path components independently, and overcoming this obstacle is at the heart of MIMO designs in mobile communications. There are several contemporary MIMO development platforms which are showing great promise in the search for enhanced bandwidth. One of the major challenges, even in certain areas of consumer electronics, is the development of intelligent digital beam-forming. Hence the rationale for investigating mobile MIMO handset or terminal designs.

The design proposed below will make use of the spatial correlations of polarisation states described in the previous chapter, rather than angle of arrival (AOA), which will allow a useful reduction in the size of the radiators comprising the antenna module [1-7]. Specifically dual band MIMO designs are investigated, as they offer flexibility between mobile terminals, such as smart phones, or wireless-LAN enabled devices.

The IEEE 802.11b/g standards utilise the 2.4 GHz ISM band, this band is license-free. Hence WLAN equipment may suffer interference from microwave ovens, cordless phones, Bluetooth devices and other appliances using this band. The IEEE 802.11a standard uses the 5 GHz band, which suffers less interference. However, the frequency band used varies from one region of the world to another: typically either the 5.15-5.35 GHz band or the 5.725-5.825 GHz band. A traveller with an 802.11a/b/g transceiver that can cover both 2.4 GHz and 5.2 GHz will be able to gain access to local WLAN networks in different parts of the world. In summary, a MIMO antenna module should be an ideal choice for such applications; but to realise this objective it is necessary to ensure that size constraints are fully satisfied, alongside the polarisation diversity. From a commercial perspective, the potential size advantage is deeply significant, especially when combined with good antenna efficiency and enhanced channel capacity.

The candidate radiator structure for the antenna module is a modified PIFA. The PIFA or planar inverted-F antenna is a variant of the inverted F antenna (IFA) [8-13]. In order to improve the bandwidth, the radiating wire element is replaced by plates. PIFA antennas can be fully accommodated within the housing of the device, and have the effect of reducing the backward radiation towards the user's head. This will minimise the electromagnetic power absorption (SAR), and thus enhances the antenna performance [14-17].

4.2 ANTENNA DESIGN METHOD

This chapter presents the practical realisation of 2×2 and 3×3 MIMO prototypes; simulated and measured results are presented. In order to build a suitable MIMO antenna module a dual band PIFA antenna has been carefully specified.

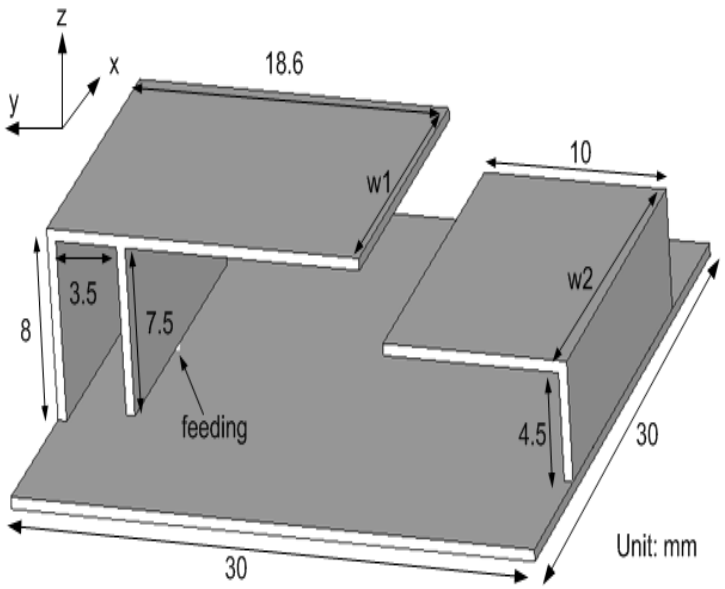

Figure 4.1: Dual-band antenna structure.

This antenna geometry is adapted from previous work [18] and modified as shown in Fig. 4.1. Firstly, the PIFA has been designed with a resonant frequency of 2.4 GHz. The inverted-L (passive) element is incorporated within λ/4 of the PIFA, this element behaves as a capacitive load, and is responsible for the second resonant frequency of 5.2 GHz. The widths w_1 and w_2 were selected as 13 mm and 11 mm to adjust the required resonances in this small antenna structure. This antenna geometry was modelled with a 50Ω matched load using Ansoft HFSS™ [19]. Generically this style of assembly will be referred to as a PIF(L)A.

Once individual dual-band antenna operation was achieved, the more challenging problem of incorporating two/three antennas to form the 2×2/3×3 MIMO prototypes was addressed. To achieve this, a metal chassis of dimensions 100mm × 50mm × 20mm was used. Orthogonal polarisations were generated by locating three of the dual-band PIF(L)A units on three orthogonal upper surfaces of the box. Figures 4.2 and 4.3 show

the full set of 2×2 and 3×3 antenna modules, including the box; once again the whole system is modelled using HFSS.

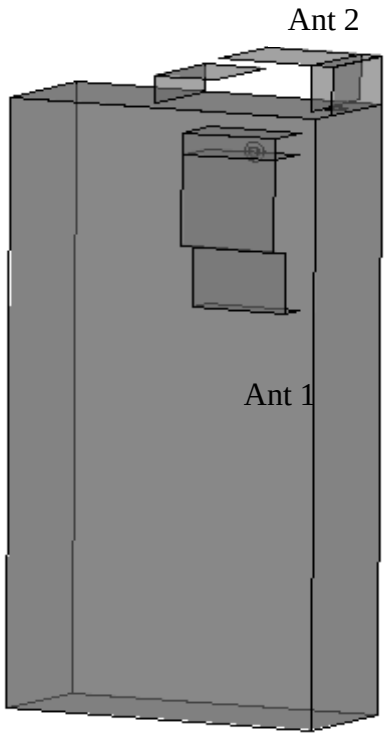

Figure 4.2: 2×2 MIMO orthogonal dual-band antennas mobile handset.

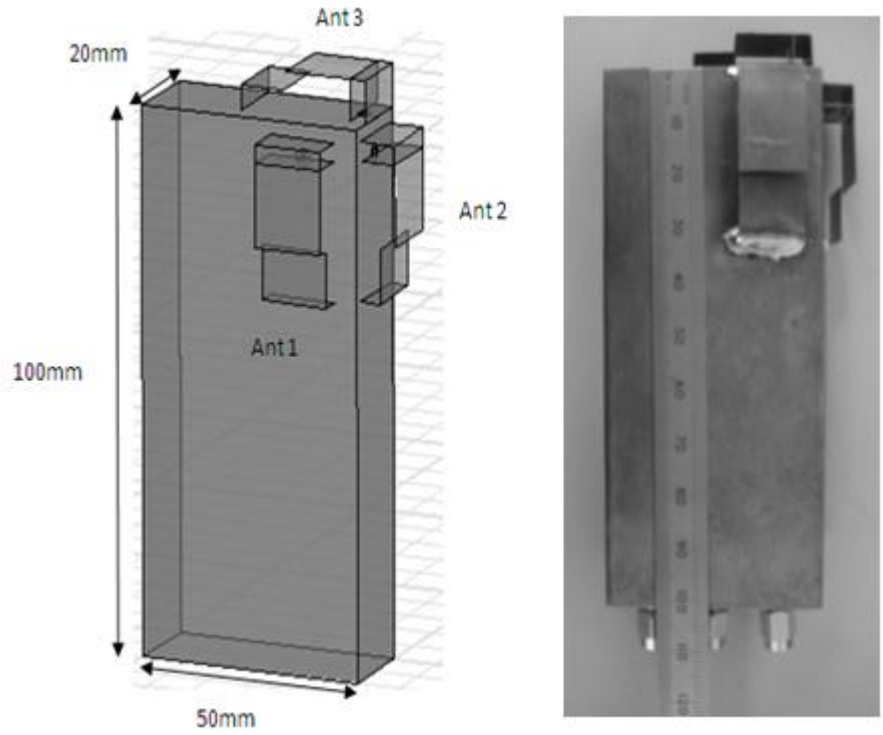

Figure 4.3: 3×3 MIMO orthogonal dual-band antennas mobile handset.

In Figure 4.3, the polarisation-diverse prototype antenna assembly is visualised. The position of each antenna has been carefully selected in order to provide suitably compact antenna geometry, with low a coupling factor between each of the three radiators. Several parameters were simulated and checked for performance with the MIMO and dual-band responses for each realisation. A 3×3 prototype module was fabricated and tested. In addition, the performance of this antenna assembly, including hand model, as shown in Figure 4.4, was tested and the simulated results are discussed.

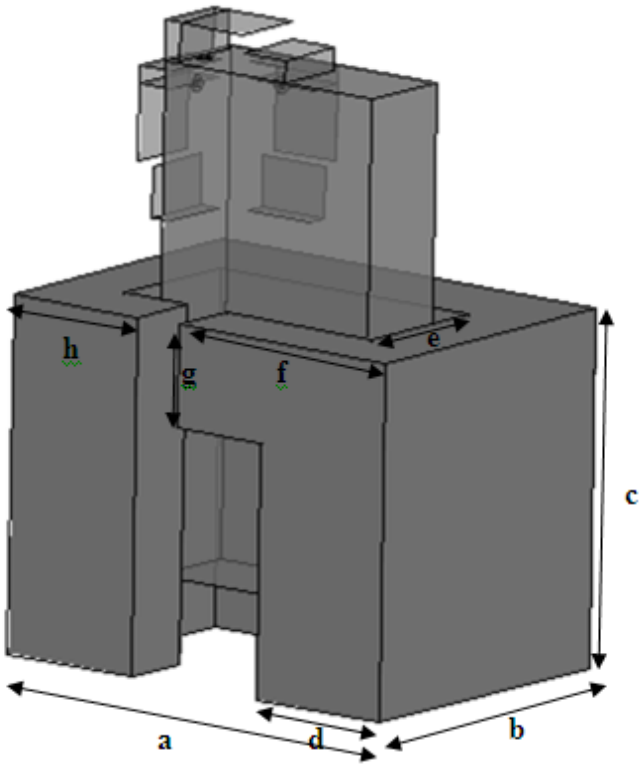

Figure 4.4: 3×3 MIMO antenna handset with hand model

Figure 4.4 illustrates the 3×3 prototype assembly, with the hand model positioned around the metal chassis. The electrical properties used for the hand model tissue at 2.5 GHz are: relative permittivity (ε_r) of 55, and conductivity (σ) of 1.45 S/m; whereas at 5.2 GHz the values are ε_r = 49, and σ = 3.7 S/m [20]. In addition, the dimensions, location and position of the hand model illustrated in Fig. 4.4 are as follows: a = 90, b = 70, c = 70, d = 20, e = 30, f = 50, g = 10, h = 25 (all the dimensions are quoted in mm). Note that the gap between the hand model and the metallic ground plate is kept at 5 mm.

4.3 MEASUREMENTS AND RESULTS

4.3.1 Return Loss and Coupling

The return loss, coupling and radiation pattern of each radiator were checked, and the simulated results verified to ensure adequate performance. Fig. 4.5 shows the return loss of 2×2 prototype. It is clear that the two elements were satisfying the requirements of a dual resonance operation at the 2.4 and 5.2 GHz frequency bands. Within these bands, both of the antennas show a return loss ranging from -13dB to -23dB, which is quite satisfactory. Antenna 1 has a return loss of -23dB and -12dB at 2.5 GHz and 5.2 GHz respectively whereas Antenna 2 has return loss of -12.5dB and -12dB at 2.5 GHz and 5.2 GHz.

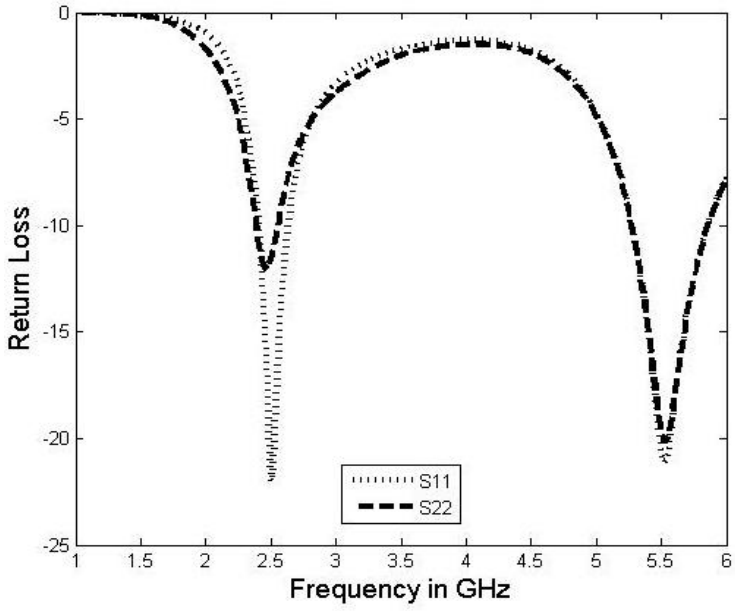

Figure 4.5: Return losses of orthogonal 2×2 MIMO antenna system

Figures 4.6(a), 4.6(b) and 4.6(c) show the simulated and measured input return losses of 3×3 prototype module. The scattering parameters S_{11}, S_{22} and S_{33} have been plotted in separate figures in order to inspect the results clearly. It is clear that in all three radiators

comprising the 3×3 prototype, each of the antennas fulfil the requirement of dual band operations at 2.4 GHz and 5.2 GHz. Within these bands, all the antennas show a return loss ranging from -10dB to -30dB, which are quite satisfactory. The simulated and measured relative (impedance) bandwidths of the radiating elements are given in Table 4.1. All the antennas show reasonable relative bandwidth at the 2.5 GHz and 5.2 GHz operating frequencies, in which they contain the total bandwidths required for the IEEE 802.11a/b/g standards.

Table 4.1: The impedance relative bandwidths (BWr) of the radiating elements of the 3 × 3 MIMO antenna handset.

	2.5 GHz		**5.2 GHz**	
	Simulated BWr %	**Measured BWr %**	**Simulated BWr %**	**Measured BWr %**
Antenna 1	9.1	6.4	13.1	6.6
Antenna 2	9.1	5	9.6	7
Antenna 3	8	6	11.5	8.7

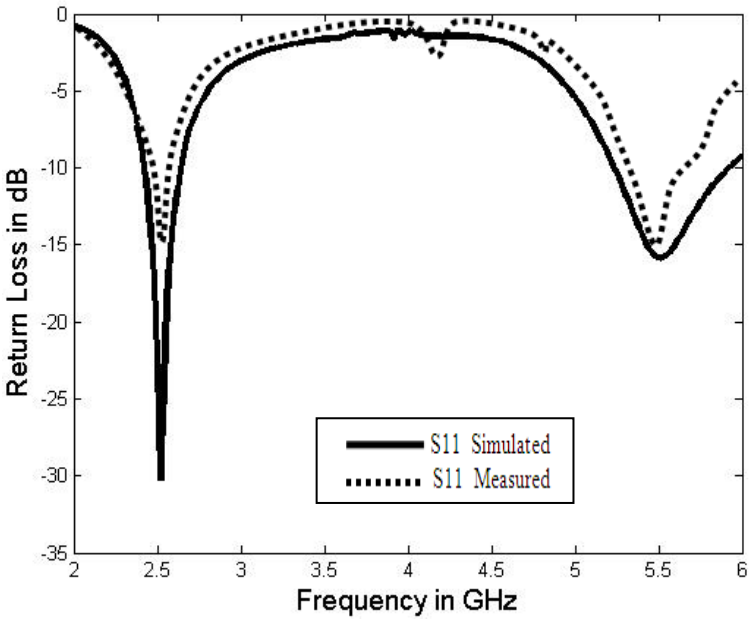
Return Loss in dB
Frequency in GHz
S11 Simulated
S11 Measured
0
-5
-10
-15
-20
-25
-30
-35
2
2.5
3
3.5
4
4.5
5
5.5
6

(a)

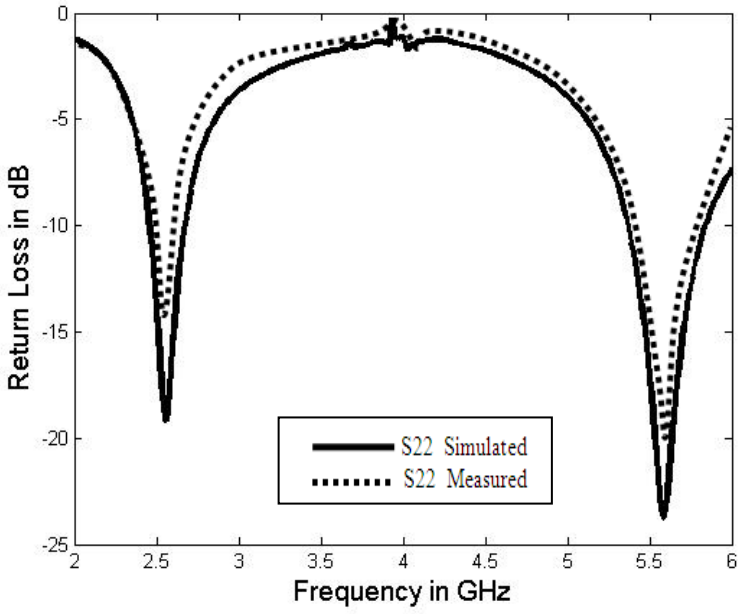
Return Loss in dB
Frequency in GHz
S22 Simulated
S22 Measured
0
-5
-10
-15
-20
-25
2
2.5
3
3.5
4
4.5
5
5.5
6

(b)

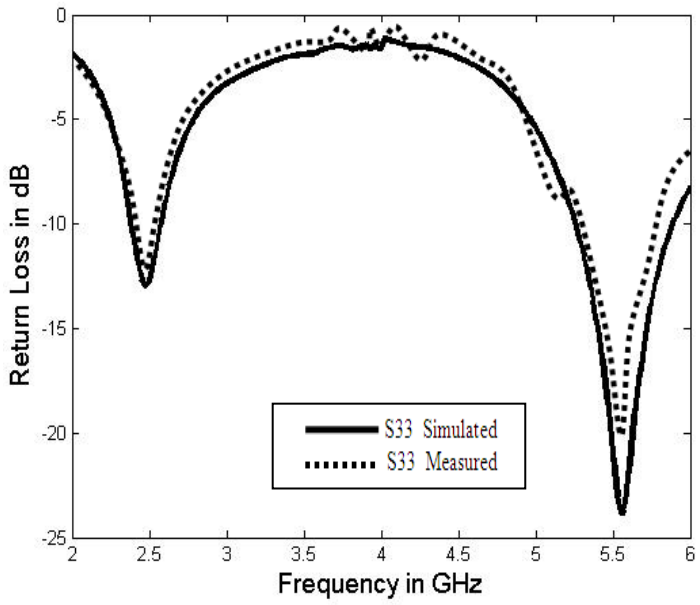

(c)

Figure 4.6: Figures (a) S_{11}, (b) S_{22} and (c) S_{33}, show return losses of orthogonal 3×3 MIMO antenna system.

The 3×3 prototype module has been simulated using the hand model positioned around the antenna assembly housing. Figure 4.7 shows the input return losses of this assembly. It has been clearly demonstrated that the effects of the hand model on the return loss is virtually negligible. The relative (impedance) bandwidth of the radiating elements of the 3×3 prototype module, including the hand model is summarized in Table 4.2. These results are quite encouraging since the available bandwidths cover the required standard bandwidth of the IEEE 802.11x standard, despite some detectable hand/antenna coupling effects.

Table 4.2: The simulated impedance relative bandwidths (BWr) of the radiating elements of the 3 × 3 MIMO antenna handset with hand model.

	2.5 GHz **BWr %**	**5.2 GHz** **BWr %**
Antenna 1	10	20
Antenna 2	8.7	22.8
Antenna 3	5	10.8

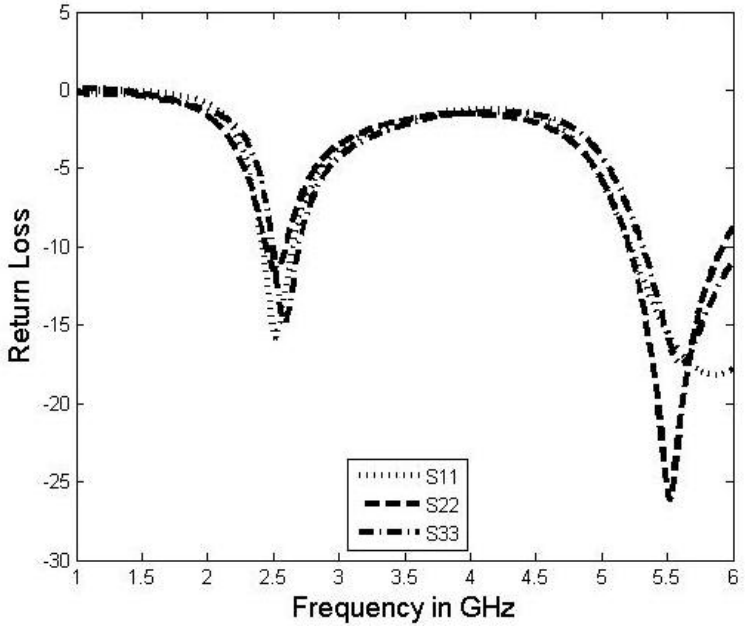

Figure 4.7: Return losses of orthogonal 3×3 MIMO antenna system with human hand

Thus far, the simulated return losses have been quite satisfactory; however, the important issue is to observe the coupling between the antennas of the 2×2/3×3 (without hand) and 3×3 (with hand) antenna modules. Figures 4.8, 4.9 and 4.10 provide the coupling factors between the antennas of all above mentioned examples.

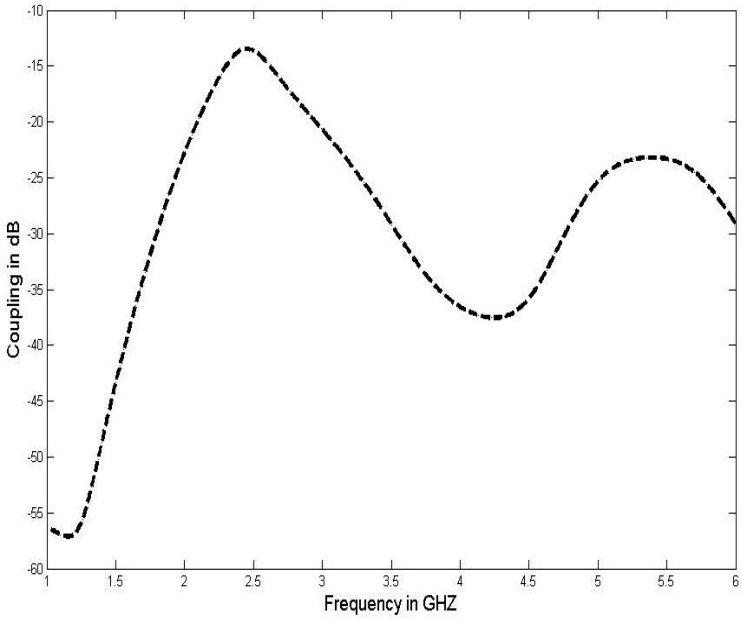

Figure 4.8: Coupling between the elements of 2×2 MIMO antenna handset.

Since the radiators are passive, so $S_{12} = S_{21}$. The coupling between both antennas is found to be less than -13dB and -23dB at the 2.4 GHz and 5.2 GHz operating frequencies respectively.

Figure 4.9a and 4.9b show the coupling factors between the three radiators in the 3×3 prototype module at 2.5GHz and 5.2GHz respectively. On close observation it has been noticed that the maximum coupling between the three radiators was -12dB in the neighbourhood of each of the operating bands. In general, the coupling factors of the 3×3 prototype module were very encouraging for its practical application in mobile terminals. In addition, the proposed geometry of this system is also in accordance with contemporary mobile size phones.

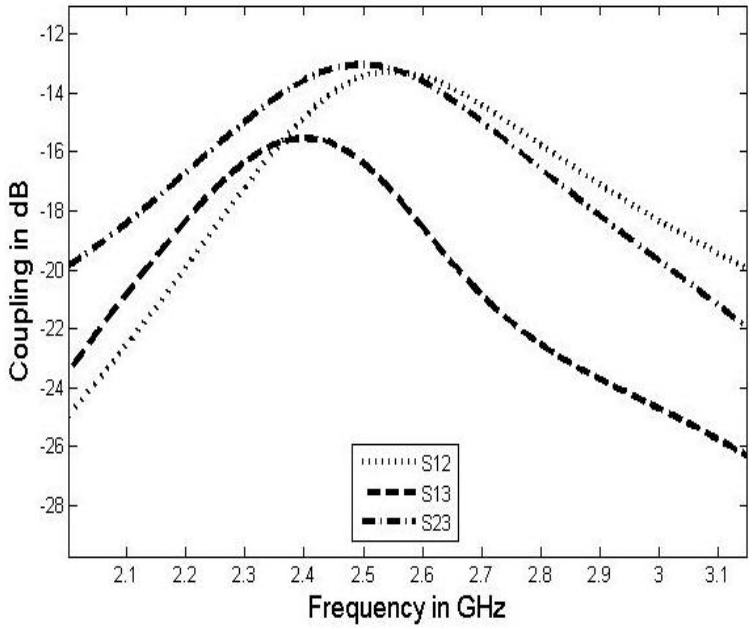

(a)

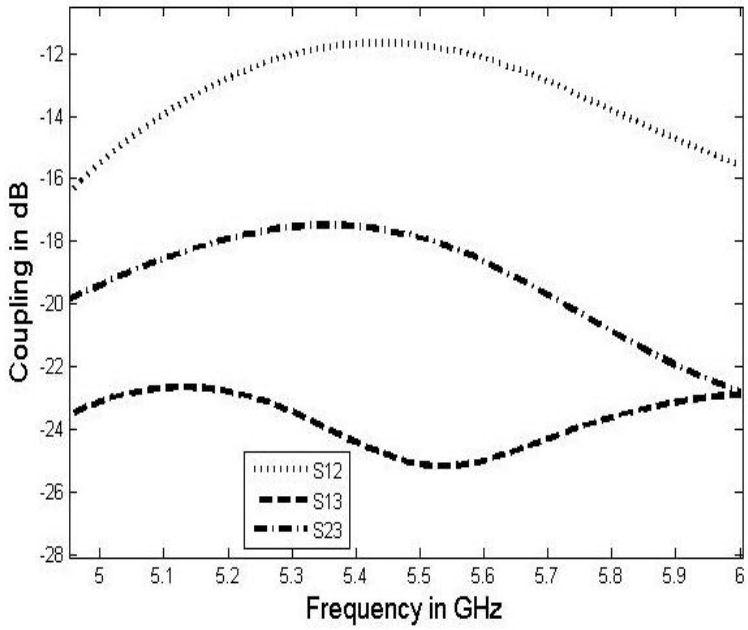

(b)

Figure 4.9: Simulated coupling factors between the elements of 3×3 MIMO system for (a) 2.5 GHz (b) 5.2 GHz band.

Figures 4.10a and 4.10b represent the coupling between the antenna elements including the model of human hand around the metal chassis of 3×3 prototype module against the target operating frequencies. In Figure 4.10a the coupling between the three antenna

elements i.e. S_{12}, S_{13} and S_{23} are found to be less than -13dB. For comparison between the results presented in Figures 4.9a and 4.10b, it can be seen that there is not much effect on the coupling factor values with the presence of hand around the handset.

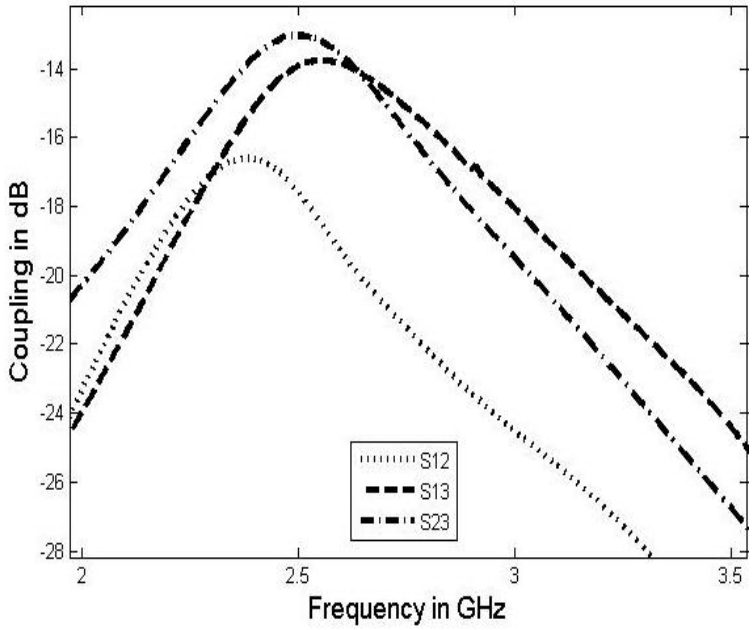

(a)

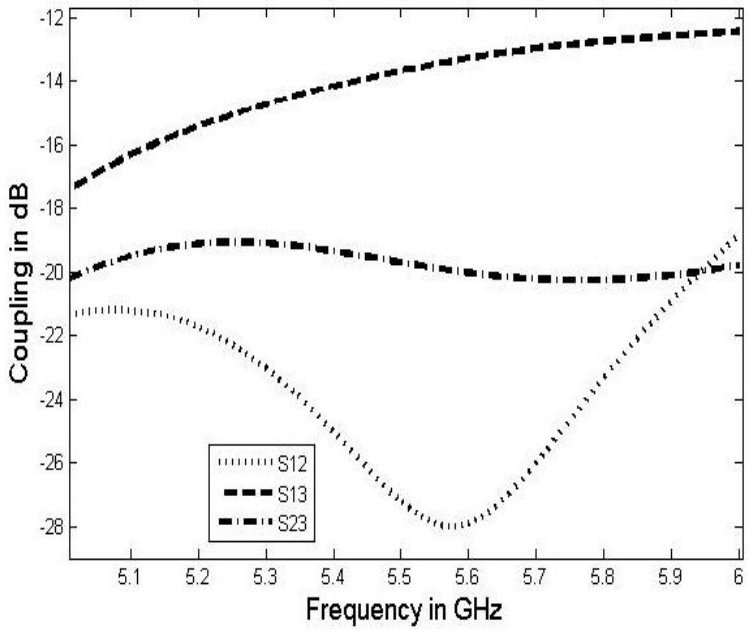

(b)

Figure 4.10: Coupling between the antenna elements of 3×3 MIMO system with hand at (a) 2.5 GHz (b) 5.2 GHz band.

Consequently, the comparison between the Figures 4.10b and 4.10b, shows the effect of human hand. In Figure 4.10b the coupling between the radiators are reduced to the values of -21.5 dB, -19 dB and -16 dB at 5.2 GHz, respectively, for the scattering parameters S_{12}, S_{13} and S_{23}.

4.4 CALCULATION OF CHANNEL CAPACITY FOR THE PROPOSED MIMO SYSTEM

The main advantage of MIMO is to increase the channel capacity of the system. A successful MIMO system design should deliver the approximately same channel capacity as of the MIMO system without any coupling.

For the calculation of channel capacity the complex values of E_θ and E_Φ field components have been extracted from the HFSS simulation. These field components were computed for the solid angle over $\theta = 0^o$ to 180^o and $\Phi = 0^o$ to 360^o with 5^o steps in both angle directions. Two frequency bands are considered, these are 2.4 GHz to 2.52 GHz and 5.2GHz to 5.8GHz. In addition to this, the 3×3 prototype module performance as a function of channel capacity has been evaluated with the effect of human hand around the mobile handset.

The channel capacity of the 3×3 module design has been calculated over a Rayleigh fading channel using Gaussian, Laplacian and secant-squared distributions along the azimuth for different values of mean and variance (Appendix B). By contrast, uniform, raised cosine and n^{th} order raised cosine distributions have been applied along the zenith angle. The channel capacity has been computed by using different combinations of these angular distributions along the azimuth and zenith for the 2.4 GHz and 5.2 GHz

bands. All the results show that the channel capacities of the prototype designs are approximately converging on the maximum of the coupling free MIMO case.

Table 4.3: Different angular distributions along azimuth and elevation

Distributions along Azimuth	**Distributions along Elevation**
Gaussian Distribution	Uniform Distribution
Uniform Distribution	Raised Cosine Distribution
Laplacian Distribution	N^{th} Order Raised Cosine Distribution
Secant Square Distribution	

Table 4.3 shows the various distributions along azimuth and elevation for the channel capacity calculation. In total, there will be twelve possible combinations for each MIMO system. This set of criteria is used throughout the subsequent discussions, in this chapter, and going forward.

4.4.1 Channel Capacity of 3×3 MIMO Antenna System

The first set of Figures 4.11 to 4.16 represent the combinations of uniform PAS over 0° to 360° and uniform, raised cosine and n^{th} order raised cosine distribution along the zenith angle. Different values of mean and variance have been set for tracking the variations of channel capacity around 2.5 GHz and 5.2 GHz frequency bands.

In Figures 4.11 and 4.12 the channel capacity of 3×3 prototype has been observed at 2.5 GHz and 5.2 GHz. The criterion for the channel capacity calculation is performed using uniform PAS in combination with uniform power spectrum over ±15° for various mean values. In Figure 4.11 it can be seen that the capacity of the system in the 2.5 GHz band

is very close to the maximum limit i.e. approximately 8.3 bps/Hz, at mean of 30°. The minimum value of 8bps/Hz has been obtained at 2.45 GHz at mean of 10°. Similarly in Figure 4.12 the minimum value of 7.6bps/Hz with variation ± 0.1bps/Hz around the 5.2GHz–5.8 GHz band can be observed. When the mean values increase from 10° to 40° the corresponding channel capacity values also increase proportionally. In Figure 4.12 the maximum value of 8.1bps/Hz can be observed with a mean of 40°. The overall variations in the capacity shown in Figures 4.11 and 4.12 are 0.2 bps/Hz and 0.1bps/Hz respectively.

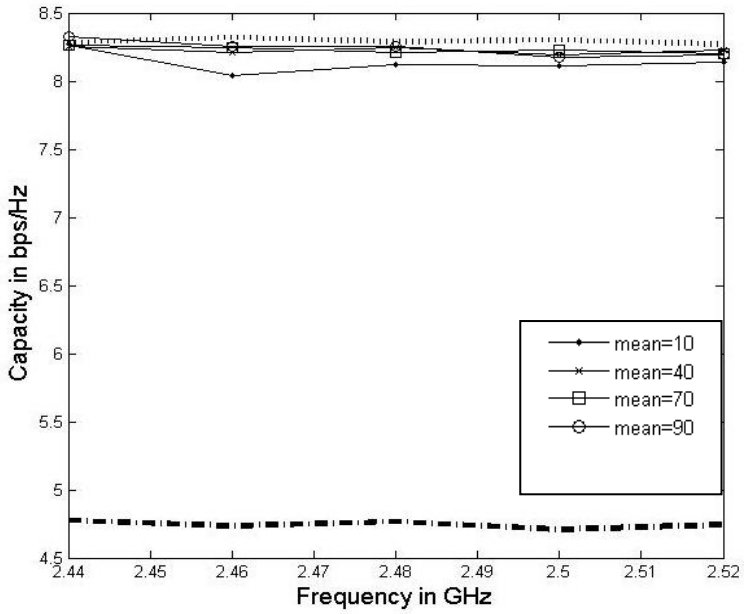

Figure 4.11: Variations of channel capacity versus operating frequency; subject to uniform PAS over 0 to 360° and uniform power spectrum over ±15° for various mean zenith angles of 10°, 40°, 70° and 90°; ('.....' upper limit of 3 × 3 MIMO), ('------'upper limit of 3 × 1 MIMO).

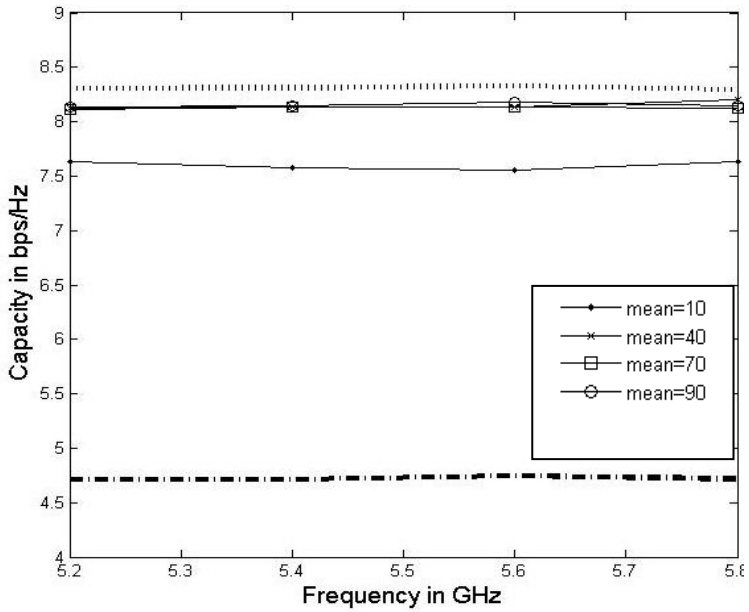

Figure 4.12: Variations of channel capacity versus operating frequency; subject to uniform PAS over 0 to 360° and raised cosine distribution power spectrum for various mean zenith angles of 70° and 90°; ('.....' upper limit of 3 × 3 MIMO), ('------'upper limit of 3 × 1 MIMO).

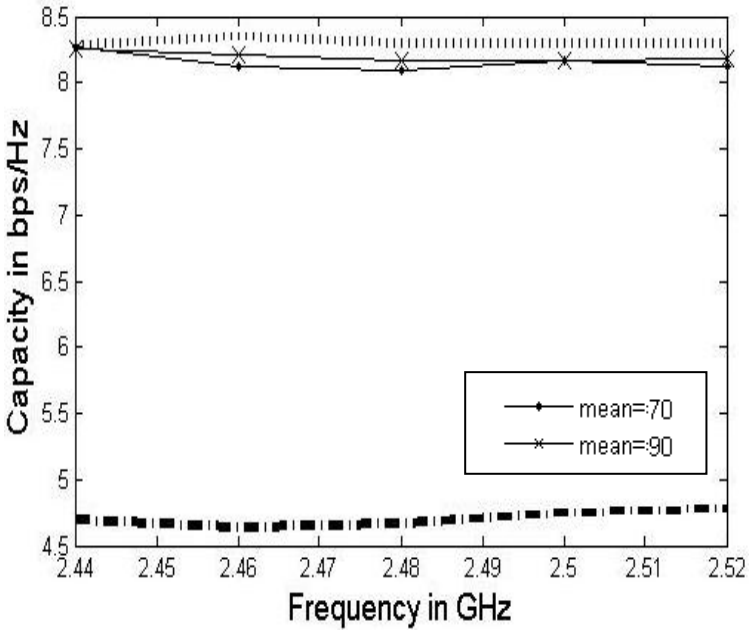

Figure 4.13: Variations of channel capacity versus operating frequency; subject to uniform PAS over 0 to 360° and raised cosine distribution power spectrum for various mean zenith angles of 70° and 90°; ('.....' upper limit of 3 × 3 MIMO), ('------'upper limit of 3 × 1 MIMO).

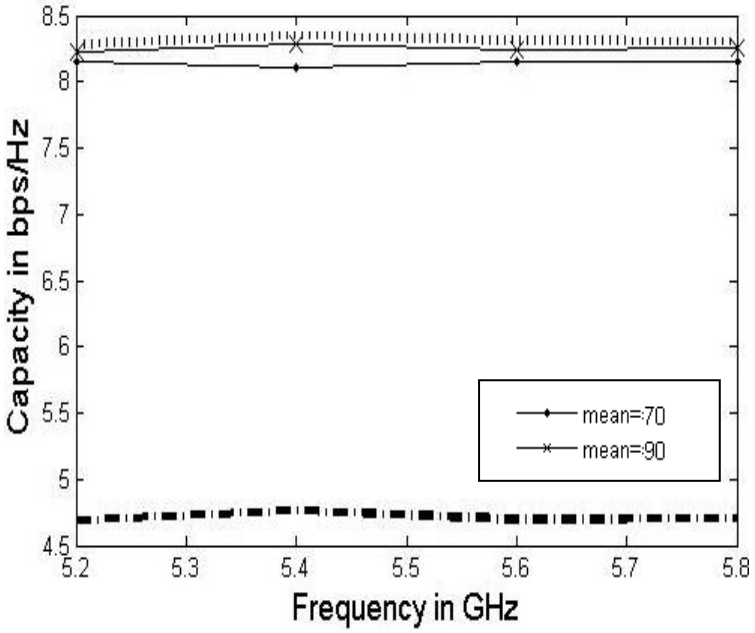

Figure 4.14: Variations of channel capacity versus operating frequency; subject to uniform PAS over 0 to 360° and raised cosine distribution power spectrum for various mean zenith angles of 70° and 90°; ('.....' upper limit of 3 × 3 MIMO), ('------'upper limit of 3 × 1 MIMO).

Figures 4.15 and 4.16 indicate the channel capacity for the 3×3 prototype with uniform PAS and n^{th} order raised cosine distribution along zenith angle. Different values of n have been used which are 2, 4 and 8. In Figure 4.15 the maximum variations of approximately 0.1bps/Hz channel capacity have been observed for all calculated values. The maximum of 8.3bps/Hz can be seen at 2.44GHz at n=8, whereas in Figure 4.16 the variation of channel capacity is almost negligible for different values of n. In each case the calculated capacity approaches the maximum limit of the 3×3 prototype module, without any coupling.

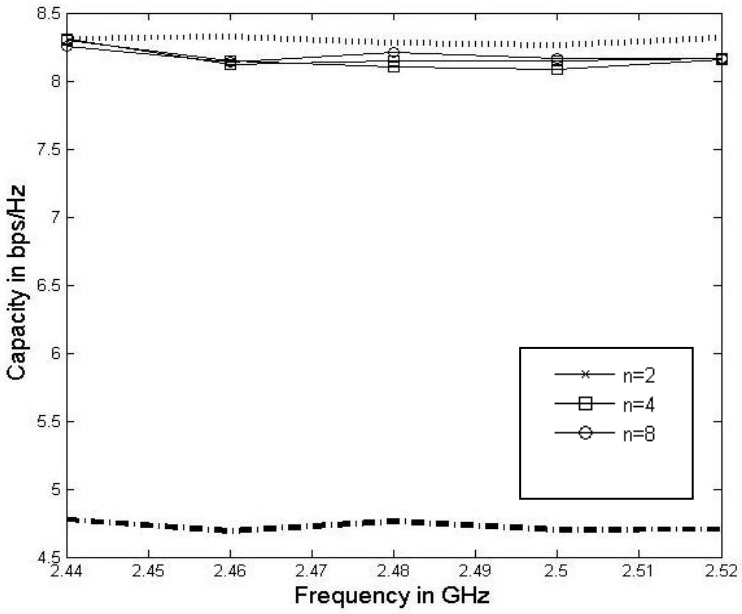

Figure 4.15: Variations of channel capacity versus operating frequency; subject to uniform PAS over 0 to 360° and n^{th} order raised cosine distribution power spectrum for mean zenith angle of 90°; ('.....' upper limit of 3 × 3 MIMO), ('------'upper limit of 3 × 1 MIMO).

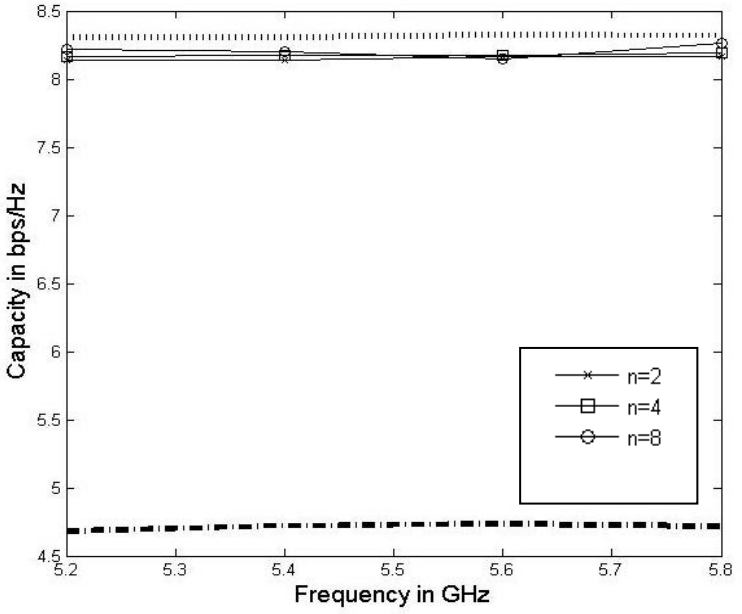

Figure 4.16: Variations of channel capacity versus operating frequency; subject to uniform PAS over 0 to 360° and n^{th} order raised cosine distribution power spectrum for mean zenith angle of 90°; ('.....' upper limit of 3 × 3 MIMO), ('------'upper limit of 3 × 1 MIMO).

Figures 4.17 to 4.26 follow the Gaussian power azimuth spectra (PAS) over 0° to 360° in combination with uniform, raised cosine and n^{th} order raised cosine distributions along the zenith angle. Sample calculations of channel capacities for different values of mean and variance have been evaluated and discussed.

Figures 4.17 and 4.18 correspond to Gaussian PAS and uniform distributions along the azimuth. These results have been calculated by keeping the mean of 45° constant for the Gaussian PAS and a mean of 90° for the Uniform distribution along the zenith, and varying the variance for Gaussian PAS, for both required frequency bands. It can be noticed that there was a linear relationship between the variances and the channel capacities are obtained. Maximum channel capacities of 8.1bps/Hz and 8 bps/Hz are observed at 2.5 GHz and 5.2GHz for 30° variance. Similarly, the minimum channel capacities of 6.5bps/Hz and 7.4bps/Hz are observed at 2.5 GHz and 5.2GHz for 5° variance.

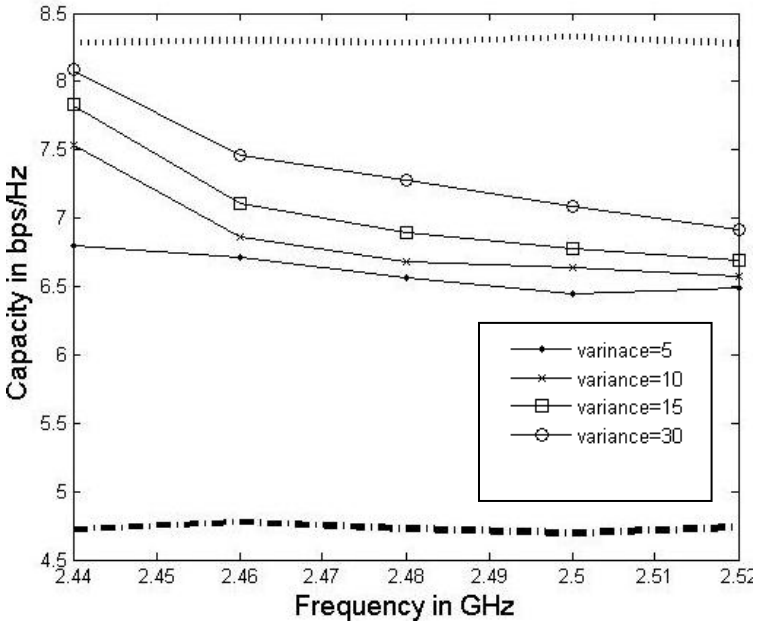

Figure 4.17: Variations of channel capacity versus operating frequency; subject to Gaussian PAS over 0 to 360° with mean 45° and different variances, and uniform power spectrum over ±15° for mean zenith angle of 90°; ('.....' upper limit of 3 × 3 MIMO), ('-----'upper limit of 3 × 1 MIMO).

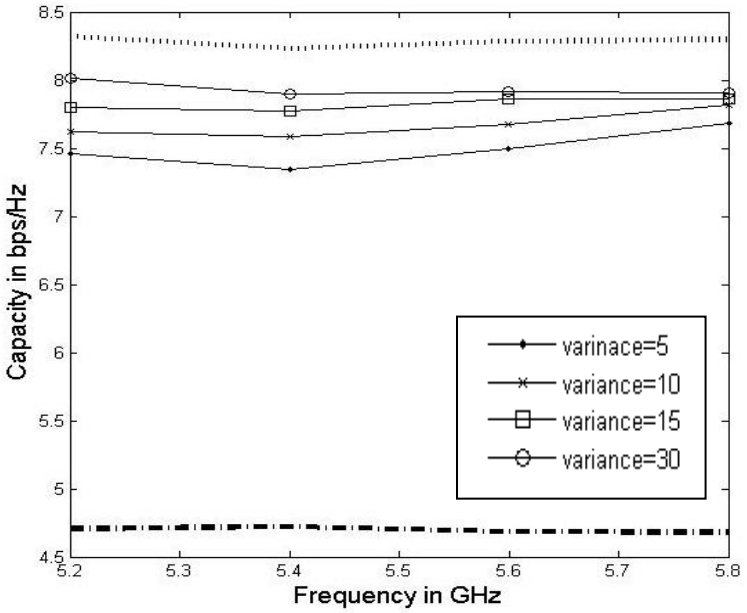

Figure 4.18: Variations of channel capacity versus operating frequency; subject to Gaussian PAS over 0 to 360° with mean 45° and different variances, and uniform power spectrum over ±15° for mean zenith angle of 90°; ('.....' upper limit of 3 × 3 MIMO), ('-----'upper limit of 3 × 1 MIMO).

If the mean and variance are kept constant (say 45° and 30°) for the Gaussian PAS and the mean of the uniform power spectrum is varied along the zenith angle at the WLAN frequencies, the corresponding channel capacities are given by Figures 4.19 and 4.20. The maximum (calculated) capacity at 2.5GHz is 8 bps/Hz (for mean 90°), the minimum capacity is 7 bps/Hz (for mean 10°). Similarly, at 5.2GHz the maximum capacity is 8 bps/Hz (for mean 70°) and the minimum capacity is 7.5 bps/Hz (for mean 90°). The maximum range of capacity variations of 0.9bps/Hz and 0.5bps/Hz were found at 2.5 GHz and 5.2 GHz respectively.

The channel capacity results shown in Figures 4.20 to 4.22 have been calculated from the Gaussian PAS and raised cosine distributions along zenith angle. Different values of variance have been used, with the means of 45° and 30° along azimuth at 2.5 GHz and 5.2GHz bands. Channel capacity variations of 1bps/Hz and 0.6bps/Hz have been seen within the band of 2.5GHz at the mean of 45° and 30° along azimuth, respectively; whereas in case of 5.2 GHz, the variations was around 0.2bps/Hz have been observed for different selected values of means and variances.

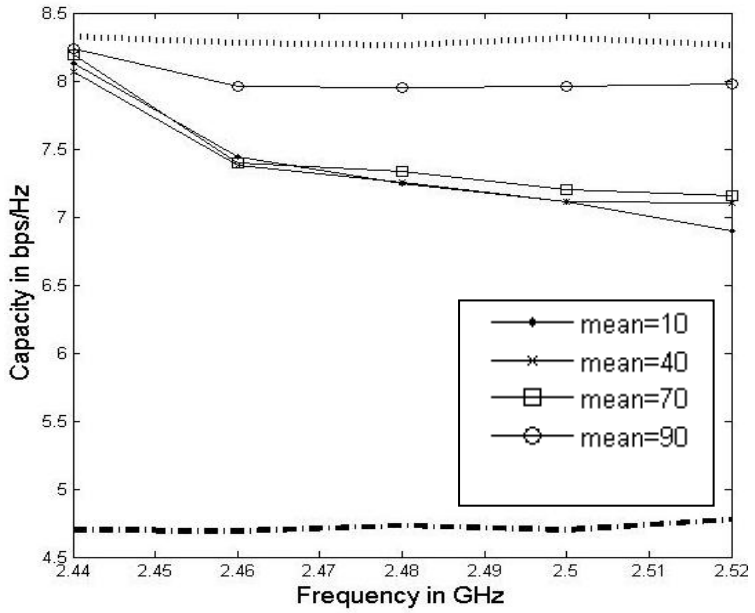

Figure 4.19: Variations of channel capacity versus operating frequency; subject to Gaussian PAS over 0 to 360° with mean 45° and uniform power spectrum over ±15° for various mean zenith angles of 10°, 40°, 70° and 90°; ('.....' upper limit of 3 × 3 MIMO), ('------'upper limit of 3 × 1 MIMO).

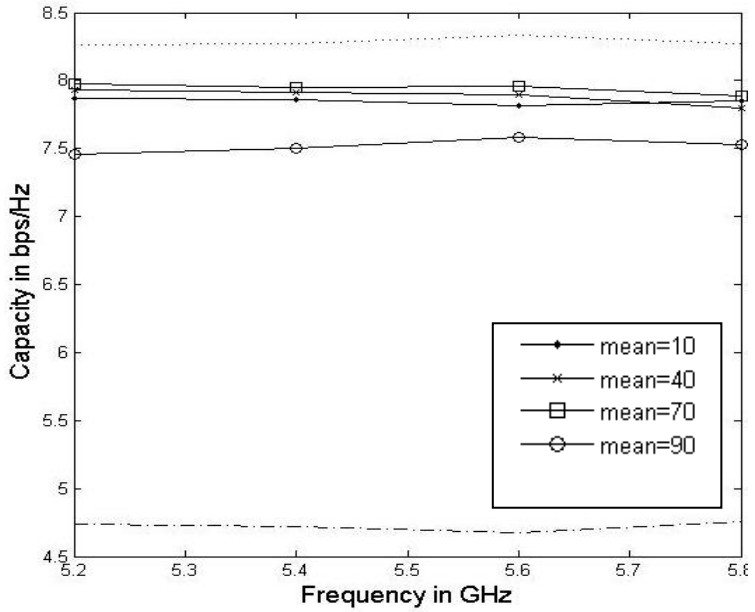

Figure 4.20: Variations of channel capacity versus operating frequency; subject to Gaussian PAS over 0 to 360° with mean 45° and uniform power spectrum over ±15° for various mean zenith angles of 10°, 40°, 70° and 90°; ('.....' upper limit of 3 × 3 MIMO), ('------'upper limit of 3 × 1 MIMO).

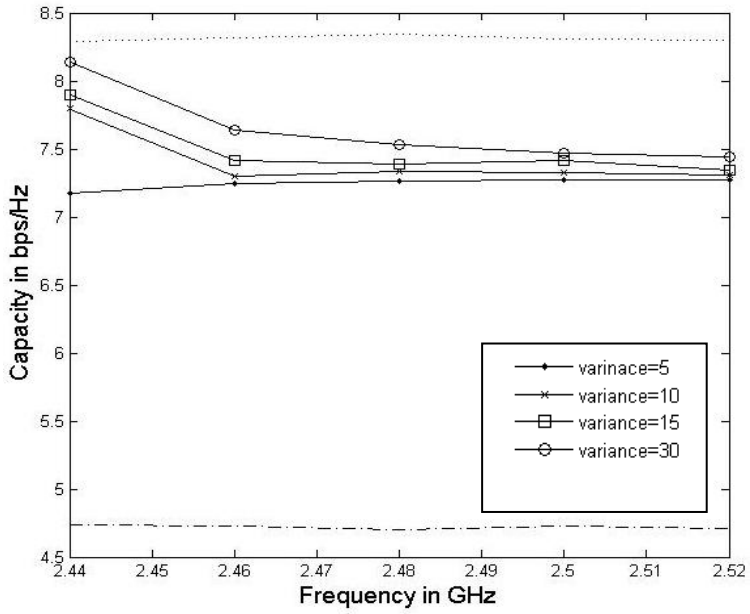

Figure 4.21: Variations of channel capacity versus operating frequency; subject to Gaussian PAS over 0 to 360° with mean 45° and different variances, and raised cosine distribution power spectrum with mean of 90°; ('.....' upper limit of 3 × 3 MIMO), ('-----'upper limit of 3 × 1 MIMO).

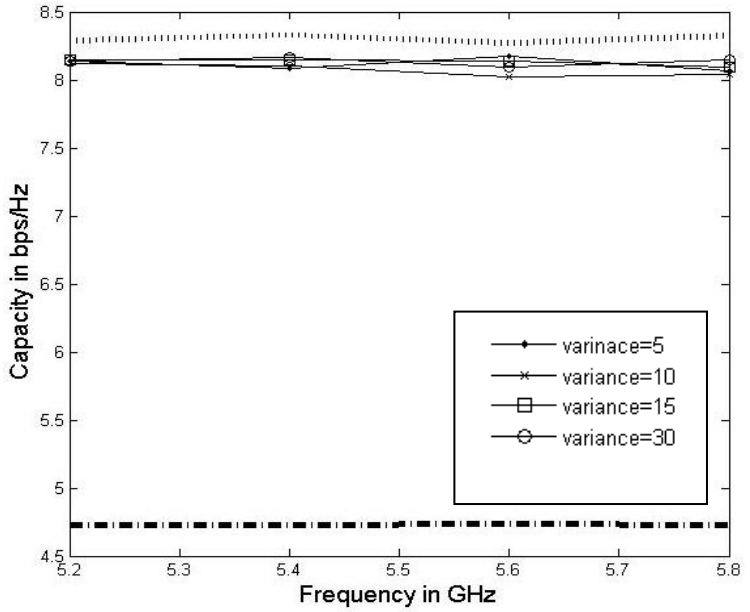

Figure 4.22: Variations of channel capacity versus operating frequency; subject to Gaussian PAS over 0 to 360° with mean 45° and different variances, and raised cosine distribution power spectrum with mean of 90°; ('.....' upper limit of 3 × 3 MIMO), ('-----'upper limit of 3 × 1 MIMO).

Moreover, the channel capacity using 2^{nd} and 4^{th} order raised cosine distributions along zenith angle including Gaussian power azimuth spectrum over 0 to 360° for mean 45°, has been elaborated in Figures 4.23 to 4.26.

Figure 4.23 shows the variation of channel capacity against operating frequency of 2.5 GHz, the maximum capacity of 8.1bps/Hz varying to 7.4 bps/Hz has been observed for the variance of 30°. The channel capacity was nearly constant at 7.1 bps/Hz over the bandwidth of interest for a variance of 5°. A similar pattern of channel capacity has occurred for the 4^{th} order raised cosine distribution along zenith angle with the maximum value of 7.9 bps/Hz, whereas the minimum value achieved was 6.9 bps/Hz. The results for both 2^{nd} and 4^{th} order raised cosine distribution are approximately similar with the slight difference of 0.1bps/Hz.

In case of channel capacity for the band of 5.2 GHz, both 2^{nd} and 4^{th} order raised cosine distributions were showing a similar pattern, with small channel variations over the operating frequency band. The maximum variations of the channel capacities for 2^{nd} and 4^{th} order distributions are 0.5bps/Hz and 0.3bps/Hz respectively. The maximum capacity for both cases were approximately around 8.1 bps/Hz.

It can also be noted from Figures 4.23 that the maximum calculated channel capcity is inversely proportional to the order of the raised cosine distributions. This is completley opposite to the use of PAS Gaussian distribution in which the channel capacity is directly proportional to the spatial spectral variance.

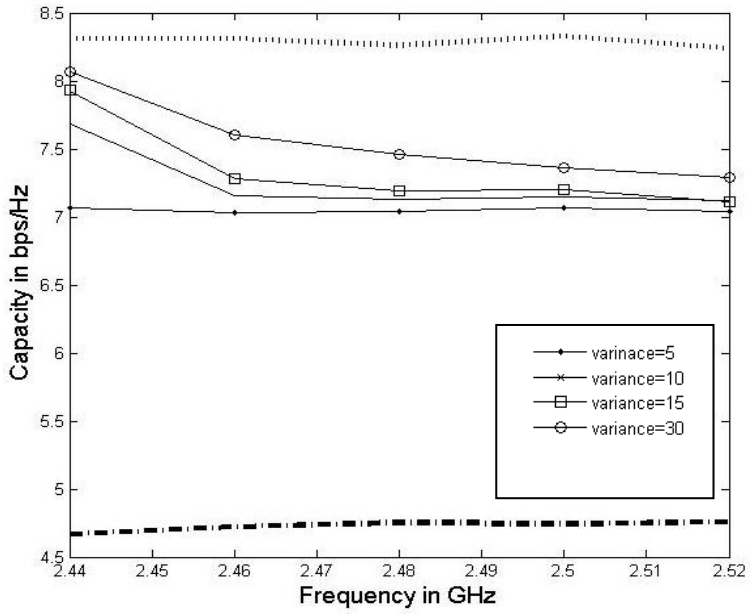

Figure 4.23: Variations of channel capacity versus operating frequency; subject to Gaussian PAS over 0 to 360° with mean 45° and different variances, and raised cosine distribution of 2nd order power spectrum with mean of 90°; ('.....' upper limit of 3 × 3 MIMO), ('------'upper limit of 3 × 1 MIMO).

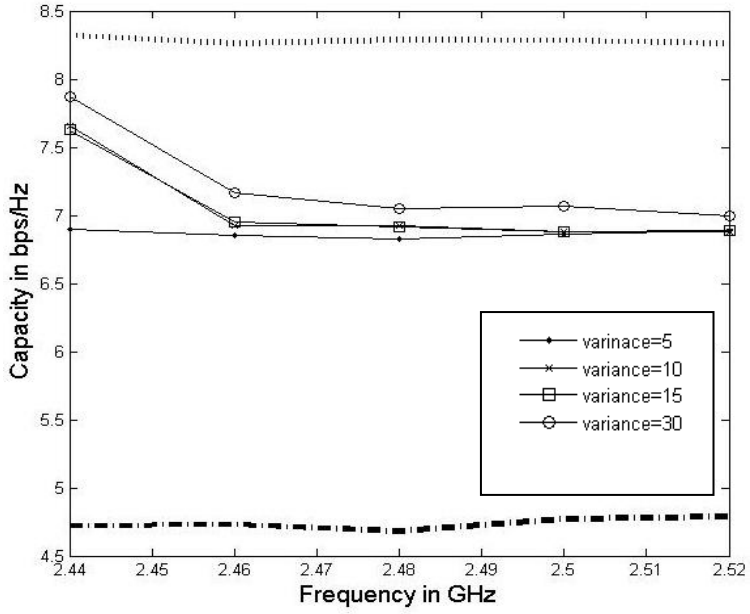

Figure 4.24: Variations of channel capacity versus operating frequency; subject to Gaussian PAS over 0 to 360° with mean 45° and different variances, and raised cosine distribution of 4th order power spectrum with mean of 90°; ('.....' upper limit of 3 × 3 MIMO), ('------'upper limit of 3 × 1 MIMO).

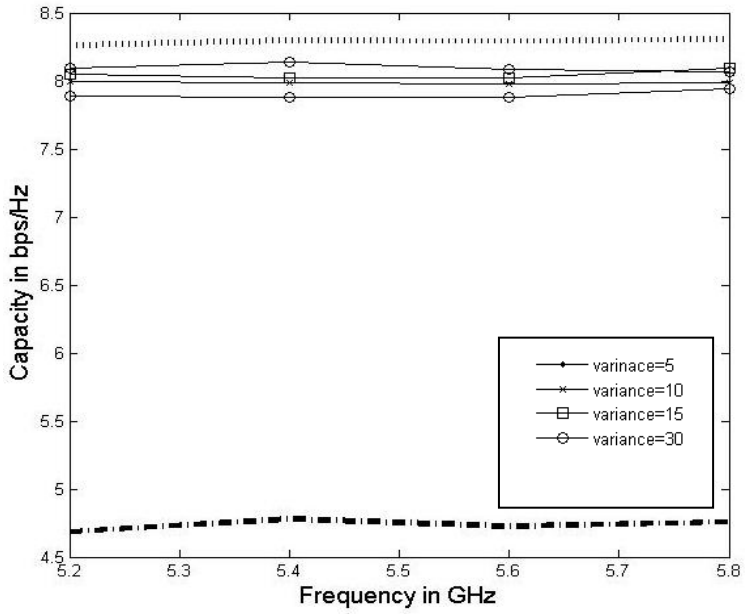

Figure 4.25: Variations of channel capacity versus operating frequency; subject to Gaussian PAS over 0 to 360° with mean 45° and different variances, and raised cosine distribution of 2nd order power spectrum with mean of 90°; ('.....' upper limit of 3 × 3 MIMO), ('------'upper limit of 3 × 1 MIMO).

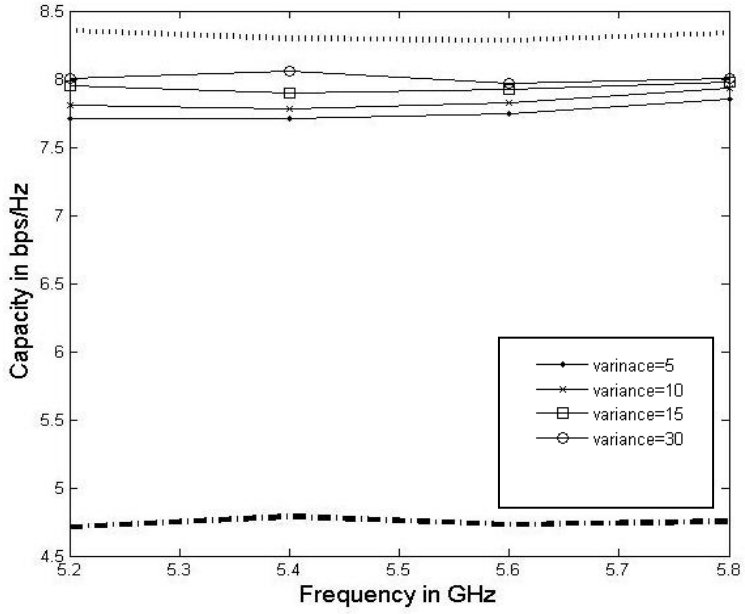

Figure 4.26: Variations of channel capacity versus operating frequency; subject to Gaussian PAS over 0 to 360° with mean 45° and different variances, and raised cosine distribution of 4th order power spectrum with mean of 90°; ('.....' upper limit of 3 × 3 MIMO), ('------'upper limit of 3 × 1 MIMO).

The set of Figures 4.27 to 4.36 correspond to a Laplacian PAS over 0° to 360° with different mean and variance in combination with uniform, raised cosine and n^{th} order raised cosine distributions along the zenith angle. The variations of the calculated channel capacity for these distributions are quite similar to the previous Gaussian PAS case.

Figure 4.27 represents the channel capacity over the 2.5 GHz band using a Laplacian PAS (mean 45°) with different variances, and a uniform distribution along the zenith with an angle of elevation of 30° (mean 90°). The maximum channel capacity of 8 bps/Hz can be observed at a variance of 30°, whereas a minimum value of 7.3 bps/Hz for a mean of 5°. For each constant value of variance, the gradual decrease in channel capacity has been observed as the operating frequency increases. This is due to the influence of the coupling effects between the three radiating elements of the MIMO system considered at this particular frequency band. However, a maximum of 1.2 bps/Hz is not a substantial capacity degradation compared to overall system performance offered by 3×1 MIMO system.

.

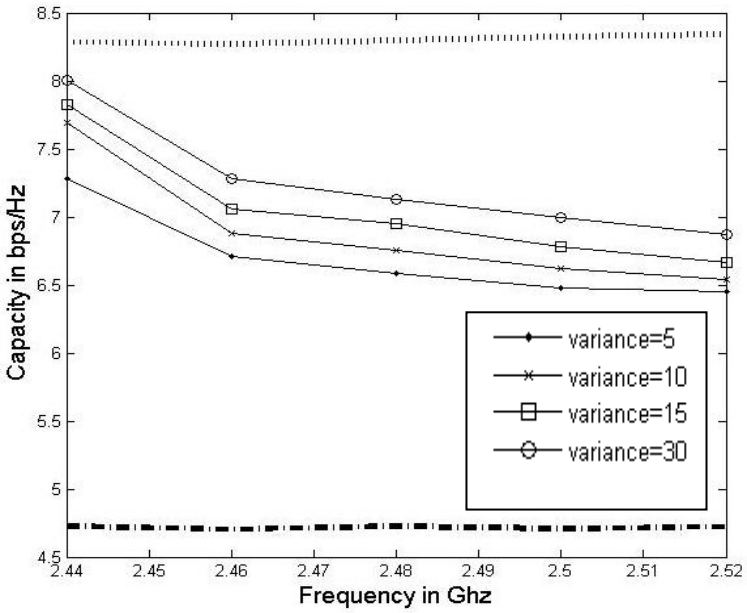

Figure 4.27: Variations of channel capacity versus operating frequency; subject to Laplacian PAS over 0 to 360° with mean 45° and different variances, and uniform power spectrum over ±15° for mean zenith angles of 90°; ('.....' upper limit of 3 × 3 MIMO), ('------'upper limit of 3 × 1 MIMO).

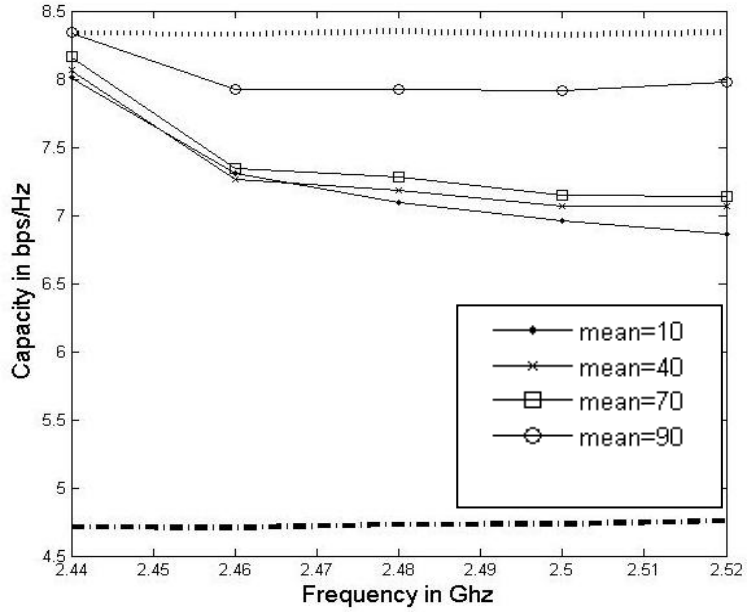

Figure 4.28: Variations of channel capacity versus operating frequency; subject to Laplacian PAS over 0 to 360° with mean 45° and variance 30°; and uniform power spectrum over ±15° for various mean zenith angles of 10°, 40°, 70° and 90°; ('.....' upper limit of 3 × 3 MIMO), ('------'upper limit of 3 × 1 MIMO).

Similarly in Figure 4.28 the channel capacity has been plotted by keeping the mean at 45° with variance at 30° unchanged for Laplacian PAS and varying the mean of the uniform power spectrum distribution in the elevation angle. The maximum and minimum capacity values of 8.2 bps/Hz and 7.4 bps/Hz were observed at mean of 90° and 10° elevations angle respectively.

The same criterion has been used to investigate the channel capacity for the 5.2 GHz band. A maximum capacity of 8 bps/Hz and minimum of 7.45bps/Hz have been observed for variances of 30°, and 10° elevation angle distributions respectively, as shown in Figure 4.31. Moreover, from Figure 4.30 the maximum and minimum capacity values of 7.9bps/Hz and 7.45 bps/Hz were obtained at mean values of 90° and 10° when uniform distribution along zenith was considered.

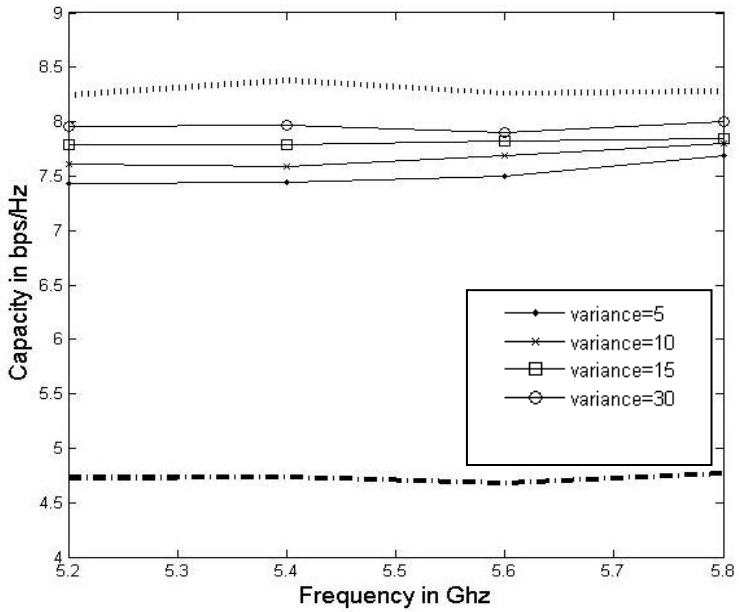

Figure 4.29: Variations of channel capacity versus operating frequency; subject to Laplacian PAS over 0 to 360° with mean 45° and different variances, and uniform power spectrum over ±15° for mean zenith angle of 90°; ('.....' upper limit of 3 × 3 MIMO), ('------'upper limit of 3 × 1 MIMO).

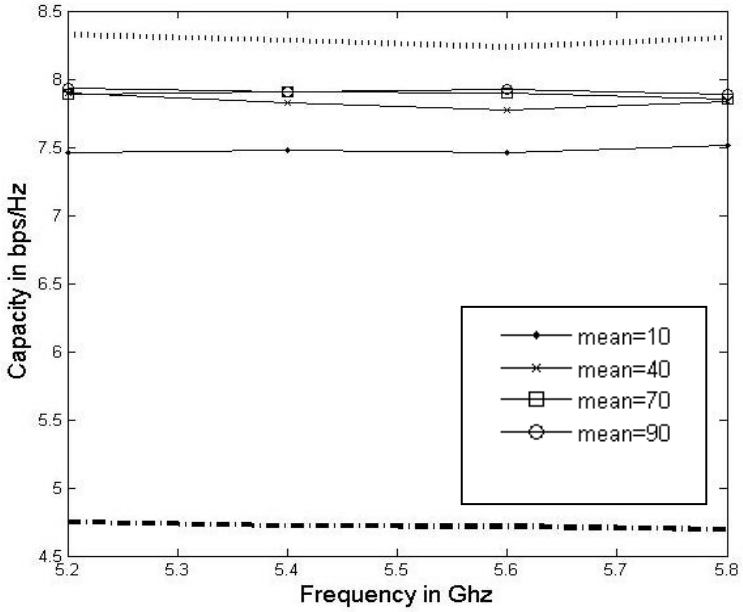

Figure 4.30: Variations of channel capacity versus operating frequency; subject to Laplacian PAS over 0 to 360° with mean 45° and variance 30°; and uniform power spectrum over ±15° for various mean zenith angles of 10°, 40°, 70° and 90°; ('.....' upper limit of 3 × 3 MIMO), ('------'upper limit of 3 × 1 MIMO).

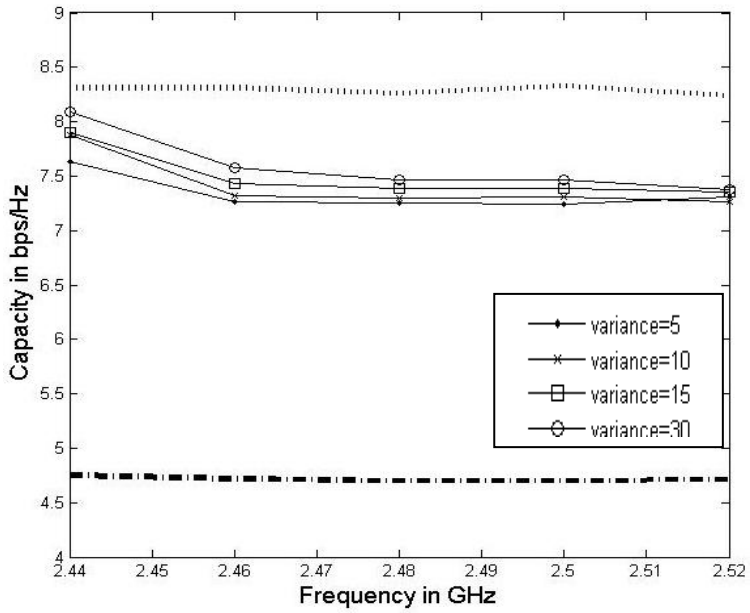

Figure 4.31: Variations of channel capacity versus operating frequency; subject to Laplacian PAS over 0 to 360° with mean 30° and different variances, and raised cosine distribution power spectrum with mean of 90°; ('.....' upper limit of 3× 3 MIMO), ('-----'upper limit of 3 × 1 MIMO).

In Figures 4.29 to 4.36 the channel capacity of 3×3 MIMO system has been investigated for the Laplacian PAS and raised cosine of n^{th} order distributions along the zenith angle. The results presented in these sets of figures are approximately similar to the previous case in which the calculated capacity ranged between 8.2 bps/Hz and 7.4 bps/Hz. The maximum variations of 1.0 bps/Hz can be clearly noted from Figures 4.373 and 4.34.

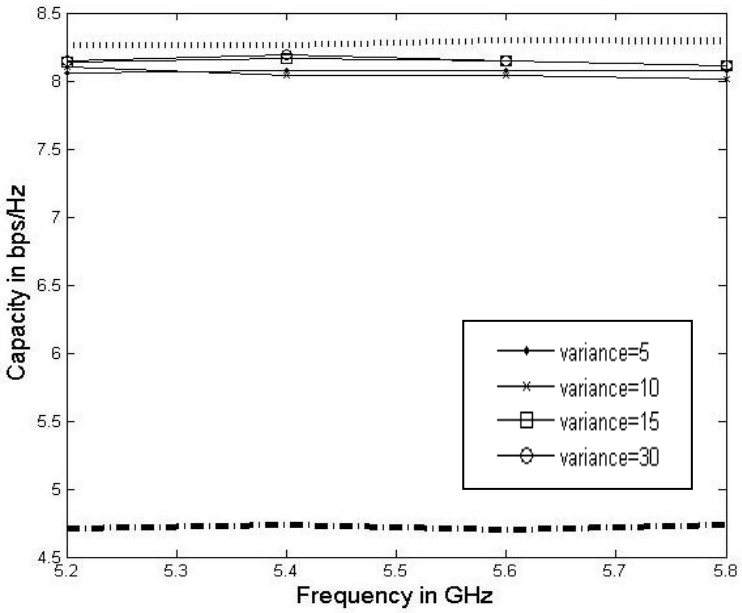

Figure 4.32: Variations of channel capacity versus operating frequency; subject to Laplacian PAS over 0 to 360° with mean 30° and different variances, and raised cosine distribution power spectrum with mean of 90°; ('.....' upper limit of 3× 3 MIMO), ('-----'upper limit of 3 × 1 MIMO).

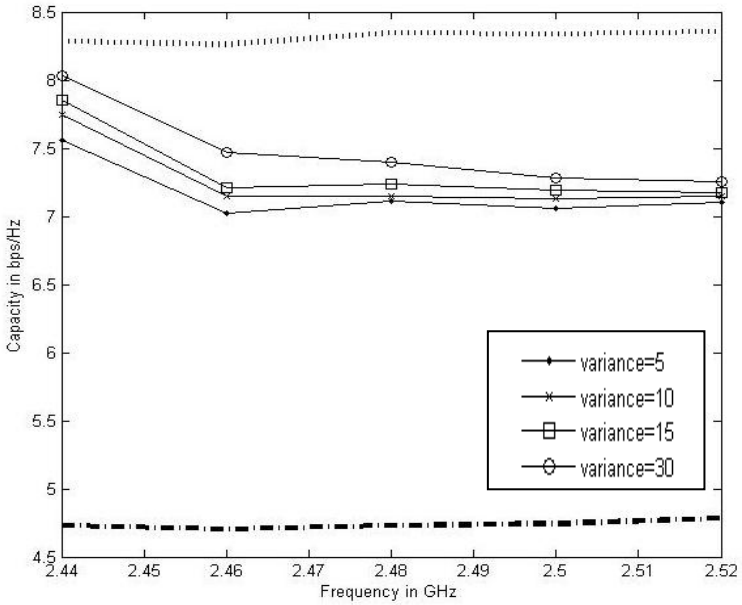

Figure 4.33: Variations of channel capacity versus operating frequency; subject to Laplacian PAS over 0 to 360° with mean 45° and different variances; and raised cosine distribution of 2nd order power spectrum with mean of 90°; ('.....' upper limit of 3 × 3 MIMO), ('------' upper limit of 3 × 1 MIMO).

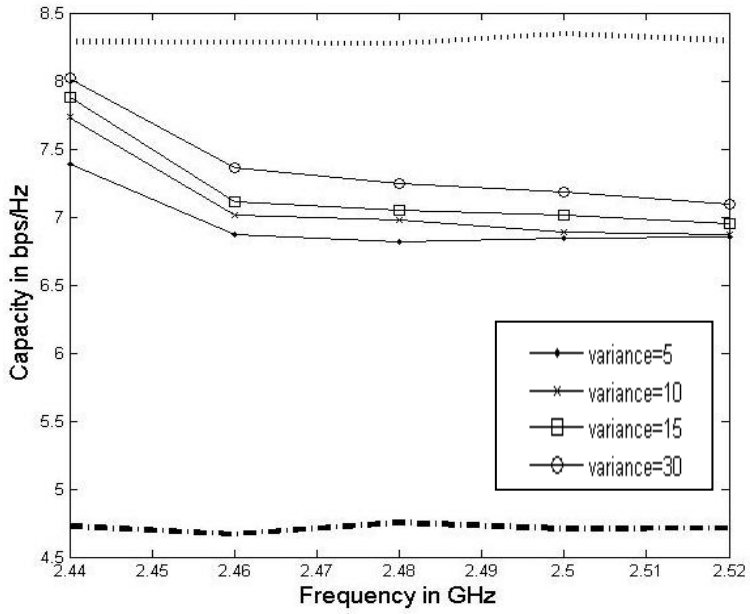

Figure 4.34: Variations of channel capacity versus operating frequency; subject to Laplacian PAS over 0 to 360° with mean 45° and different variances; and raised cosine distribution of 4th order power spectrum with mean of 90°; ('.....' upper limit of 3 × 3 MIMO), ('------' upper limit of 3 × 1 MIMO).

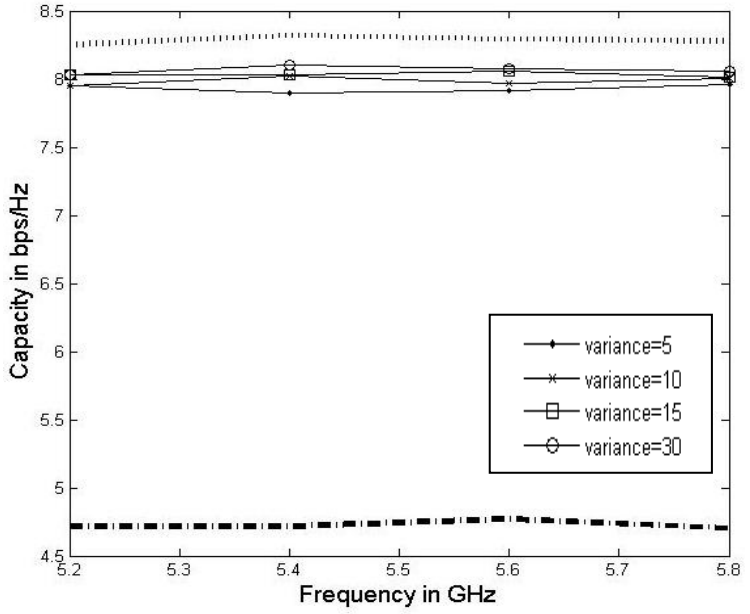

Figure 4.35: Variations of channel capacity versus operating frequency; subject to Laplacian PAS over 0 to 360° with mean 45° and different variances; and raised cosine distribution of 2nd order power spectrum with mean of 90°; ('.....' upper limit of 3 × 3 MIMO), ('------' upper limit of 3 × 1 MIMO).

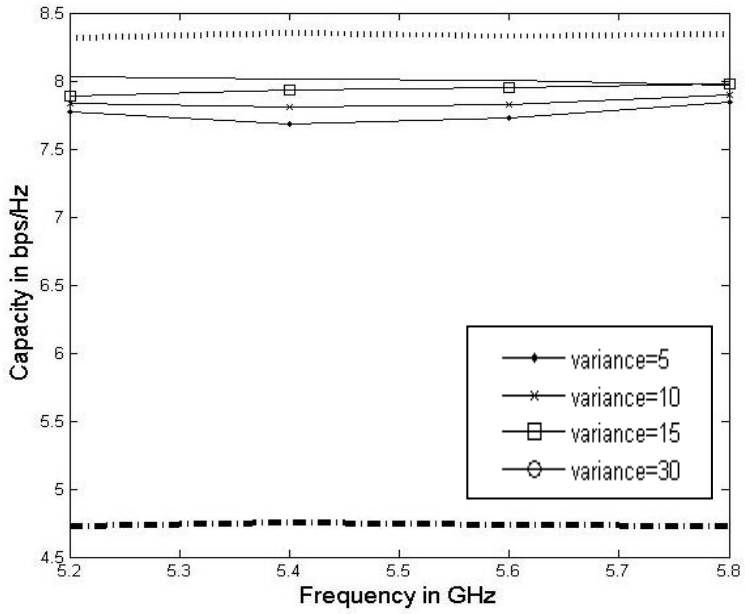

Figure 4.36: Variations of channel capacity versus operating frequency; subject to Laplacian PAS over 0 to 360° with mean 45° and different variances; and raised cosine distribution of 4th order power spectrum with mean of 90°; ('.....' upper limit of 3 × 3 MIMO), ('------' upper limit of 3 × 1 MIMO).

In Figure 4.37the channel capacity is plotted around 2.5 GHz band applying the secant-squared PAS over 0 to 360° (mean 45°) with different values of variance in combination with uniform power spectrum distribution over ±15° of the zenith angle (mean 90°). All the plotted results at different variances indicate the same pattern with minimum capacity variations of 0.2 bps/Hz.

The channel capacity is plotted Figure 4.38 for same frequency band for a mean of 45° and variance of 30° along the azimuth. Then, the capacity was computed for different mean values of uniform distribution along the zenith angle. The maximum capacities of 8.25 bps/Hz and 8.1 bps/Hz can be observed (mean 40° and 90° respectively). Almost negligible differences appeared over the operating frequency band.

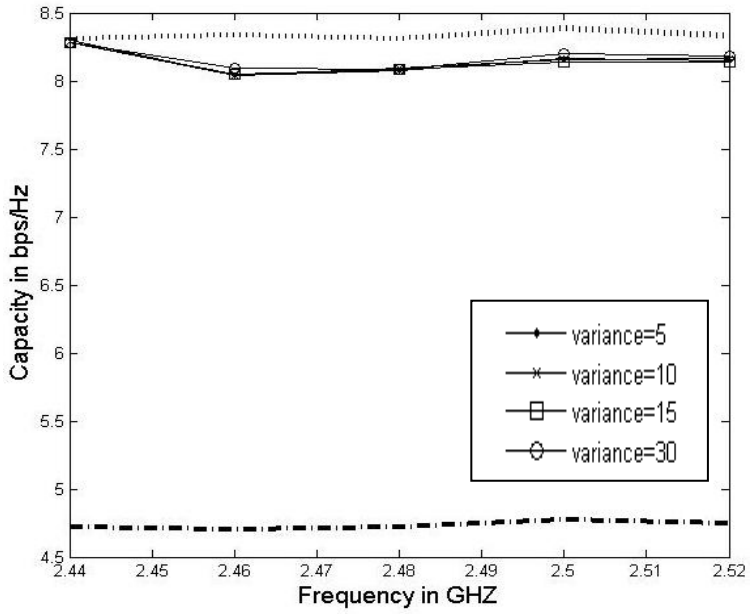

Figure 4.37: Variations of channel capacity versus operating frequency; subject to Secant Square PAS over 0 to 360° with mean 45° and different variances, and uniform power spectrum over ±15° for mean zenith angle of 90°; ('.....' upper limit of 3 × 3 MIMO), ('------'upper limit of 3 × 1 MIMO).

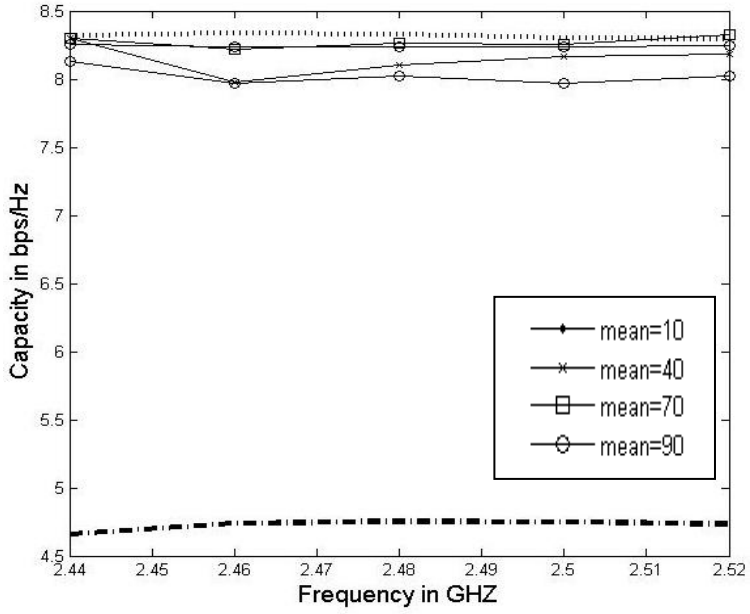

Figure 4.38: Variations of channel capacity versus operating frequency; subject to Secant Square PAS over 0 to 360° with mean 45° and uniform power spectrum over ±15° for various mean zenith angles of 10°, 40°, 70° and 90°; ('.....' upper limit of 3 × 3 MIMO), ('------'upper limit of 3 × 1 MIMO).

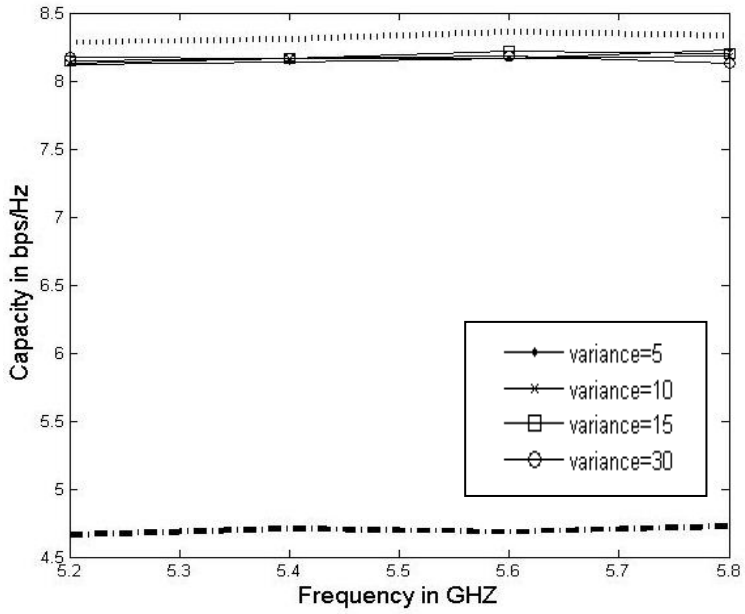

Figure 4.39: Variations of channel capacity versus operating frequency; subject to Secant Square PAS over 0 to 360° with mean 45° and different variances, and uniform power spectrum over ±15° for mean zenith angle of 90°; ('.....' upper limit of 3 × 3 MIMO), ('------'upper limit of 3 × 1 MIMO).

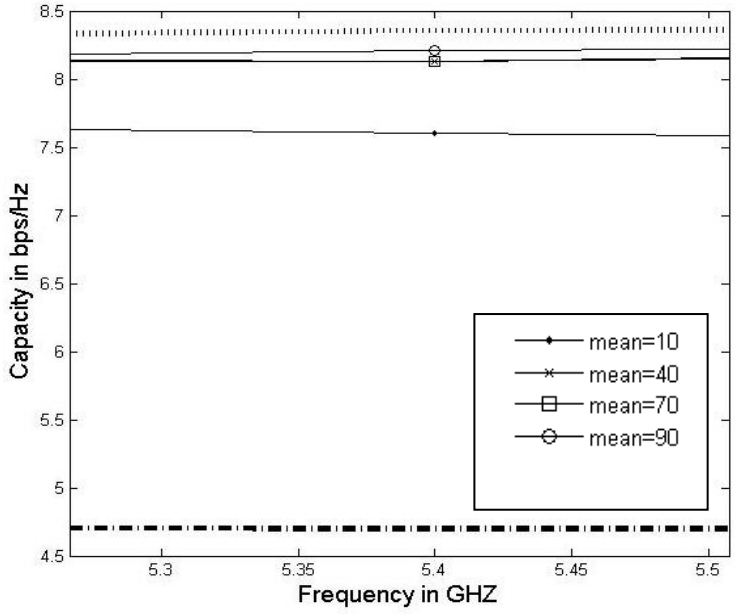

Figure 4.40: Variations of channel capacity versus operating frequency; subject to Secant Square PAS over 0 to 360° with mean 45° and uniform power spectrum over ±15° for various mean zenith angles of 10°, 40°, 70° and 90°; ('.....' upper limit of 3 × 3 MIMO), ('------'upper limit of 3 × 1 MIMO).

Figures 4.41 and 4.42 summarize the response of the channel capacities over the operating frequency bands when secant-squared PAS (over 0 to 360°), with mean 45° used in combination with raised cosine distribution (mean 90°) along zenith angle. Maximum channel capacity variations of 0.3 bps/Hz and 0.1 bps/Hz have been observed over the 2.5 GHz and 5.2GHz frequency bands respectively. In Figure 4.41 the maximum capacity is approximately 8.2 bps/Hz. A maximum capacity of 8.2 bps/Hz was achieved at 5.2 GHz frequency band, as shown in Figures 4.42.

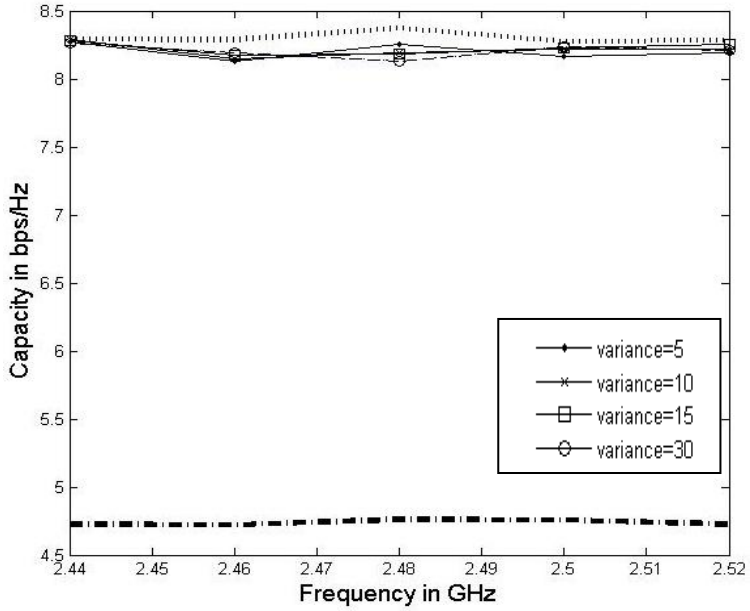

Figure 4.41: Variations of channel capacity versus operating frequency; subject to Secant Square PAS over 0 to 360° with mean 45° and different variances, and raised cosine distribution power spectrum with mean of 90°; ('.....' upper limit of 3 × 3 MIMO), ('------'upper limit of 3 × 1 MIMO).

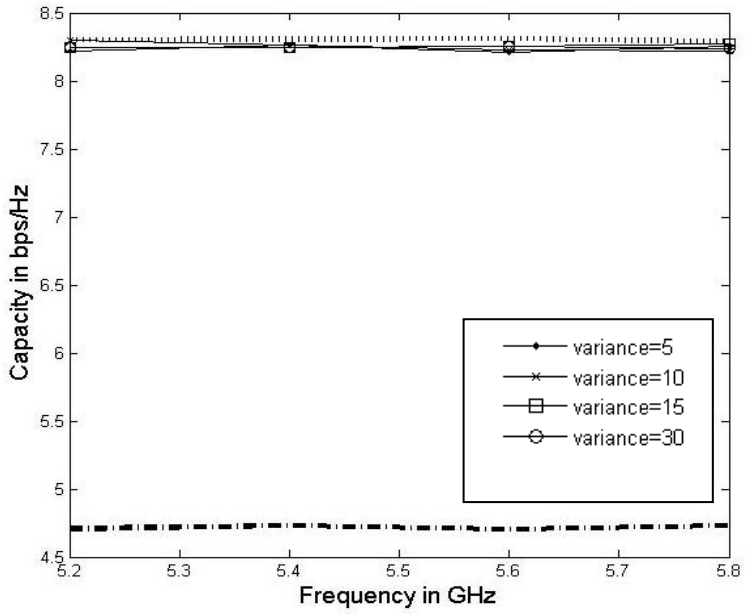

Figure 4.42: Variations of channel capacity versus operating frequency; subject to Secant Square PAS over 0 to 360° with mean 45° and different variances, and raised cosine distribution power spectrum with mean of 90°; ('.....' upper limit of 3 × 3 MIMO), ('------'upper limit of 3 × 1 MIMO).

Figures 4.43 to 4.46 show the calculated channel capacity for N^{th} order raised cosine distribution along zenith angle and secant-squared PAS over 0 to 360°.

In Figure 4.43, the 2^{nd} order raised cosine distribution has been used in combination with secant square PAS, with a mean of 45° and different values of variances. Very small variations of 0.1 bps/Hz channel capacity are observed for the different values of variances. The maximum value of 8.25bps/Hz has been obtained for the 2.5GHz frequency band.

Similarly using the 4^{th} order raised cosine distribution along the zenith angle and keeping the secant PAS parameters unchanged, the observed capacity variations are shown in Figure 4.44.

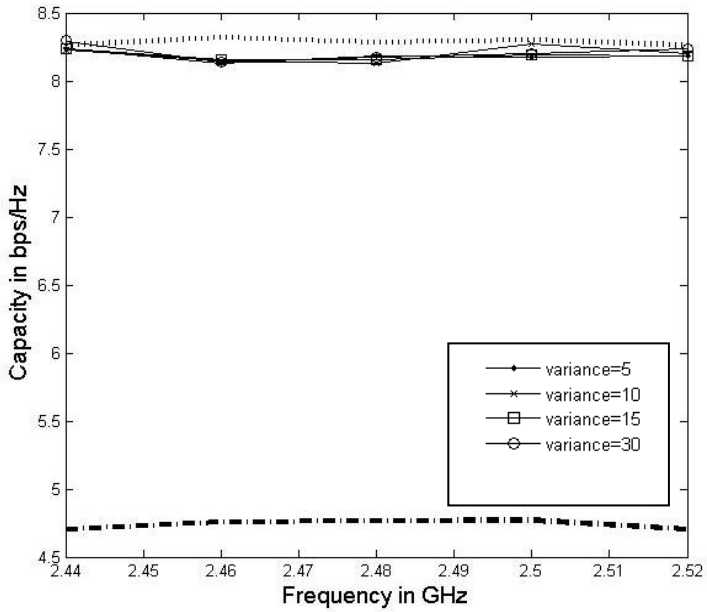

Figure 4.43: Variations of channel capacity versus operating frequency; subject to Secant Square PAS over 0 to 360° with mean 45° and different variances; and raised cosine distribution of 2nd order power spectrum with mean of 90°; ('.....' upper limit of 3 × 3 MIMO), ('------'upper limit of 3 × 1 MIMO).

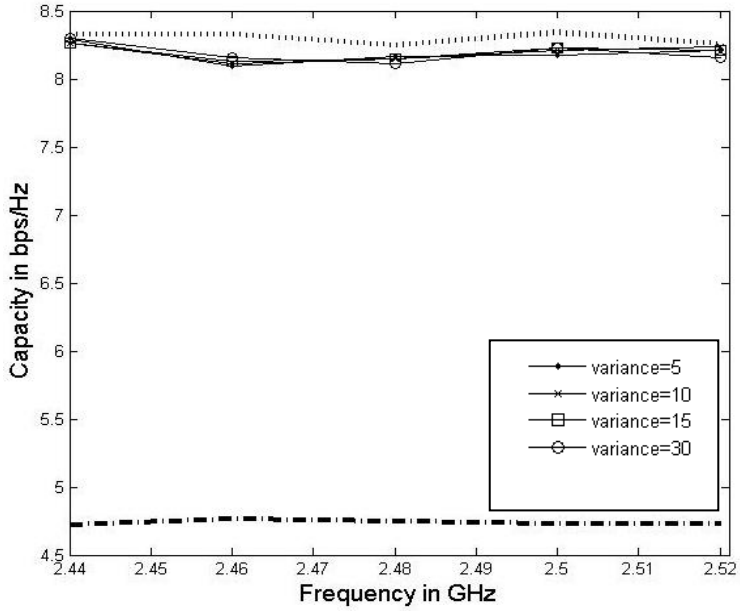

Figure 4.44: Variations of channel capacity versus operating frequency; subject to Secant Square PAS over 0 to 360° with mean 45° and different variances; and raised cosine distribution of 4th order power spectrum with mean of 90°; ('.....' upper limit of 3 × 3 MIMO), ('------'upper limit of 3 × 1 MIMO).

Figures 4.45 and 4.46 are showing the channel capacity for the 5.2GHz frequency band. These results have been plotted using the 2nd and 4th order raised cosine distribution along zenith and secant PAS. There is negligible variation in the capacity with variance. The maximum capacities are approximately 8.25 bps/Hz and 8.2 bps/Hz, as observed for 2nd and 4th orders respectively.

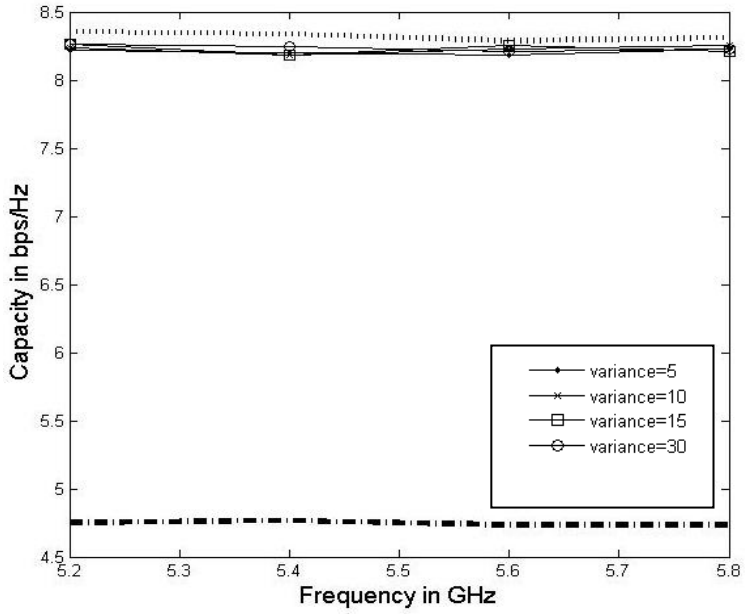

Figure 4.45: Variations of channel capacity versus operating frequency; subject to Secant Square PAS over 0 to 360° with mean 45° and different variances; and raised cosine distribution of 2nd order power spectrum with mean of 90°; ('.....' upper limit of 3 × 3 MIMO), ('------'upper limit of 3 × 1 MIMO).

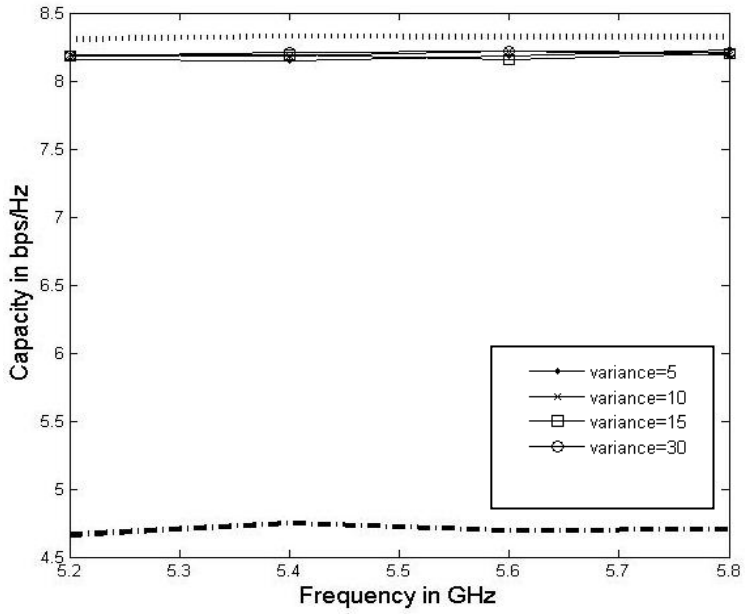

Figure 4.46: Variations of channel capacity versus operating frequency; subject to Secant Square PAS over 0 to 360° with mean 45° and different variances; and raised cosine distribution of 4th order power spectrum with mean of 90°; ('.....' upper limit of 3 × 3 MIMO), ('------'upper limit of 3 × 1 MIMO).

Thus far most of the presented results show the theoretical maximum values of the channel capacities of the 3×3 MIMO systems (shown in Figure 4.3) for the free space environment. The maximum capacity values approach the maximum limit, in other words, the capacity values were around 8.2 bps/Hz to 8.4 bps/Hz. It should be noted that the mean values of channel capacities for all cases studied are varied between 7.16 and 8.25 bps/Hz as summarized in Table 4.4. These results are very encouraging for real world implementations of this simple antenna geometry

Table 4.4: Summarised channel capacity of the antenna geometry shown in Fig 4.3.

Power Distributions		**Mean of Calculated Channel Capacity (Bps/Hz)**	
Azimuth	**Elevation**	**2.44 to 2.52 GHz**	**5.2 to 5.8 GHz**
Uniform	Uniform	8.15	7.75
Uniform	Raised Cosine	8.21	8.25
Uniform	n^{th} Order raised Cosine	8.13	8.23
Gaussian	Uniform	7.23	7.75
Gaussian	Raised Cosine	7.41	7.51
Gaussian	2^{nd} Order raised Cosine	7.32	8.05
Gaussian	4^{th} Order raised Cosine	7.24	7.85
Laplacian	Uniform	7.16	7.74
Laplacian	Raised Cosine	7.61	8.15
Laplacian	2^{nd} Order raised Cosine	7.27	7.91
Laplacian	4^{th} Order raised Cosine	7.32	7.81
Secant Square	Uniform	8.17	8.21
Secant Square	Raised Cosine	8.19	8.23
Secant Square	2^{nd} Order raised Cosine	8.2	8.23
Secant Square	4^{th} Order raised Cosine	8.19	8.2

4.4.2 Channel Capacity of 3×3 MIMO System with Hand Model

This section is concerned with the calculation of channel capacity for the 3×3 prototype module shown in Figure 4.4, in which a human hand model is coupled to the antenna module. The same criterion used in previous section was applied here, to compute the MIMO channel capacity.

The first part of the results, given in Figures 4.47 to 4.51, in which a uniform PAS over 0° to 360° with different means and variances are presented with combinations of uniform, raised cosine, and n^{th} order raised cosine distributions in zenith angle.

Comparison with Fig. 4.11 illustrates the effect of the hand around the handset on the forecast values of channel capacity, which appear to be slightly larger (around 0.7 bps/Hz). Similar results can also be seen for the 5.2GHz frequency band.

The lower capacity values have been recorded for 2.5 GHz compared to the those at 5.2 GHz as shown in Figure 4.48. The maximum capacity values of 8.2 bps/Hz and 7.6 bps/Hz have been observed for 90° and 10° means respectively.

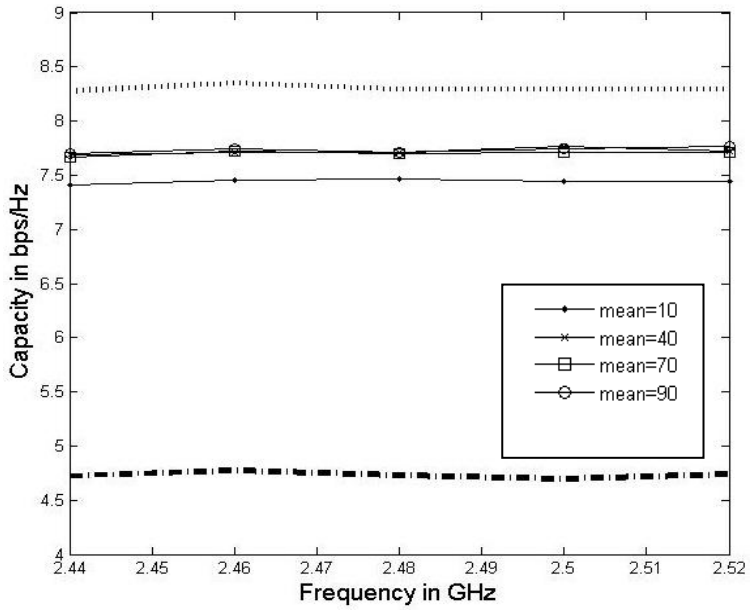

Figure 4.47: Variations of channel capacity versus operating frequency; subject to uniform PAS over 0 to 360° and uniform power spectrum over ±15° for various mean zenith angles of 10°, 40°, 70° and 90°; ('.....' upper limit of 3 × 3 MIMO), ('------'upper limit of 3 × 1 MIMO).

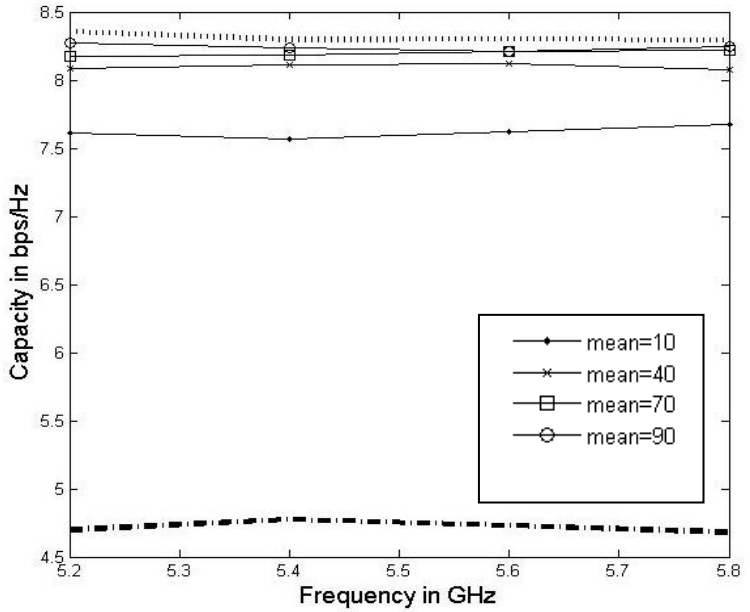

Figure 4.48: Variations of channel capacity versus operating frequency; subject to uniform PAS over 0 to 360° and uniform power spectrum over ±15° for various mean zenith angles of 10°, 40°, 70° and 90°; ('.....' upper limit of 3 × 3 MIMO), ('------'upper limit of 3 × 1 MIMO).

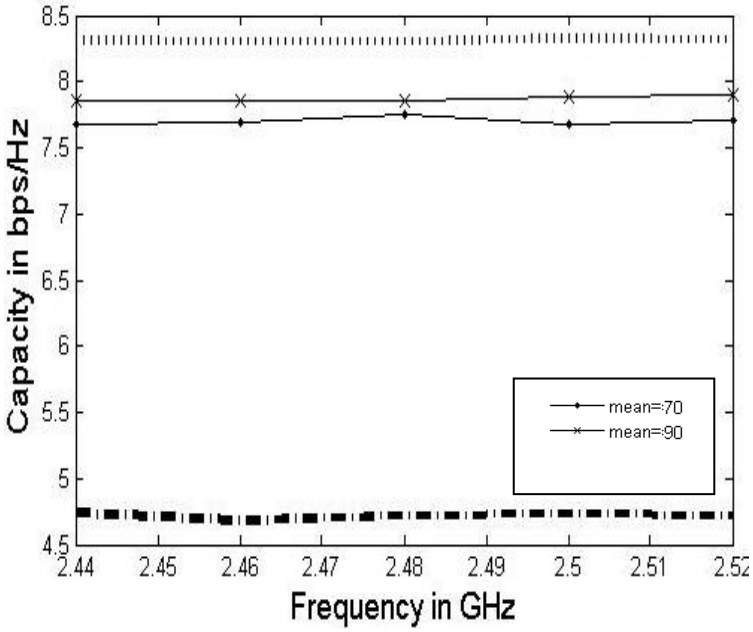

Figure 4.49: Variations of channel capacity versus operating frequency; subject to uniform PAS over 0 to 360° and raised cosine distribution power spectrum for various mean zenith angles of 70° and 90°; ('.....' upper limit of 3 × 3 MIMO), ('------'upper limit of 3 × 1 MIMO).

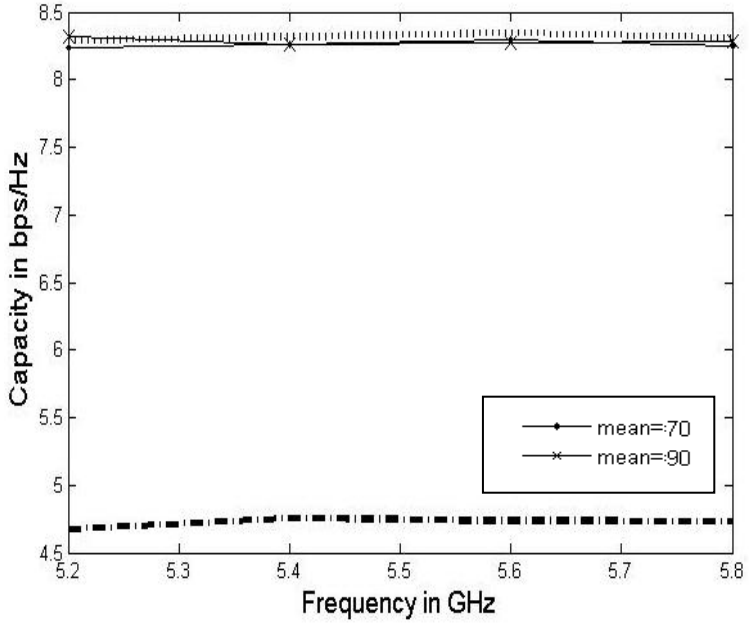

Figure 4.50: Variations of channel capacity versus operating frequency; subject to uniform PAS over 0 to 360° and raised cosine distribution power spectrum for various mean zenith angles of 70° and 90°; ('.....' upper limit of 3 × 3 MIMO), ('------'upper limit of 3 × 1 MIMO).

For the n^{th} order distribution along zenith angle, a maximum capacity of 7.7bps/Hz has been obtained at $n = 2$, which is 0.5 bps/Hz less than the one shown in Figure 4.15. In addition, the capacity values over the 5.2 GHz frequency band shown in Figure 4.52 are similar to one depicted in Figure 4.16 (i.e. without the hand model present), in which the maximum capacity was 8.2 bps/Hz.

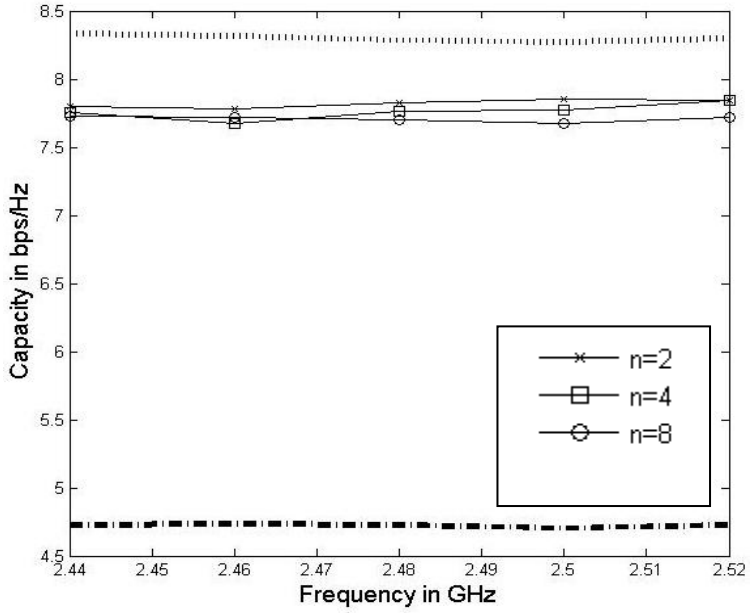

Figure 4.51: Variations of channel capacity versus operating frequency; subject to uniform PAS over 0 to 360° and n^{th} order raised cosine distribution power spectrum for mean zenith angle of 90°; ('.....' upper limit of 3 × 3 MIMO), ('------'upper limit of 3 × 1 MIMO).

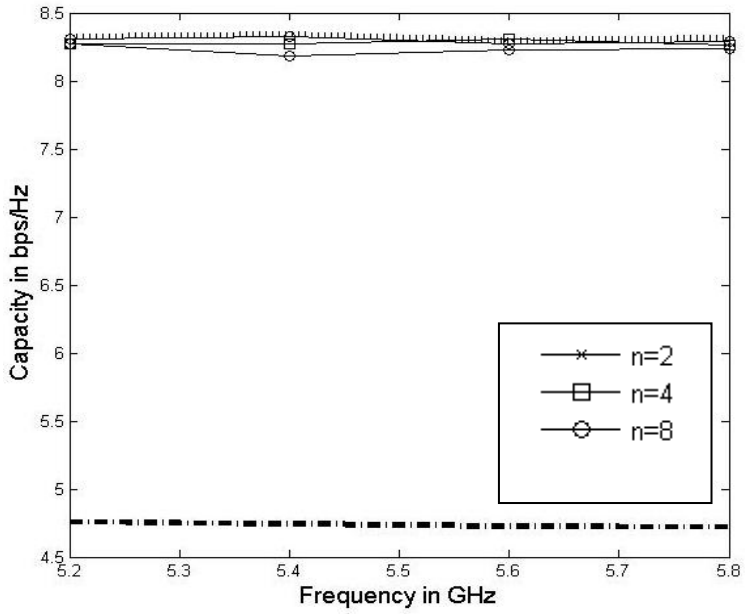

Figure 4.52: Variations of channel capacity versus operating frequency; subject to uniform PAS over 0 to 360° and n^{th} order raised cosine distribution power spectrum for mean zenith angle of 90°; ('.....' upper limit of 3 × 3 MIMO), ('------'upper limit of 3 × 1 MIMO).

Figures 4.53 to 4.56 report the channel capacities calculated by using a Gaussian PAS over 0 to 360° with mean of 45° and different variances in combination with a uniform power spectrum over ±15° and different values of mean along the zenith angle.

In Figure 4.53 the maximum value of 7.4 bps/Hz has been observed for a variance of 30°. The capacity was 0.6 bps/Hz lower than the value reported in Figure 4.17. For Figures 4.59 the maximum and minimum capacity values are 7.4 bps/Hz and 7.2bps/Hz, located around the means 10° and 90°, respectively. The maximum variation range is 0.2 bps/Hz observed over the full band.

Figures 4.55 and 4.56 show the channel capacity results for 5.2 GHz band. The maximum values of 8 bps/Hz and 7.9bps/Hz are located at the variances 30° and 10°, respectively.

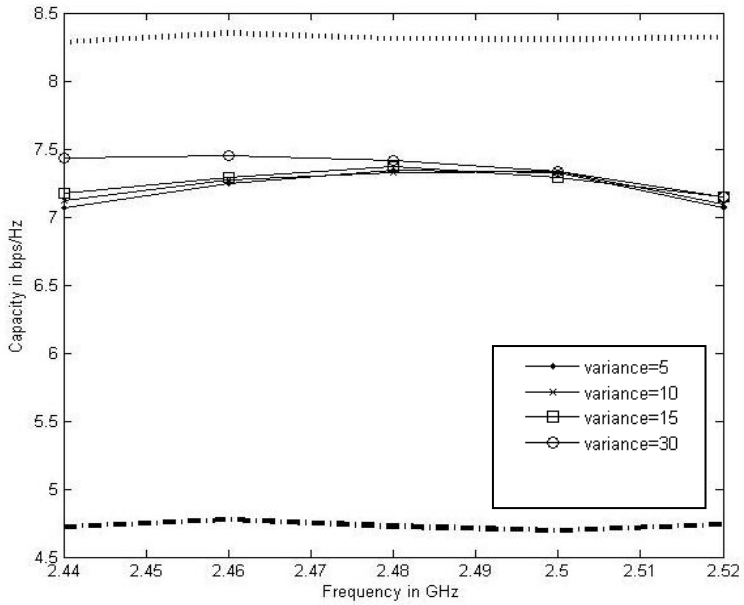

Figure 4.53: Variations of channel capacity versus operating frequency; subject to Gaussian PAS over 0 to 360° with mean 45° and different variances, and uniform power spectrum over ±15° for mean zenith angle of 90°; ('.....' upper limit of 3 × 3 MIMO), ('------'upper limit of 3 × 1 MIMO).

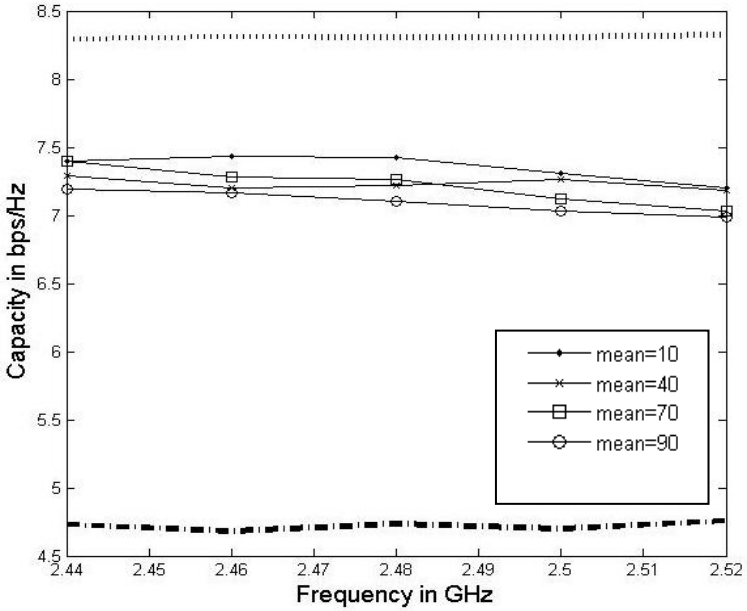

Figure 4.54: Variations of channel capacity versus operating frequency; subject to Gaussian PAS over 0 to 360° with mean 45° and uniform power spectrum over ±15° for various mean zenith angles of 10°, 40°, 70° and 90°; ('.....' upper limit of 3 × 3 MIMO), ('------'upper limit of 3 × 1 MIMO).

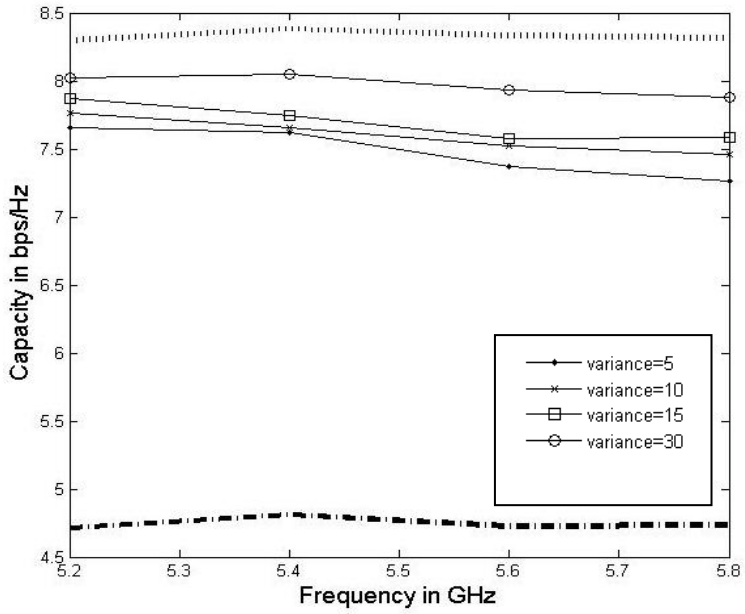

Figure 4.55: Variations of channel capacity versus operating frequency; subject to Gaussian PAS over 0 to 360° with mean 45° and different variances, and uniform power spectrum over ±15° for mean zenith angle of 90°; ('.....' upper limit of 3 × 3 MIMO), ('------'upper limit of 3 × 1 MIMO).

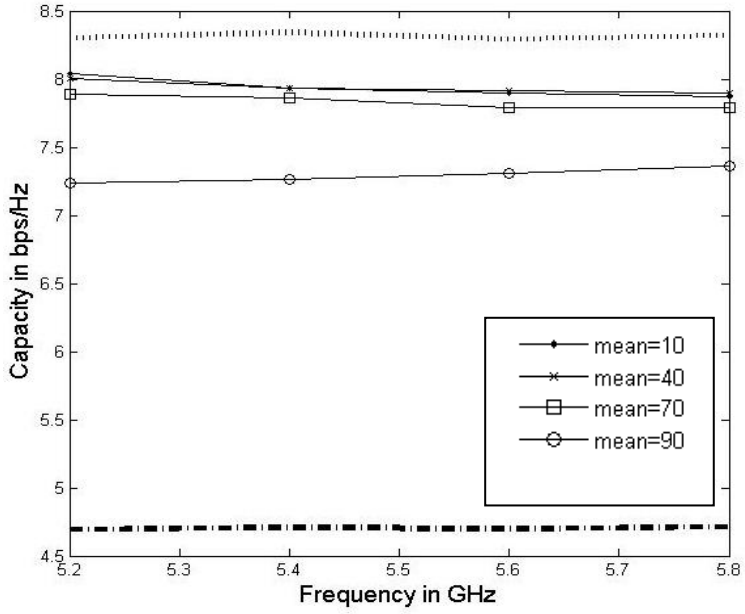

Figure 4.56: Variations of channel capacity versus operating frequency; subject to Gaussian PAS over 0 to 360° with mean 45° and uniform power spectrum over ±15° for various mean zenith angles of 10°, 40°, 70° and 90°; ('.....' upper limit of 3 × 3 MIMO), ('------'upper limit of 3 × 1 MIMO).

The channel capacity variation in Figure 4.57 is small, around 0.1 bps/Hz. This is based on a combination of Gaussian PAS with variance 45° with a raised cosine distribution applied along the zenith; the maximum capacity is 7.6bps/Hz. Further comparison with the results in figure 4.21 shows that the variations of channel capacity with the hand model were smaller than expected.

Consequently, in Figure 4.58 the channel capacity calculated in the neighbourhood of 5.2GHz band is found to have small variations around 0.1 bps/Hz, but the maximum value reaches 8.2 bps/Hz.

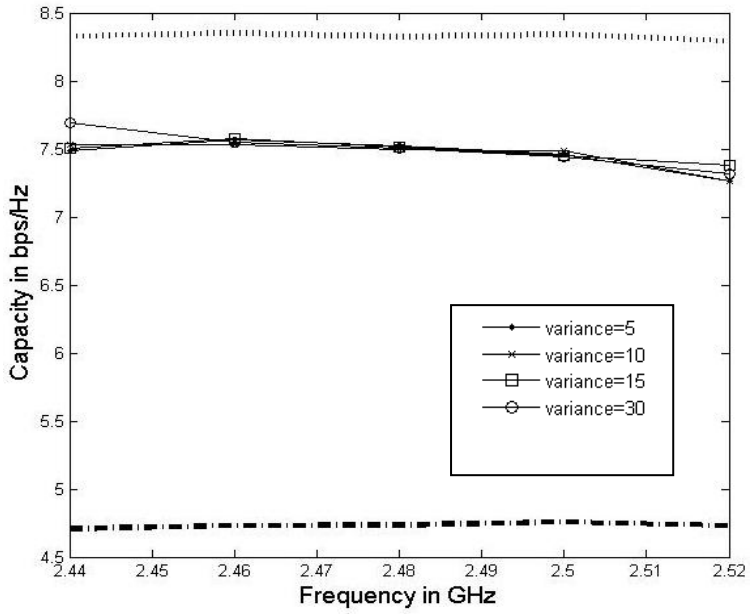

Figure 4.57: Variations of channel capacity versus operating frequency; subject to Gaussian PAS over 0 to 360° with mean 45° and different variances, and raised cosine distribution power spectrum with mean of 90°; ('.....' upper limit of 3 × 3 MIMO), ('-----'upper limit of 3 × 1 MIMO).

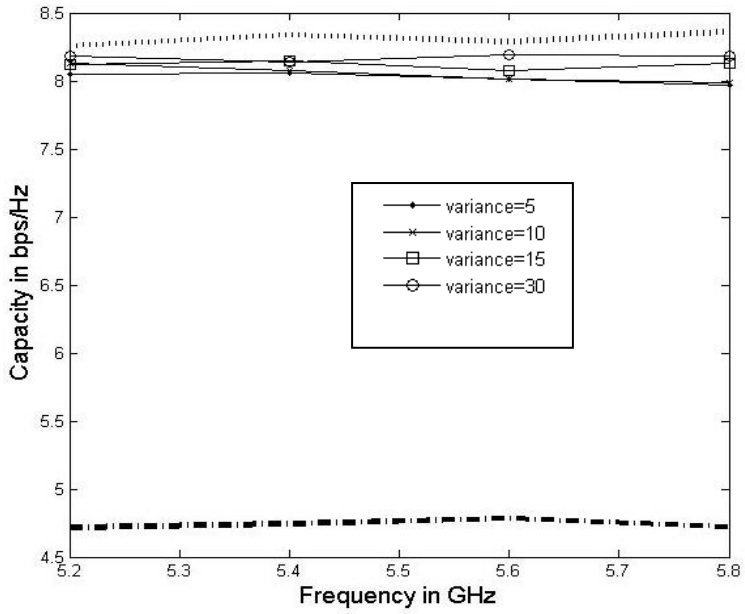

Figure 4.58: Variations of channel capacity versus operating frequency; subject to Gaussian PAS over 0 to 360° with mean 45° and different variances, and raised cosine distribution power spectrum with mean of 90°; ('.....' upper limit of 3 × 3 MIMO), ('-------' upper limit of 3 × 1 MIMO).

2nd and 4th order raised cosine distributions combined with Gaussian PAS were used to compute the channel capacities shown in Figures 4.59 to 4.62. The small difference between the 2nd and 4th order capacity leads to notably different variances. The capacity values were approximately 7.5 bps/Hz with maximum variations of 0.1 bps/Hz at 2.5GHz, and 8.1 bps/Hz with a comparable variation of 0.2 bps/Hz at 5.2GHz. These capacity values were lower than the one recorded at 2.5 GHz without the hand model shown in Figures 4.23 and 4.24. Moreover, a similar relationship of capacity values was also observed for the 5.2 GHz band without hand model.

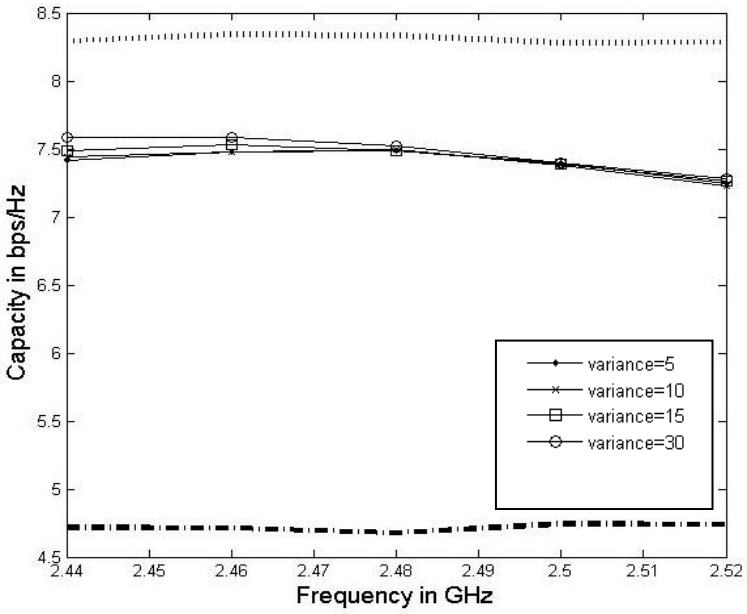

Figure 4.59: Variations of channel capacity versus operating frequency; subject to Gaussian PAS over 0 to 360° with mean 45° and different variances, and raised cosine distribution of 2nd order power spectrum with mean of 90°; ('.....' upper limit of 3 × 3 MIMO), ('------'upper limit of 3 × 1 MIMO).

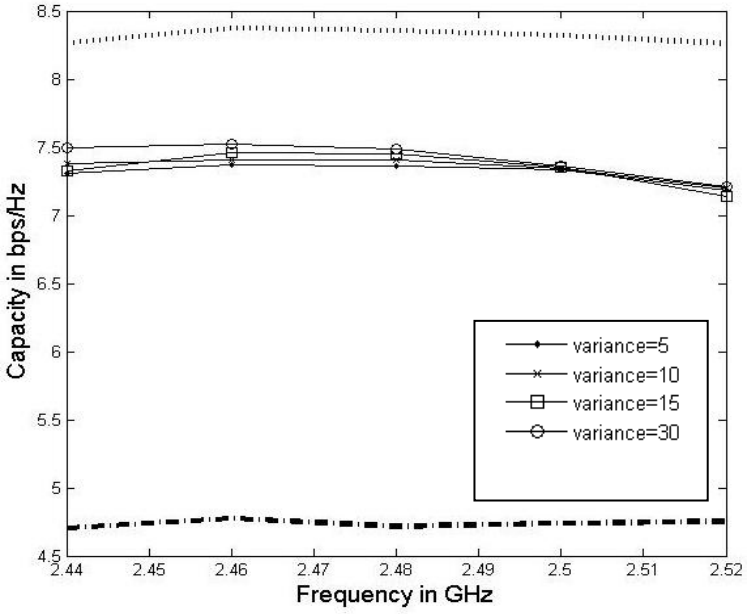

Figure 4.60: Variations of channel capacity versus operating frequency; subject to Gaussian PAS over 0 to 360° with mean 45° and different variances, and raised cosine distribution of 4th order power spectrum with mean of 90°; ('.....' upper limit of × 3 MIMO), ('------'upper limit of 3 × 1 MIMO).

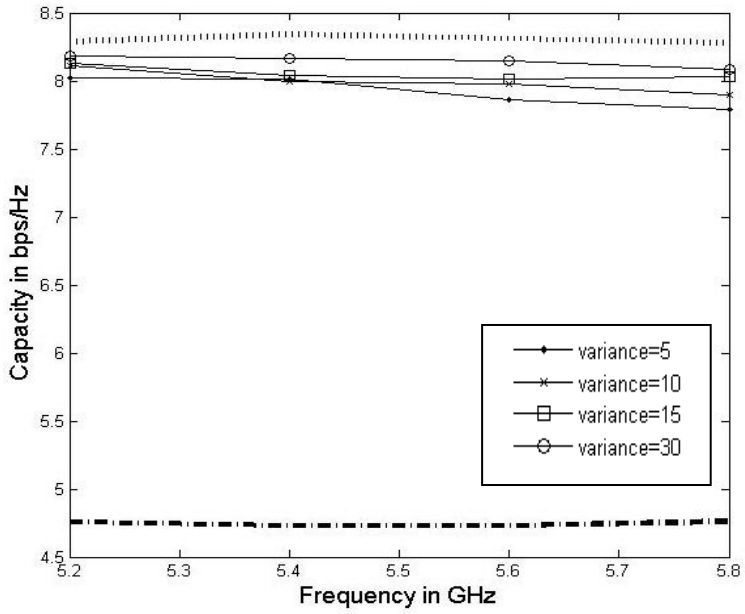

Figure 4.61: Variations of channel capacity versus operating frequency; subject to Gaussian PAS over 0 to 360° with mean 45° and different variances, and raised cosine distribution of 2nd order power spectrum with mean of 90°; ('.....' upper limit of 3 × 3 MIMO), ('------'upper limit of 3 × 1 MIMO).

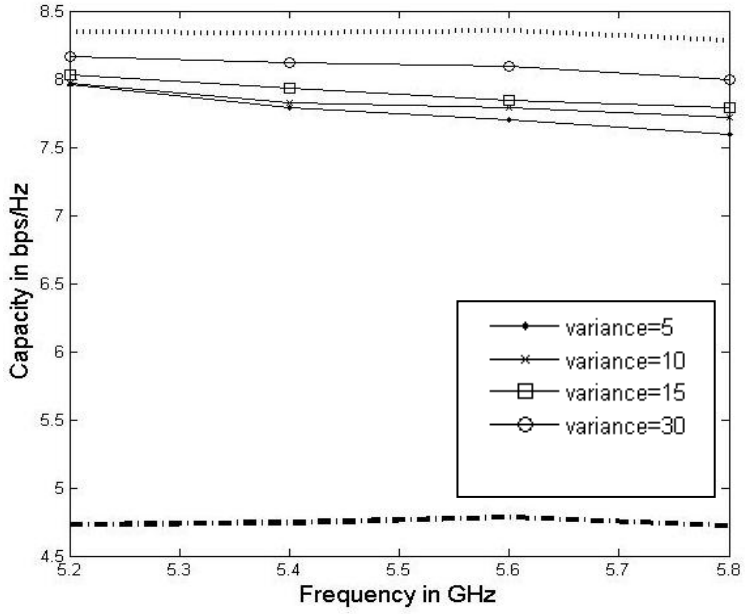

Figure 4.62: Variations of channel capacity versus operating frequency; subject to Gaussian PAS over 0 to 360° with mean 45° and different variances, and raised cosine distribution of 4th order power spectrum with mean of 90°; ('.....' upper limit of × 3 MIMO), ('------' upper limit of 3 × 1 MIMO).

Figures from 4.63 to 4.82 show the channel capacity results calculated with Laplacian and secant-squared PAS's combined with uniform, raised cosine and, n^{th} order raised cosine distributions along the zenith angle.

The trend at 2.5GHz shows lower channel capacities as compared with the results calculated in section 4.4.1. However, similar capacity values are observed at 5.2GHz.

The maximum capacity value was 7.6 bps/Hz over the 2.5 GHz band with variations of 0.3 bps/Hz, as depicted in Figures 4.74 and 4.77; also the variations of channel capacity over the 5.2GHz band are negligible.

A summarized mean channel capacities for all cases investigated with hand model included are presented in Table 4.5. These values were varied between 7.23 and 8.26 bps/Hz, which is quite similar to that achieved without hand model.

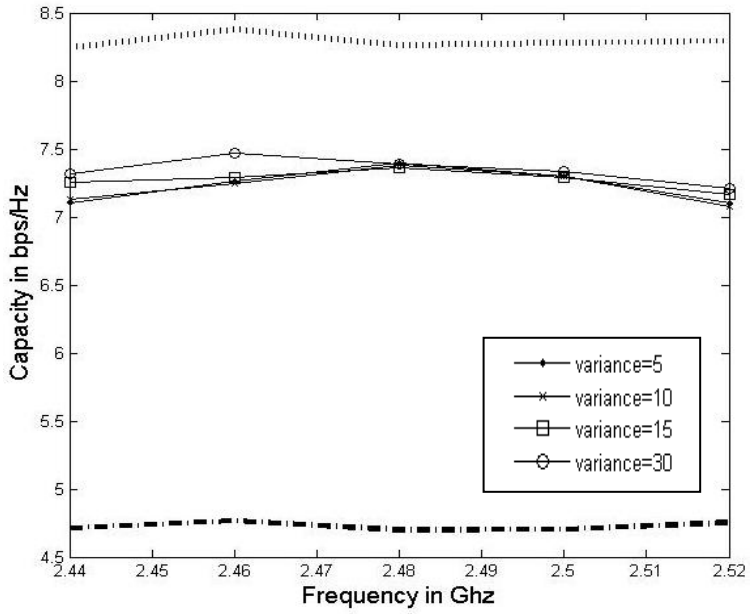

Figure 4.63: Variations of channel capacity versus operating frequency; subject to Laplacian PAS over 0 to 360° with mean 45° and different variances, and uniform power spectrum over ±15° for mean zenith angle of 90°; ('.....' upper limit of 3 × 3 MIMO), ('------'upper limit of 3 × 1 MIMO).

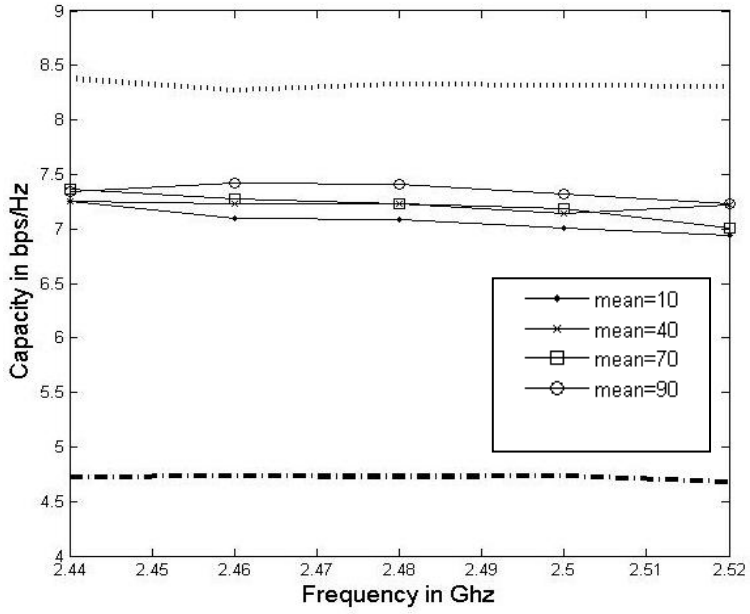

Figure 4.64: Variations of channel capacity versus operating frequency; subject to Laplacian PAS over 0 to 360° with mean 45° and variance 30°; and uniform power spectrum over ±15° for various mean zenith angles of 10°, 40°, 70° and 90°; ('.....' upper limit of 3 × 3 MIMO), ('------'upper limit of 3 × 1 MIMO).

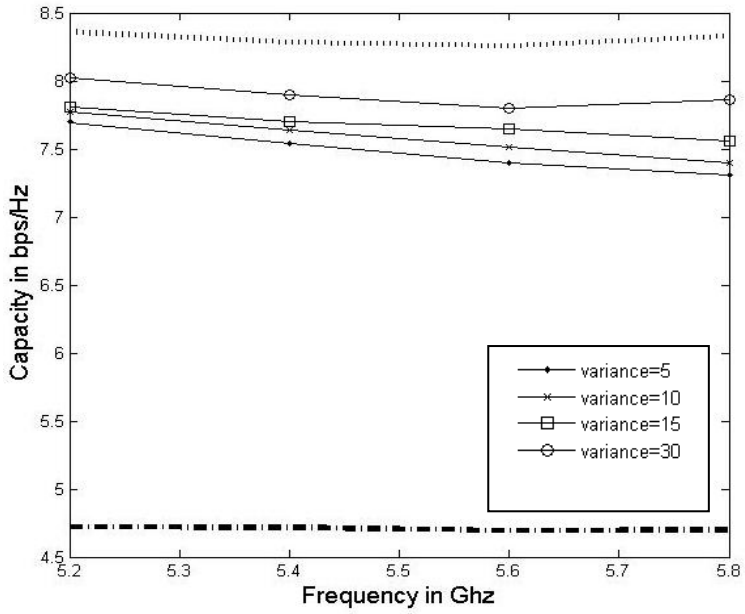

Figure 4.65: Variations of channel capacity versus operating frequency; subject to Laplacian PAS over 0 to 360° with mean 45° and different variances, and uniform power spectrum over ±15° for mean zenith angle of 90°; ('.....' upper limit of 3 × 3 MIMO), ('------'upper limit of 3 × 1 MIMO).

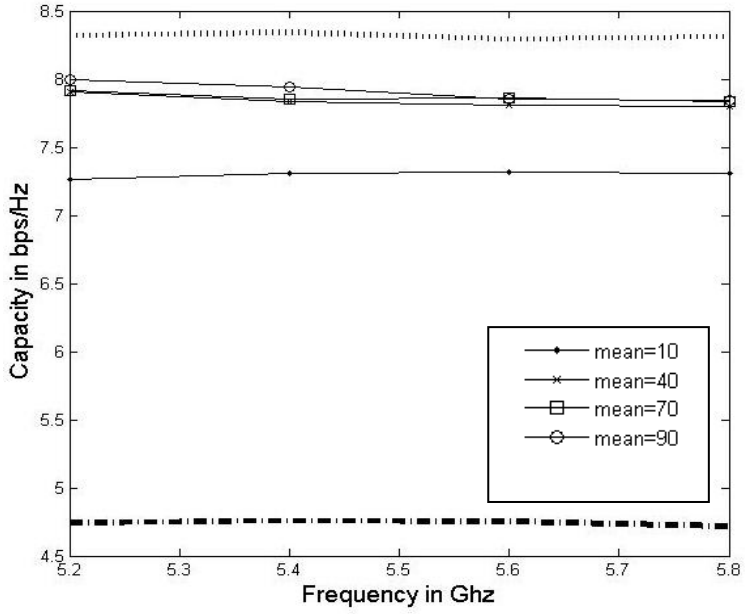

Figure 4.66: Variations of channel capacity versus operating frequency; subject to Laplacian PAS over 0 to 360° with mean 45° and variance 30°; and uniform power spectrum over ±15° for various mean zenith angles of 10°, 40°, 70° and 90°; ('.....' upper limit of 3 × 3 MIMO), ('------'upper limit of 3 × 1 MIMO).

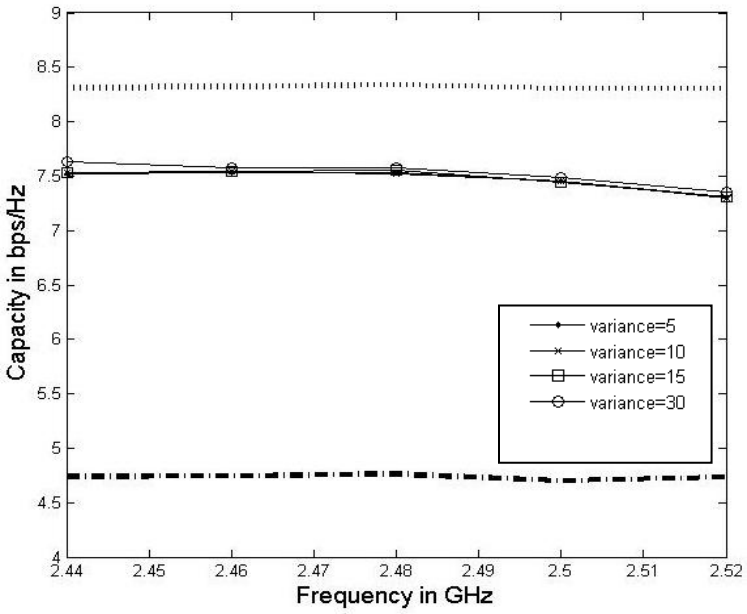

Figure 4.67: Variations of channel capacity versus operating frequency; subject to Laplacian PAS over 0 to 360° with mean 30° and different variances, and raised cosine distribution power spectrum with mean of 90°; ('.....' upper limit of 3 × 3 MIMO), ('-----'upper limit of 3 × 1 MIMO).

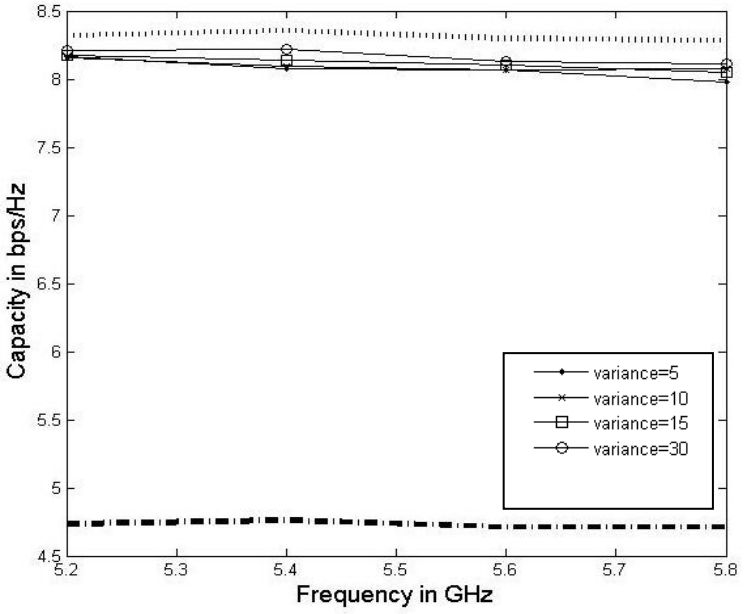

Figure 4.68: Variations of channel capacity versus operating frequency; subject to Laplacian PAS over 0 to 360° with mean 30° and different variances, and raised cosine distribution power spectrum with mean of 90°; ('.....' upper limit of 3 × 3 MIMO), ('-----'upper limit of 3 × 1 MIMO).

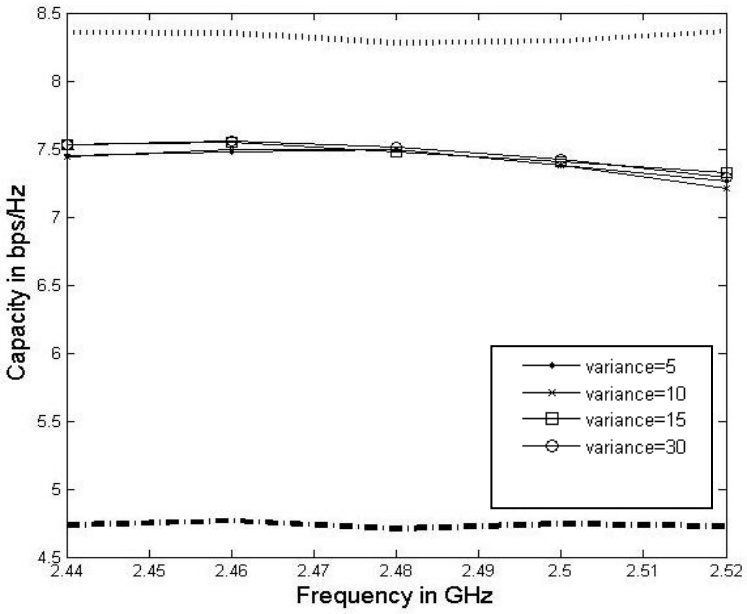

Figure 4.69: Variations of channel capacity versus operating frequency; subject to Laplacian PAS over 0 to 360° with mean 45° and different variances; and raised cosine distribution of 2nd order power spectrum with mean of 90°; ('.....' upper limit of 3 × 3 MIMO), ('------'upper limit of 3 × 1 MIMO).

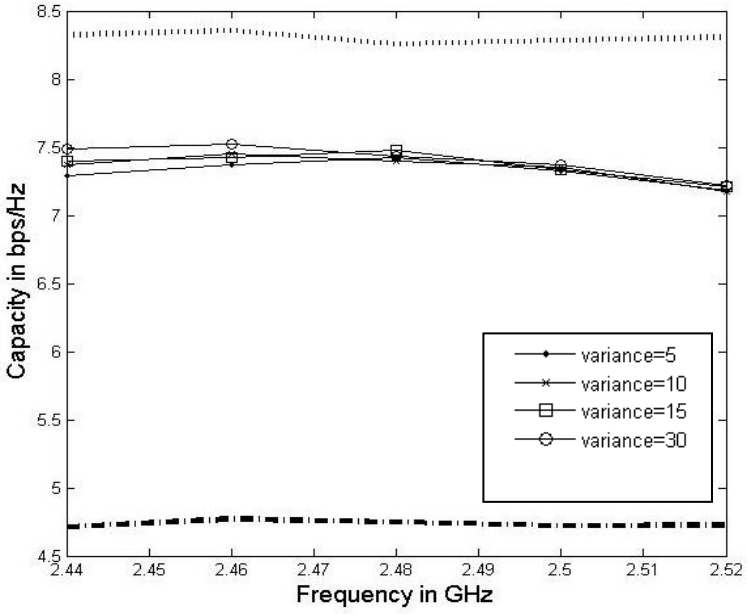

Figure 4.70: Variations of channel capacity versus operating frequency; subject to Laplacian PAS over 0 to 360° with mean 45° and different variances; and raised cosine distribution of 4th order power spectrum with mean of 90°; ('.....' upper limit of 3 × 3 MIMO), ('------'upper limit of 3 × 1 MIMO).

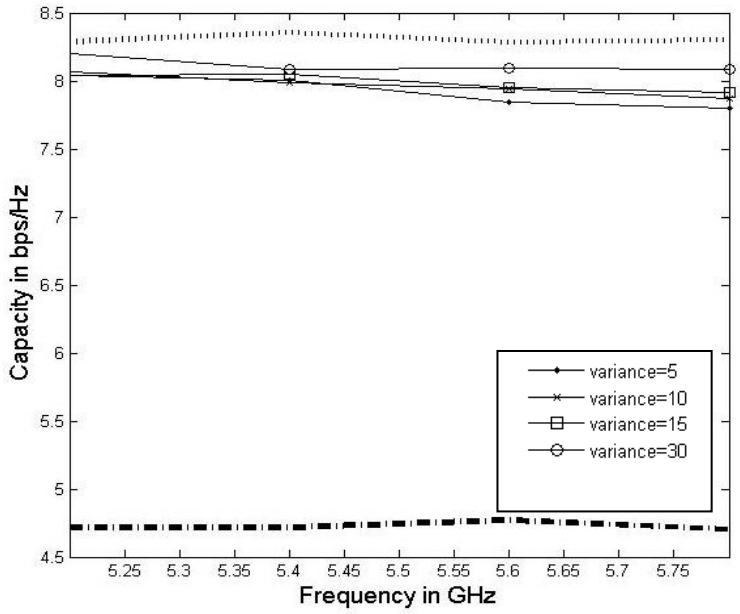

Figure 4.71: Variations of channel capacity versus operating frequency; subject to Laplacian PAS over 0 to 360° with mean 45° and different variances; and raised cosine distribution of 2nd order power spectrum with mean of 90°; ('.....' upper limit of 3 × 3 MIMO), ('------'upper limit of 3 × 1 MIMO).

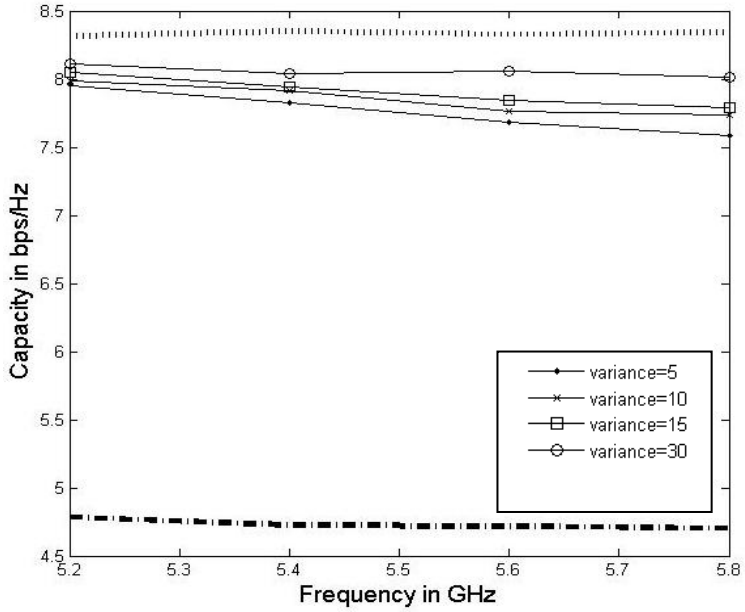

Figure 4.72: Variations of channel capacity versus operating frequency; subject to Laplacian PAS over 0 to 360° with mean 45° and different variances; and raised cosine distribution of 4th order power spectrum with mean of 90°; ('.....' upper limit of 3 × 3 MIMO), ('------'upper limit of 3 × 1 MIMO).

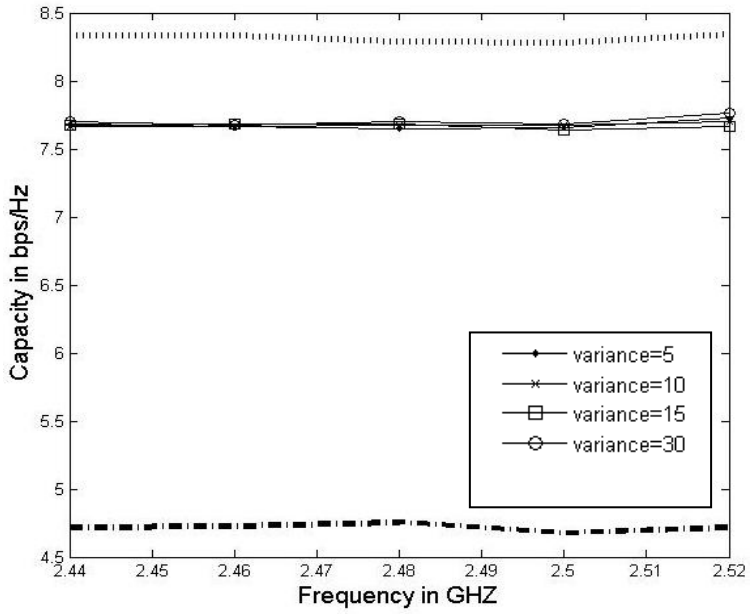

Figure 4.73: Variations of channel capacity versus operating frequency; subject to Secant Square PAS over 0 to 360° with mean 45° and different variances, and uniform power spectrum over ±15° for mean zenith angle of 90°; ('.....' upper limit of 3 × 3 MIMO), ('------'upper limit of 3 × 1 MIMO).

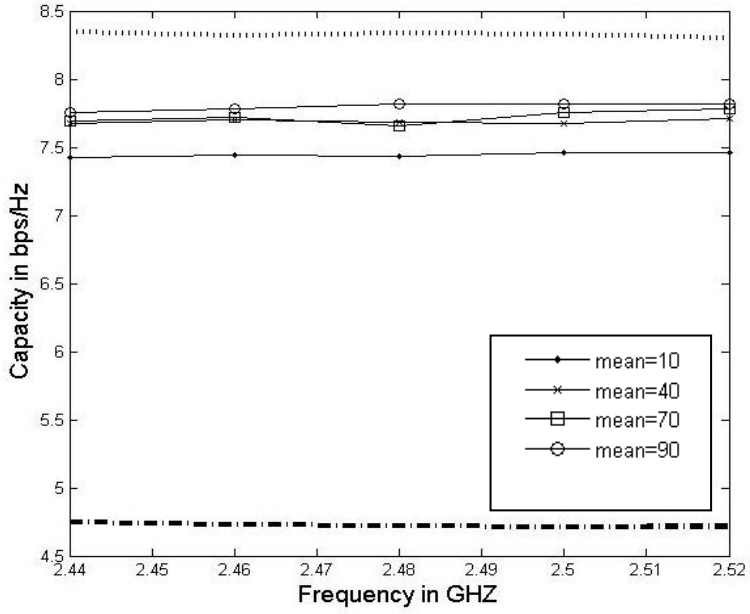

Figure 4.74: Variations of channel capacity versus operating frequency; subject to Secant Square PAS over 0 to 360° with mean 45° and uniform power spectrum over ±15° for various mean zenith angles of 10°, 40°, 70° and 90°; ('.....' upper limit of 3 × 3 MIMO), ('------'upper limit of 3 × 1 MIMO).

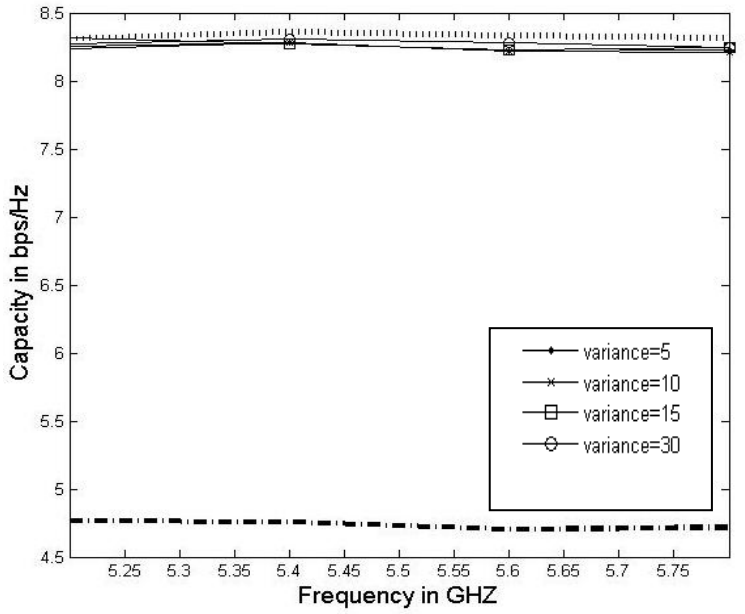

Figure 4.75: Variations of channel capacity versus operating frequency; subject to Secant Square PAS over 0 to 360° with mean 45° and different variances, and uniform power spectrum over ±15° for mean zenith angle of 90°; ('.....' upper limit of 3 × 3 MIMO), ('------'upper limit of 3 × 1 MIMO).

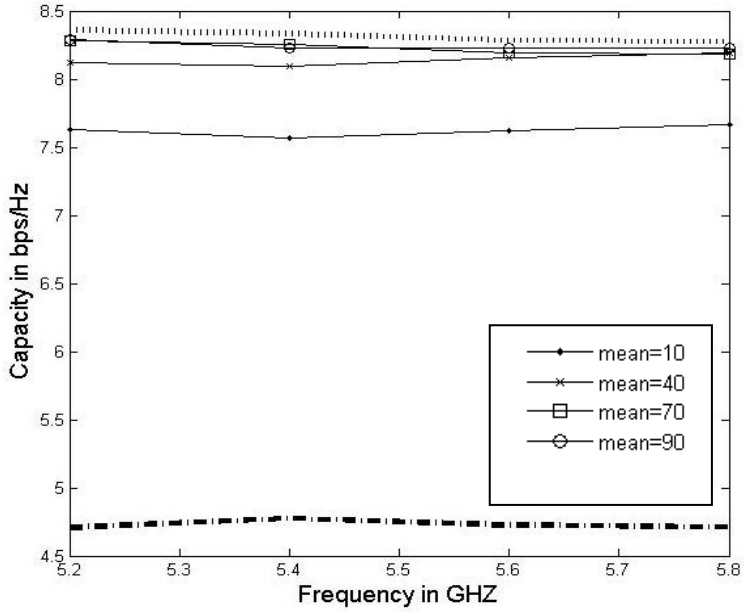

Figure 4.76: Variations of channel capacity versus operating frequency; subject to Secant Square PAS over 0 to 360° with mean 45° and uniform power spectrum over ±15° for various mean zenith angles of 10°, 40°, 70° and 90°; ('.....' upper limit of 3 × 3 MIMO), ('------'upper limit of 3 × 1 MIMO).

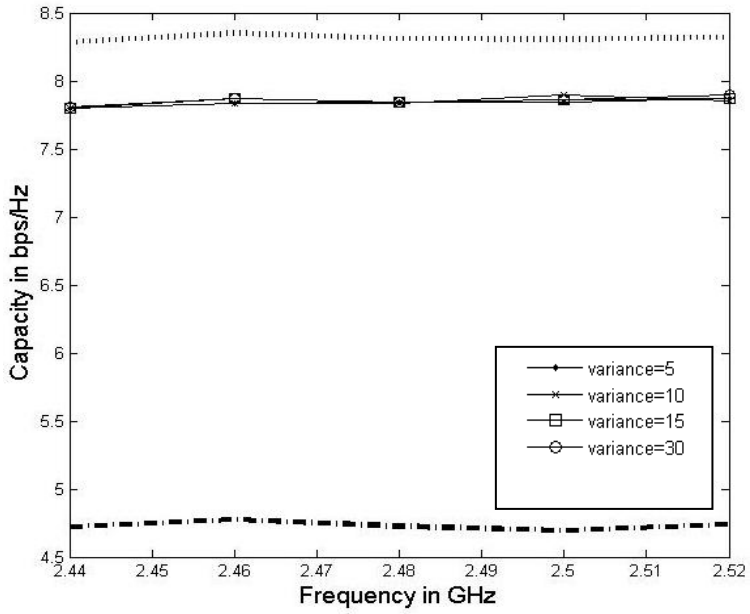

Figure 4.77: Variations of channel capacity versus operating frequency; subject to Secant Square PAS over 0 to 360° with mean 45° and different variances, and raised cosine distribution power spectrum with mean of 90°; ('.....' upper limit of 3 × 3 MIMO), ('------'upper limit of 3 × 1 MIMO).

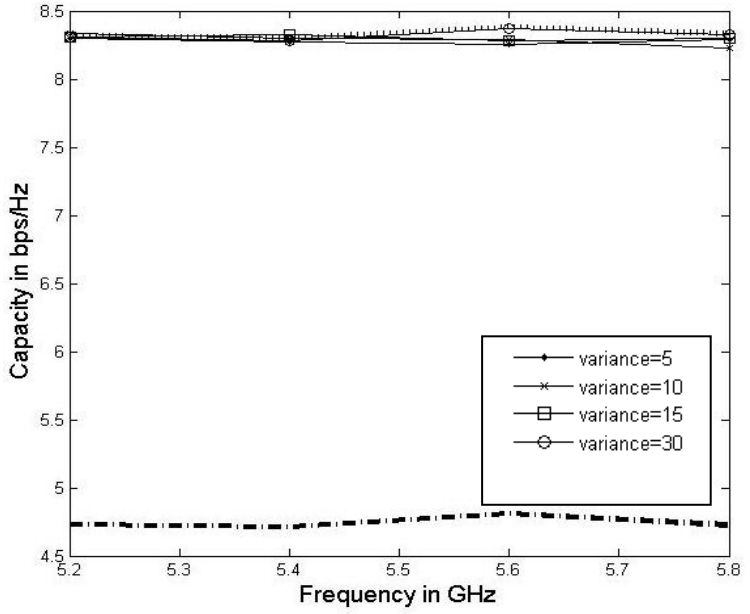

Figure 4.78: Variations of channel capacity versus operating frequency; subject to Secant Square PAS over 0 to 360° with mean 45° and different variances, and raised cosine distribution power spectrum with mean of 90°; ('.....' upper limit of 3 × 3 MIMO), ('------'upper limit of 3 × 1 MIMO).

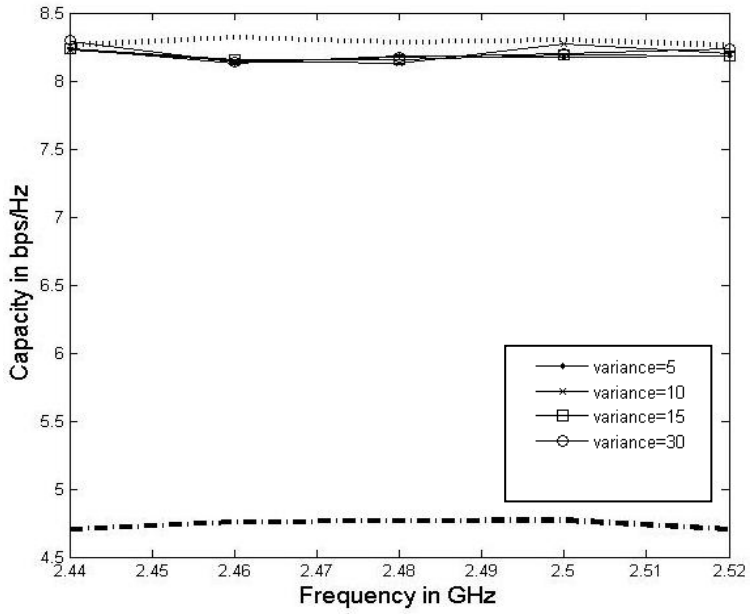

Figure 4.79: Variations of channel capacity versus operating frequency; subject to Secant Square PAS over 0 to 360° with mean 45° and different variances; and raised cosine distribution of 2nd order power spectrum with mean of 90°; ('.....' upper limit of 3 × 3 MIMO), ('------'upper limit of 3 × 1 MIMO).

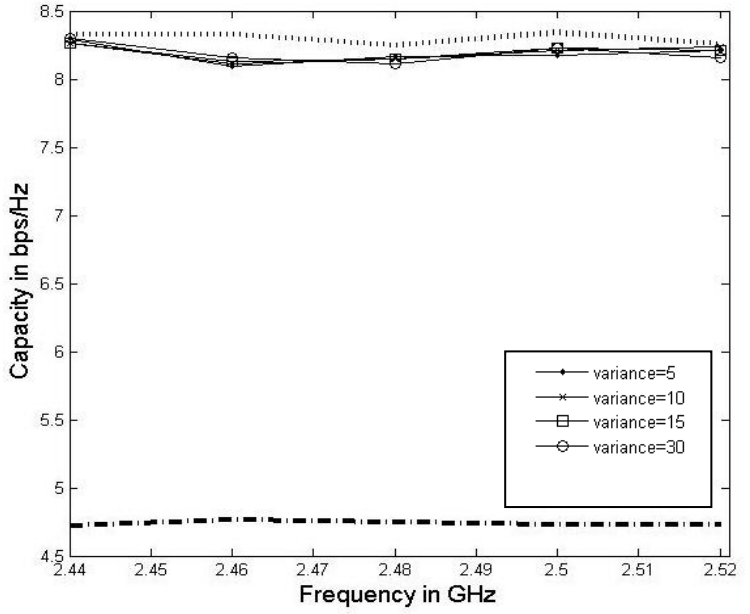

Figure 4.80: Variations of channel capacity versus operating frequency; subject to Secant Square PAS over 0 to 360° with mean 45° and different variances; and raised cosine distribution of 4th order power spectrum with mean of 90°; ('.....' upper limit of 3 × 3 MIMO), ('------' upper limit of 3 × 1 MIMO).

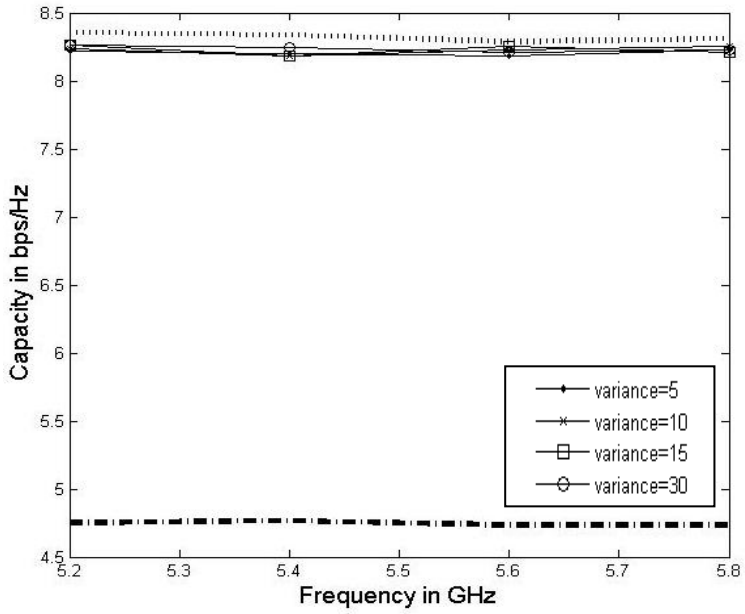

Figure 4.81: Variations of channel capacity versus operating frequency; subject to Secant Square PAS over 0 to 360° with mean 45° and different variances; and raised cosine distribution of 2nd order power spectrum with mean of 90°; ('.....' upper limit of 3 × 3 MIMO), ('------' upper limit of 3 × 1 MIMO).

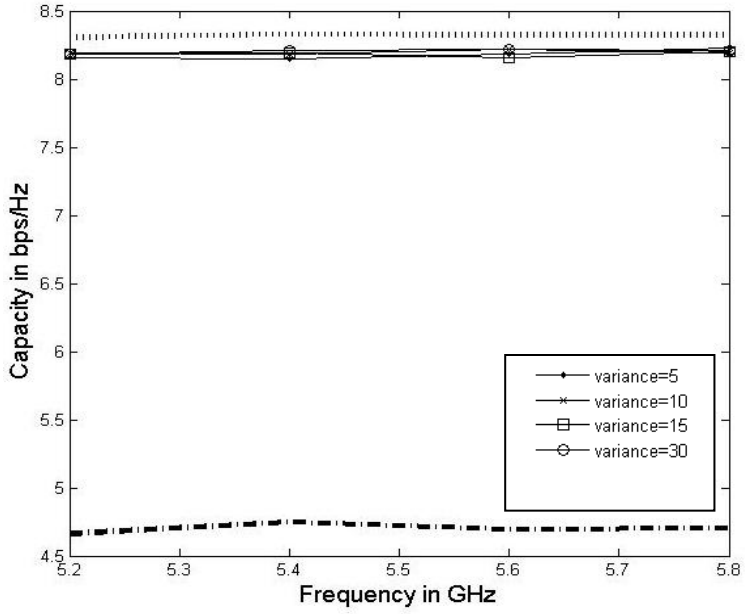

Figure 4.82: Variations of channel capacity versus operating frequency; subject to Secant Square PAS over 0 to 360° with mean 45° and different variances; and raised cosine distribution of 4th order power spectrum with mean of 90°; ('.....' upper limit of 3 × 3 MIMO), ('------' upper limit of 3 × 1 MIMO).

Table 4.5 : Summarised channel capacity of the antenna geometry shown in Fig. 4.4.

Power Distributions		**Mean of Calculated Channel Capacity (Bps/Hz)**	
Azimuth	**Elevation**	**2.44 to 2.52 GHz**	**5.2 to 5.8 GHz**
Uniform	Uniform	7.51	7.86
Uniform	Raised Cosine	7.63	8.25
Uniform	n^{th} Order raised Cosine	7.78	8.27
Gaussian	Uniform	7.25	7.82
Gaussian	Raised Cosine	7.57	8.15
Gaussian	2^{nd} Order raised Cosine	7.53	8.16
Gaussian	4^{th} Order raised Cosine	7.38	8.12
Laplacian	Uniform	7.23	7.78
Laplacian	Raised Cosine	7.52	8.23
Laplacian	2^{nd} Order raised Cosine	7.46	8.18
Laplacian	4^{th} Order raised Cosine	7.38	8.07
Secant Square	Uniform	7.62	8.26
Secant Square	Raised Cosine	7.72	8.26
Secant Square	2^{nd} Order raised Cosine	8.23	8.16
Secant Square	4^{th} Order raised Cosine	8.19	8.2

4.4.3 Radiation Patterns for 3x3 MIMO Systems

Figures 4.83 – 4.85 show the principal plane radiation patterns for $\boldsymbol{E}_{\theta}$ and $\boldsymbol{E}_{\phi}$ in the xy-planes and xz-planes for each radiator, at each dual band resonance. The radiation patterns of the three radiating elements show a reasonable field diversity to contribute

towards a suitable RX/TX capacity, vis. broad dipole-like patterns covering the majority of the sphere. The power gains for each radiating antenna were approximately 2.5 dB and 4.5 dB at 2.45 GHz and 5.2 GHz, respectively.

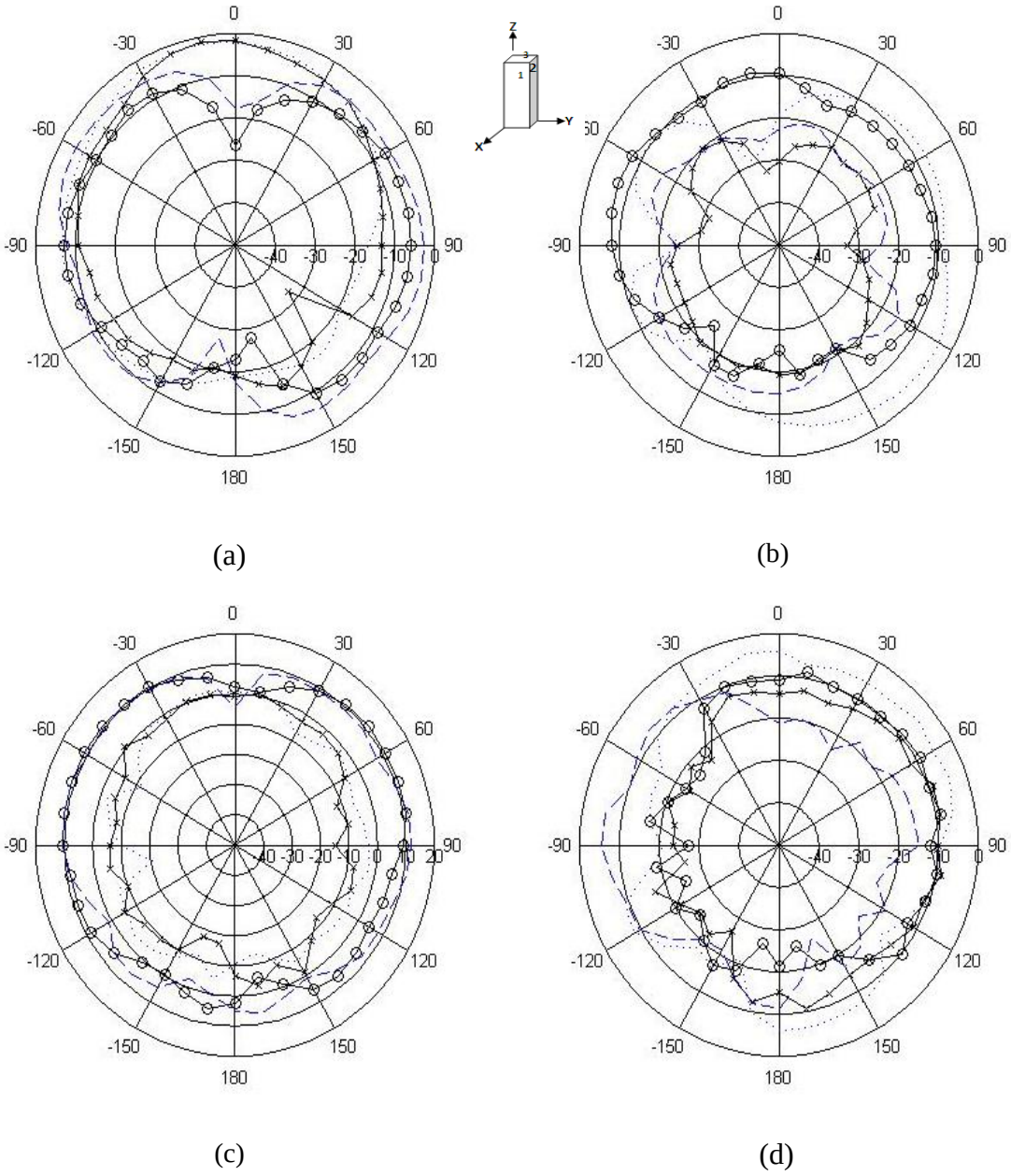

Figure 4.83: Radiation pattern of antenna element 1 for two different cuts; (a) θ=90, Φ=0-360, at 2.5 GHz; (b) θ=0-360, Φ=0 at 2.5 GHz; (c) θ=90, Φ=0-360, at 5.2 GHz; (d) θ=0-360, Φ=0 at 5.2 GHz; ('ooo' measured E_{Φ}, 'xxx' measured E_{θ}, '-----' Simulated E_{Φ}, '…...'Simulated E_{θ})

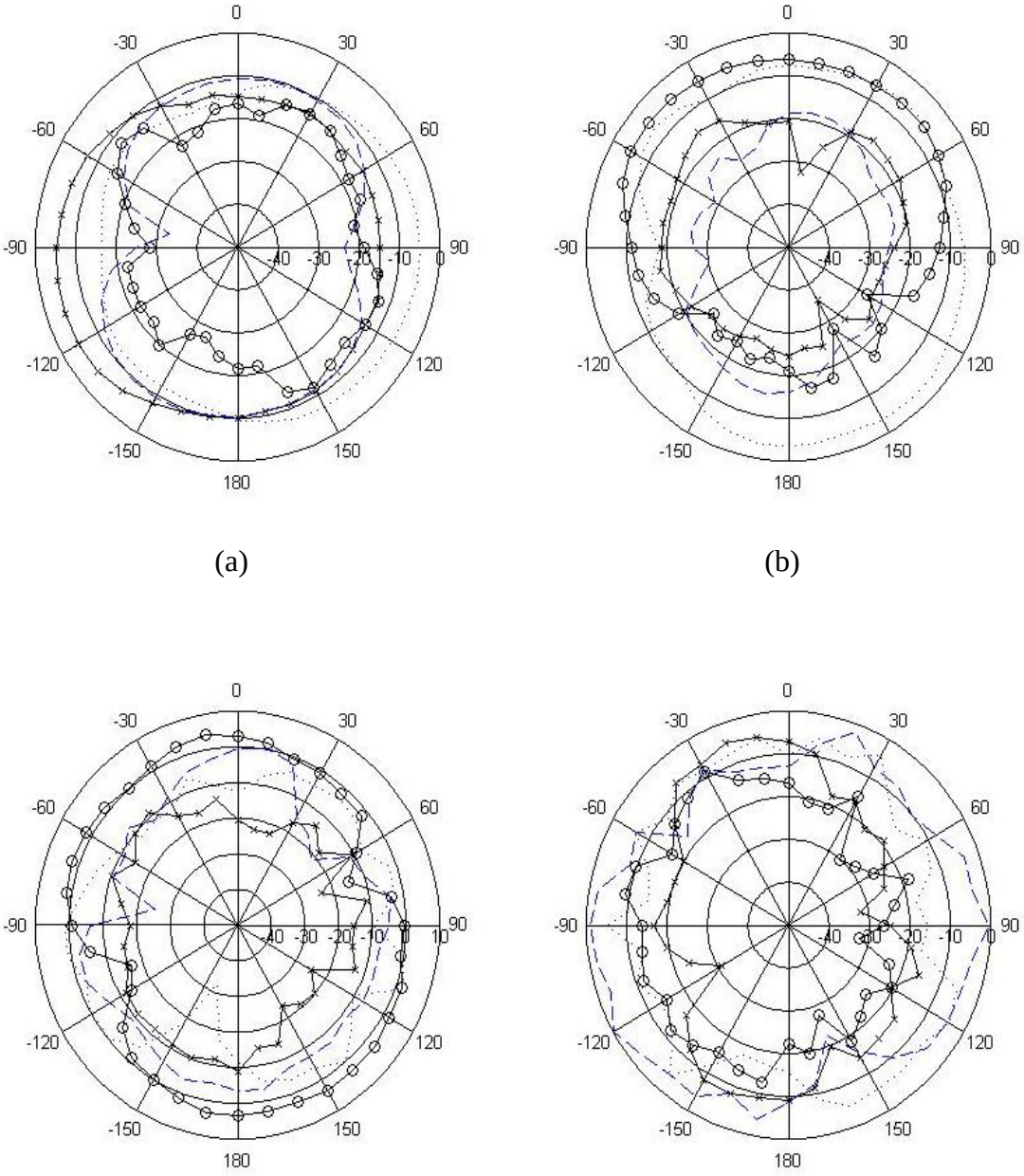

(a) (b)

(c) (d)

Figure 4.84: Radiation pattern of antenna element 2 for two different cuts; (a) θ=90, Φ=0-360, at 2.5 GHz; (b) θ=0-360, Φ=0 at 2.5 GHz; (c) θ=90, Φ=0-360, at 5.2 GHz; (d) θ=0-360, Φ=0 at 5.2 GHz; (‘ooo’ measured E_{Φ}, ’xxx’ measured E_{θ}, ’-----’ Simulated E_{Φ}, ‘…...’Simulated E_{θ})

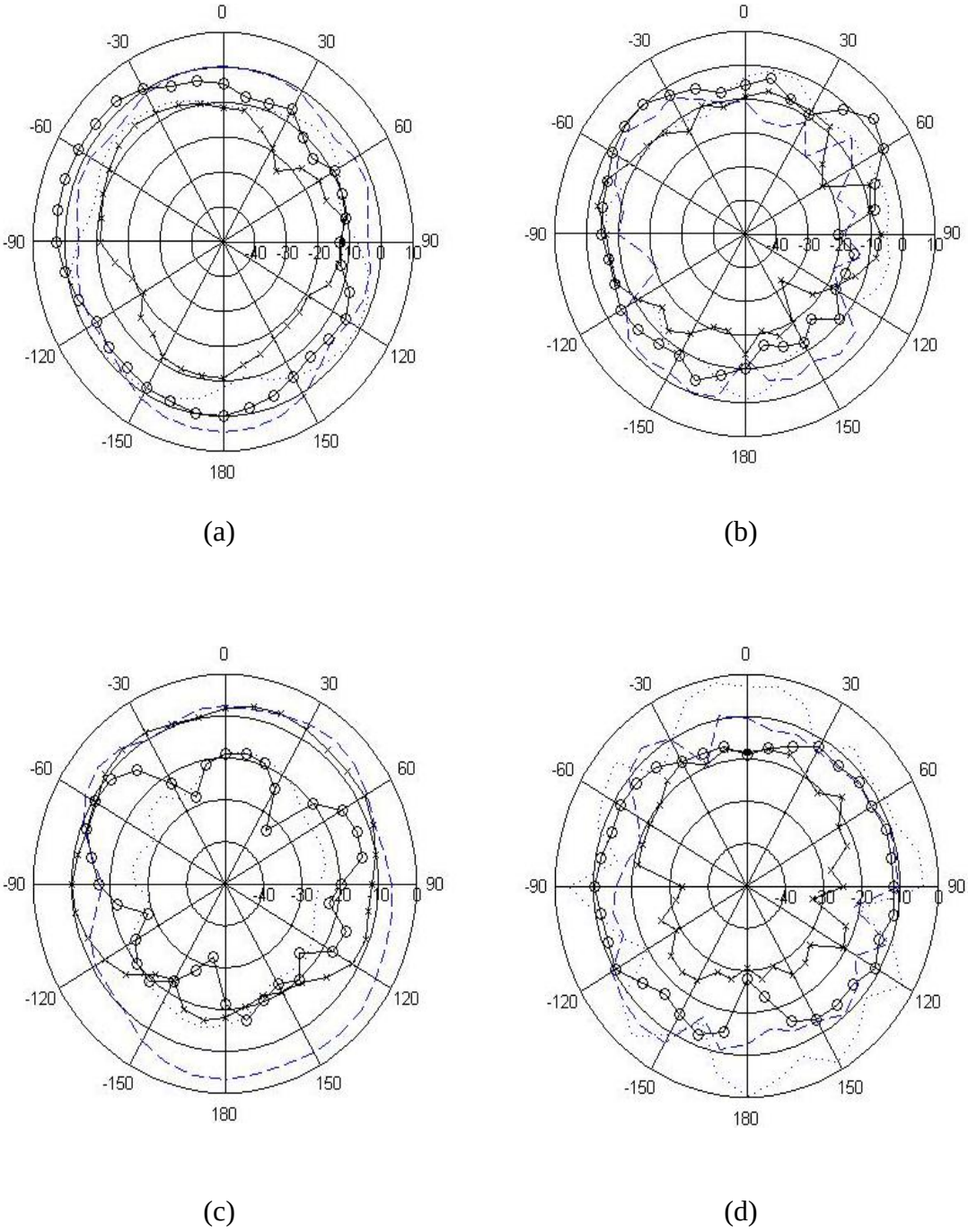

(a) (b)

(c) (d)

Figure 4.85: Radiation pattern of antenna element 3 for two different cuts; (a) θ=90, Φ=0-360, at 2.5 GHz; (b) θ=0-360, Φ=0 at 2.5 GHz; (c) θ=90, Φ=0-360, at 5.2 GHz; (d) θ=0-360, Φ=0 at 5.2 GHz; ('ooo' measured E_{Φ}, 'xxx' measured E_{θ}, '-----' Simulated E_{Φ}, '…...'Simulated E_{θ})

4.5 REDUCED SIZE OF 3×3 MIMO SYSTEM

4.5.1 Proposed Antenna Design Concept

Several antenna size reduction techniques have been proposed for microstrip antennas over the last decade. A representative sub-set of these methods includes: the use of high permittivity substrate, shorting pins, shorting walls, and modifications to the internal radiator structure [21-23]. More recently the use of magnetic symmetry walls [24,25] have been proposed; significantly it has been found that most performance metrics (return losses, gains, and radiation efficiencies) and radiation patterns of U-slot, E-slot, and certain UWB, microstrip antennas are comparable to their full structures [26].

In an extension of the previous research [27], this section proposes a possible 50% size reduction of the dual frequency PIF(L)A antennas. Using the earlier PIF(L)A prototype structure this suggests an overall size of 30mm×15mm×8mm mounted over a 30mm×15mm ground plane. This is an attractive prospect for integration into a variety of mobile terminals, such notebook computers, as well as smart phones. This analysis was carried out using HFSS. The models were developed with the IEEE 802.11x standard in mind, using the antenna type in [27], but with suitably modified structure parameters (Figure 4.86) and a magnetic symmetry wall aligned with the antenna surface [26-28].

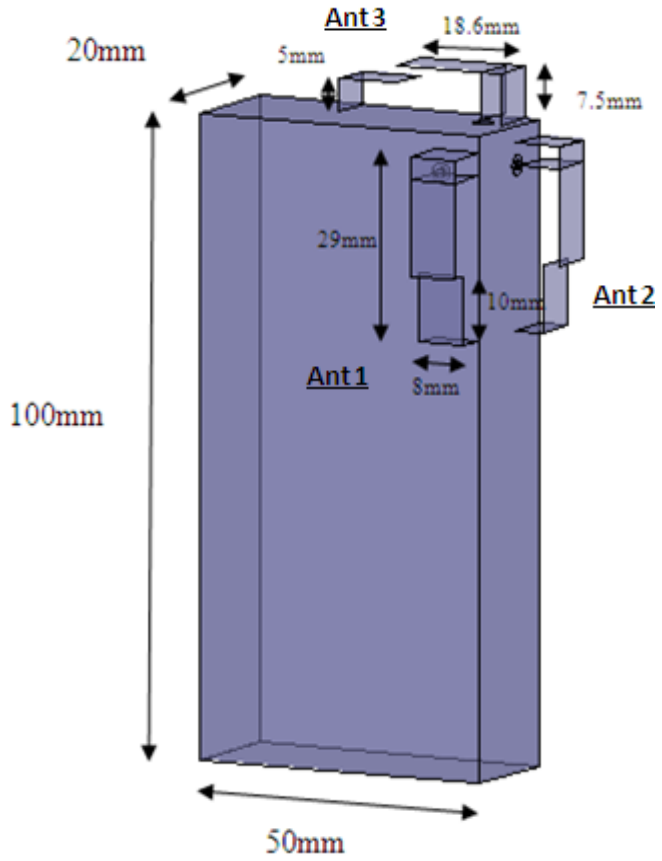

Figure 4.86: The basic geometry model of the reduced size 3×3 MIMO Antenna mobile handset.

Due to their traditional wire feed mechanism, PIFA modules have limited bandwidth performance (4%-12 %) [28]. By changing to a different feed plane silhouette [29], the impedance bandwidth can be significantly increased from 18% to 25%. Possibilities include triangular plate, bi-triangular plate, rectangular plate, rounded rectangular plate, or U-shaped strip plate; a rectangular plate feed is selected in this instance.

The proposed miniaturisation follows from the removal of half of the patch antenna along the line of structure symmetry of the PIF(L)A module, as in [27]. Hence, the volume of the patch antenna is reduced to half of the overall volume of the PIF(L)A module described in [27]. This allows a new prototype assembly to be fabricated, as previously, three PIF(L)As are arranged into an orthogonal set over a metal box of

dimensions 100mm×50mm×20mm (see Figure 4.86). In essence a new 3×3 MIMO antenna prototype has been created with dual resonances set at 2.5GHz and 5.2GHz.

4.5.2 Input Return Loss and Coupling

The coupling between the three radiators for the dual bands is less than -10 dB, as presented in Figure 4.10. The proposed 'half width' 3×3 prototype design provides a good trade off between the bandwidth and the geometrical size of each radiator comprising the module.

The return loss for each antenna in the new prototype assembly is -18dB over both frequency bands (see Figure 4.87). The coupling between the three radiator elements was found to be less than -10 dB (Figure 4.87a/b/c). This 'half width' 3×3 prototype design seems to offer a good trade-off between bandwidth and antenna size.

Figure 4.87a shows that the 'half width' design resonates at 2.5 and 5.2 GHz; but a slight frequency drift away from centre frequency was observed for 5.2GHz. Proper coverage of the upper band frequency range is still observed, and with good return loss (2.5 GHz and 5.2GHz were -50 dB and -18dB respectively).

Similarly Figure 4.87b shows a maximum value of S_{22} (-23 dB) at 2.5GHz, where it is improved in comparison with return loss of full width S_{22}. This is also be repeated over the 5.2GHz band for which a maximum of -36 dB is achieved, with a slight shift in the resonant frequency.

Similar improvements in the maximum return loss can be observed for the half size third element as shown in Figure 4.87c compared to a full size radiating element. Improvements of 4 dB and 11 dB were achieved using the half size element at both resonant frequencies.

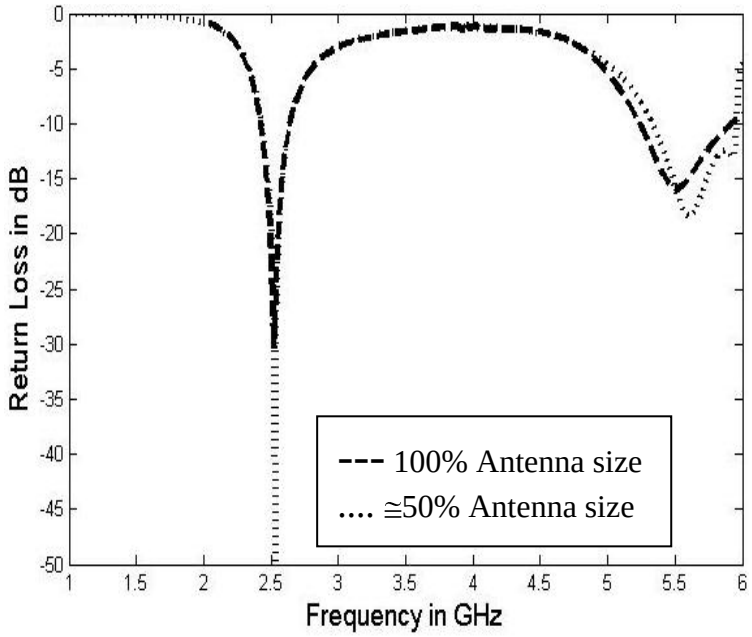

(a)

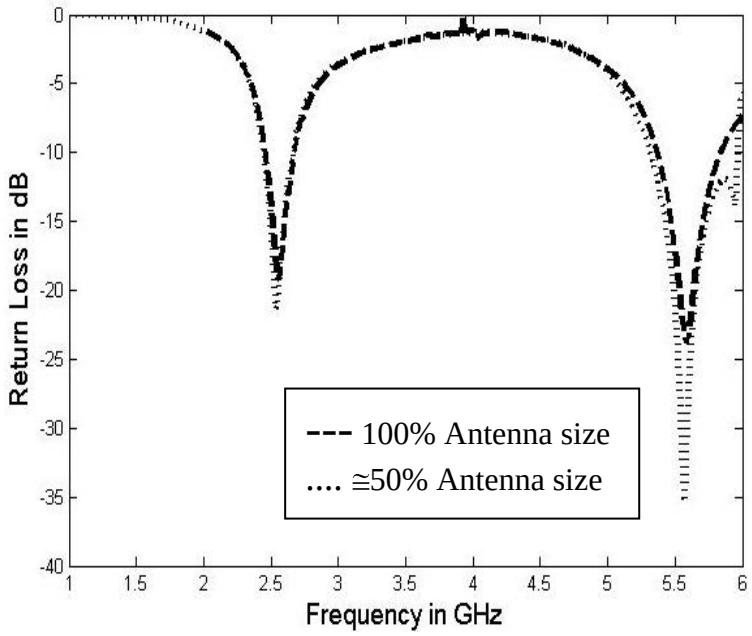

(b)

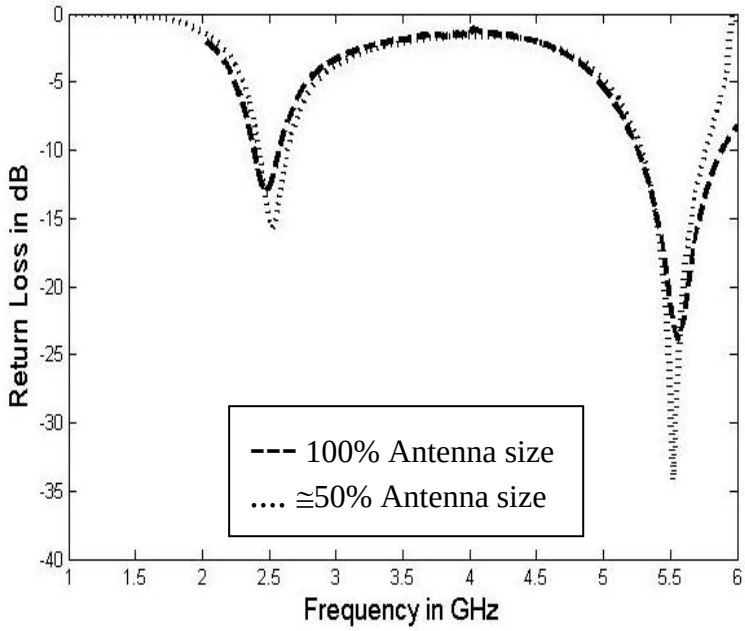

Figure 4.87: Input return loss of (a) Ant 1, (b) Ant 2 and (c) Ant 3, for the 3×3 MIMO antenna handset.

The simulated relative impedance bandwidths of the radiators for both the full size and half size 3×3 prototype modules are summarized in Table 4.6. All the antenna elements show reasonable relative bandwidth at 2.5 GHz and 5.2 GHz, in which they conform to the IEEE 802.11a/b/g standards.

Table 4.6: The impedance relative bandwidths (BWr) of the proposed 3 × 3 MIMO antenna handsets.

	2.5 GHz		**5.2 GHz**	
	Full Width BWr %	**Half Width BWr %**	**Full Width BWr %**	**Half Width BWr %**
Antenna 1	9.1	9.1	13.1	10.7
Antenna 2	9.1	9.1	9.6	12.8
Antenna 3	8	8.3	11.5	9.6

Coupling between the reduced size radiating elements of both the 3×3 prototype module is shown in Figure 4.88.

Improvements of 4 dB and 5 dB in the S_{12} coupling factor were found using the reduced size antenna prototype model compared to full size version (Figure 4.88a), for 2.5 GHz and 5.2GHz respectively.

The variation of S_{13} for half size prototype was similar to full size version (Figure 4.88b), except for a 5 dB coupling improvement around the upper band resonance. Similarly, S_{23} shows a similar variations, except for a 3 dB difference found around the lower band resonance.

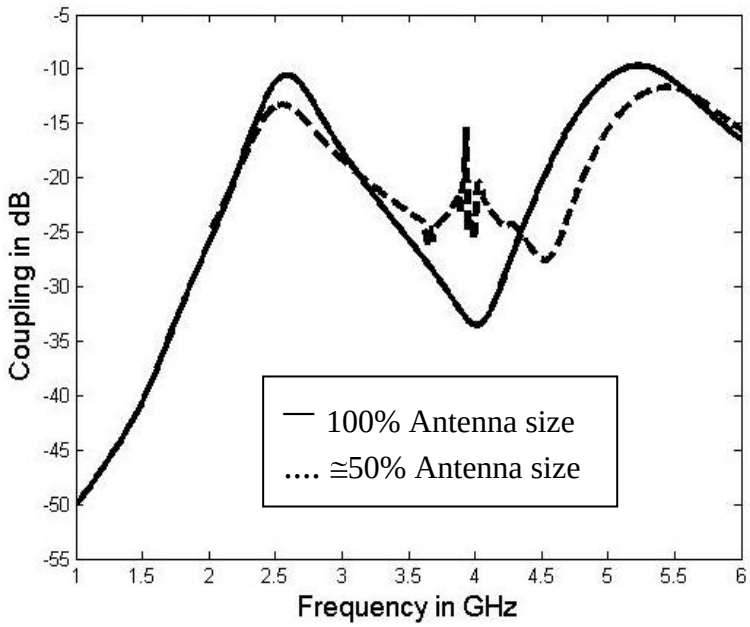

(a)

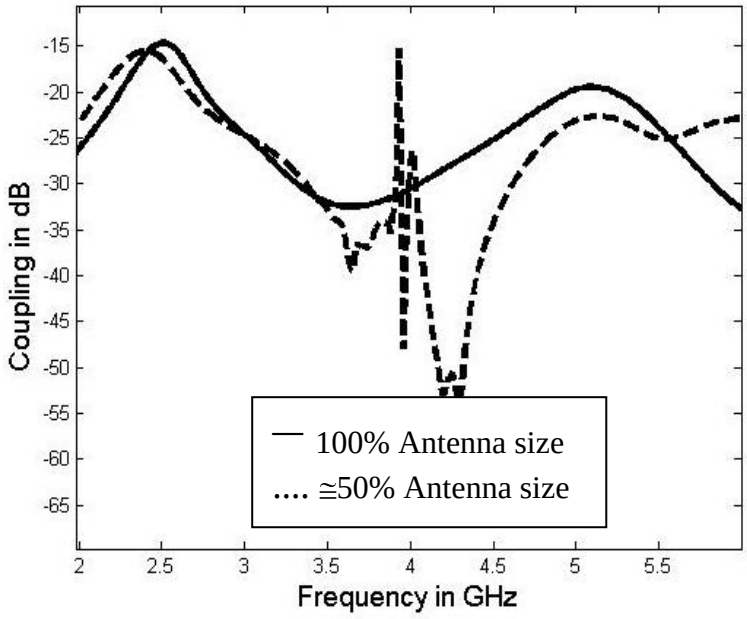

(b)

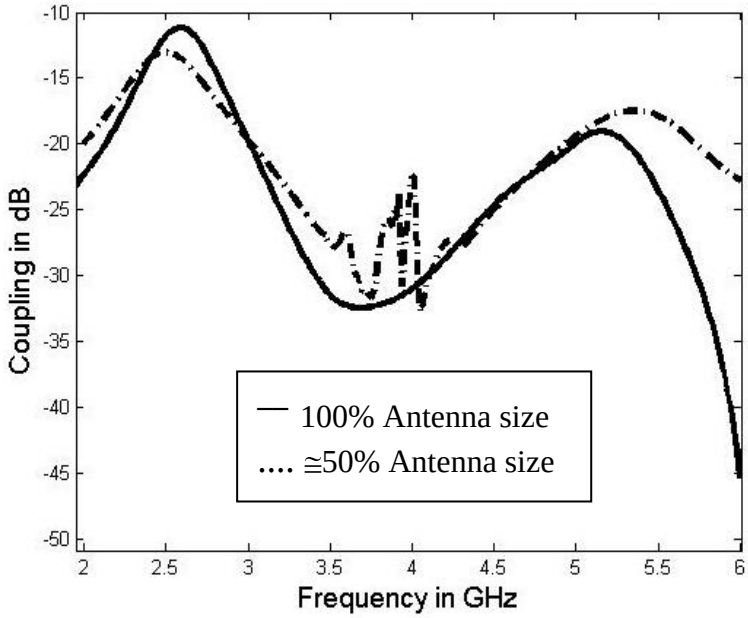

Figure 4.88: The coupling of 3×3 MIMO antenna handset (a) S_{12} (b) S_{13} and (c) S_{23}.

4.5.3 Channel Capacity of Reduced Size 3×3 MIMO System

The angle and magnitude of E_θ and E_Φ have been extracted from the simulation for the two bands of frequencies around 2.5 GHz and 5.2 GHz. These fields have been utilized in the Matlab for the channel capacity calculation. The channel capacity calculation criterion is same as that used in sections 4.4.1 and 4.4.2. The results indicate that the channel capacities are approximately same as for the 3×3 prototype (Figure 4.2), and also reaching to the maximum channel capacity of the ideal 3×3 MIMO system, i.e. in free space without coupling. Examples are performed to discuss the performance of the proposed design as follows.

Figures 4.89 to 4.93 illustrate the channel capacity of the 'half size' 3×3 prototype using uniform PAS over 0 to 360° in combination of uniform raised cosine and n^{th} order raised cosine distribution along the zenith angle.

Figure 4.89 considers the channel capacity for the uniform distribution over azimuth and uniform power spectrum over ±15° with different values of mean along the zenith angle. The maximum capacity of 8.1 bps/Hz is observed at mean of 40° in which it is almost comparable to the channel capacity obtained in Section 4.4.1, Figure 4.11, applying the similar channel assumptions at the 2.5 GHz frequency band.

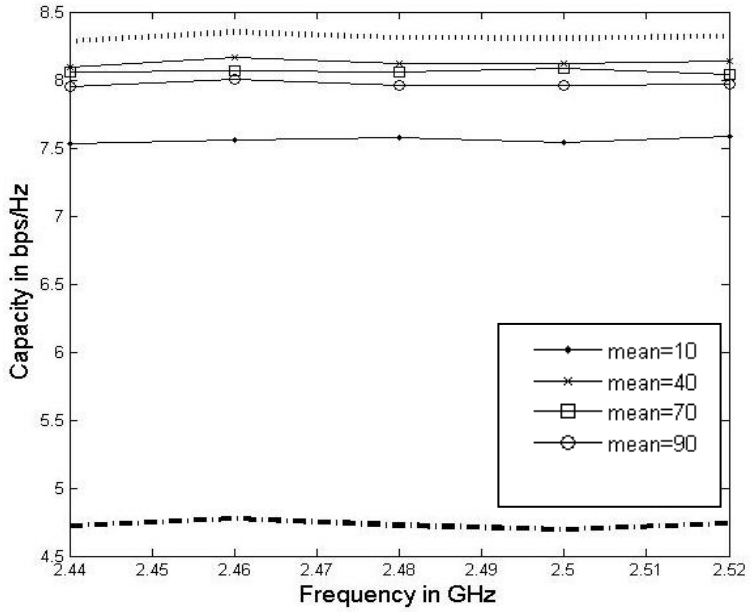

Figure 4.89: Variations of channel capacity versus operating frequency; subject to uniform PAS over 0 to 360° and uniform power spectrum over ±15° for various mean zenith angles of 10°, 40°, 70° and 90°; ('.....' upper limit of 3 × 3 MIMO), ('------'upper limit of 3 × 1 MIMO).

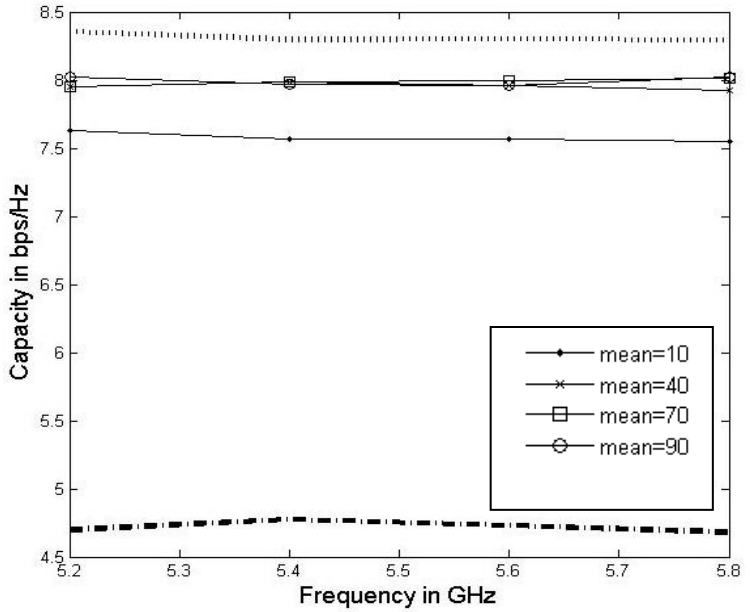

Figure 4.90: Variations of channel capacity versus operating frequency; subject to uniform PAS over 0 to 360° and uniform power spectrum over ±15° for various mean zenith angles of 10°, 40°, 70° and 90°; ('.....' upper limit of 3 × 3 MIMO), ('------'upper limit of 3 × 1 MIMO).

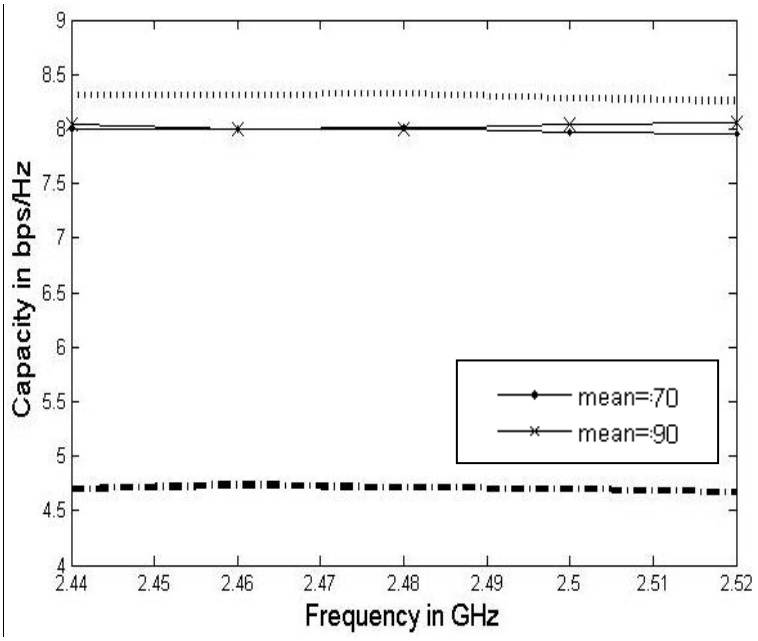

Figure 4.91: Variations of channel capacity versus operating frequency; subject to uniform PAS over 0 to 360° and raised cosine distribution power spectrum for various mean zenith angles of 70° and 90°; ('.....' upper limit of 3 × 3 MIMO), ('------'upper limit of 3 × 1 MIMO).

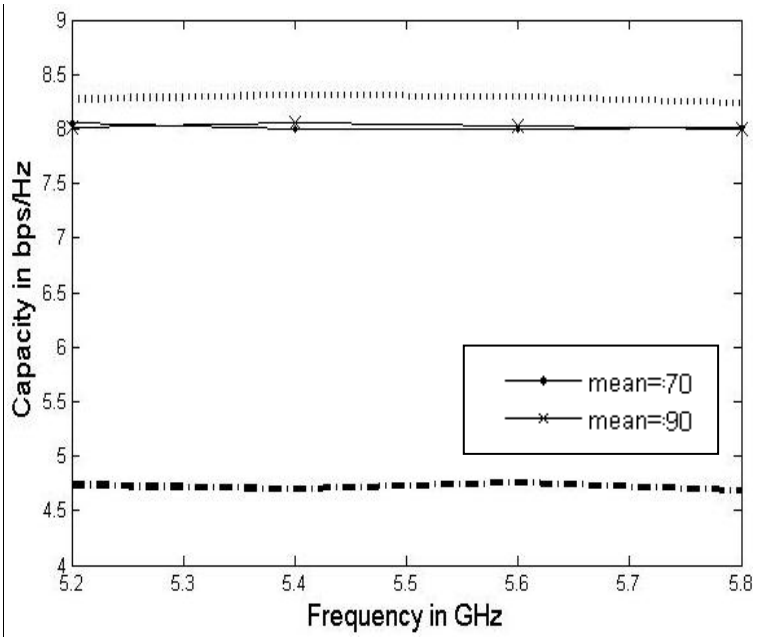

Figure 4.92: Variations of channel capacity versus operating frequency; subject to uniform PAS over 0 to 360° and raised cosine distribution power spectrum for various mean zenith angles of 70° and 90°; ('.....' upper limit of 3 × 3 MIMO), ('------'upper limit of 3 × 1 MIMO).

Figures 4.93 and 4.94 demonstrate the computed channel capacities using uniform PAS with n^{th} order raised cosine distribution along zenith angle for the bands 2.5 and 5.2GHz respectively. The maximum channel capacities are around 8 bps/Hz over the two bands, and these were 0.5 bps/Hz lower than that calculated in Figure 4.15 and 4.16. There was 0.1 bps/Hz maximum variations appear for the different values of n^{th} order raised cosine functions at 2.5 and 5.2GHz bands.

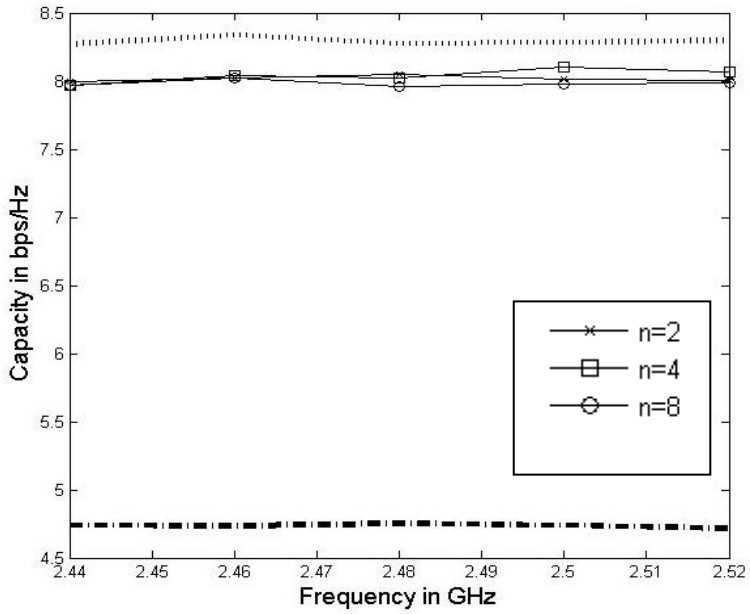

Figure 4.93: Variations of channel capacity versus operating frequency; subject to uniform PAS over 0 to 360° and n^{th} order raised cosine distribution power spectrum for mean zenith angle of 90°; ('.....' upper limit of 3 × 3 MIMO), ('------'upper limit of 3 × 1 MIMO).

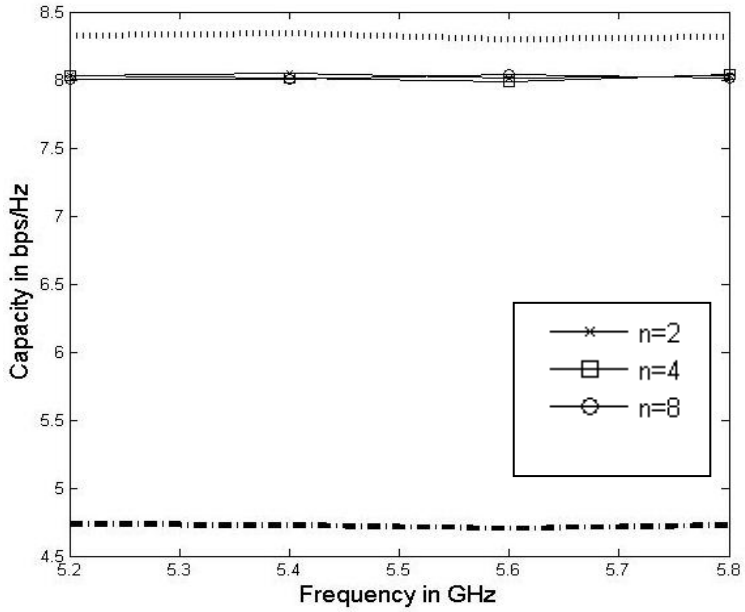

Figure 4.94: Variations of channel capacity versus operating frequency; subject to uniform PAS over 0 to 360° and n^{th} order raised cosine distribution power spectrum for mean zenith angle of 90°; ('.....' upper limit of 3 × 3 MIMO), ('------'upper limit of 3 × 1 MIMO).

Figures 4.95 to 4.104 show the channel capacity for 'half size' prototype using Gaussian PAS over 0 to 360° with different values of varinace in combination of uniform, raised cosine and n^{th} order raised cosine distribution along the zenith angle. The results alomost similar to that appeared in Section 4.4.1 in which the capcity values ranging from 6.5 bps/Hz to 8.1 bps/Hz.

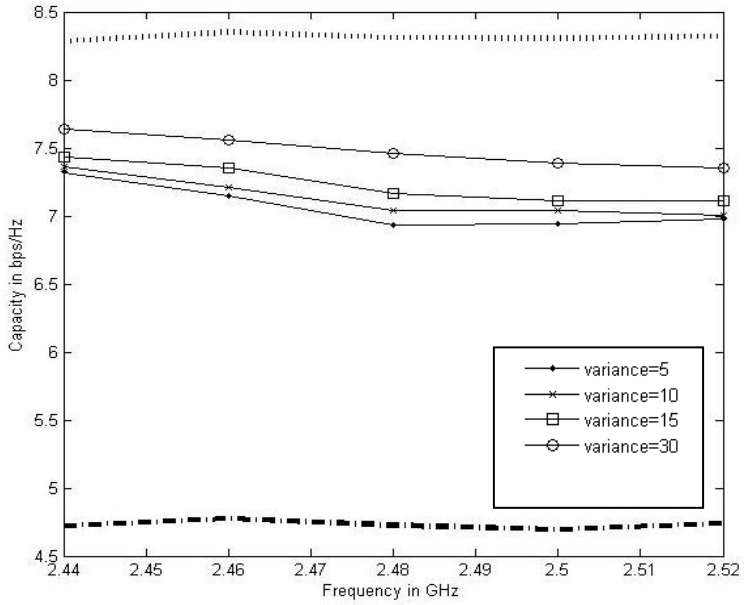

Figure 4.95: Variations of channel capacity versus operating frequency; subject to Gaussian PAS over 0 to 360° with mean 45° and different variances, and uniform power spectrum over ±15° for mean zenith angle of 90°; ('.....' upper limit of 3 × 3 MIMO), ('------'upper limit of 3 × 1 MIMO).

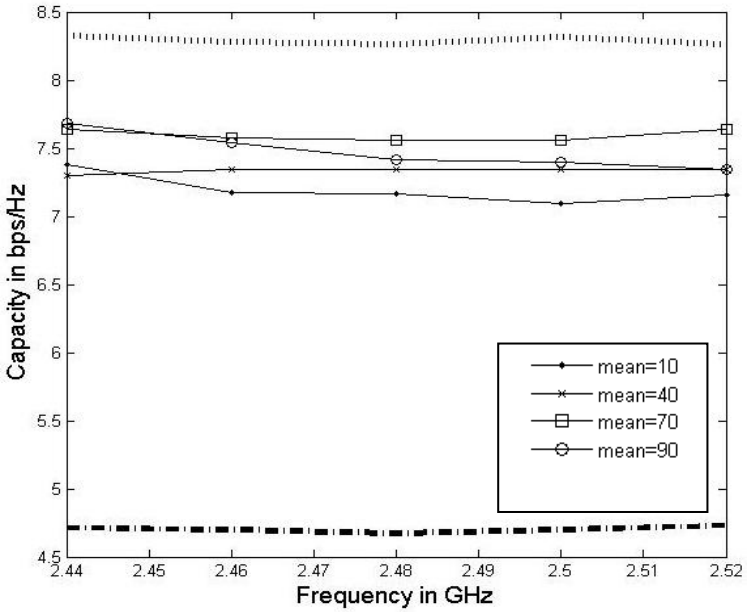

Figure 4.96: Variations of channel capacity versus operating frequency; subject to Gaussian PAS over 0 to 360° with mean 45° and uniform power spectrum over ±15° for various mean zenith angles of 10°, 40°, 70° and 90°; ('.....' upper limit of 3 × 3 MIMO), ('------'upper limit of 3 × 1 MIMO).

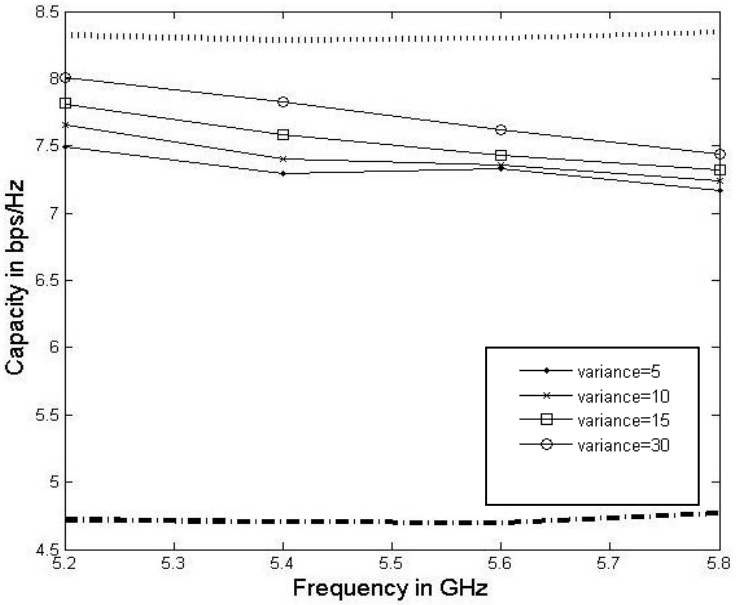

Figure 4.97: Variations of channel capacity versus operating frequency; subject to Gaussian PAS over 0 to 360° with mean 45° and different variances, and uniform power spectrum over ±15° for mean zenith angle of 90°; ('.....' upper limit of 3 × 3 MIMO), ('------'upper limit of 3 × 1 MIMO).

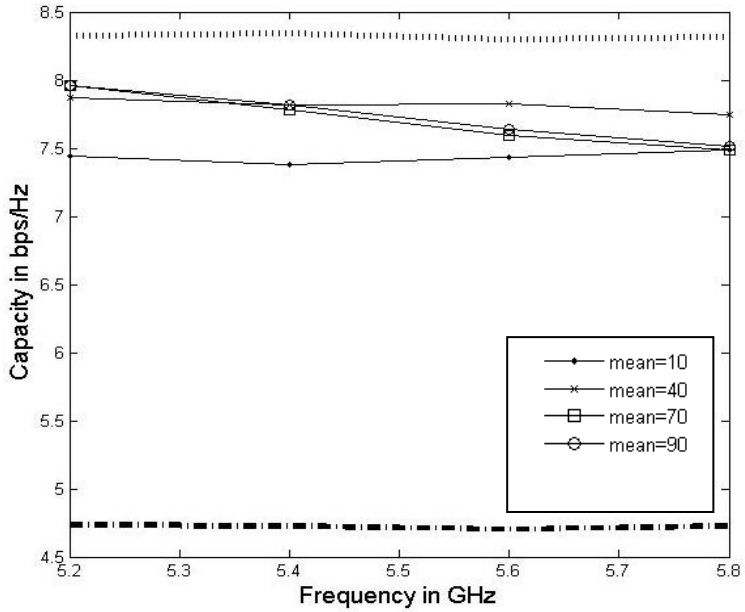

Figure 4.98: Variations of channel capacity versus operating frequency; subject to Gaussian PAS over 0 to 360° with mean 45° and uniform power spectrum over ±15° for various mean zenith angles of 10°, 40°, 70° and 90°; ('.....' upper limit of 3 × 3 MIMO), ('------'upper limit of 3 × 1 MIMO).

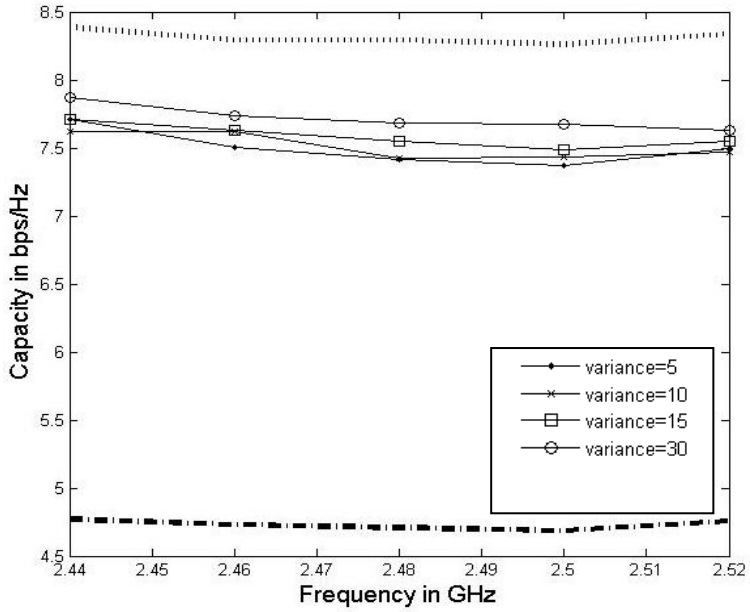

Figure 4.99: Variations of channel capacity versus operating frequency; subject to Gaussian PAS over 0 to 360° with mean 45° and different variances, and raised cosine distribution power spectrum with mean of 90°; ('.....' upper limit of 3 × 3 MIMO), ('-----'upper limit of 3 × 1 MIMO).

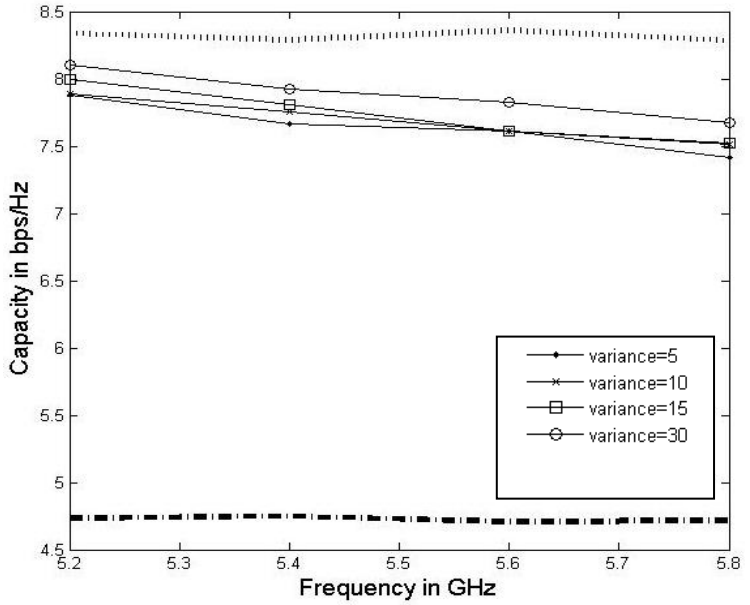

Figure 4.100: Variations of channel capacity versus operating frequency; subject to Gaussian PAS over 0 to 360° with mean 45° and different variances, and raised cosine distribution power spectrum with mean of 90°; ('.....' upper limit of 3 × 3 MIMO), ('-----'upper limit of 3 × 1 MIMO).

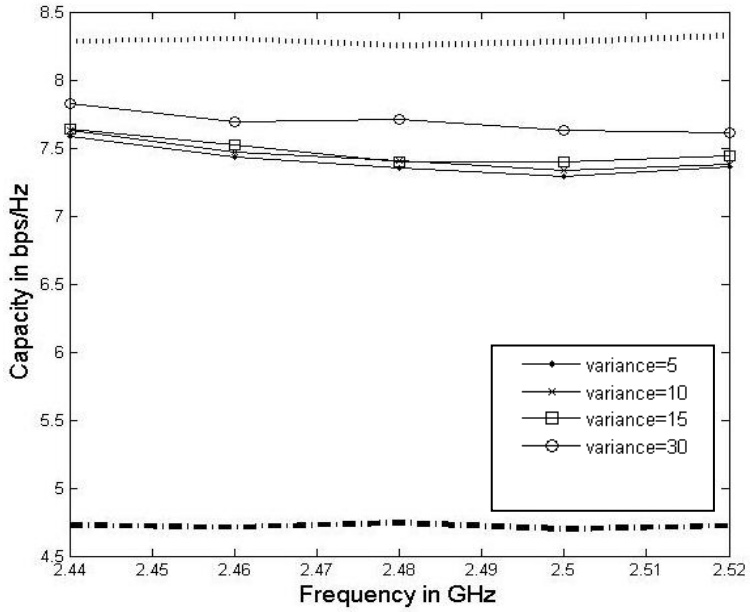

Figure 4.101: Variations of channel capacity versus operating frequency; subject to Gaussian PAS over 0 to 360° with mean 45° and different variances, and raised cosine distribution of 2nd order power spectrum with mean of 90°; ('.....' upper limit of 3 × 3 MIMO), ('------'upper limit of 3 × 1 MIMO).

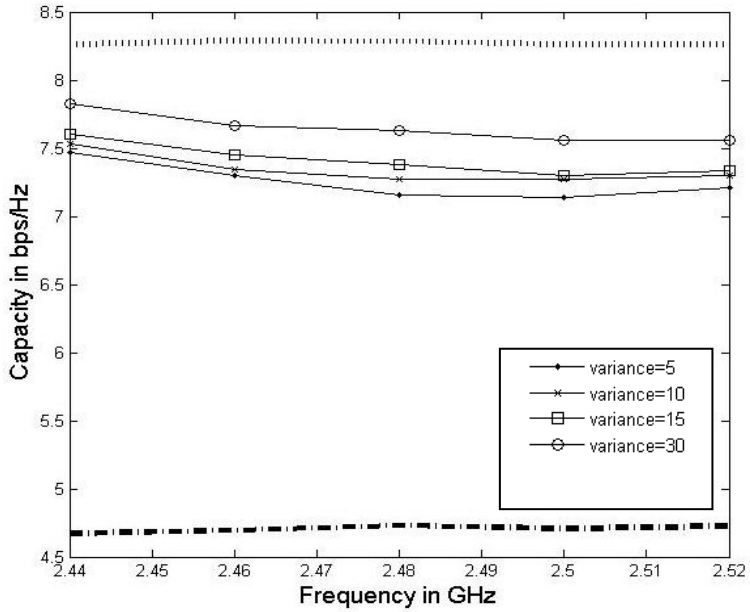

Figure 4.102: Variations of channel capacity versus operating frequency; subject to Gaussian PAS over 0 to 360° with mean 45° and different variances, and raised cosine distribution of 4th order power spectrum with mean of 90°; ('.....' upper limit of 3 × 3 MIMO), ('------'upper limit of 3 × 1 MIMO).

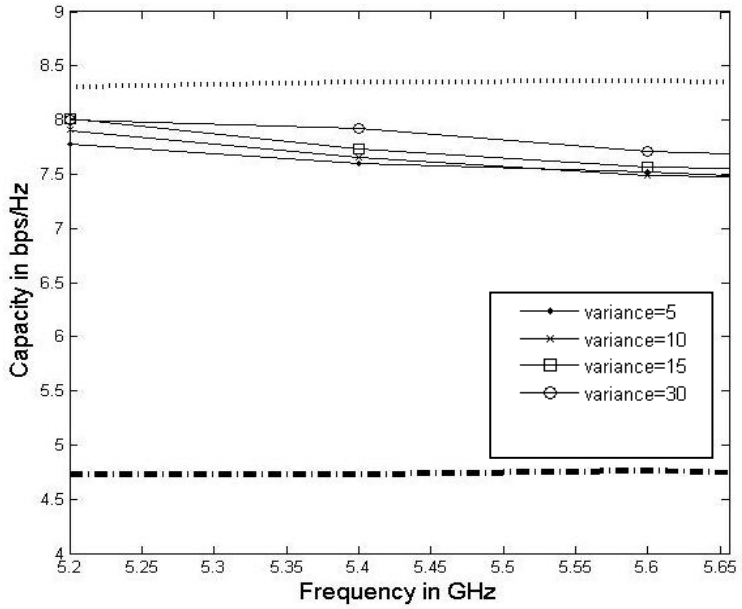

Figure 4.103: Variations of channel capacity versus operating frequency; subject to Gaussian PAS over 0 to 360° with mean 45° and different variances, and raised cosine distribution of 2nd order power spectrum with mean of 90°; ('.....' upper limit of 3 × 3 MIMO), ('------'upper limit of 3 × 1 MIMO).

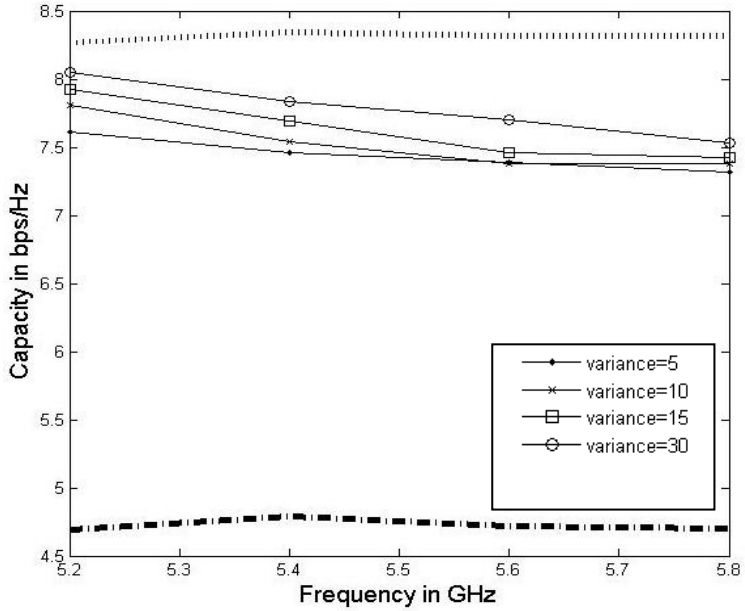

Figure 4.104: Variations of channel capacity versus operating frequency; subject to Gaussian PAS over 0 to 360° with mean 45° and different variances, and raised cosine distribution of 4th order power spectrum with mean of 90°; ('.....' upper limit of 3 × 3 MIMO), ('------'upper limit of 3 × 1 MIMO).

Similarly Figures 4.105 to 4.124 are showing the channel capacities using Laplacian and secant-squared PAS in combination with the uniform, raised cosine and n^{th} order raised cosine distribution along the zenith angle. The results were almost comparable to that observed for full size MIMO antenna handset shown in Section 4.4.1.

The mean channel capacities of the reduced size MIMO system for all cases considered are presented in Table 4.7. These values also show quite similar range to the values of the results summarised in Tables 4.4 and 4.5.

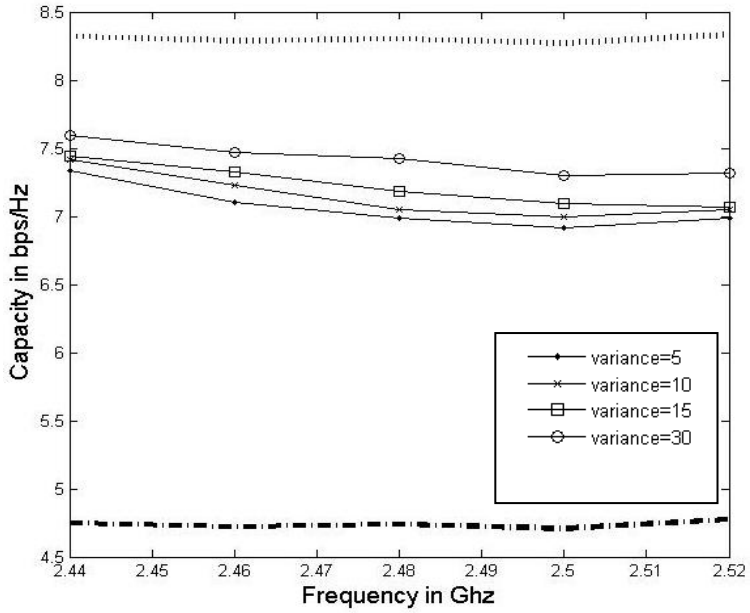

Figure 4.105: Variations of channel capacity versus operating frequency; subject to Laplacian PAS over 0 to 360° with mean 45° and different variances, and uniform power spectrum over ±15° for various mean zenith angle of 90°; ('.....' upper limit of 3 × 3 MIMO), ('------'upper limit of 3 × 1 MIMO).

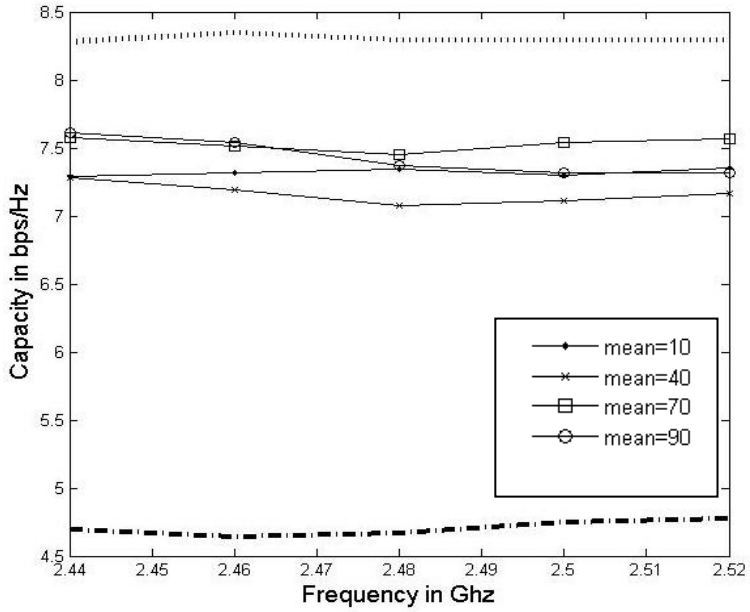

Figure 4.106: Variations of channel capacity versus operating frequency; subject to Laplacian PAS over 0 to 360° with mean 45° and variance 30°; and uniform power spectrum over ±15° for various mean zenith angles of 10°, 40°, 70° and 90°; ('.....' upper limit of 3× 3 MIMO), ('------'upper limit of 3 × 1 MIMO).

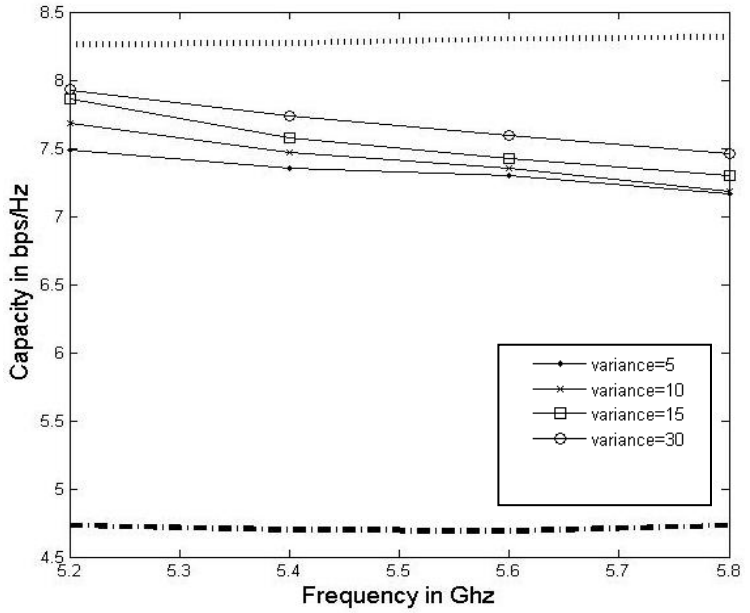

Figure 4.107: Variations of channel capacity versus operating frequency; subject to Laplacian PAS over 0 to 360° with mean 45° and different variances, and uniform power spectrum over ±15° for mean zenith angle of 90°; ('.....' upper limit of 3 × 3 MIMO), ('------'upper limit of 3 × 1 MIMO).

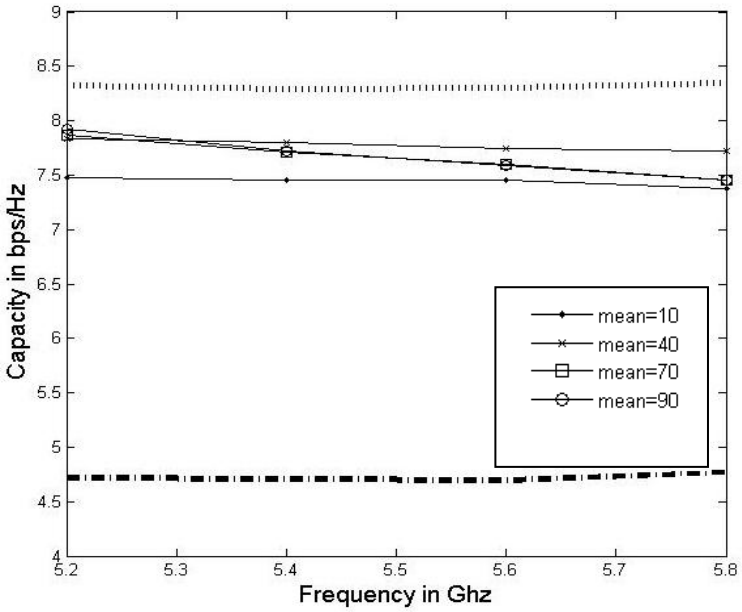

Figure 4.108: Variations of channel capacity versus operating frequency; subject to Laplacian PAS over 0 to 360° with mean 45° and variance 30°; and uniform power spectrum over ±15° for various mean zenith angles of 10°, 40°, 70° and 90°; ('.....' upper limit of 3× 3 MIMO), ('------'upper limit of 3 × 1 MIMO).

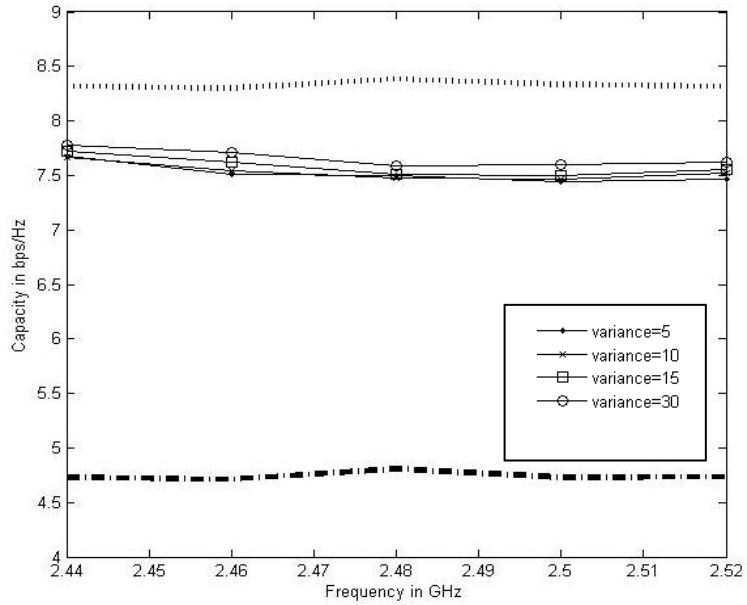

Figure 4.109: Variations of channel capacity versus operating frequency; subject to Laplacian PAS over 0 to 360° with mean 30° and different variances, and raised cosine distribution power spectrum with mean of 90°; ('.....' upper limit of 3 × 3 MIMO), ('------'upper limit of 3 × 1 MIMO).

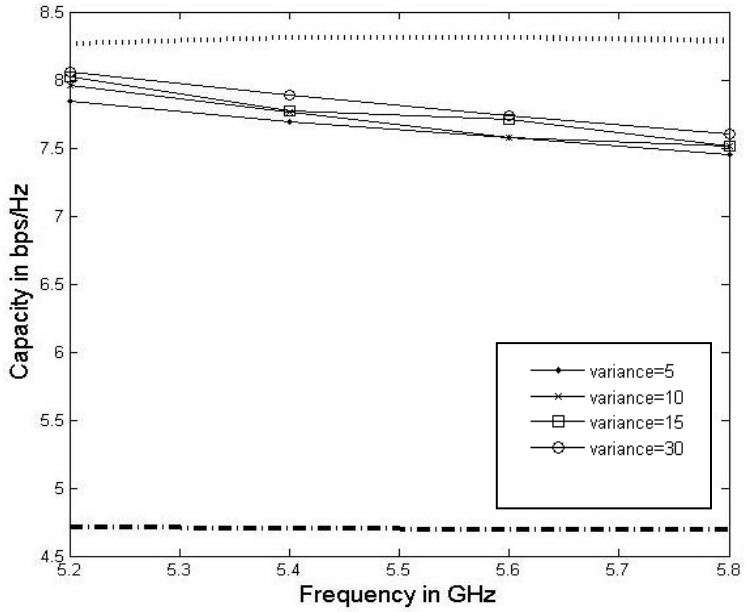

Figure 4.110: Variations of channel capacity versus operating frequency; subject to Laplacian PAS over 0 to 360° with mean 30° and different variances, and raised cosine distribution power spectrum with mean of 90°; ('.....' upper limit of 3 × 3 MIMO), ('-----'upper limit of 3 × 1 MIMO).

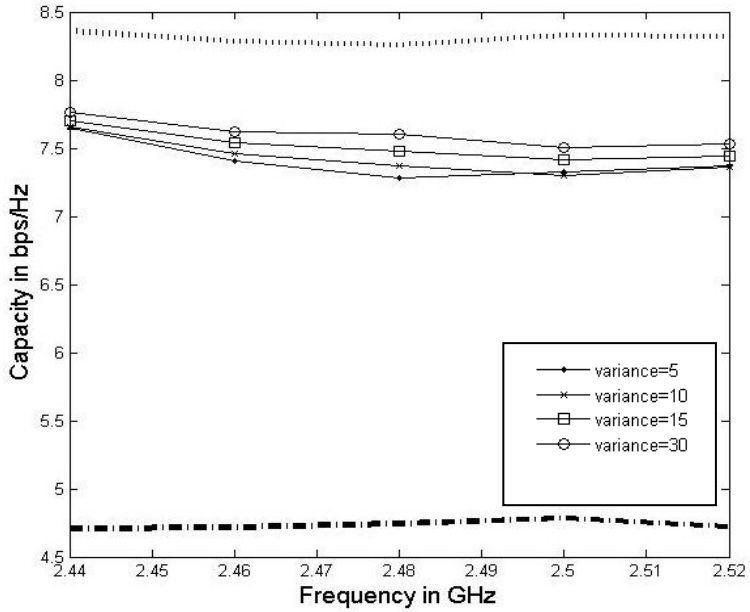

Figure 4.111: Variations of channel capacity versus operating frequency; subject to Laplacian PAS over 0 to 360° with mean 45° and different variances; and raised cosine distribution of 2nd order power spectrum with mean of 90°; ('.....' upper limit of 3 × 3 MIMO), ('------'upper limit of 3 × 1 MIMO).

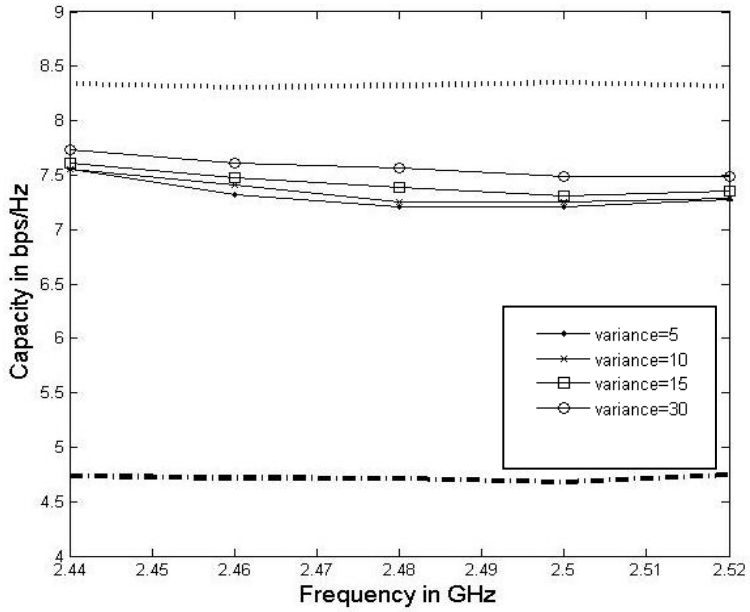

Figure 4.112: Variations of channel capacity versus operating frequency; subject to Laplacian PAS over 0 to 360° with mean 45° and different variances; and raised cosine distribution of 4th order power spectrum with mean of 90°; ('.....' upper limit of 3 × 3 MIMO), ('------'upper limit of 3 × 1 MIMO).

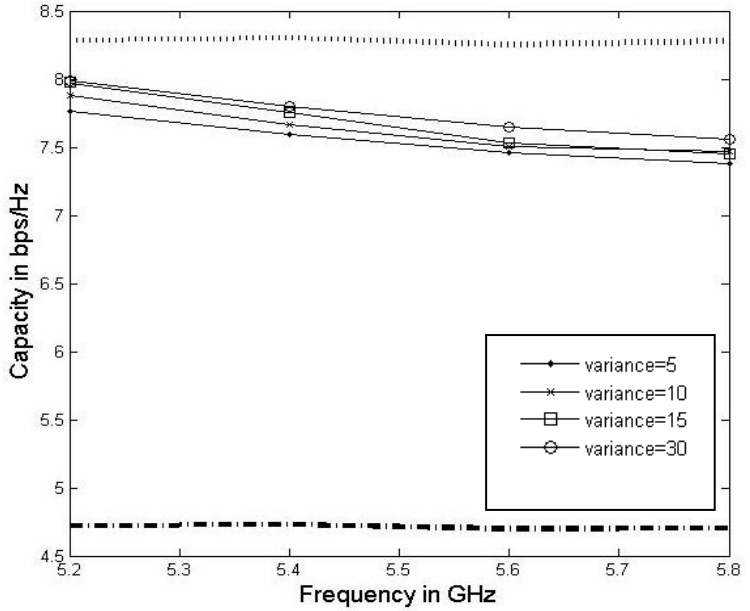

Figure 4.113: Variations of channel capacity versus operating frequency; subject to Laplacian PAS over 0 to 360° with mean 45° and different variances; and raised cosine distribution of 2nd order power spectrum with mean of 90°; ('.....' upper limit of 3 × 3 MIMO), ('------'upper limit of 3 × 1 MIMO).

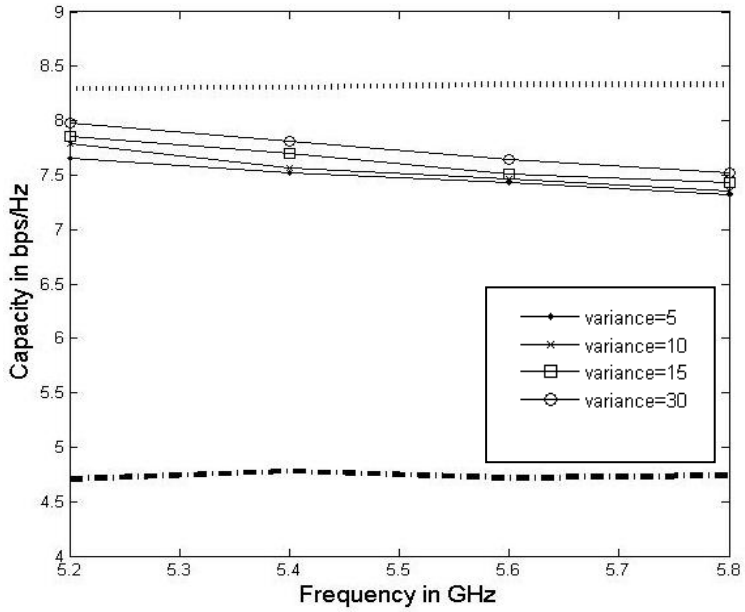

Figure 4.114: Variations of channel capacity versus operating frequency; subject to Laplacian PAS over 0 to 360° with mean 45° and different variances; and raised cosine distribution of 4th order power spectrum with mean of 90°; ('.....' upper limit of 3 × 3 MIMO), ('------'upper limit of 3 × 1 MIMO).

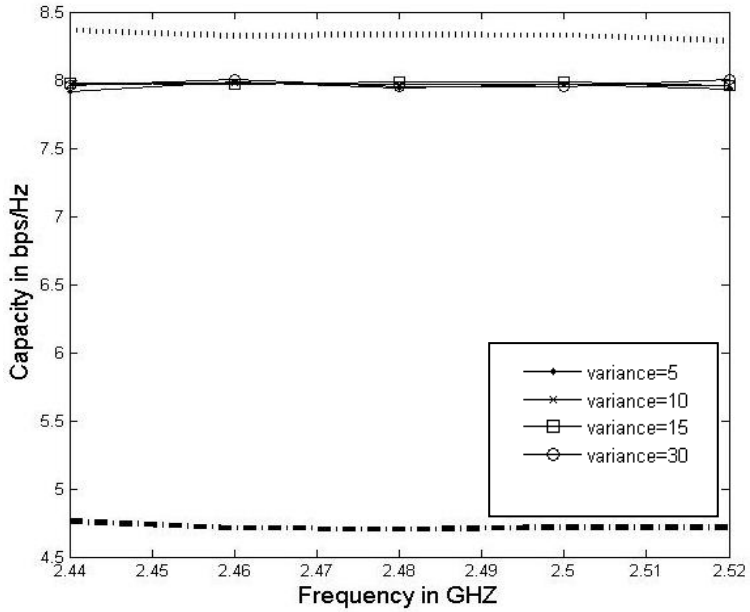

Figure 4.115: Variations of channel capacity versus operating frequency; subject to Secant Square PAS over 0 to 360° with mean 45° and different variances, and uniform power spectrum over ±15° for various mean zenith angle of 90°; ('.....' upper limit of 3× 3 MIMO), ('------'upper limit of 3 × 1 MIMO).

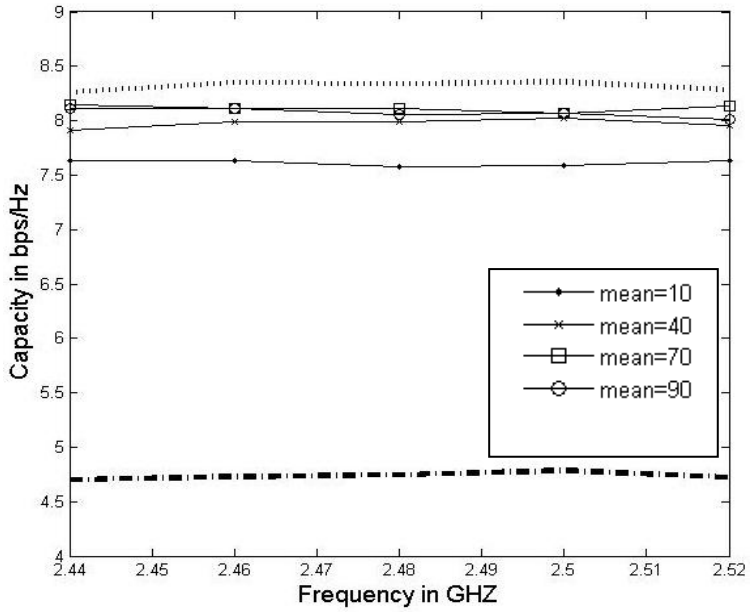

Figure 4.116: Variations of channel capacity versus operating frequency; subject to Secant Square PAS over 0 to 360° with mean 45° and uniform power spectrum over ±15° for various mean zenith angles of 10°, 40°, 70° and 90°; ('.....' upper limit of 3 × 3 MIMO), ('------'upper limit of 3 × 1 MIMO).

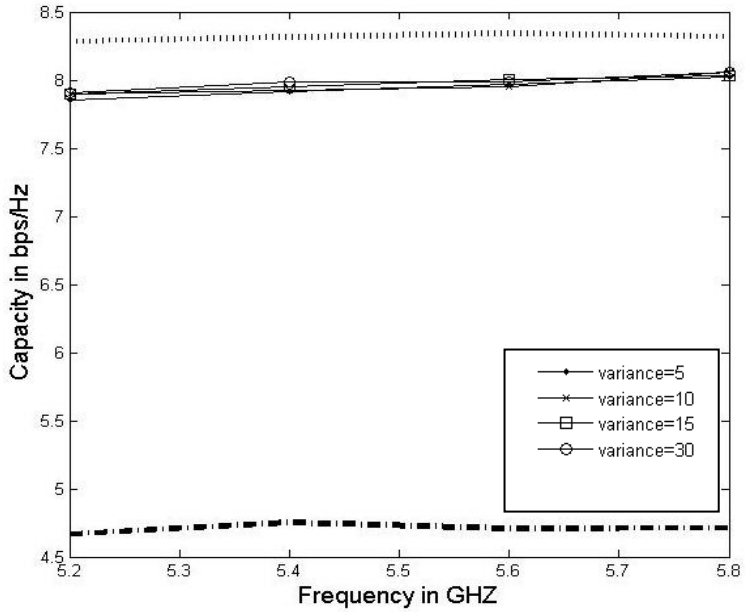

Figure 4.117: Variations of channel capacity versus operating frequency; subject to Secant Square PAS over 0 to 360° with mean 45° and different variances, and uniform power spectrum over ±15° for mean zenith angle of 90°; ('.....' upper limit of 3 × 3 MIMO), ('------'upper limit of 3 × 1 MIMO).

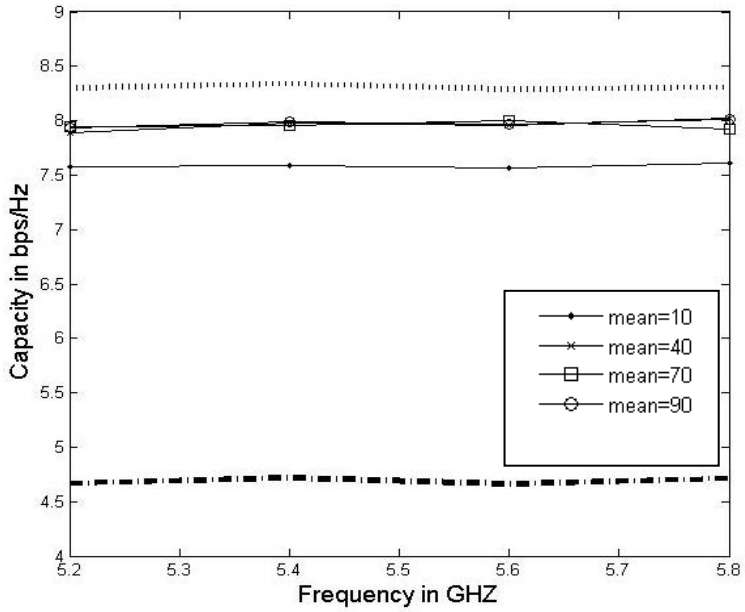

Figure 4.118: Variations of channel capacity versus operating frequency; subject to Secant Square PAS over 0 to 360° with mean 45° and uniform power spectrum over ±15° for various mean zenith angles of 10°, 40°, 70° and 90°; ('.....' upper limit of 3 × 3 MIMO), ('------'upper limit of 3 × 1 MIMO).

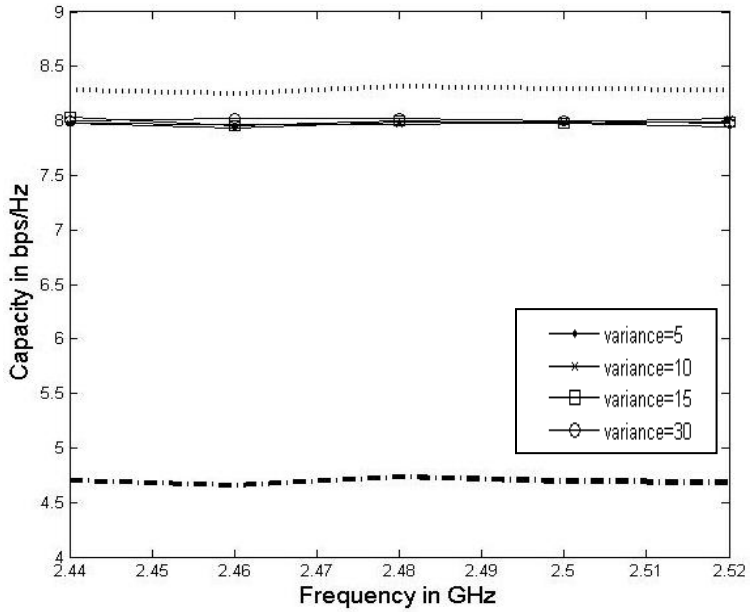

Figure 4.119: Variations of channel capacity versus operating frequency; subject to Secant Square PAS over 0 to 360° with mean 45° and different variances, and raised cosine distribution power spectrum with mean of 90°; ('.....' upper limit of 3 × 3 MIMO), ('------'upper limit of 3 × 1 MIMO).

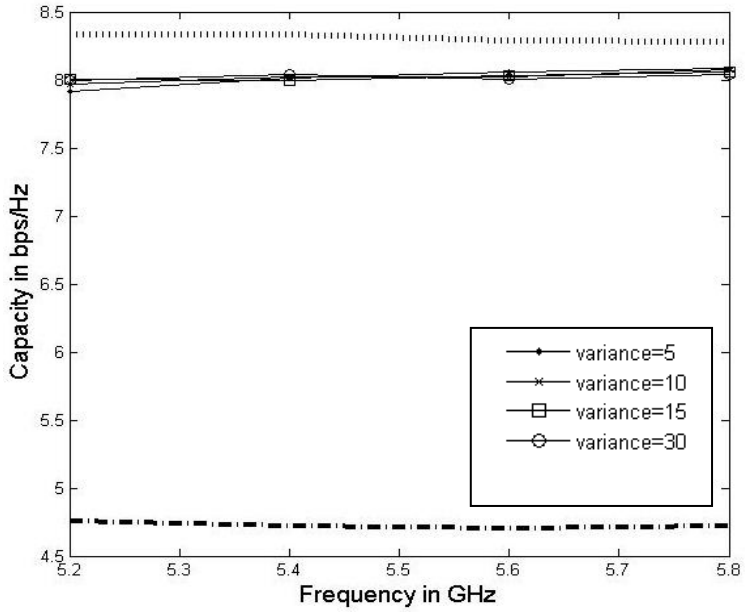

Figure 4.120: Variations of channel capacity versus operating frequency; subject to Secant Square PAS over 0 to 360° with mean 45° and different variances, and raised cosine distribution power spectrum with mean of 90°; ('.....' upper limit of 3 × 3 MIMO), ('------'upper limit of 3 × 1 MIMO).

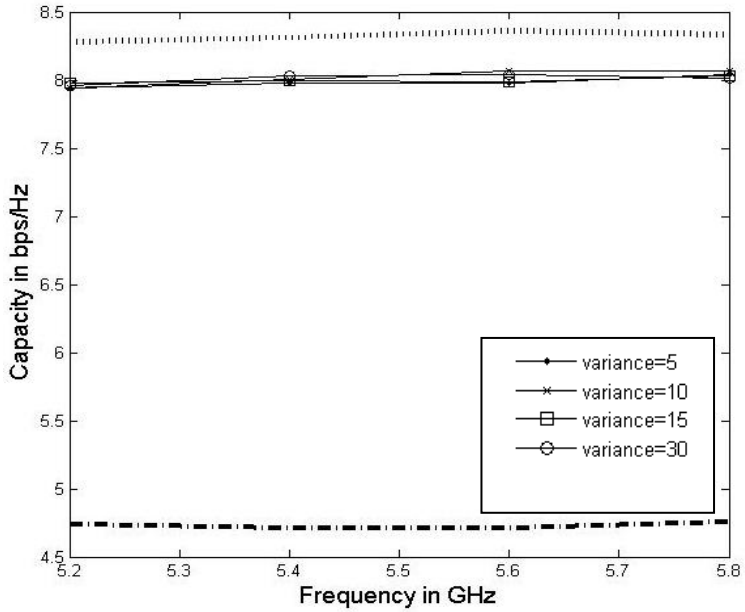

Figure 4.121: Variations of channel capacity versus operating frequency; subject to Secant Square PAS over 0 to 360° with mean 45° and different variances; and raised cosine distribution of 2nd order power spectrum with mean of 90°; ('.....' upper limit of 3 × 3 MIMO), ('------'upper limit of 3 × 1 MIMO).

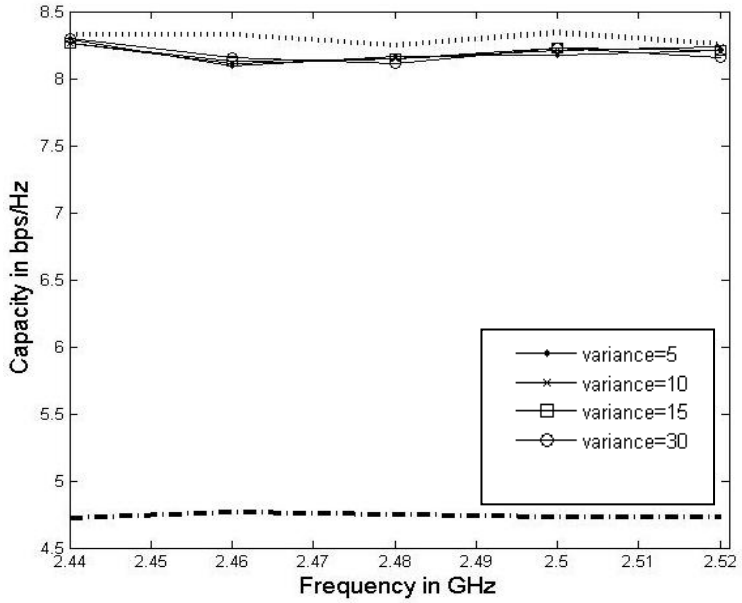

Figure 4.122: Variations of channel capacity versus operating frequency; subject to Secant Square PAS over 0 to 360° with mean 45° and different variances; and raised cosine distribution of 4th order power spectrum with mean of 90°; ('.....' upper limit of 3 × 3 MIMO), ('------'upper limit of 3 × 1 MIMO).

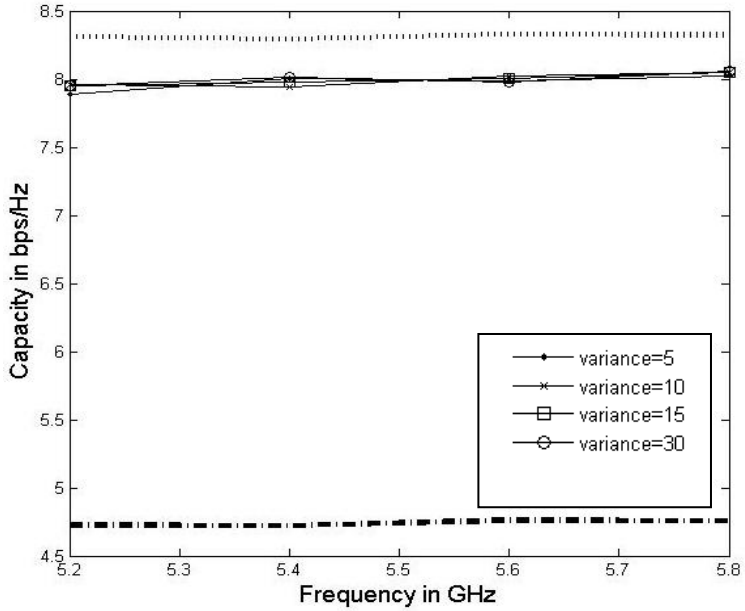

Figure 4.123: Variations of channel capacity versus operating frequency; subject to Secant Square PAS over 0 to 360° with mean 45° and different variances; and raised cosine distribution of 2nd order power spectrum with mean of 90°; ('.....' upper limit of 3 × 3 MIMO), ('------'upper limit of 3 × 1 MIMO).

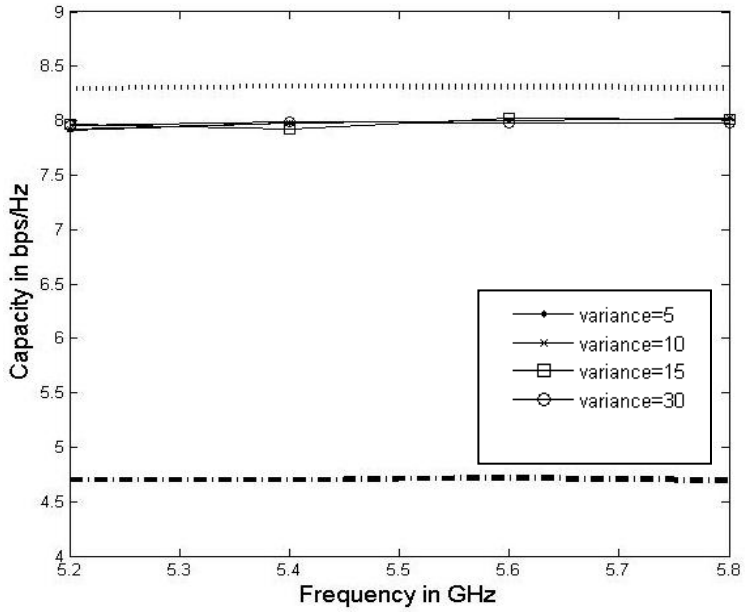

Figure 4.124: Variations of channel capacity versus operating frequency; subject to Secant Square PAS over 0 to 360° with mean 45° and different variances; and raised cosine distribution of 4th order power spectrum with mean of 90°; ('.....' upper limit of 3 × 3 MIMO), ('------'upper limit of 3 × 1 MIMO).

Table 4.7: Summarised channel capacity of the antenna geometry shown in Fig. 4.86.

Power Distributions		**Mean of Calculated Channel Capacity (Bps/Hz)**	
Azimuth	**Elevation**	**2.44 to 2.52 GHz**	**5.2 to 5.8 GHz**
Uniform	Uniform	7.81	7.75
Uniform	Raised Cosine	8.04	8.25
Uniform	n^{th} Order raised Cosine	8.05	8.03
Gaussian	Uniform	7.42	7.62
Gaussian	Raised Cosine	7.72	7.93
Gaussian	2^{nd} Order raised Cosine	7.65	7.82
Gaussian	4^{th} Order raised Cosine	7.63	7.83
Laplacian	Uniform	7.45	7.78
Laplacian	Raised Cosine	7.58	7.82
Laplacian	2^{nd} Order raised Cosine	7.72	7.85
Laplacian	4^{th} Order raised Cosine	7.61	7.75
Secant Square	Uniform	7.94	7.98
Secant Square	Raised Cosine	7.81	8.04
Secant Square	2^{nd} Order raised Cosine	7.83	8.06
Secant Square	4^{th} Order raised Cosine	8.25	8.02

4.5.4 Radiation Patterns

Figures 4.125 – 4.127 show the principal plane radiation patterns for E_θ and E_ϕ in the xy-planes and xz-planes for each radiator in the 'half size' 3×3 prototype design, for each dual band resonance. The radiation patterns of the three radiating elements show a reasonable field diversity to contribute towards a suitable RX/TX capacity. The

maximum power gain for both horizontal and vertical components were varied between the 0.1 to 4.1 for 2.5 GHz band and 1.2 to 5.6 at 5.2 GHz band. The radiation patterns were almost covering a solid angle at the 2.5 and 5.2GHz operating frequencies.

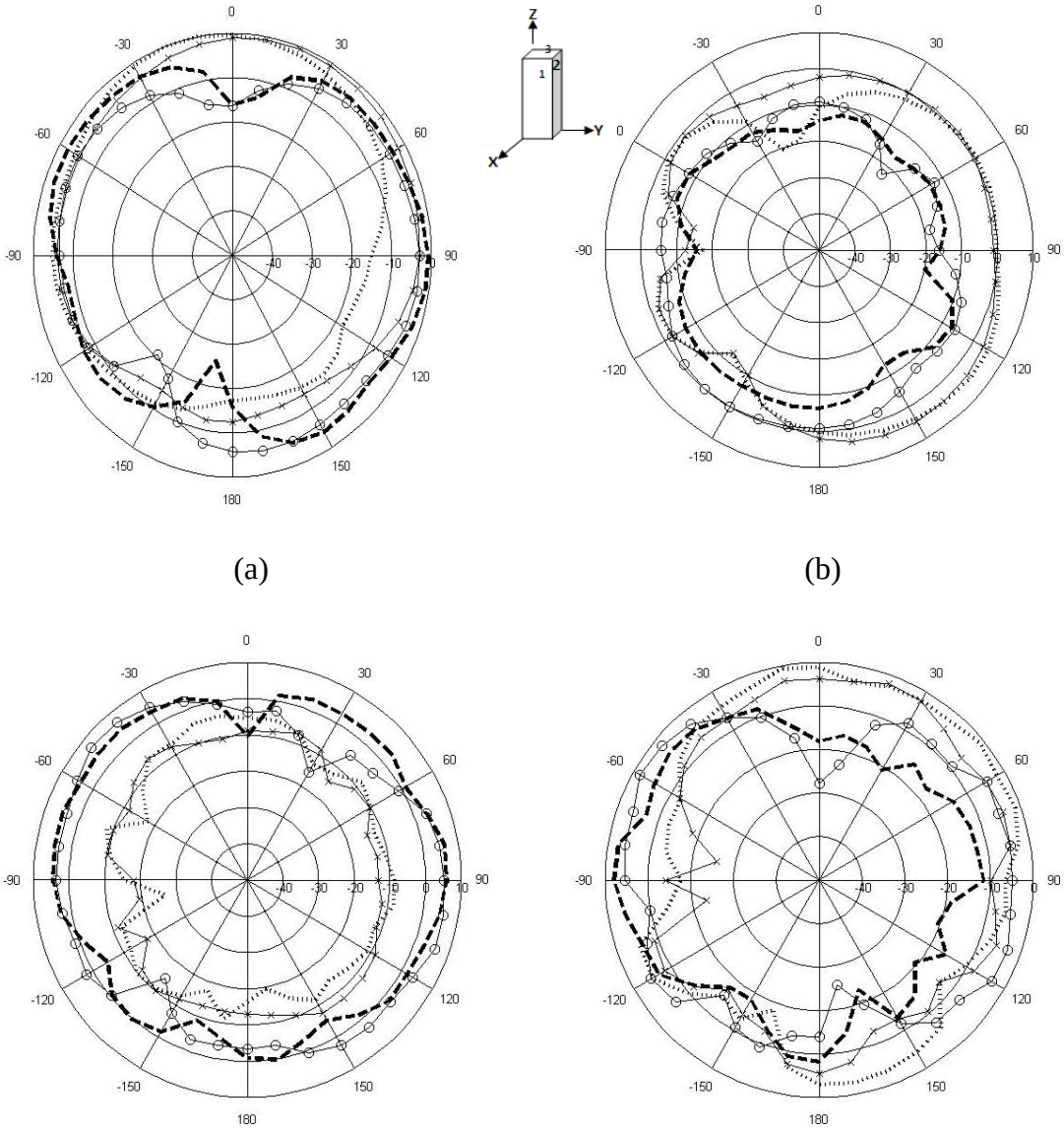

(a) (b)

(c) (d)

Figure 4.125: Radiation pattern of antenna element 1 for two different cuts; (a) θ=90, Φ=0-360, at 2.5 GHz; (b) θ=0-360, Φ=0 at 2.5 GHz; (c) θ=90, Φ=0-360, at 5.2 GHz; (d) θ=0-360, Φ=0 at 5.2 GHz; (‘ooo’ Half Antenna Size E_{Φ}, ’xxx’ Half Antenna Size E_{θ}, ’-----’ Full Antenna Size E_{Φ}, ‘…...’ Full Antenna Size E_{θ})

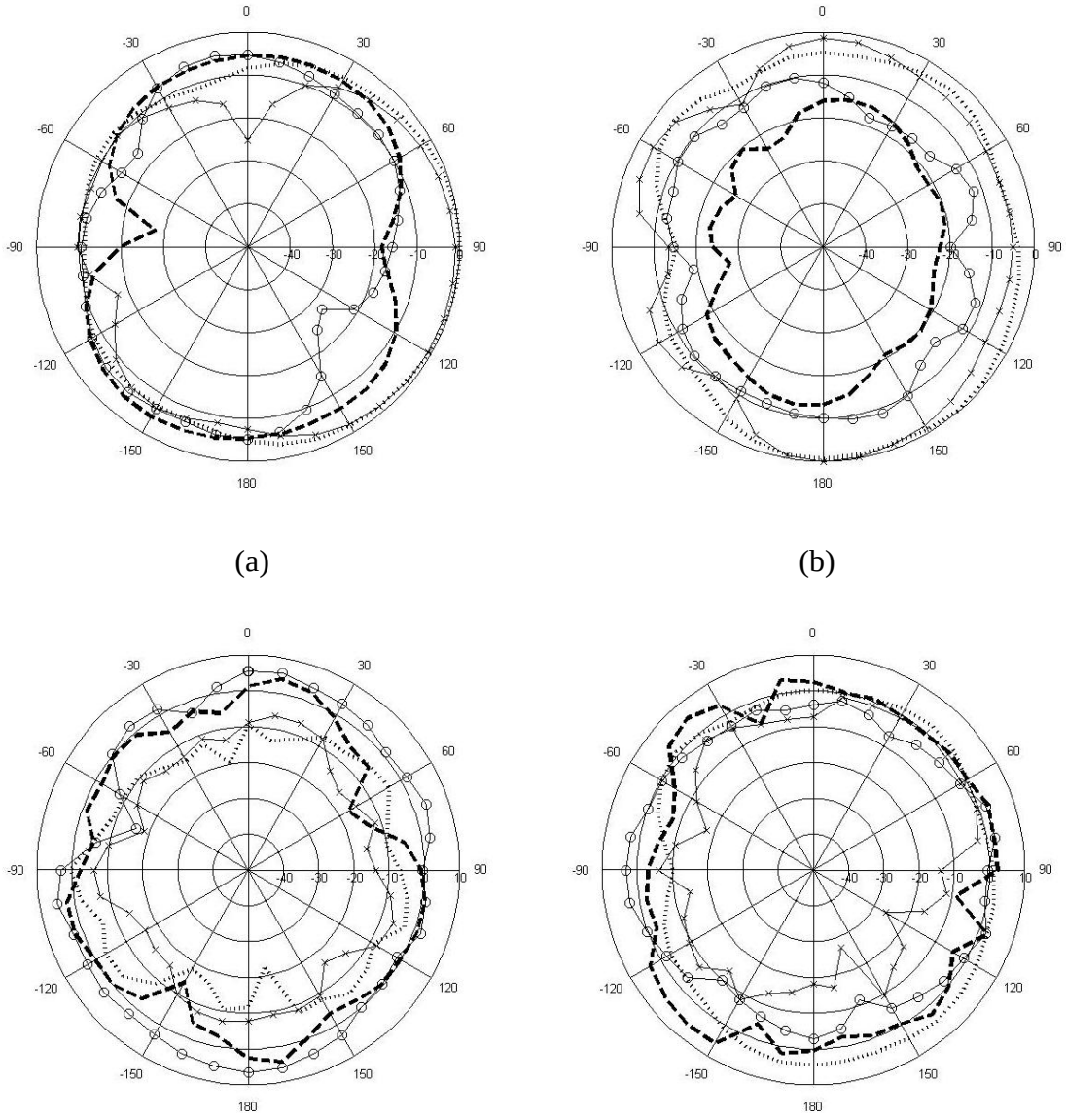

Figure 4.126: Radiation pattern of antenna element 2 for two different cuts; (a) θ=90, Φ=0-360, at 2.5 GHz; (b) θ=0-360, Φ=90 at 2.5 GHz; (c) θ=90, Φ=0-360, at 5.2 GHz; (d) θ=0-360, Φ=90 at 5.2 GHz; ('ooo' Half Antenna Size E_{Φ}, 'xxx' Half Antenna Size E_{θ}, '-----' Full Antenna Size E_{Φ}, '…...' Full Antenna Size E_{θ})

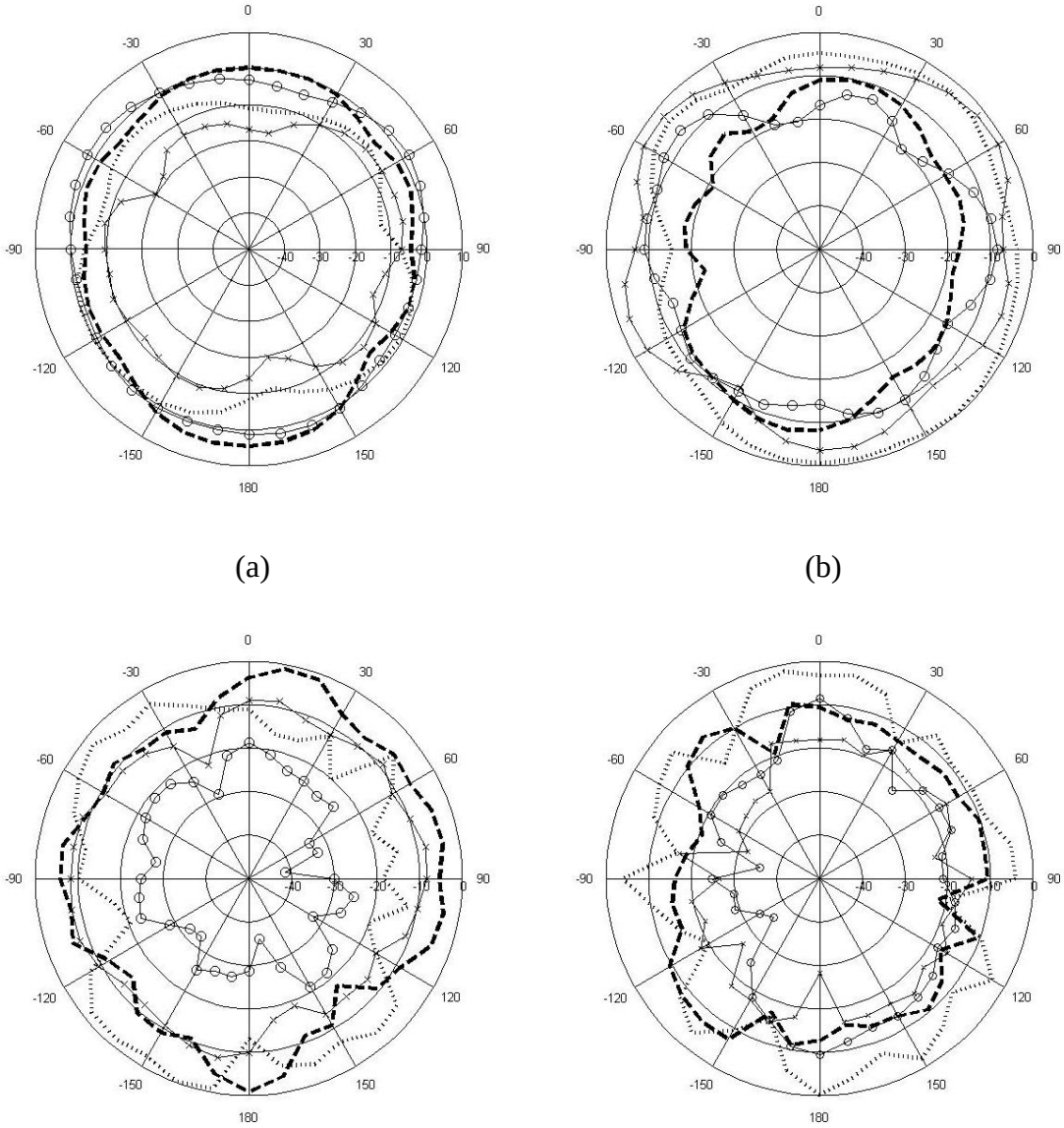

(a) (b)

(c) (d)

Figure 4.127: Radiation pattern of antenna element 3 for two different cuts; (a) θ=0-360, Φ=0, at 2.5 GHz; (b) θ=0-360, Φ=90 at 2.5 GHz; (c) θ=0-360, Φ=0, at 5.2 GHz; (d) θ=0-360, Φ=90 at 5.2 GHz; ('ooo' Half Antenna Size E_{Φ}, 'xxx' Half Antenna Size E_{θ}, '-----' Full Antenna Size E_{Φ}, '…...' Full Antenna Size E_{θ})

4.6 CONCLUSION

In this chapter the design and characterisation of dual band PIF(L)A (planar inverted F & L antenna) radiators has been presented; and the feasibility of using such antennas within a prototype multi-antenna module for future MIMO mobile terminal applications has been reviewed. The system performance relies on the multi-polarisation diversity inherent in the multi-path (i.e. mobile) environment, rather than the more traditional AOA approach. Through balancing the size and bandwidth constraints, a set of antennas are proposed with suitably dimensioned structural parameters which make the best use of the small surface area available on the terminal's chassis, whilst meeting the antenna air-interface requirements for IEEE 802.11 a/b/g/n mobile terminal operations.

It has been found that the working channel capacity in each of the operating bands almost equalled the ideal (i.e. coupling free) MIMO system capacity, based on AOA diversity. However, this would require an unfeasibly bulky antenna module. This motivated the study of a more favourable reduced size PIF(L)A for the 3×3 MIMO case, this modified prototype was 50% smaller (derived from a magnetic symmetry operation), and its performance was compared vs. the full size prototype module. Similar results, and system performance, were found for both devices. This suggests that these designs are useful candidates for mobile terminal MIMO applications.

4.7 REFERENCES

[1] L. Dong, H. Choo, R. W. Heath and H. Ling, "Simulation of MIMO Channel Capacity with Antenna Polarization Diversity", IEEE Transactions on Wireless Communications, vol. 4, no. 4, July 2005, pp. 1869-1873.

[2] J. H. Winters, J. Salz, and R. D. Gitlin, “The impact of antenna diversity on the capacity of wireless communication systems,” IEEE Trans. Commun., vol. 42, pp. 1740–1751, Feb. 1994.

[3] M. R. Andrews, P. P. Mitra and R. de Carvalho, “Tripling the capacity of wireless communications using electromagnetic polarization”, Nature, vol. 409, no. 6818, pp. 316–318, Jan. 2001.

[4] T. Svantesson, “On capacity and correlation of multi-antenna systems employing multiple polarizations”, in IEEE Int. Antennas Propagation Symp. Digest, San Antonio, TX, Jun. 2002, pp. 202–205.

[5] D. D. Stancil, A. Berson, J. P. Van’t Hof, R. Negi, S. Sheth and P. Patel, “Doubling wireless channel capacity using co-polarised, co-located electric and magnetic dipoles”, Electron. Lett., vol. 38, no. 14, pp. 746–747, Jul. 2002.

[6] J. B. Andersen and B. N. Getu, “The MIMO cube—A compact MIMO antenna”, in 5th Int. Symp. Wireless Personal Multimedia communications, Honolulu, HI, Oct. 2002, pp. 112–114.

[7] H. Xu, M. J. Gans, N. Amitay and R. A. Valenzuela, “Experimental verification of MTMR system capacity in controlled propagation environment”, Electron. Lett., vol. 37, no. 15, pp. 936–937, Jul. 2001.

[8] C. Soras, M. Karaboikis, M. Tsachtsiris, G. Makios, “Analysis and design of an inverted-F antenna printed on a PCMCIA card for the 2.4 GHz ISM band”, Antennas and Propagation Magazine, IEEE, Volume: 44 (1) , pp: 37-44, Feb 2002 .

[9] T. Itoh, Y. Murakami; S. Sekine, and H. Shoki, “A wideband inverted F-type antenna for dual-frequency operation”, Antennas and Propagation Society International Symposium, 2002. IEEE, Volume: 4, pp: 512- 515, 2002.

[10] L. Pazin, N. Telzhensky, and Y. Leviatan, “Multiband Flat-Plate Inverted-F Antenna for Wi-Fi/WiMAX Operation”, Antennas and Wireless Propagation Letters, IEEE, Volume 7, pp: 197-200, 2008.

[11] B. T. Jiang and J. F. Mao, “Design of an PIFA-IFA-monopole in dual-SIM mobile phone for GSM/DCS/Bluetooth operations”, Microwave and Millimeter Wave Technology, 2008. ICMMT 2008. International Conference on 21-24 April 2008, Volume: 3, pp: 1050-1053.

[12] Pey-Ling Teng, Shyh-Tirng Fang, Kin-Lu Wong, “PIFA with a bent, meandered radiating arm for GSM/DCS dual-band operation”, Antennas and Propagation Society International Symposium, 2003. IEEE, Volume: 3, pp: 107-110, 22-27 June 2003.

[13] M-C. Huynh and W. Stutzman, “Ground plane effects on planar inverted-F antenna (PIFA) performance”, Microwaves, Antennas and Propagation, IEEE Proceedings, Volume: 150, Issue: 4, pp: 209- 213, 8 Aug. 2003.

[14] Yu-Shin Wang, Ming-Chou Lee and Shyh-Jong Chung, “Two PIFA-Related Miniaturized Dual-Band Antennas”, Antennas and Propagation, IEEE Transactions, Volume: 55 Issue: 3, Part=2, Page(s): 805-811, March 2007.

[15] Yue Gao, Xiaodong Chen, Zhinong Ying and C. Parini, “Design and Performance Investigation of a Dual-Element PIFA Array at 2.5 GHz for MIMO

Terminal", Antennas and Propagation, IEEE Transactions, Volume: 55 Issue: 12, pp: 3433-3441, Dec. 2007.

[16] Il-Young Oh; Sang-Hyuk Wi; Yongshik Lee and Jong-Gwan Yook, "Bandwidth property of folded planar inverted-F antennas", Antennas and Propagation Society International Symposium, pp: 1-4, 5-11 July 2008.

[17] Cheng-Tse Lee and Kin-Lu Wong, "Uniplanar Printed Coupled-Fed PIFA With a Band-Notching Slit for WLAN/WiMAX Operation in the Laptop Computer", Antennas and Propagation, IEEE Transactions, Volume: 57 Issue: 4 Part=2, pp: 1252-1258, April 2009.

[18] C. H. See, R. A. Abd-Alhameed, D. W. Zhou and P. S. Excell, "Dual-Frequency Planar F-L Antenna (PIFLA) for WLAN and Short Range Communication Systems", IEEE Trans. On Antennas and Propag., Oct 2008, vol.56, pp.3318-3320.

[19] The High Frequency Structure Simulator (HFSS^{TM} Version 11) Users Manual, AnsoftCorportation, Pittsburgh (USA), http://www.ansoft.com/products/hf/hfss/, (part of theANSYS Group).

[20] Teruo Onishi and Shinji Uebayashi, "Biological Tissue-Equivalent Phantoms Usable in Broadband Frequency Range", NTT DOCOMO Technical Journal Vol.7 No.4, pp. 61-65, March 2006.

[21] A.K. Skrivervik, J.-F. Zurcher, O. Staub, and J.R. Mosig, "PCS Antenna Design: The Challenge of Miniaturization", IEEE Antennas and Propagation Magazine, vol. 43, pp. 12, 27, August 2001.

[22] C.S. Lee and K-H. Tseng, “Size reduction of microstrip antennas”, Electron. Lett., Vol. 37, pp.1274-1275, 2001.

[23] K. Shackelford, K. F. Lee, and K. M. Luk, “Design of small-size wideband widthmicrostrip-patch antennas”, IEEE Antennas Propag. Mag., vol. 45, no. 1, pp. 75–83, Feb. 2003.

[24] A. A. Deshmukh and G. Kumar, “Half U-slot loaded rectangular microstrip antenna”, in IEEE AP-S Int. Symp. USNC/CNC/URSI National Radio Science Meeting, vol. 2, 2003, pp. 876–879.

[25] R. Chair, C-L. Mak, K-F. Lee, K-M. Luk and A.A. Kishk, “Miniature Wide-Band Half U-Slot and Half E-Shaped Patch Antennas”, IEEE Transactions on AP, Vol.53, No.8, pp.2645 2651 August 2008.

[26] L. Guo, S. Wang, X. Chen and C. Parini, “Miniaturised Antennas for UWBCommunications”, in Proceeding of Eucap2009, 23-27 March, Berlin Germany, pp-3774 3778

[27] M. Usman, R.A. Abd-Alhameed, Peter. S. Excell, “Dual Band Three Antenna Polarisation Diverse MIMO System for Mobile Devices”, Proceedings of 3rd International Conference on Internet Technologies and Applications, 8th – 11th Sep, 2009, Glyndŵr University, Wrexham, Wales, UK. ISBN: 978-0-946881-65-9.

[28] H. Nakano, N. Ikeda, Y-Y. Wu, R. Suzuki, H. Mimaka and J. Yamauchi, “Realization of Dual-Frequency and Wide-Band VSWR Performances Using Normal-Mode Helical and Inverted-F Antenna”, IEEE Trans. On Antennas and Propagation, vol.46, pp.788-793, June 1998.

[29] R. Feick, H. Carrasco, M. Olmos and H.D. Hristov, “PIFA input bandwidth enhancement by changing feed plate silhouette”, Electronics Letters, vol.40, pp.921-922, July 2004.

CHAPTER 5

DUAL-BAND BALANCED MIMO ANTENNA SYSTEM FOR MOBILE PHONES

5.1 INTRODUCTION

In recent years, balanced antennas have formed a major trend in mobile antenna designs, due in part because of their stable performance when held adjacent to the user's body [1-4]. In such an antenna, balanced currents only flow on the radiator, thus dramatically reducing the effect of current flow over the ground plane (chassis).

Dipoles and loops are the most common balanced antennas, although meander-line, helical and microstrip forms are also possible. In earlier research [5-9], it has been demonstrated that the folded dipole and loop antennas produce small induced currents on the ground plane, together with stable radiation performance and low SAR. There is a possible drawback, in that the lack of impedance bandwidth with respect to frequency coverage in many of the common mobile bands. Some novel techniques have been proposed for the enhancement of impedance bandwidth for balanced antennas. For example, a genetic algorithm technique has been implemented to improve the impedance bandwidth and wider bandwidth for the folded loop antenna system has been

obtained by performing a parametric study on the length and width of strip lines for such an antenna [10, 11].

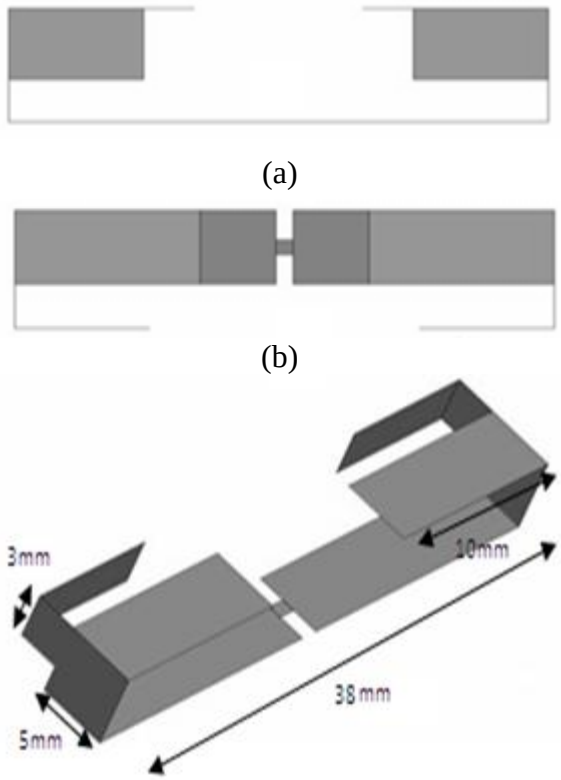

Figure 5.1: Antenna design; (a) Front view, (b) Top View, (c) 3D view.

5.2 ANTENNA GEOMETRY AND DESIGN

The main objective in this chapter is to design a MIMO antenna module, comprising radiators and ground plane compatible with a mobile handset operating in the dual band configuration used in the previous chapter (vis. 2.5GHz and 5.2GHz). The proposed antenna is made of two balanced radiating elements placed in parallel, as shown in Figure 5.1, and the structure was analyzed using HFSS [12]. The antenna is fed at the centre with a differential feed mechanism which provides equal magnitudes of phase current for the two arms, but which are 180° degrees out of phase. The input impedance

is 50Ω, and the optimisation goal is arranged to minimize the coupling between the radiators, and maximum return loss at the two resonant frequencies. Actually, more complex optimisations may be realised in which different radiator locations can be used to excite one or more polarisation components, but this possibility is not explored here. In the prototype model the distance between the radiators is 24mm. The design is completed by analysing the mutual coupling between the user's hand, positioned around the chassis, and the prototype module (Figure 5.2b).

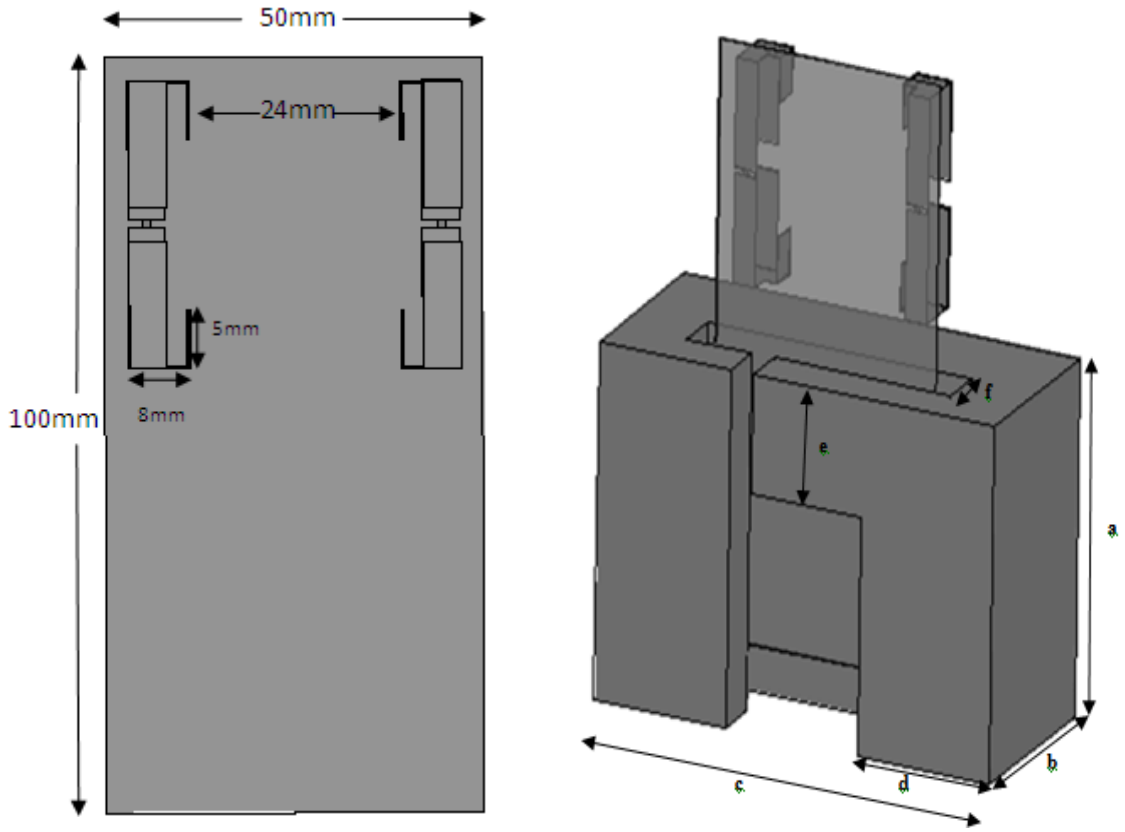

(a) (b)

Figure 5.2: 2 × 2 Balanced MIMO antenna handset; (a) front view handset only, (b) 3D hand phantom model with the proposed antenna MIMO design.

The electrical properties used in the hand model are as for Chapter 4 (section 4.2). The dimensions and position of the hand model that are as follows: a = 60, b = 40, c = 90, d

= 30, e = 25 and f = 10 (all dimensions in mm, Figure 5.2b). The gap between the hand model and the metallic ground plane is 4 mm in the model.

5.3 MEASUREMENTS AND RESULTS

For a balanced antenna (e.g. dipole) configuration, a balun is conventionally required as a feeding network [13-15]. These circuits provide a balanced feed from an unbalanced source. The input impedance or return loss of the balanced antenna measured in this way is from the antenna as well as the balun, rather than a simple measurement at the antenna feed point. Consequently, two different methods were adopted to verify and validate the impedance of the proposed balanced antenna. The first is an S-Parameter method [16], in which balanced antennas are considered as two-port devices, and the S-Parameters can be routinely measured. A simple formula is used to derive the differential input impedance of the balanced antennas. This method has been successfully used to calculate the input impedance of the balanced antenna [16-19]. Finally, a monopole over a ground plane using mirror theory [20-22] is used as the other method to compare the results obtained from the first measurement method.

5.3.1 Input Return Loss and Antenna Coupling

Figure 5.3 shows the input return loss of the 2×2 balanced module at the two feeding ports of the radiating elements. The S_{11} and S_{22} represent the input return loss of the two balanced antennas comprising the 2×2 balanced module. The measured results show an acceptable agreement on the variation of the input return losses.

The bandwidths of the both radiators are very encouraging since the relative bandwidth at return loss of 10 dB (equivalent to VSWR ≤ 2), obtained at 2.5 GHz is around 10%

measured vs. 12% simulated; at 5.2 GHz is 14% measured vs. 16% simulated. Both radiators are resonant at 2.5 GHz and 5.2 GHz, with corresponding maximum return losses of 20 dB and 32 dB, respectively.

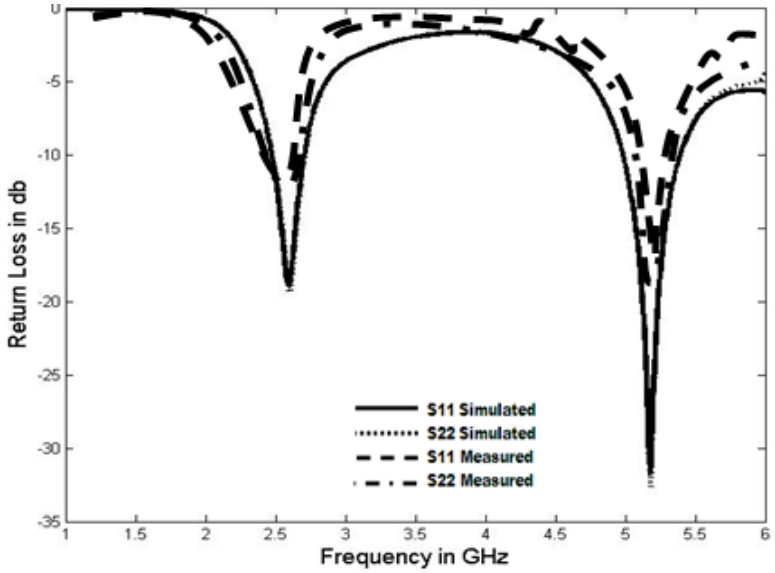

(a)

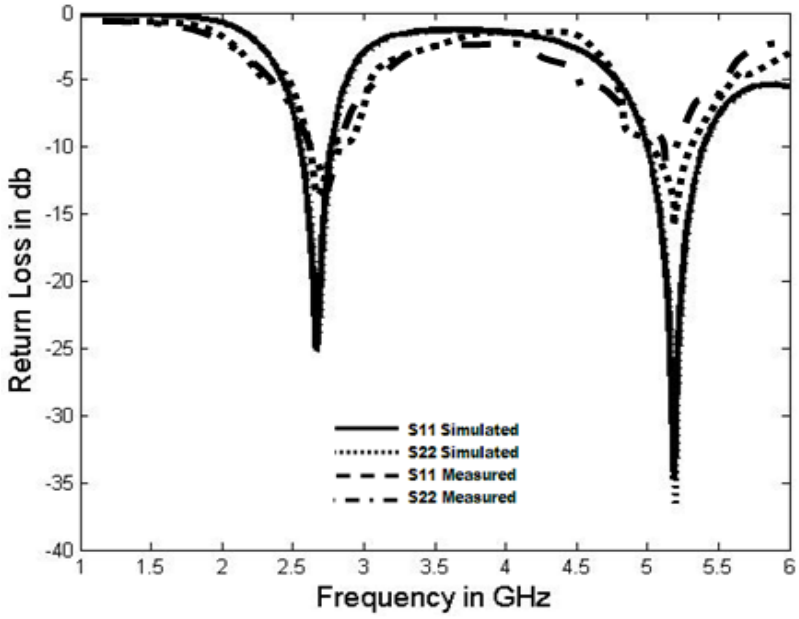

(b)

Figure 5.3: Return loss at the input ports of 2 × 2 Balanced MIMO antenna handset. (a) Without Hand (b) With Hand

Fig. 5.3(b) shows the antenna return loss with and with the hand model. The results have an enhanced acceptable input return loss at both frequency bands. As can be seen, the resultant two plots have almost identical variations with the variations of return loss shown in Figure 5.3a. The results indicate the proposed design have low sensitivity of impedance de-tuning when the phone is held and reduced dependence of the antenna on the ground plane. It is easily be noted that the corresponding maximum return loss of 25 dB and 36 dB, observed at 2.5 GHz and 5.2 GHz, respectively. Similar or slightly better bandwidth performances for both bands also noted, this is the due to the loss introduced by the user's hand.

Figure 5.4 shows the coupling between the two radiators of the 2 × 2 balanced prototype module. As both antennas are considered passive elements, $S_{12} = S_{21.}$ The results show that the coupling between both balanced antennas at 2.5 and 5.2 GHz is less than 10 dB and 12 dB, respectively. The coupling factor between the antennas predicted from the handset-hand model was quite improved by 2-3 dB at the 2.5 GHz frequency band. These coupling values are quite acceptable for practical implementation. This coupling can be reduced further by placing the radiators in orthogonal positions with respect to their local geometries. This results in the required spatial polarization diversity for the 2×2 balanced module.

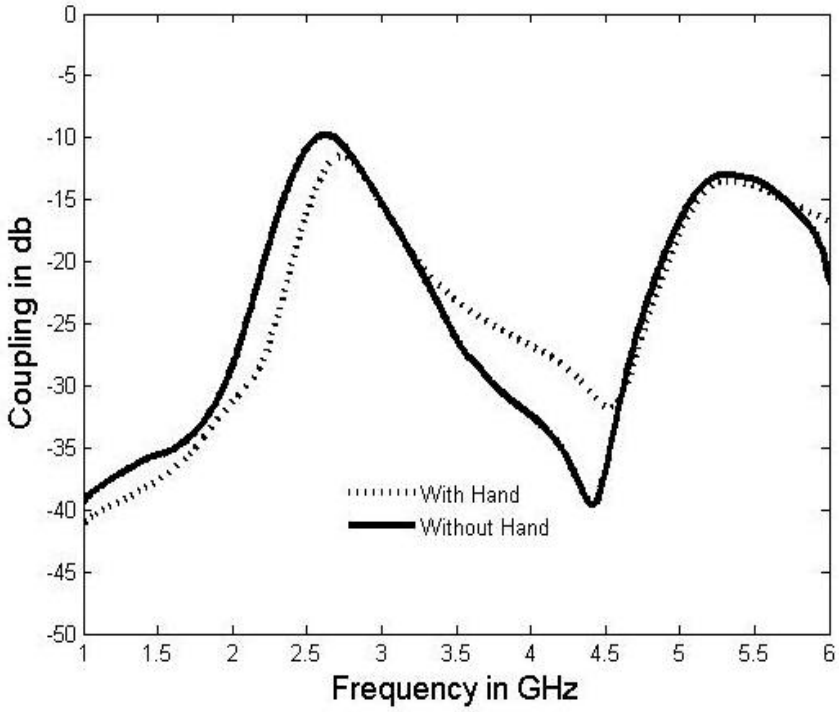

Figure 5.4: Coupling between antennas of 2×2 balanced MIMO antenna system.

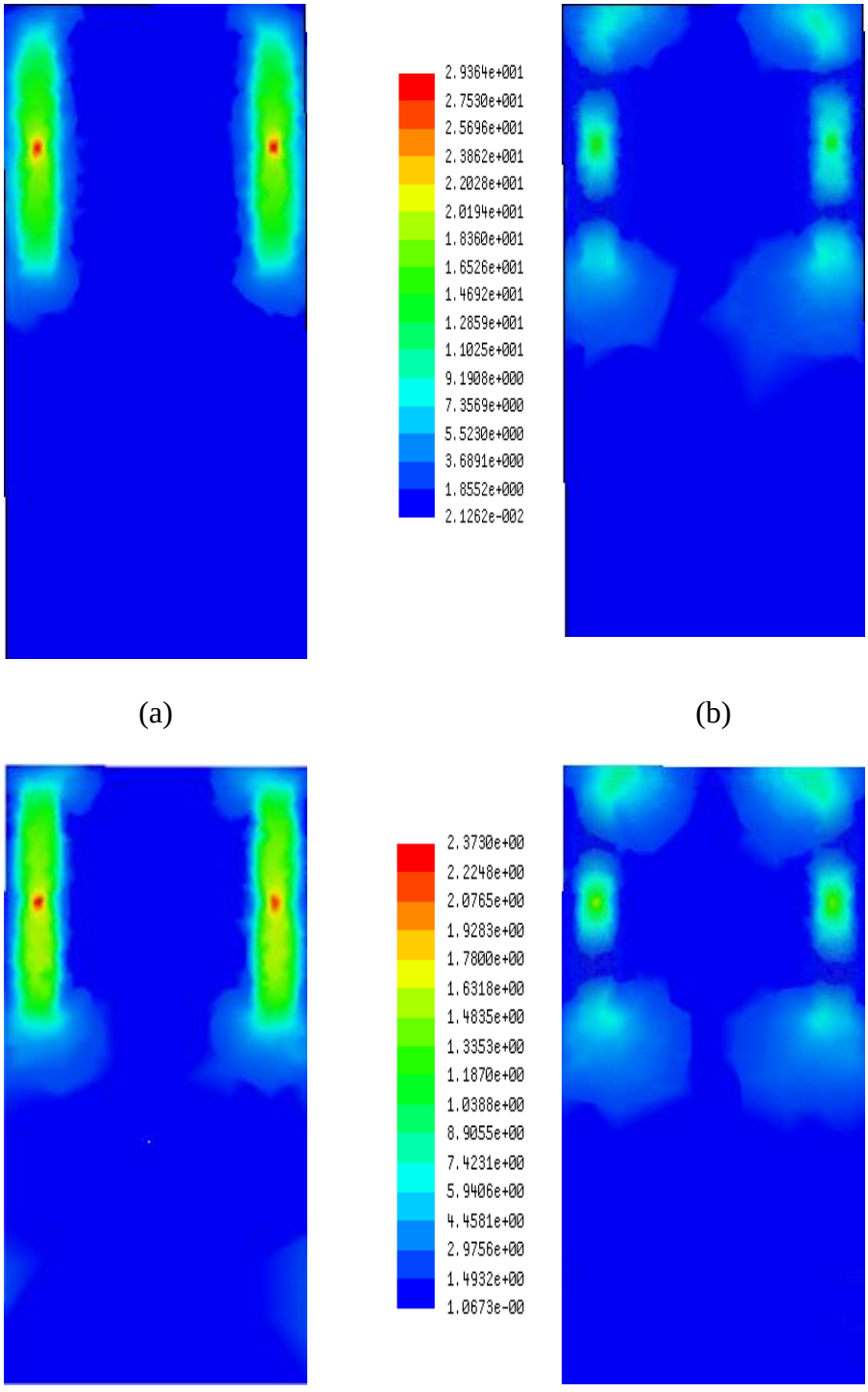

Figure 5.5: Surface current distributions on handset for the proposed balanced MIMO antenna; (a) without hand at 2.5 GHz; (b) without hand at 5.2 GHz; (c) with hand at 2.5 GHz; (d) with hand at 5.2 GHz.

The computed surface currents on the 2×2 prototype module, with and without the user's hand are shown in Figure 5.5 for two operating frequencies. These currents almost are negligible, except underneath the balanced antenna. These results indicate that the proposed module also features a low degree of sensitivity with respect to the ground plane size in comparisons with the use of unbalanced antennas in which the ground (i.e. handset) has extremely effect when hand model included [2]. This implies that the present antenna design may be adapted with some flexibility for a variety of mobile terminal technologies.

5.3.2 Calculation of the Channel Capacity

The rationale for designing a MIMO antenna module is the enhancement of channel capacity. The implementation of a balanced MIMO antenna module not only increases the channel capacity, but also reduces the coupling effects within the device, and between the device and the user's hand, as described above. The channel capacity of the 2×2 balanced module has been computed over a Rayleigh fading channel using the regime described in Chapter 4 for the dual frequency bands. All the results indicate that these channel capacities are approximately equal to the free coupled MIMO system (i.e. no hand is present). The corresponding lower limit of the channel capacity represents the MIMO model of 2×1 system. These maximum limits are similar to the limits applied to MIMO system models using orthogonal polarization diversity.

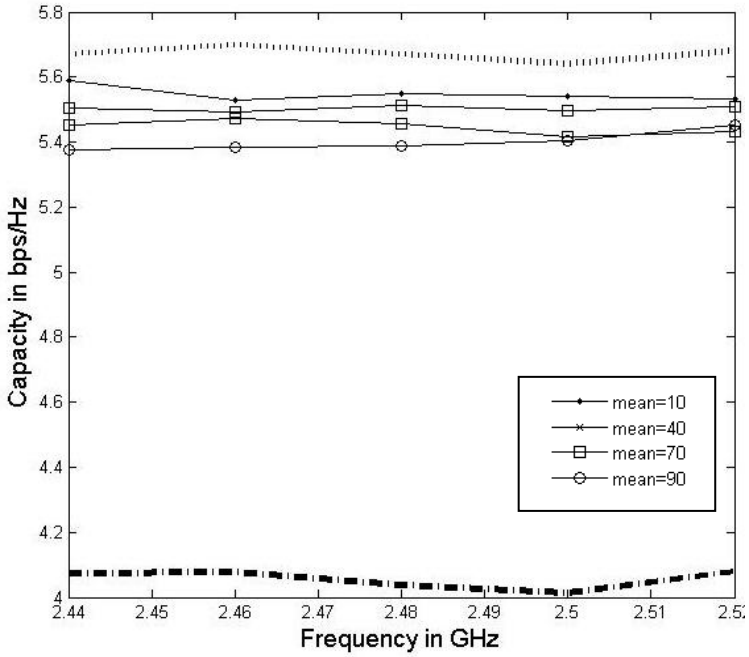

Figure 5.6: Variations of channel capacity versus operating frequency; subject to uniform PAS over 0 to 360° and uniform power spectrum over ±15° for various mean zenith angles of 10°, 40°, 70° and 90°; ('.....' upper limit of 2 × 2 MIMO), ('------'upper limit of 2 × 1 MIMO).

Figures 5.6 to 5.10 represent the channel capacities of the 2 × 2 balanced MIMO system calculated for uniform PAS over 0 to 360°, and various elevation distributions such as uniform, raised cosine and n^{th} order raised cosine. The channel capacities of 10 dB SNR have been investigated over the operating frequency bands. On close observation of each result, it was found that there were slight variations of channel capacity. These values were approximately 0.2 bps/Hz with different values of means and variances assumed for the PAS and elevation angles. The computed results approximately exhibit the maximum capacity limits considered by a simple 2×2 MIMO system.

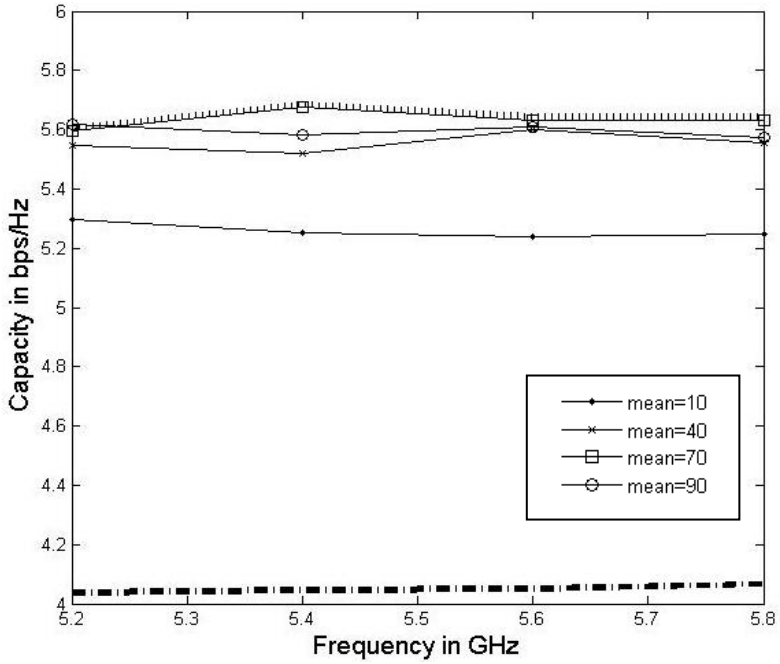

Figure 5.7: Variations of channel capacity versus operating frequency; subject to uniform PAS over 0 to 360° and uniform power spectrum over ±15° for various mean zenith angles of 10°, 40°, 70° and 90°; ('.....' upper limit of 2 × 2 MIMO), ('------'upper limit of 2 × 1 MIMO).

Figure 5.11 to 5.20 represent the calculated channel capacities for the 2×2 balanced module with angular distributions of Gaussian PAS over 0° to 360° and uniform, raised cosine and n^{th} order raised cosine along zenith angle. In Figure 5.11 a maximum of 0.8 bps/Hz capacity was observed for different values of variance along azimuth. Linear variations were found between the higher values of the variances and the resulting capacities. The highest capacity of 5.21bps/Hz can be seen, the variance of 30° along the azimuth. By contrast, in Figure 5.12, the capacity of 5.62 bps/Hz has been achieved at uniform power spectrum over ±15° with mean of 10°, at the lower operating frequency. The channel capacity calculated at 5.2 GHz showed fewer variations compared to capacity values presented in Figures 5.13 and 5.14.

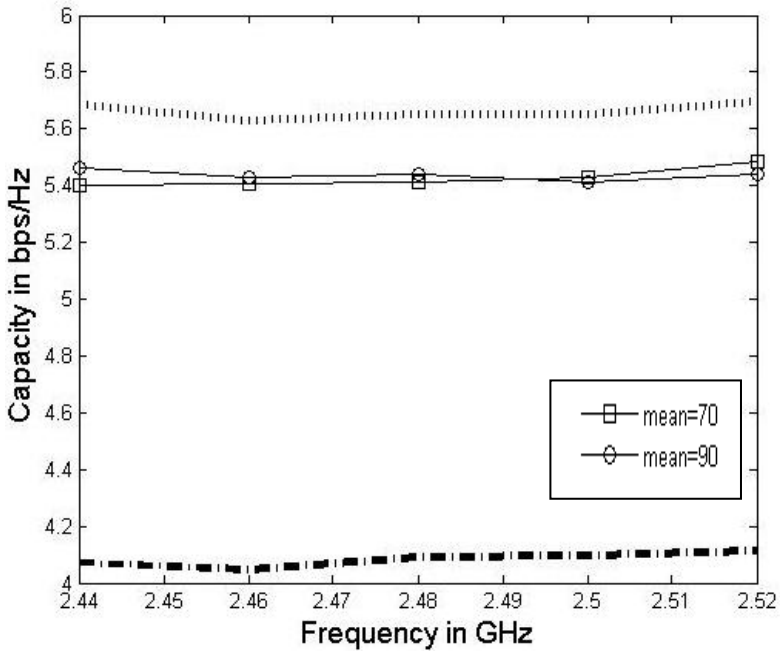

Figure 5.8: Variations of channel capacity versus operating frequency; subject to uniform PAS over 0 to 360° and raised cosine distribution power spectrum for various mean zenith angles of 70° and 90°; ('.....' upper limit of 2 × 2 MIMO), ('------'upper limit of 2 × 1 MIMO).

Figures from 5.21 to 5.39 describe the Laplacian and secant-squared PAS distributions over 0° to 360° and uniform, raised cosine and n^{th} order raised cosine power spectrum along the zenith. The maximum variation of 0.9bps/Hz has been observed in Figure 5.27. This figure corresponds to Laplacian PAS and 4^{th} order raised cosine distribution along the zenith angle. The mean of 45° along the azimuth, and 90° along the zenith are fixed, and the variance along this angle has been varied. At variance of 30° a capacity of 5.25 bps/Hz is obtained, whereas at variance of 5° the capacity of 4.4 bps/Hz has been achieved. It should be noted that higher values of the variances along azimuth correspond to the higher values of channel capacity. A generalized summary of the channel capacity values for all cases considered are tabulated in Table 5.1. It is clear evidence from Table 5.1 that the mean variations of the channel capacities were varied but very close to the maximum achievable capacity of the 2×2 MIMO system.

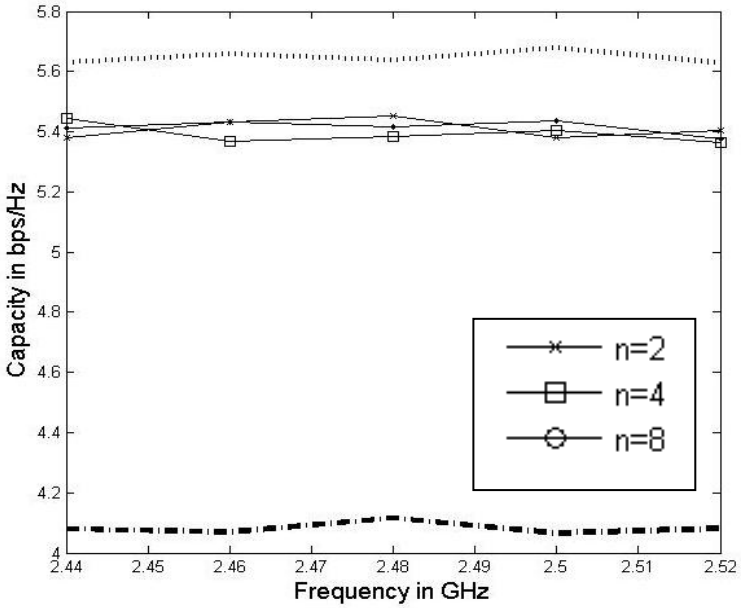

Figure 5.9: Variations of channel capacity versus operating frequency; subject to uniform PAS over 0 to 360° and n^{th} order raised cosine distribution power spectrum for mean zenith angle of 90°; ('.....' upper limit of 2 × 2 MIMO), ('------'upper limit of 2 × 1 MIMO).

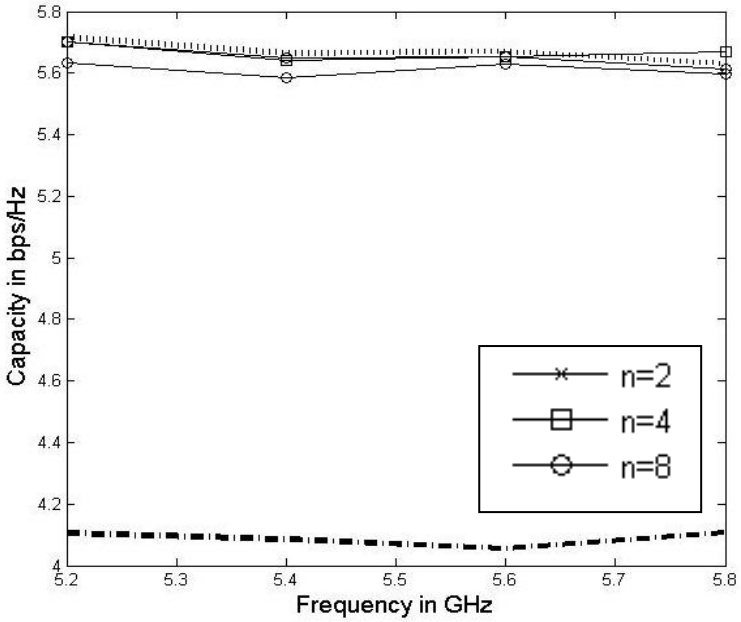

Figure 5.10: Variations of channel capacity versus operating frequency; subject to uniform PAS over 0 to 360° and n^{th} order raised cosine distribution power spectrum for mean zenith angle of 90°; ('.....' upper limit of 2 × 2 MIMO), ('------'upper limit of 2 × 1 MIMO).

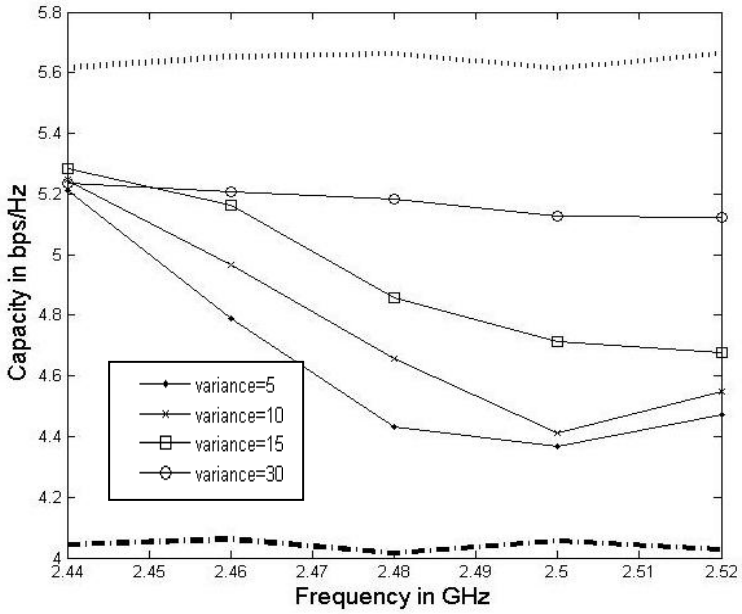

Figure 5.11: Variations of channel capacity versus operating frequency; subject to Gaussian PAS over 0 to 360° with mean 45° and different variances, and uniform power spectrum over ±15° for mean zenith angle of 90°; (‘.....’ upper limit of 2 × 2 MIMO), (‘------‘upper limit of 2 × 1 MIMO).

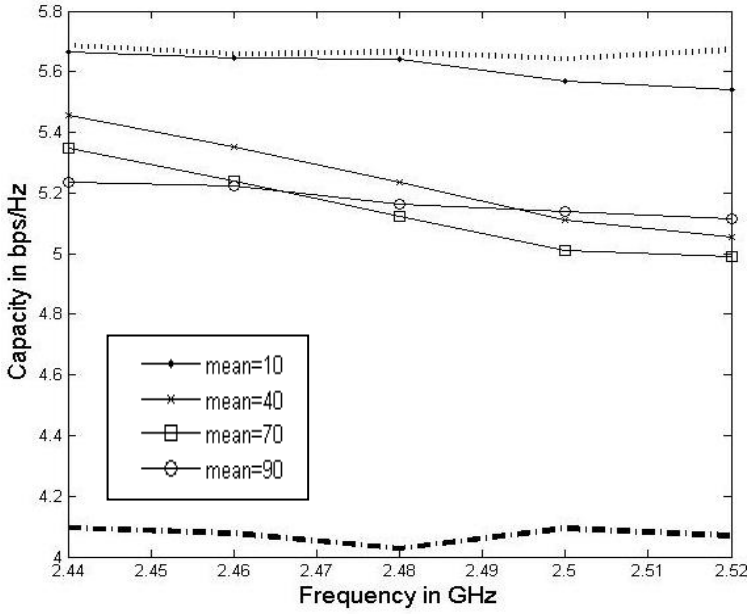

Figure 5.12: Variations of channel capacity versus operating frequency; subject to Gaussian PAS over 0 to 360° with mean 45° and uniform power spectrum over ±15° for various mean zenith angles of 10°, 40°, 70° and 90°; (‘.....’ upper limit of 2 × 2 MIMO), (‘------‘upper limit of 2 × 1 MIMO).

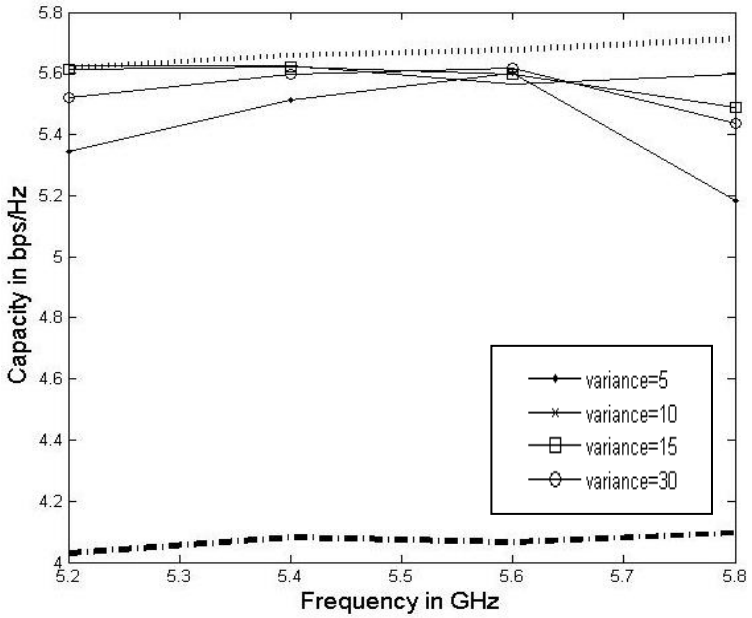

Figure 5.13: Variations of channel capacity versus operating frequency; subject to Gaussian PAS over 0 to 360° with mean 45° and different variances, and uniform power spectrum over ±15° for mean zenith angle of 90°; ('.....' upper limit of 2 × 2 MIMO), ('------'upper limit of 2 × 1 MIMO).

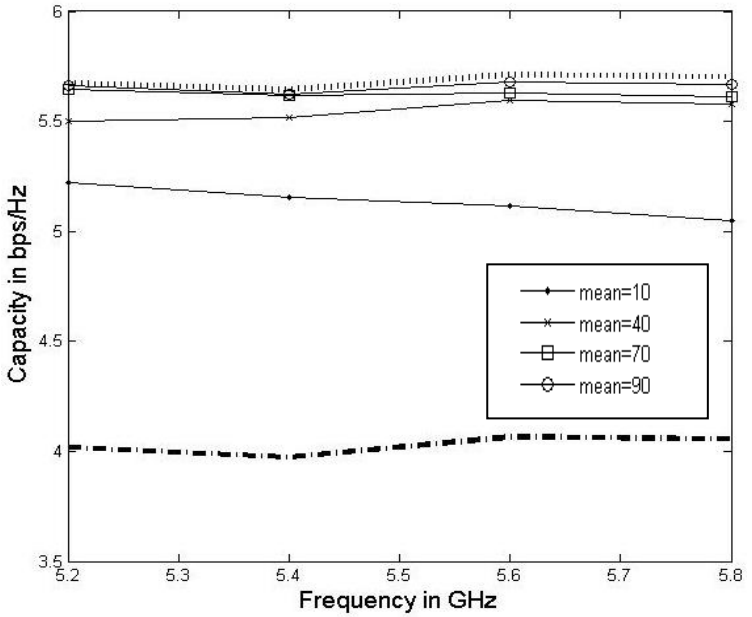

Figure 5.14: Variations of channel capacity versus operating frequency; subject to Gaussian PAS over 0 to 360° with mean 45° and uniform power spectrum over ±15° for various mean zenith angles of 10°, 40°, 70° and 90°; ('.....' upper limit of 2 × 2 MIMO), ('------'upper limit of 2 × 1 MIMO).

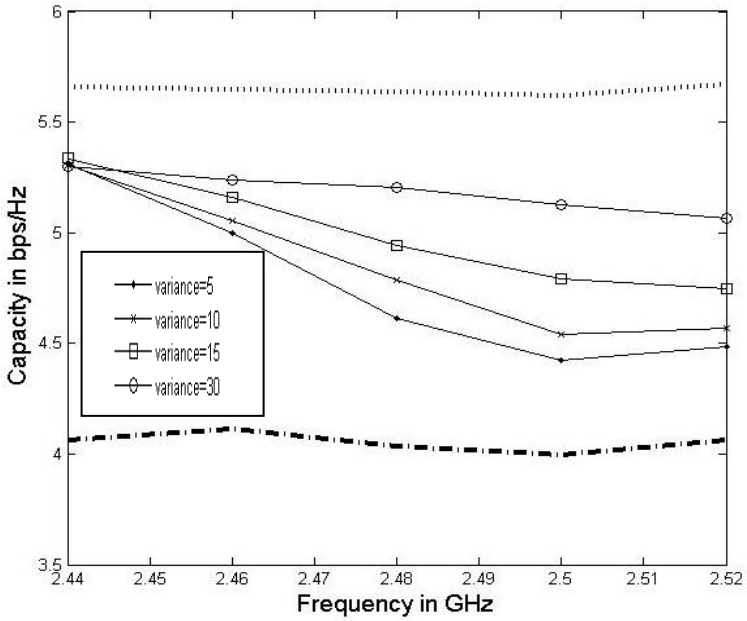

Figure 5.15: Variations of channel capacity versus operating frequency; subject to Gaussian PAS over 0 to 360° with mean 45° and different variances, and raised cosine distribution power spectrum with mean of 90°; ('.....' upper limit of 2 × 2 MIMO), ('-----'upper limit of 2 × 1 MIMO).

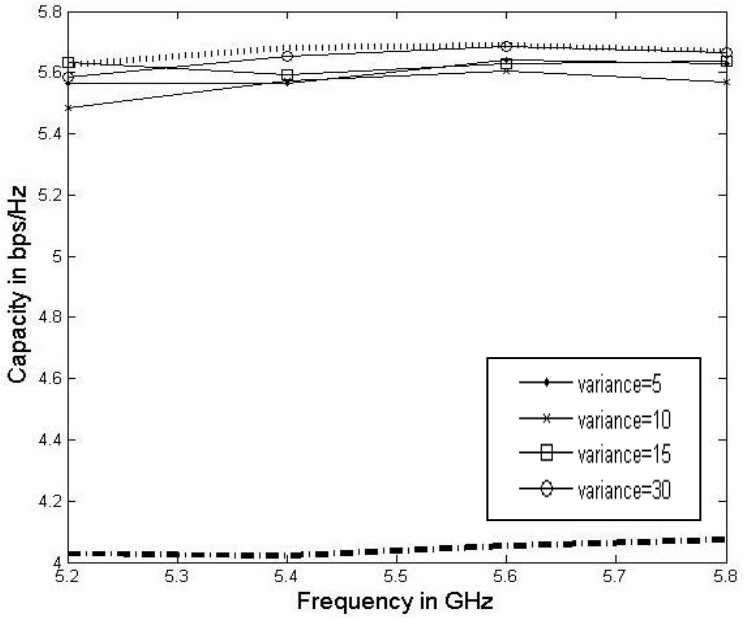

Figure 5.16: Variations of channel capacity versus operating frequency; subject to Gaussian PAS over 0 to 360° with mean 45° and different variances, and raised cosine distribution power spectrum with mean of 90°; ('.....' upper limit of 2 × 2 MIMO), ('-----'upper limit of 2 × 1 MIMO).

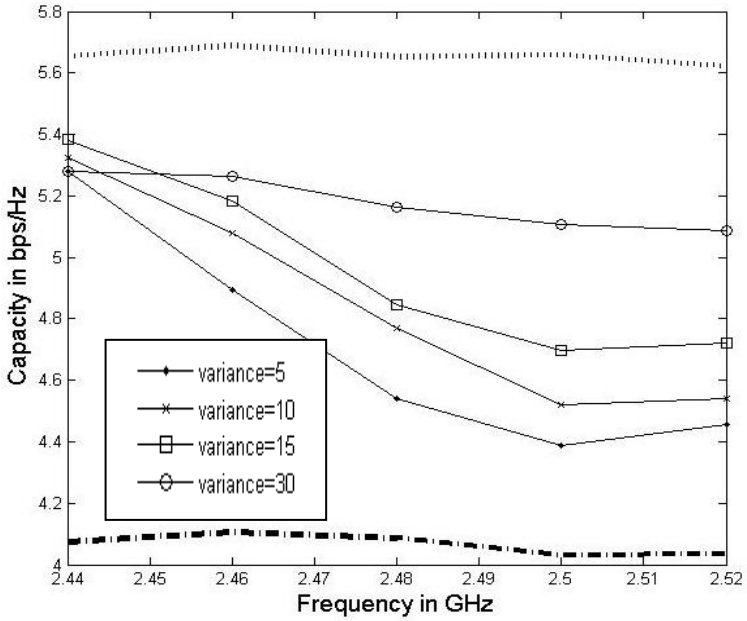

Figure 5.17: Variations of channel capacity versus operating frequency; subject to Gaussian PAS over 0 to 360° with mean 45° and different variances, and raised cosine distribution of 2nd order power spectrum with mean of 90°; ('.....' upper limit of 2 × 2 MIMO), ('------'upper limit of 2 × 1 MIMO).

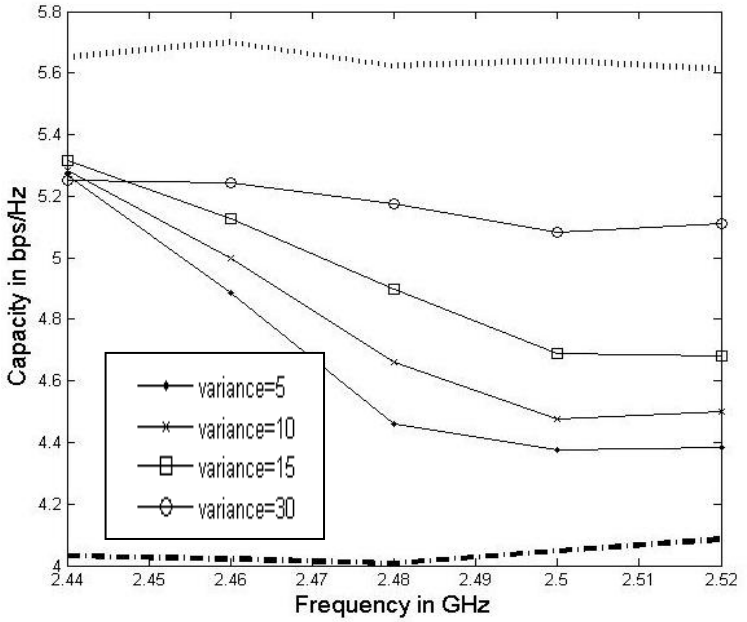

Figure 5.18: Variations of channel capacity versus operating frequency; subject to Gaussian PAS over 0 to 360° with mean 45° and different variances, and raised cosine distribution of 4th order power spectrum with mean of 90°; ('.....' upper limit of 2 × 2 MIMO), ('------'upper limit of 2 × 1 MIMO).

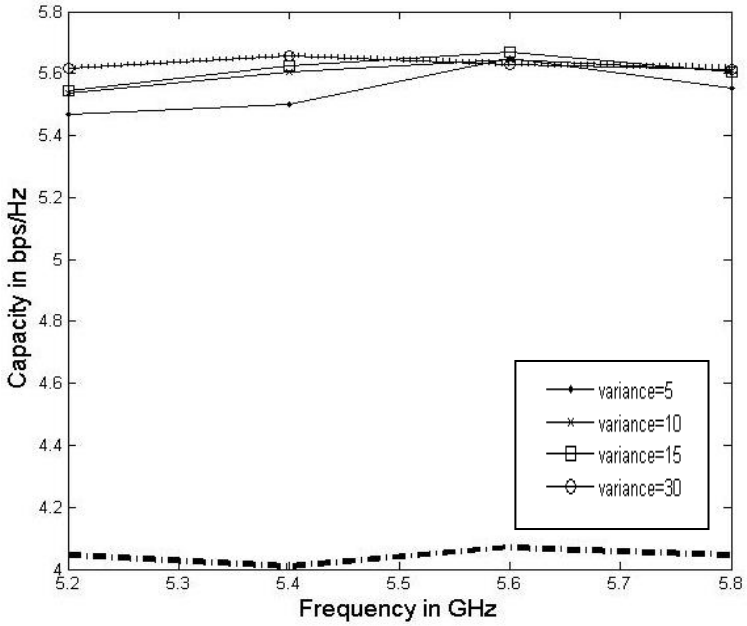

Figure 5.19: Variations of channel capacity versus operating frequency; subject to Gaussian PAS over 0 to 360° with mean 45° and different variances, and raised cosine distribution of 2nd order power spectrum with mean of 90°; ('.....' upper limit of 2 × 2 MIMO), ('------'upper limit of 2 × 1 MIMO).

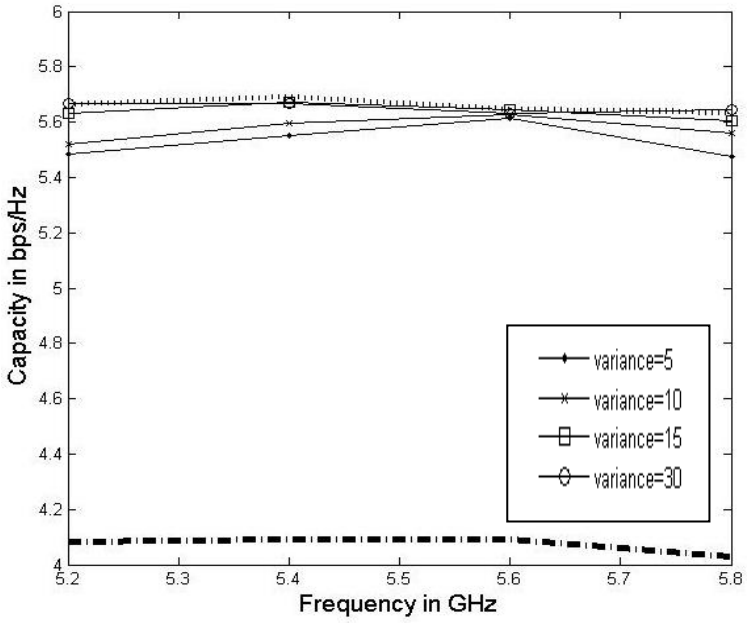

Figure 5.20: Variations of channel capacity versus operating frequency; subject to Gaussian PAS over 0 to 360° with mean 45° and different variances, and raised cosine distribution of 4th order power spectrum with mean of 90°; ('.....' upper limit of 2 × 2 MIMO), ('------'upper limit of 2 × 1 MIMO).

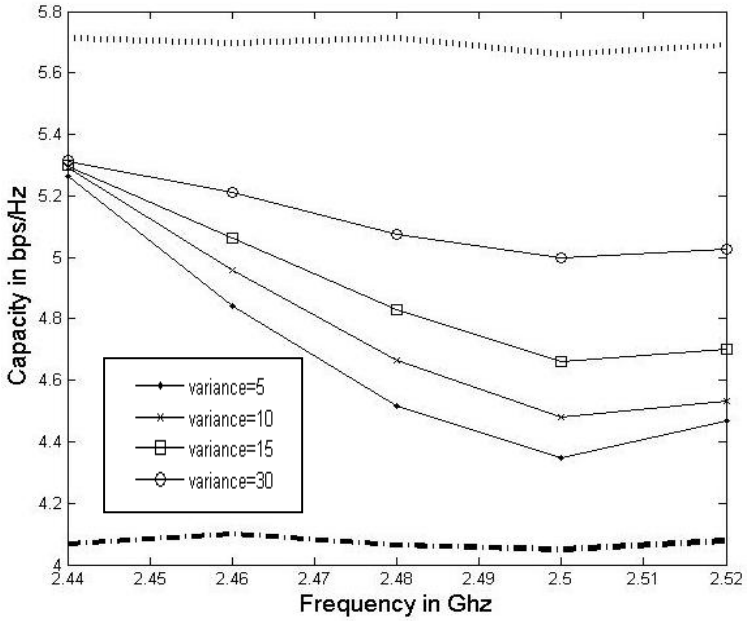

Figure 5.21: Variations of channel capacity versus operating frequency; subject to Laplacian PAS over 0 to 360° with mean 45° and different variances, and uniform power spectrum over ±15° for mean zenith angle of 90°; ('.....' upper limit of 2 × 2 MIMO), ('------'upper limit of 2 × 1 MIMO).

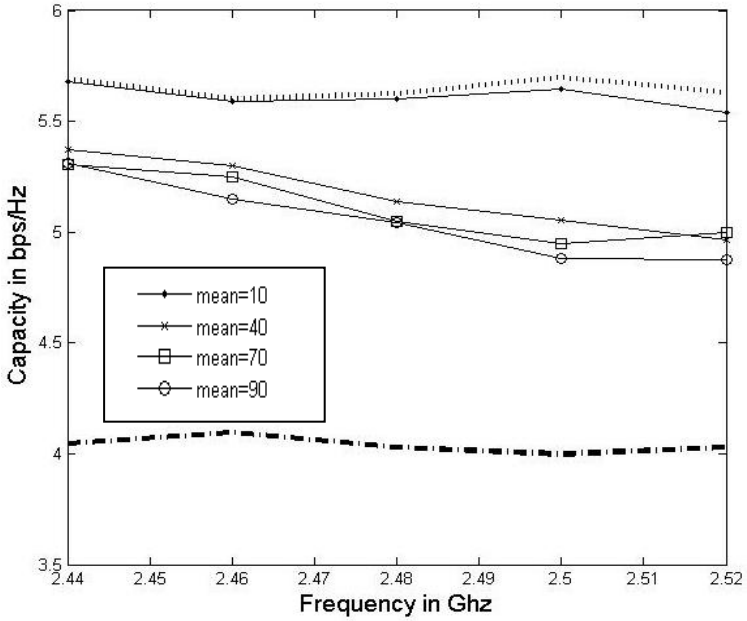

Figure 5.22: Variations of channel capacity versus operating frequency; subject to Laplacian PAS over 0 to 360° with mean 45° and variance 30°; and uniform power spectrum over ±15° for various mean zenith angles of 10°, 40°, 70° and 90°; ('.....' upper limit of 2 × 2 MIMO), ('------'upper limit of 2 × 1 MIMO).

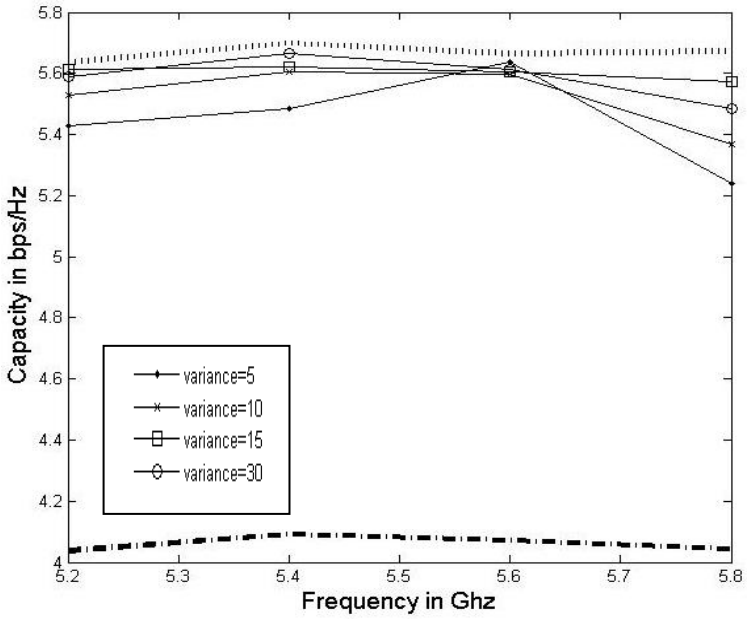

Figure 5.23: Variations of channel capacity versus operating frequency; subject to Laplacian PAS over 0 to 360° with mean 45° and different variances, and uniform power spectrum over ±15° for mean zenith angle of 90°; ('.....' upper limit of 2 × 2 MIMO), ('------'upper limit of 2 × 1 MIMO).

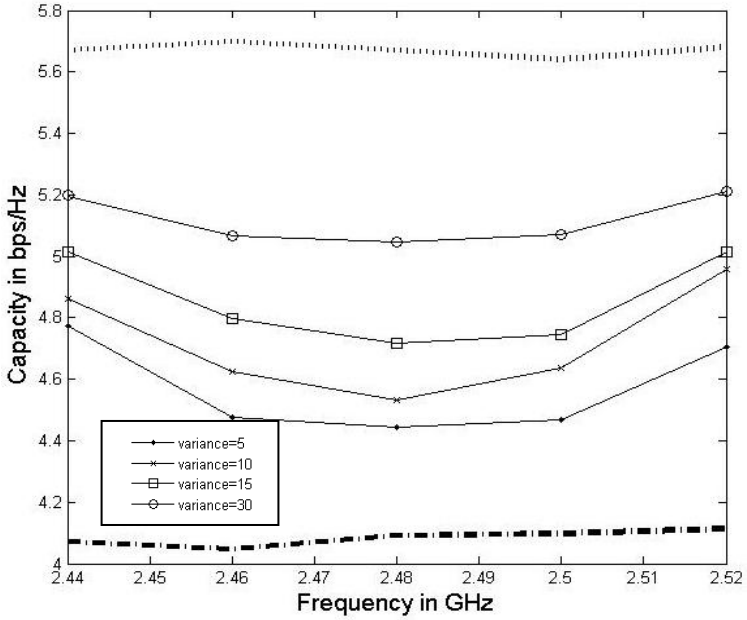

Figure 5.24: Variations of channel capacity versus operating frequency; subject to Laplacian PAS over 0 to 360° with mean 60° and different variances, and raised cosine distribution power spectrum with mean of 90°; ('.....' upper limit of 2 × 2 MIMO), ('------'upper limit of 2 × 1 MIMO).

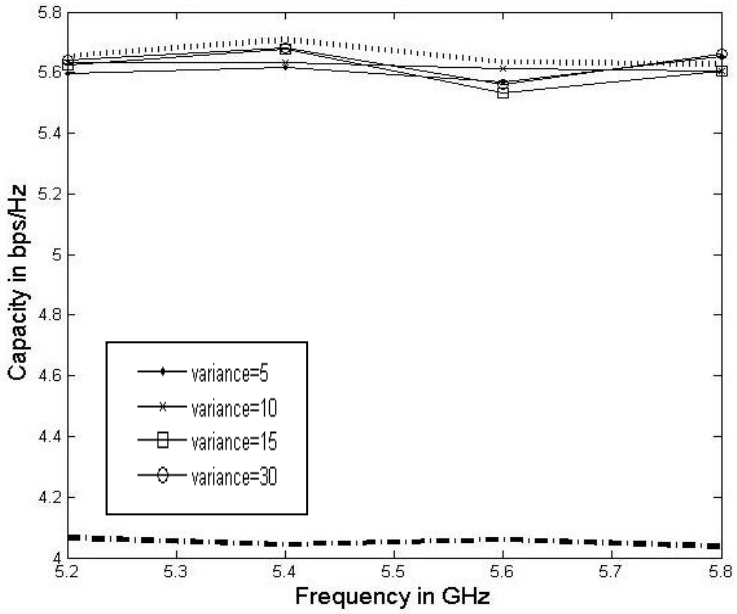

Figure 5.25: Variations of channel capacity versus operating frequency; subject to Laplacian PAS over 0 to 360° with mean 60° and different variances, and raised cosine distribution power spectrum with mean of 90°; ('.....' upper limit of 2 × 2 MIMO), ('-----'upper limit of 2 × 1 MIMO).

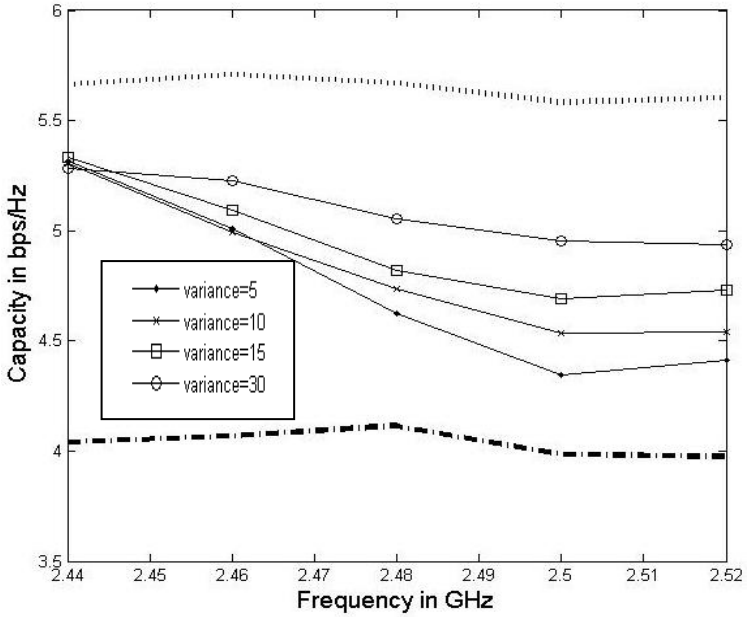

Figure 5.26: Variations of channel capacity versus operating frequency; subject to Laplacian PAS over 0 to 360° with mean 45° and different variances; and raised cosine distribution of 2nd order power spectrum with mean of 90°; ('.....' upper limit of 2 × 2 MIMO), ('------'upper limit of 2 × 1 MIMO).

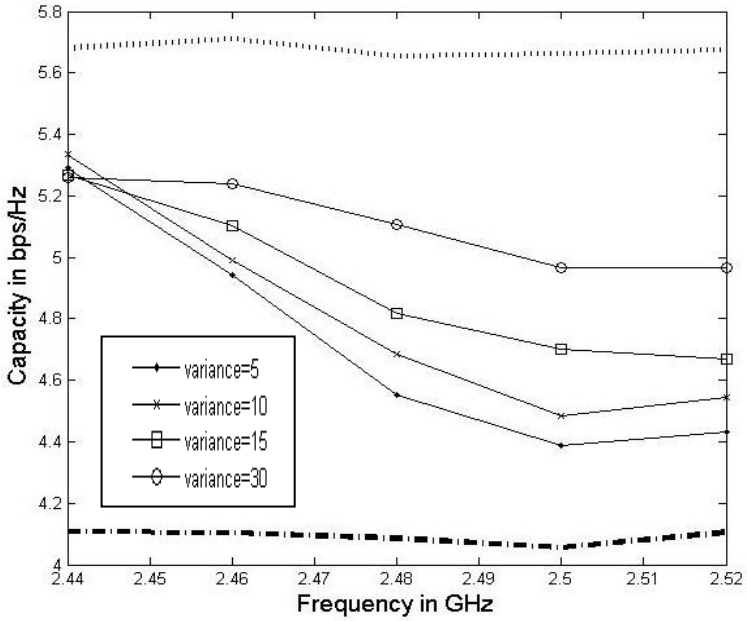

Figure 5.27: Variations of channel capacity versus operating frequency; subject to Laplacian PAS over 0 to 360° with mean 45° and different variances; and raised cosine distribution of 4th order power spectrum with mean of 90°; ('.....' upper limit of 2 × 2 MIMO), ('------'upper limit of 2 × 1 MIMO).

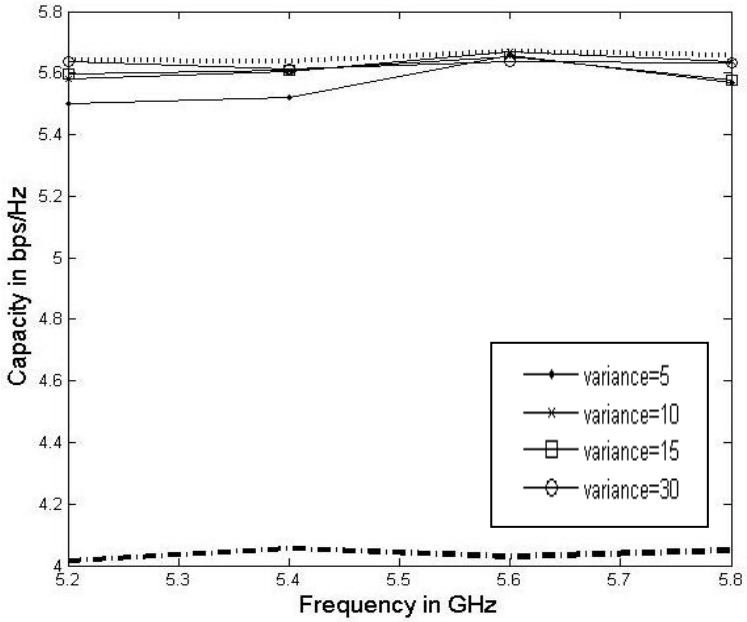

Figure 5.28: Variations of channel capacity versus operating frequency; subject to Laplacian PAS over 0 to 360° with mean 45° and different variances; and raised cosine distribution of 2nd order power spectrum with mean of 90°; ('.....' upper limit of 2 × 2 MIMO), ('------'upper limit of 2 × 1 MIMO).

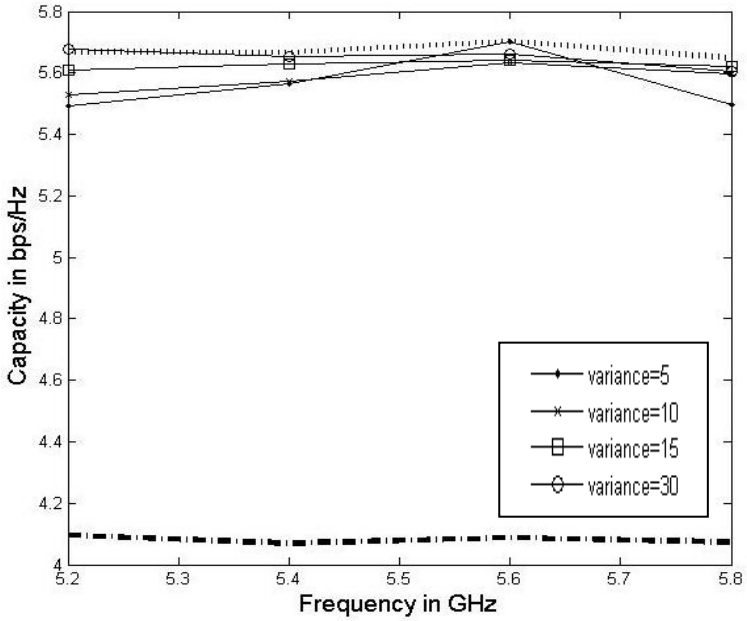

Figure 5.29: Variations of channel capacity versus operating frequency; subject to Laplacian PAS over 0 to 360° with mean 45° and different variances; and raised cosine distribution of 4th order power spectrum with mean of 90°; ('.....' upper limit of 2 × 2 MIMO), ('------'upper limit of 2 × 1 MIMO).

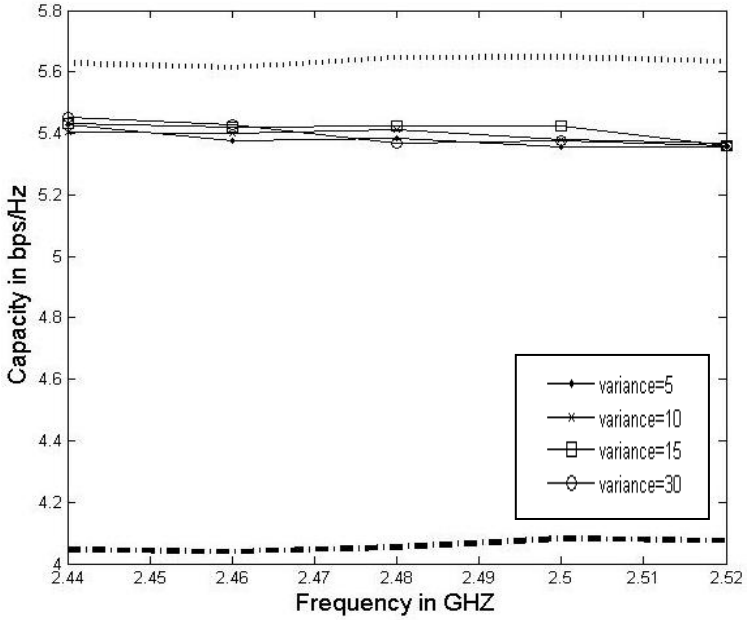

Figure 5.30: Variations of channel capacity versus operating frequency; subject to Secant Square PAS over 0 to 360° with mean 45° and different variances, and uniform power spectrum over ±15° for mean zenith angle of 90°; ('.....' upper limit of 2 × 2 MIMO), ('------'upper limit of 2 × 1 MIMO).

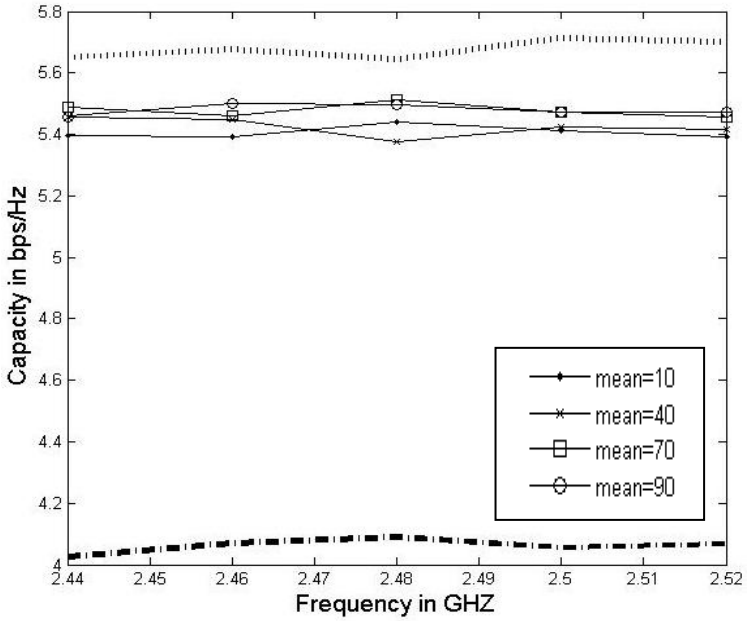

Figure 5.31: Variations of channel capacity versus operating frequency; subject to Secant Square PAS over 0 to 360° with mean 45° and uniform power spectrum over ±15° for various mean zenith angles of 10°, 40°, 70° and 90°; ('.....' upper limit of 2 × 2 MIMO), ('------'upper limit of 2 × 1 MIMO).

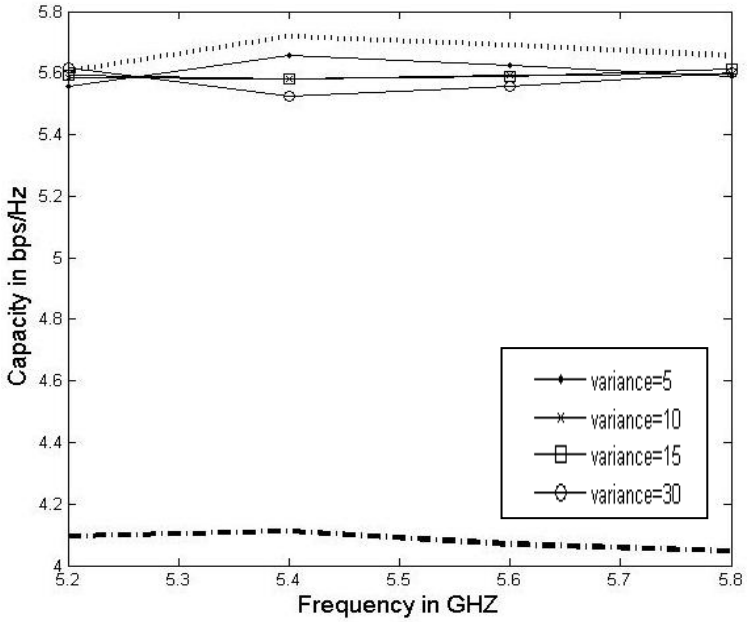

Figure 5.32: Variations of channel capacity versus operating frequency; subject to Secant Square PAS over 0 to 360° with mean 45° and different variances, and uniform power spectrum over ±15° for mean zenith angles of 90°; ('.....' upper limit of 2 × 2 MIMO), ('------'upper limit of 2 × 1 MIMO).

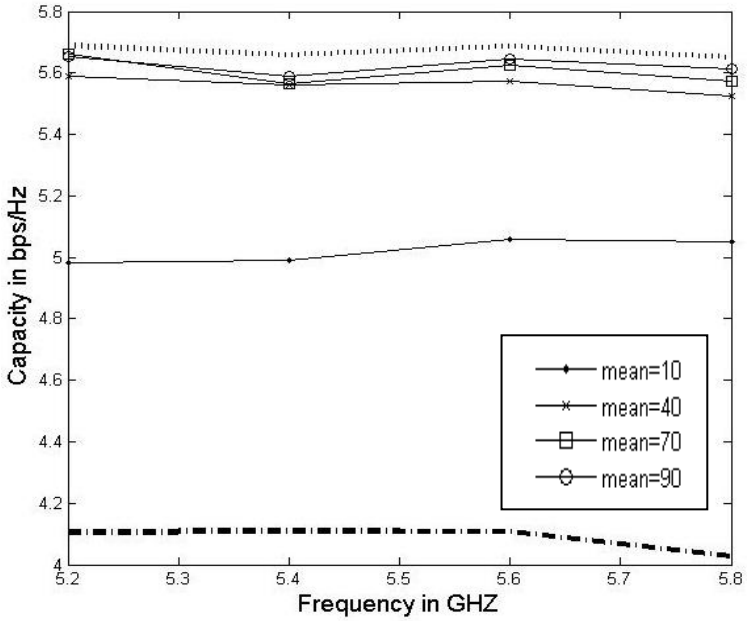

Figure 5.33: Variations of channel capacity versus operating frequency; subject to Secant Square PAS over 0 to 360° with mean 45° and uniform power spectrum over ±15° for various mean zenith angles of 10°, 40°, 70° and 90°; ('.....' upper limit of 2 × 2 MIMO), ('------'upper limit of 2 × 1 MIMO).

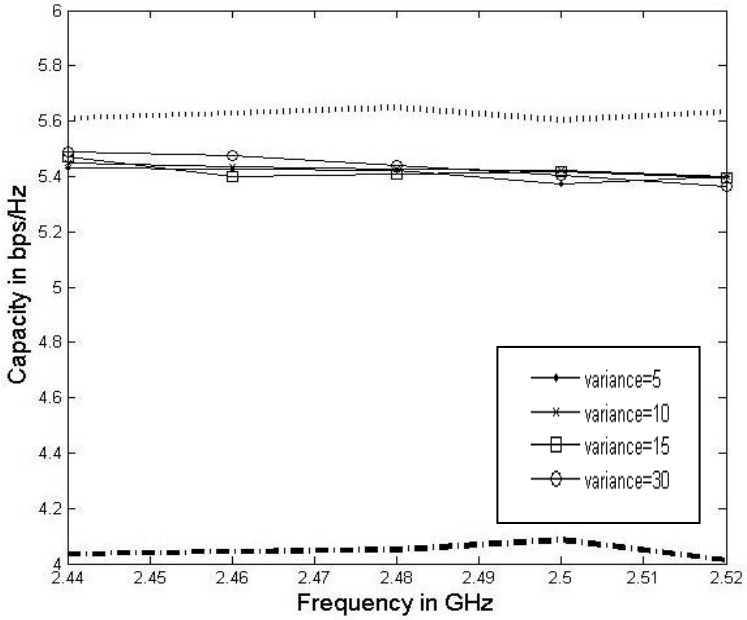

Figure 5.34: Variations of channel capacity versus operating frequency; subject to Secant Square PAS over 0 to 360° with mean 45° and different variances, and raised cosine distribution power spectrum with mean of 90°; ('.....' upper limit of 2 × 2 MIMO), ('------'upper limit of 2 × 1 MIMO).

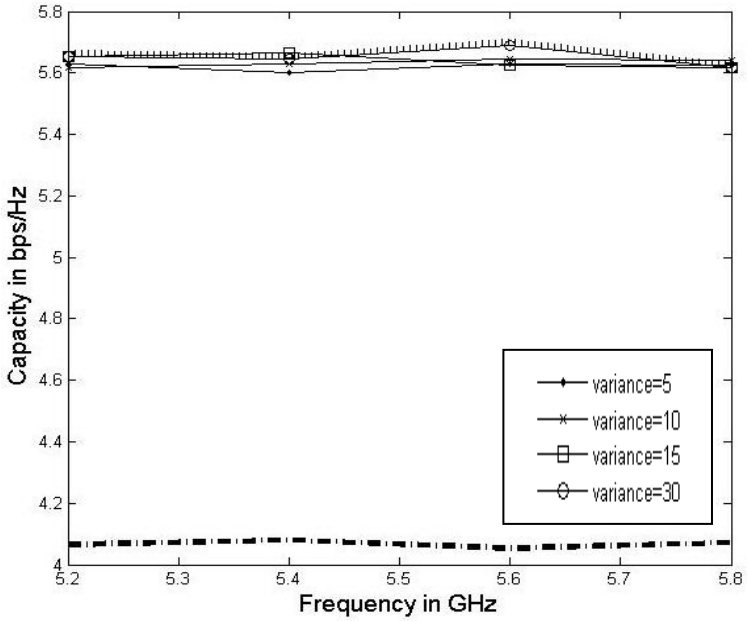

Figure 5.35: Variations of channel capacity versus operating frequency; subject to Secant Square PAS over 0 to 360° with mean 45° and different variances, and raised cosine distribution power spectrum with mean of 90°; ('.....' upper limit of 2 × 2 MIMO), ('------'upper limit of 2 × 1 MIMO).

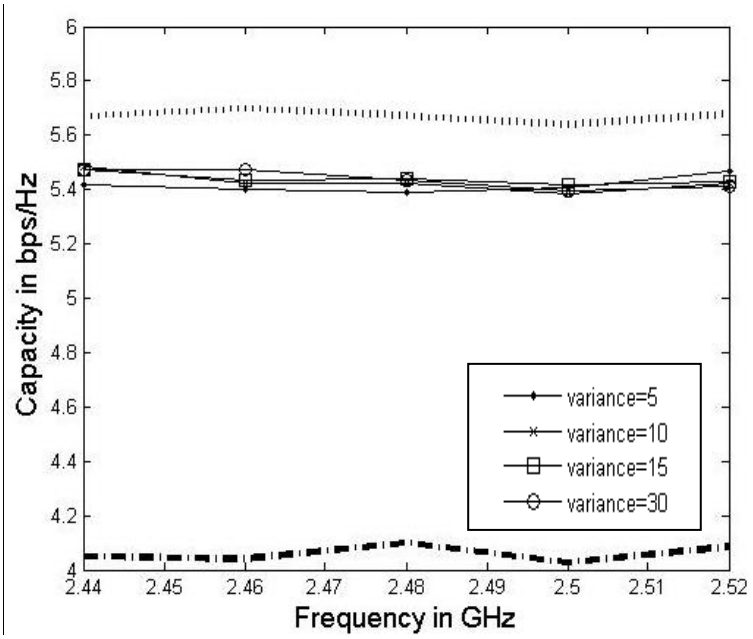

Figure 5.36: Variations of channel capacity versus operating frequency; subject to Secant Square PAS over 0 to 360° with mean 45° and different variances; and raised cosine distribution of 2nd order power spectrum with mean of 90°; ('.....' upper limit of 2 × 2 MIMO), ('------'upper limit of 2 × 1 MIMO).

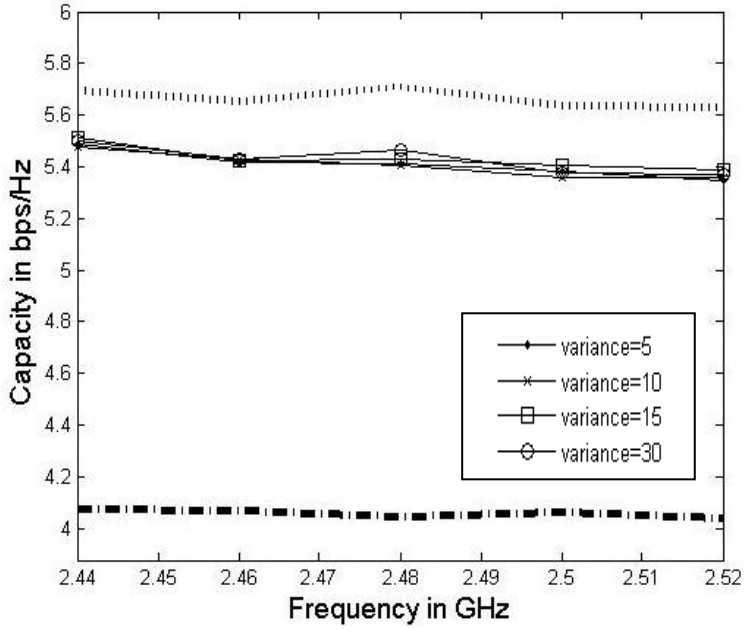

Figure 5.37: Variations of channel capacity versus operating frequency; subject to Secant Square PAS over 0 to 360° with mean 45° and different variances; and raised cosine distribution of 4th order power spectrum with mean of 90°; ('.....' upper limit of 2 × 2 MIMO), ('------'upper limit of 2 × 1 MIMO).

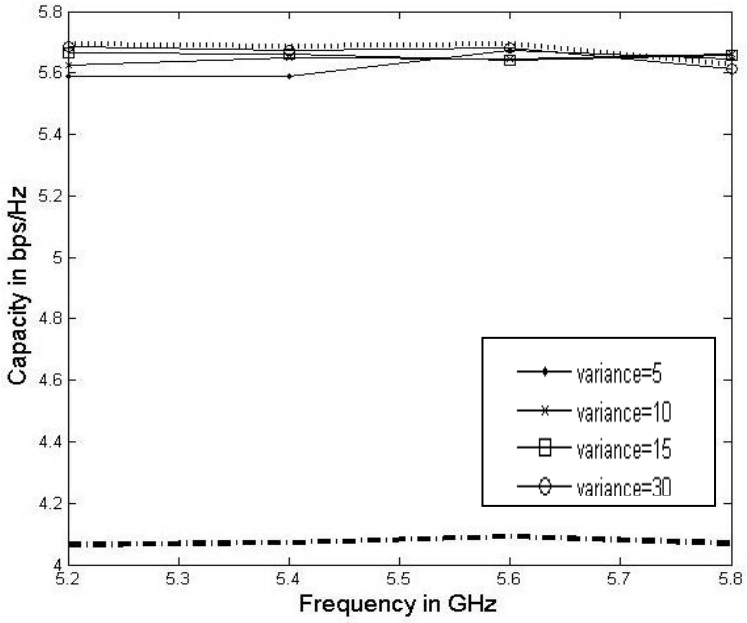

Figure 5.38: Variations of channel capacity versus operating frequency; subject to Secant Square PAS over 0 to 360° with mean 45° and different variances; and raised cosine distribution of 2nd order power spectrum with mean of 90°; ('.....' upper limit of 2 × 2 MIMO), ('------'upper limit of 2 × 1 MIMO).

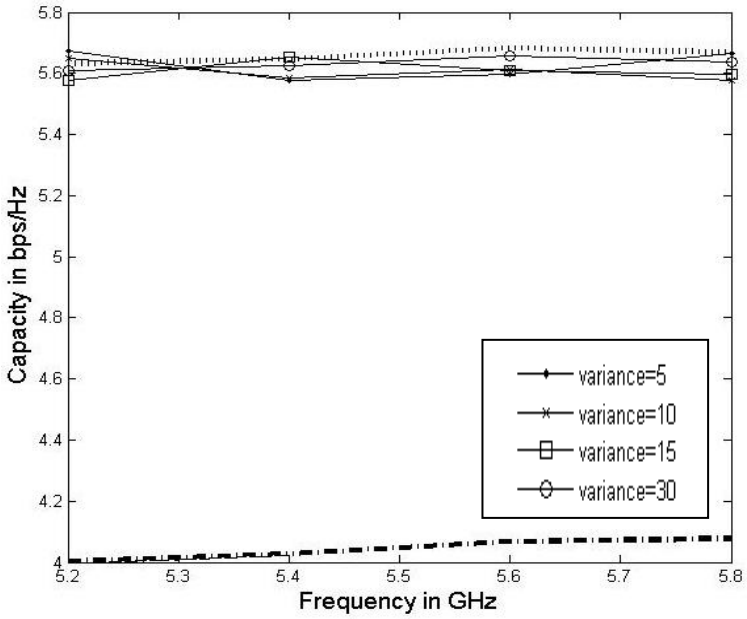

Figure 5.39: Variations of channel capacity versus operating frequency; subject to Secant Square PAS over 0 to 360° with mean 45° and different variances; and raised cosine distribution of 4th order power spectrum with mean of 90°; ('.....' upper limit of 2 × 2 MIMO), ('------'upper limit of 2 × 1 MIMO).

Table 5.1: Summarised channel capacity of the antenna geometry shown in Fig. 5.2.

Power Distributions		**Mean of Calculated Channel Capacity (Bps/Hz)**	
Azimuth	**Elevation**	**2.44 to 2.52 GHz**	**5.2 to 5.8 GHz**
Uniform	Uniform	5.48	5.51
Uniform	Raised Cosine	5.43	5.46
Uniform	n^{th} Order raised Cosine	5.41	5.64
Gaussian	Uniform	4.85	5.48
Gaussian	Raised Cosine	4.81	5.52
Gaussian	2^{nd} Order raised Cosine	4.88	5.52
Gaussian	4^{th} Order raised Cosine	4.86	5.58
Laplacian	Uniform	4.78	5.56
Laplacian	Raised Cosine	4.82	5.58
Laplacian	2^{nd} Order raised Cosine	4.75	5.56
Laplacian	4^{th} Order raised Cosine	4.81	5.51
Secant Square	Uniform	5.42	5.58
Secant Square	Raised Cosine	4.43	5.62
Secant Square	2^{nd} Order raised Cosine	5.43	5.62
Secant Square	4^{th} Order raised Cosine	5.51	5.59

5.3.3 Radiation Patterns

The radiation patterns for both balanced antennas are investigated with and without the user's hand at two different vertical planes as shown in Figures 5.40 – 5.41. The first plane was considered at $\Phi = 0°$, $\theta = 0°$ to $360°$; and the other at $\Phi = 90°$ and $\theta = 0°$ to $360°$. These radiated fields were observed at the operating frequencies. The radiation

patterns for radiating element #1 without and with hand model are shown in Figures 5.40 and 5.41 respectively. In spite the asymmetry of the hand model used in Figure 5.3, the far field of the radiating element #2 is not presented here. This is due to the internal symmetry of the antenna geometry, and the low effects of the induced surface currents on the chassis.

It can be clearly seen that the E_{Φ} and E_{θ} almost cover the sphere, the radiation patterns for this 2×2 balanced module are acceptable for mobile terminal applications. The maximum gains observed in figure 5.40 at 2.5 and 5.2 GHz are 5.1dB and 4.8dB, respectively. This gain can be more improved by changing the geometry of the antenna, but this will affect the coupling between the two radiators. Hence the current distributions, and geometry of both antennas deliver a good tradeoff between the gain and the coupling.

Figure 5.41 represents the radiation pattern of 2x2 balanced module with the user's hand present. The radiation patterns are still spherical, and ideal for use in mobile applications. On closer observation, it can be seen that gain of the antenna has not been affected. The maximum gains observed with the user's hand present, are 3.2db and 7db at 2.5 and 5.2 GHz.

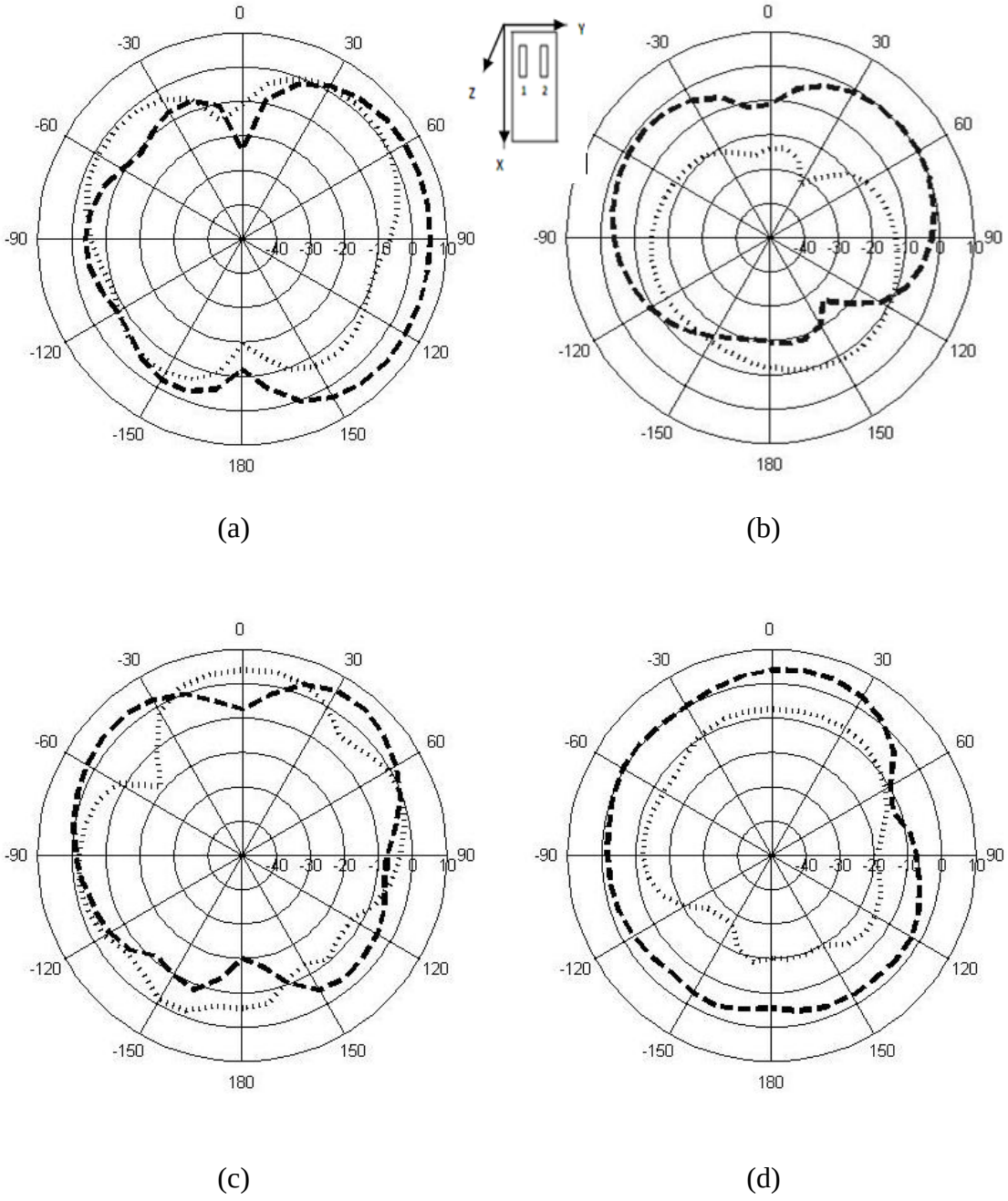

Figure 5.40: The radiation pattern of antenna 1 of the MIMO antenna configuration shown in Figure 3 versus the zenith angle without the hand model; (a) Φ = 0° at 2.5 GHz, (b) Φ = 90° at 2.5, (c) Φ = 0° at 5.2 GHz, (d) Φ = 90° at 5.2 GHz; ('_ _' E_{Φ}, '…….' E_{θ})

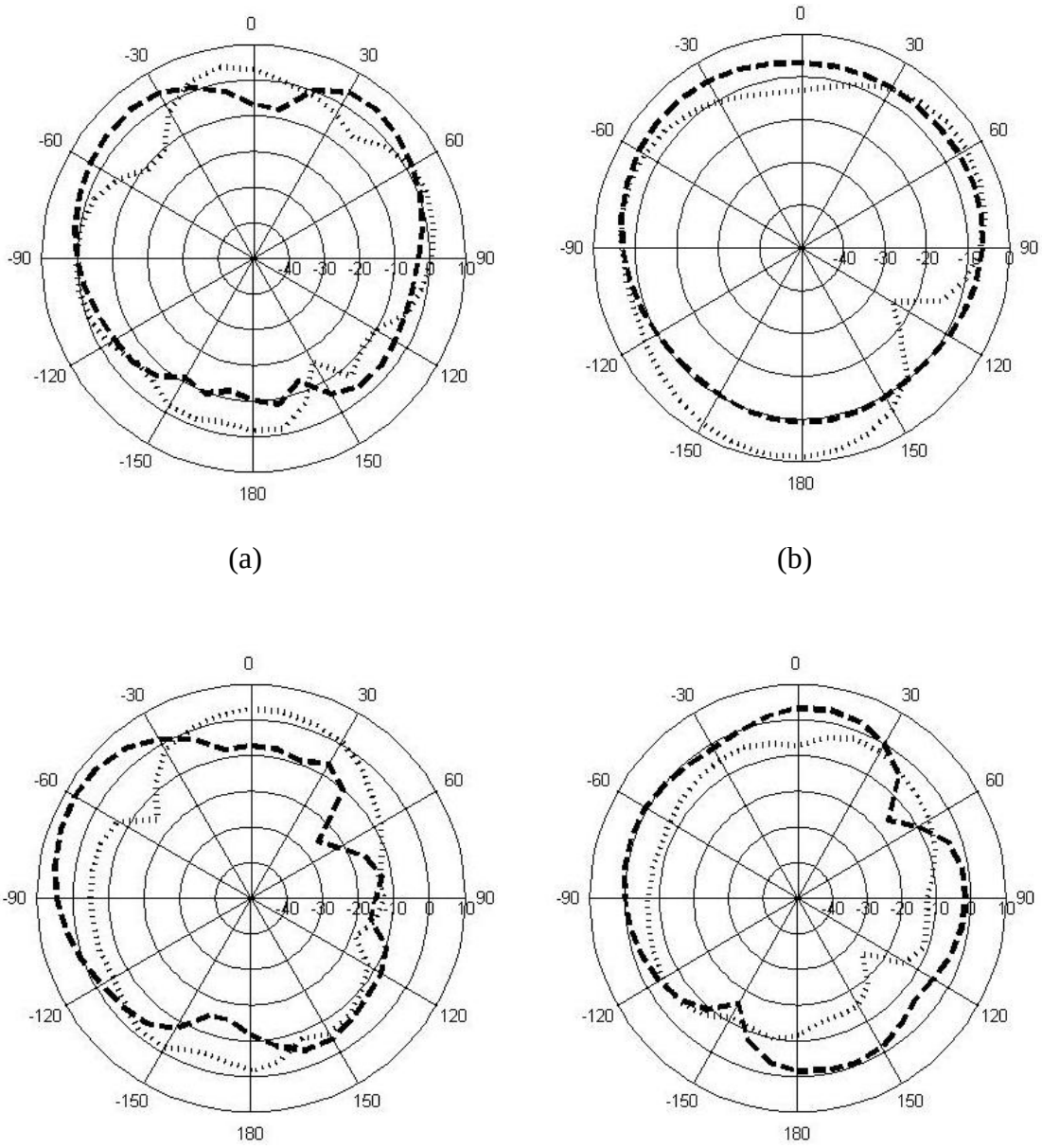

Figure 5.41: The radiation pattern of antenna 1 of the MIMO antenna configuration shown in Figure 3 versus the zenith angle with the hand model; (a) Φ = 0° at 2.5 GHz, (b) Φ = 90° at 2.5, (c) Φ = 0° at 5.2 GHz, (d) Φ = 90° at 5.2 GHz; ('_ _' E_{Φ}, '…….' E_{θ})

5.4 CONCLUSION

A new 2×2 balanced MIMO antenna module, based on a folded arm dipole structure, and designed to operate over the 2.5 GHz and 5.2 GHz wireless-LAN bands has been analysed and realised in hardware. Calculation of their channel capacity shows good agreement with the computational predictions; the variations in channel capacity are close to the maximum, as for the 2×2 coupling free MIMO system. The prototype performance shows that the induced handset currents are reduced, thus giving an enhanced immunity to the effect of adjacent human body components. This results in an enhanced stability of the proposed antenna under realistic mobile operating conditions, in this case the IEEE 802.11b/g standard.

5.5 REFERENCES

[1] H. Morishita, H. Furuuchi and K. Fujimoto, "Performance of balance-fed antenna system for handsets in vicinity of a human head or hand", IEE Proc.-Microw. Antennas Propag., Vol. 149, No, 2, pp. 85-91, April 2002.

[2] R.A. Abd-Alhameed, P.S. Excell, K. Khalil, R. Alias and J. Mustafa, "SAR and radiation performance of balanced and unbalanced mobile antennas using a hybrid formulation", IEE Proceedings-Science, Measurement and Technology, Vol. 151, No. 6, pp. 440-444, November 2004.

[3] H. Morishita, Y. Kim, Y. Koyanagi and K. Fujimoto, “A folded loop antenna system for handsets”, IEEE Antennas and Propagation Symp. Proc., Vol. 3, pp. 440-443, July 2001.

[4] Navsariwala. U, Svigelj. J, “ A reduced sized balanced antenna for 2.4 GHz wLAN”, Antennas and Propagation Society International Symposium, 2003. IEEE, Vol. 2, no.2 ,pp. 6- 9 , June 2003.

[5] S. Hayashita, H. Morishita, Y. Koyanagi and K. Fujimoto, “Wideband folded loop antenna for handsets”, IEEE Antennas and Propagation Symp. Proc., Vol. 3, pp. 2-5, July 2002.

[6] M.J. Ammann and Z.N. Chen, “Wideband Monopole Antennas for Multi-Band Wireless Systems”, IEEE Antennas and Propagation Magazine, Vol. 45, No. 2, pp. 146-150, April 2003.

[7] W. L. Stutzman, G. A. Thiele, “Antenna Theory and Design”, 2nd edition, John Wiley & Sons, Inc., New York,1998.

[8] K.-L. Wong, C.-H. Wu and S.-W. Su, “Ultrawide-band square planar metal-plate monopole antenna with a trident-shaped feeding strip”, IEEE Transaction on Antennas and Propagation, Vol. 53, No. 4, pp. 1262-1269, April 2005.

[9] D. Valderas, J. Legarda, I. Gutierrez and J.I. Sancho, “Design of UWB folded-plate monopole antennas based on TLM”, IEEE Transactions on Antennas and Propagation, Vol. 54, No. 6, pp. 1676-1687, June 2006.

[10] D. Zhou, R.A. Abd-Alhameed and P.S. Excell, "Bandwidth enhancement of balanced folded loop antenna design for mobile handsets using genetic algorithms", PIERS Online, Vol. 4, No. 1, pp.136-139, 2008.

[11] D. Zhou, R.A. Abd-Alhameed and P.S. Excell, "Wideband balanced folded dipole antenna for mobile handsets", 2nd European Conference on Antennas and Propagation, Session MoPA, Paper no.39, Edinburgh, UK, 11-16 November 2007.

[12] Agilent Technologies, Santa Rosa, CA, Advanced Design Systems, Version 2005A.

[13] Teruo Onishi and Shinji Uebayashi, "Bioloical Tissue-Equivalent Phantoms Usable in Broadband Frequency Range", NTT DOCOMO Technical Journal Vol.7 No.4, pp. 61-65, March 2006.

[14] Z.Y. Zhang, Y.X. Guo and L.C. Ong, "A new wideband planar balun on a single-layer PCB", IEEE Microwave and Wireless Components Letters, Vol. 15, no. 6, pp. 416-418, June 2005.

[15] K. Tilley, X.-D. Wu and K. Chang, "Coplanar waveguide fed coplanar strip dipole antenna", Electronics Letters, Vol. 30, No. 3, pp. 176-177, 1994.

[16] R. Meys and F. Janssens, "Measuring the impedance of balanced antennas by an S-Parameter method", IEEE Antennas and Propagation magazine, vol. 40, no. 6, pp. 62-65, December 1998.

[17] Kaldjob, E.B.; Geck, B.; Eul, H, “Impedance Measurement of Properly Excited Small Balanced Antennas”, Antennas and Wireless Propagation Letters, IEEE, vol.8, pp. 193-195, 2009.

[18] Koskinen, T.; Rajagopalan, H.; Rahmat-Samii, Y, “Impedance measurements of various types of balanced antennas with the differential probe method”, Antenna Technology, 2009. iWAT 2009. IEEE International Workshop ,pp.1-4, march 2009.

[19] K. D. Palmer and M. W. van Rooyen, “Simple broadband measurements of balanced loads using a network analyzer”, IEEE Transactions on Instrumentation and Measurement, vol. 55, no. 1, pp. 266–272, Feb. 2006.

[20] S. Tanaka, S. Hayashida, H. Morishita and Y. Atsumi, “Wideband and compact folded loop antenna”, Electronics Letters, vol. 41, no. 17, pp. 945-946, 18th August 2005.

[21] Y. Tikhov, Y.J. Kim and Y.H. Min, “Compact low cost antenna for passive RFID transponder”, IEEE Antennas and Propagation Society International Symposium, pp. 1015-1018, 2006.

[22] D. A. Frickey, “Conversions between S, Z, Y, h, ABCD, and T parameters which are valid for complex source and load impedances”, IEEE Transactions on Microwave Theory and Techniques, vol. 42, no. 2, pp. 205–211, Feb. 1994.

CHAPTER 6

COMPACT DIPOLE ANTENNA DESIGN FOR POLARISATION-DIVERSITY MIMO COMMUNICATIONS

6.1 INTRODUCTION TO CONCEPT

The possibility of using multiple polarisations to achieve Multiple Input-Multiple Output (MIMO) communications was announced in a landmark paper by Andrews et al [1]. In earlier MIMO realisations, having multiple antennas at each end of a communication link, co-polarised linear arrays were used. Information theory has shown that with multipath propagation, multiple antennas at both the transmitter and the receiver can establish multiple parallel channels that operate simultaneously on the same frequency band and at the same time. This gives high spectral efficiencies in a rich scattering environment such as indoors or in cityscapes. Depending on the angular spread of scattered multipath ray paths in the environment between source and receiver, substantial increases in the theoretical spectral efficiency in b/s/Hz may be obtained [2]. This system normally requires array antennas at each end which have physical dimensions of at least a half-wavelength, a size that may be unacceptable on a mobile terminal, since a half-wavelength is approximately 190 mm in the lower mobile band

(around 800 MHz) and approximately 80 mm in the upper band (around 1.8 GHz).

The possibility offered by the use of multi-polarisation MIMO is that the antennas could be far smaller, since discrimination between the channels is no longer by angle of arrival alone. The use of polarisation discrimination permits antenna elements to be used which may theoretically be physically very small (i.e. much smaller than a half-wavelength) and these elements can be collocated at a point, rather than being required to be spaced out.

Classically, radio communications have relied on one channel per frequency, although it is well understood that the two polarisation states of planar waves on a line-of-sight path allow two distinct information channels and techniques such as 'polarisation diversity' already take advantage of this [3-6]. However, by allowing for different angles of arrival discriminated by polarisation, the paper [1] showed that three independent channels can be created using electrically small arrays of orthogonal arrays of three electric dipoles.

The physics of polarisation limits the number of channels to three in this system, whereas for spatial-diversity MIMO; the link capacity grows, in principle, with the number of transmitter and receiver antennas [7-24]. In [8-9], dual polarized MIMO systems have been presented in terms the system performance and channel capacity. Generally, the spatial correlation effects and the beam forming of polarized MIMO were discussed for wireless and mobile access points in [10-16]. In addition the wide band spatial channel model using polarization concept is discussed in [17-18], for which a 3D model polarized MIMO system was discussed using ray tracing method in [18]. A

more detailed work on system performance evaluation of MIMO system employed combined polarization and transmit diversity was discussed in [19]. Some experimental results using polarization diversity of MIMO system can be found in [13, 20-22]. Recent prove of channel capacity of multiple-input–multiple-output (MIMO) antenna systems using polarization diversity on handsets for next generation wireless devices were presented in [23-24].

However, by using three magnetic dipoles, a parallel system can be created and the electric and magnetic systems can then, in principle, be overlaid to create a six-channel system. To achieve this, however, sets of three superimposed electric and magnetic dipoles are required and the present work investigated prototype designs for one of these.

In more details, a dual-polarisation dipole antenna is investigated, intended for use as one of three collocated orthogonal antennas in a polarisation-diversity Multiple-Input Multiple-Output (MIMO) communication system. The antenna actually consists of two overlaid dipoles, one electric and the other magnetic, such that their radiation patterns are nominally identical but they are cross-polarised and hence only interact minimally. Using Finite Difference Time Domain (FDTD) and HFSS simulation, it was found that the antenna performed broadly as expected, although the engineering to create a physical realisation would be challenging. In principle, however, a system using two of the triplicated antennas could, in a richly scattering environment, achieve a six-fold increase in channel capacity for the same bandwidth as a traditional line-of-sight link. Unlike established MIMO systems, the antennas could be electrically small (less than a half-wavelength maximum dimension), which is essential for use in mobile terminals.

6.2 DESIGN AND MODEL CONSIDERATIONS

Magnetic loops provide the most direct realisation of magnetic dipole antennas, but they suffer in several ways for the design objectives here. Electrically small magnetic loops have poor antenna efficiencies, but the dipole behaviour is eroded as the electrical size approaches $\lambda/2$. This dilemma may be resolved by adding a rod of high-permeability lossless material on the axis of the loop: this then becomes the well-known "ferrite rod antenna". The selection of a suitable ferromagnetic material is critical, the intended application requires a relatively high permeability (see Sections 6.3 and 6.4), but the loss performance is also significant, in addition to the usual capacitive effects, the influence of hysteresis and eddy currents may also have a non trivial influence on the final design. For the immediate modelling tasks [25] is used for guidance on ferrites and non conductive iron powders.

For the initial design, a standard electric dipole antenna was located in close juxtaposition with a ferromagnetic rod antenna, as shown in Figure 6.1. In principle, the electric dipole should be invisible to fields from the magnetic dipole, because its conductor is normal to the electric field from the ferromagnetic rod. Conversely, the magnetic dipole should be relatively invisible to fields from the electric dipole, because its conductor is also normal to the electric field from the latter. However, the permittivity ($\mu_r > 1$) of the non-conducting ferromagnetic rod can be expected to cause some distortion of the electric field from the electric dipole, and investigation of this must be a priority.

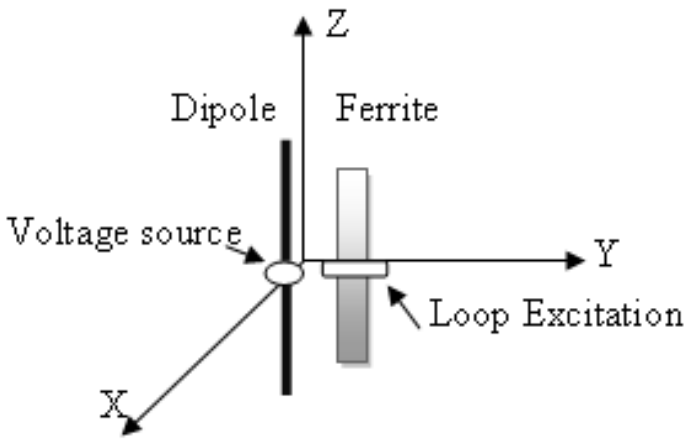

Figure 6.1: Electric dipole and magnetic (ferromagnetically-loaded) dipole in close juxtaposition.

In the first instance, a simple conceptual using FDTD codes was build up and analysed [26]. Both antennas were located close to the centre of the problem space of the FDTD model, as shown in Fig. 6.1. An ideal ferromagnetic material with a purely real permeability and permittivity, and no loss mechanisms was assumed. This was surrounded by a loop at its centre. The operating frequency used was 900 MHz.

The FDTD model used the following parameters:

- FDTD increment (cell) size: 5mm
- Length of the electric dipole: 170 mm (34 cells)
- Length of the ferromagnetic rod: 60 mm (12 cells)
- Width of the ferromagnetic rod: 20 mm (4 cells)
- Relative permeability of ferromagnetic rod: 4.3

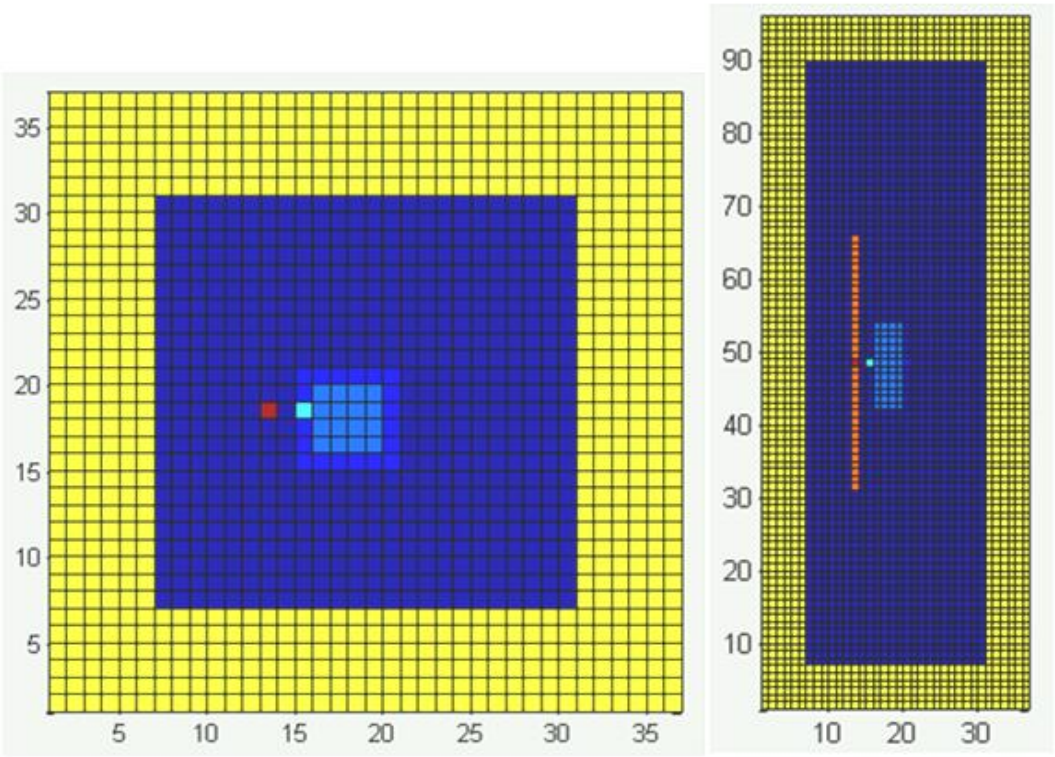

Figure 6.2: Conceptual FDTD model of a problem space surrounding the antennas in Fig.6.1. Left: cross-section; right: side view (note differing scales). Yellow: absorbing boundary condition; dark blue: air; red: electric dipole conductor; light blue: ferromagnetic rod; medium blue: loop of conductor around ferromagnetic rod; light turquoise: excitation point for conducting loop.

For a more advanced design, the ferromagnetic component was configured as a hollow tube, with the electric dipole threaded down its centre. This is technically feasible and it was thought that the radiation pattern from the electric dipole would be more axi-symmetric than for the first design. This modified design should simplify collocation of the three orthogonal replicas of the twin-dipole structure. The structure is shown in Figure 6.3, and its conceptual FDTD model is shown in Figure 6.4.

In Figure 6.4, the dimensional choices were:

- FDTD increment (cell) size: 3mm
- Length of the electric dipole: 168 mm (56 cells)

- Length of the ferromagnetic tube: 54 mm (18 cells)
- Width of the ferromagnetic tube: 30 mm (10 cells)
- Tube aperture width: 12 mm (4 cells)

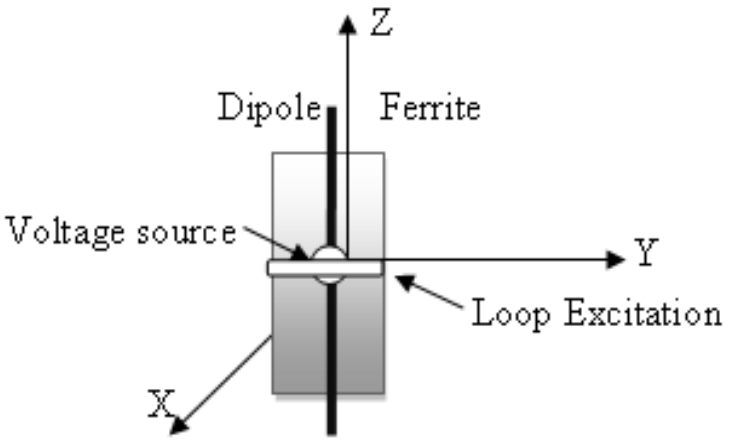

Figure 6.3: Coaxial electric and magnetic dipoles, using ferromagnetic tube for the latter.

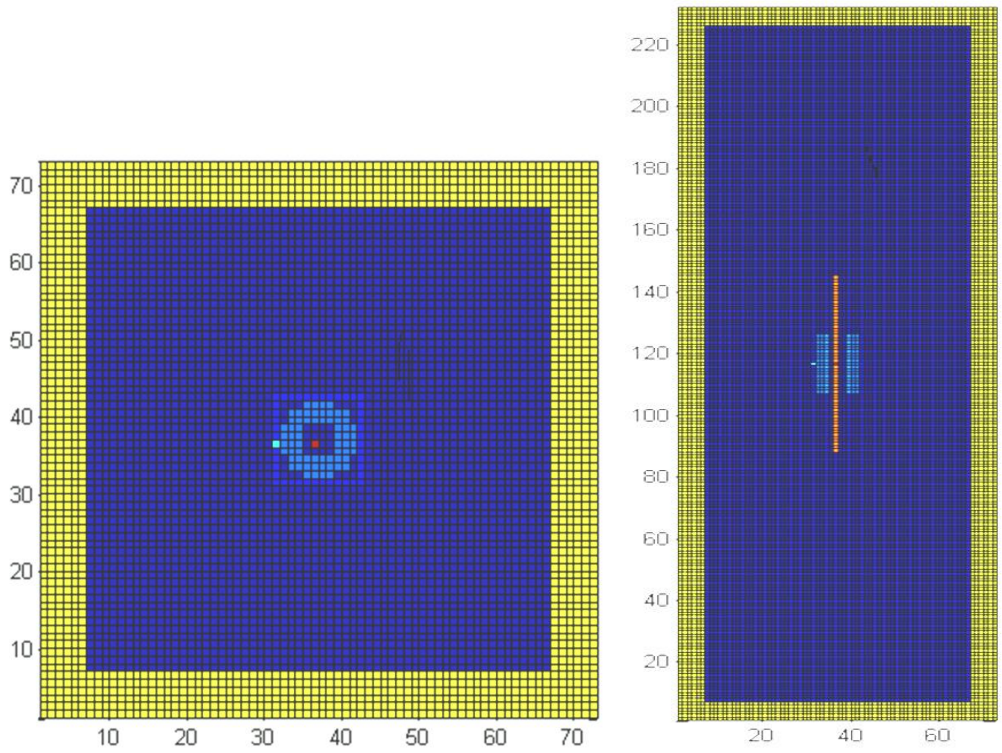

Figure 6.4: Geometry model of the problem space of Figure 3, using FDTD. Legend: as for Fig.6.2.

6.3 SIMULATION AND RESULTS

The return losses for the dipole and the ferromagnetically-loaded loop were 5dB and -4.6dB, respectively for the simple geometry (Fig. 2). For the coaxial geometry (Fig 6.4), the simulated return losses were -3.1dB and -3.5dB, respectively. These figures are close to practical values, and can be improved by using external matching networks.

The radiation patterns for the two designs were computed from the FDTD code. The patterns in the principal orthogonal planes for the antenna geometries shown in Figures 6.1 and 6.3, are shown in Figures 6.5 and 6.6, respectively. The shapes of the patterns for the electric dipole and the ferromagnetic rod are similar, although not identical. The curve for the magnetic antenna was particularly skewed with the simple design. This is probably due to the interaction between the two antennas, since they were not exactly collocated. The results for the coaxial case are much better, the only difference being a small filling of the nulls.

It was noted that mismatch at the feed point caused some gain attenuation for the magnetic dipole, this has been compensated out in the curves shown. Perhaps using a multi-turn coil in place of a single-turn loop to drive the ferromagnetic rod would be more practical, but the modelling of this using FDTD is significantly more involved, requiring local sub-gridding around the windings. A matching network and a balun would also be needed for both antenna elements.

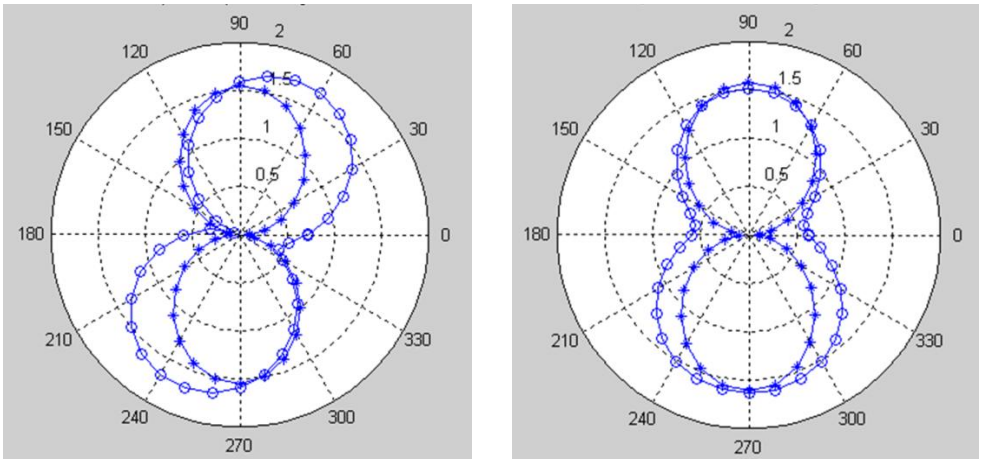

(a) (b)

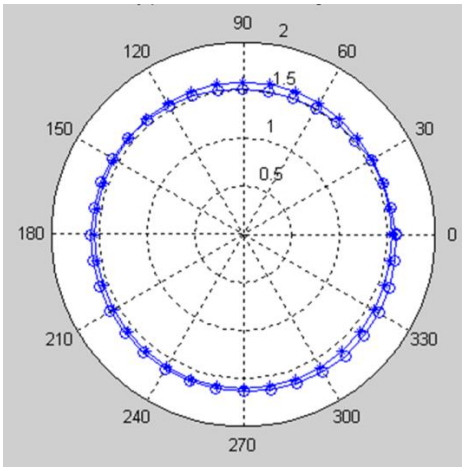

(c)

Figure 6.5: Radiation pattern of antenna geometry shown in Fig.6.1. Note that antenna is rotated to be horizontal for these plots.(a) x-z plane i.e., $\phi = 0°$. (b) y-z plane i.e., $\phi = 90°$.(c) x-y plane i.e., $\theta = 90°$. ¨*¨ Electric dipole -o- Ferromagnetically loaded loop antenna.

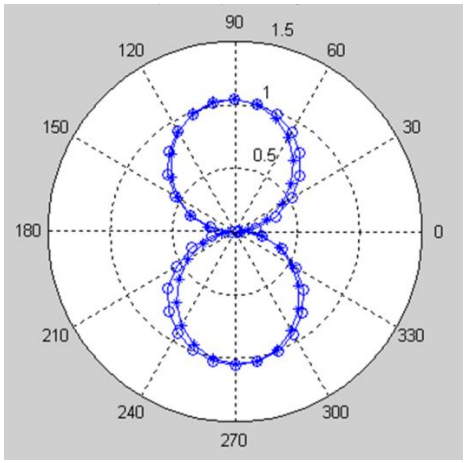

(a)

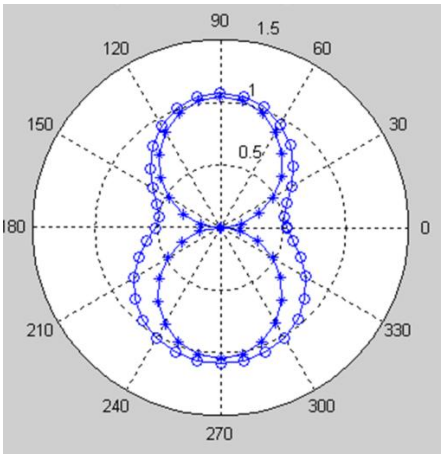

(b)

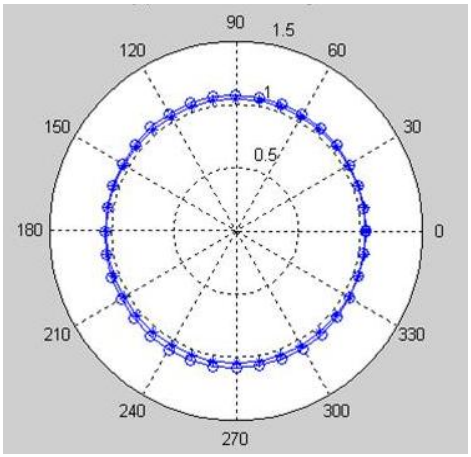

(c)

Figure 6.6: Radiation pattern of antenna geometry shown in Fig.6.2. Note that antenna is rotated to be horizontal for these plots.(a) x-z plane i.e., ϕ= 0°. (b) y-z plane i.e., ϕ= 90°.(c) x-y plane i.e., θ=90°. ¨*¨ Electric dipole -o- Ferromagnetically loaded loop antenna.

6.4 ANTENNA DESIGN USING HFSS

The concept of having compact dual dipole antennas with electrical and magnetic dipoles was very attractive in terms the compact antenna size that might be considered as a useful application for the next generation of Mobile handsets. The design concept presented in earlier sections were proved the possible operation of dual polarization

subject to spatial fields distribution, however, this also needs some design considerations to implement the antenna with acceptable radiation efficiency.

This section extends and optimizes the FDTD modelling to further prove the operational concept, subject to several design constraints using HFSS [27]. This has been employed since the cell structure grid used in FDTD of modelling the antenna geometry were not sufficiently accurate due to the intrinsic limitations of the stair-casing procedure used over the curved surfaces. Additionally, the polarization diversity and channel capacity over azimuth and zenith angular power spectra have been investigated and discussed. This includes raised cosine power spectrum over zenith and four three PAS functions such as: Uniform, Gaussian, Laplacian and Secant-Square for azimuth distributions.

The more realistic antenna structure consists of: an inner dipole of a conducting material, and the outer hollow cylindrical dipole of ferromagnetic material ($\mu_r = 22$). The choice of permeability is influenced by the desire to increase the magnetic properties of the outer coax. In other words to create a stronger magnetic field for the outer dipole, an establish an improved isolation with the electric fields in the inner coax. The total length of the inner dipole after several iterations was optimised at 206mm, and its corresponding diameter was 4mm. The length, thickness and diameter of the outer dipole were found to be 150mm, 10mm and 25mm, respectively.

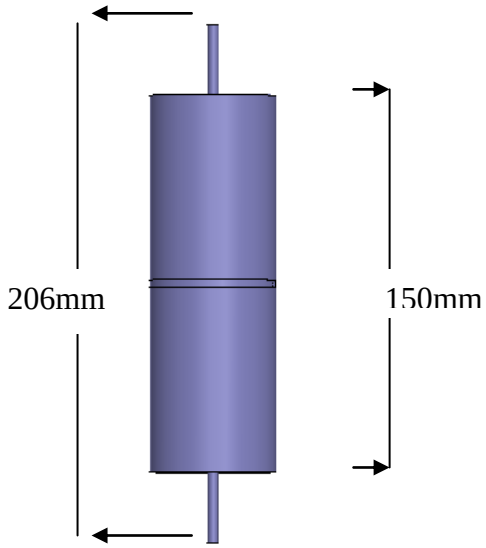

Figure 6.7: Side view of the proposed antenna geometry.

Simulation results attempted to prove the design concept of both inner and outer dipoles to resonant around 900 MHz band with input ports return loss less than -10 dB. Figures 6.7 and 6.8 show the side and cross sectional views of the proposed antenna structure respectively. Antenna geometry of other design frequency band is possible, however, is not considered in this present work. The curved surface model is quietly improved using the HFSS for accurately predicting the antenna performance.

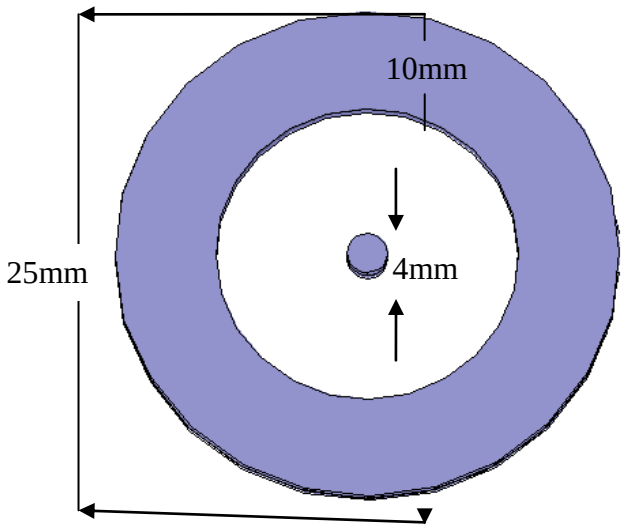

Figure 6.8: Cross-sectional view of the antenna geometry shown in Figure 6.7.

6.5 INPUT RETURN LOSS AND ANTENNA COUPLING

Figure 6.9 shows the input return loss of the antenna system at the two feed ports of the radiating elements. S_{22} represents the input return loss of the inner dipole, whereas S_{11} is the return loss considered by the outer magnetic dipole. It has been observed that the bandwidth of the magnetic dipole is less than the inner conducting dipole at the return loss of -10 dB.

Nevertheless, these results are quite encouraging. Reasonable computed relative impedance bandwidths exist for the GSM 900 band. These are 8.6% for magnetic dipole, and 60% for the inner dipole, at 6dB return loss that is equivalent to VSWR ≤ 3. Furthermore, the computed relative impedance bandwidth of the inner dipole at 10dB return loss is around 33%. It is plausible that the sharp bandwidth response of magnetic dipole is due to the high relative permeability of the magnetic material used for this particular design.

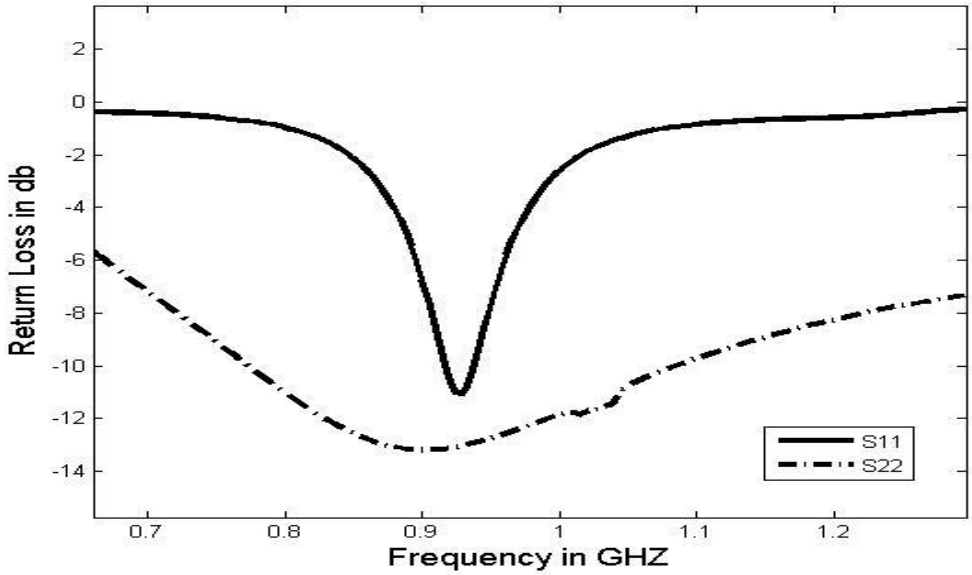

Figure 6.9: Input ports return loss of the antenna geometry depicts in Figure 6.7.

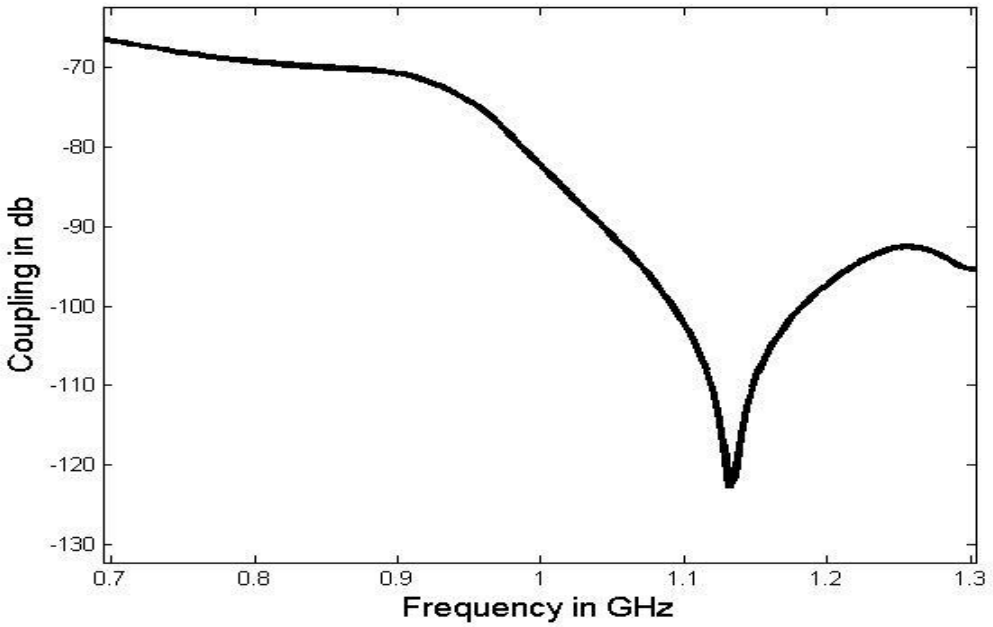

Figure 6.10: The mutual coupling between inner and outer dipoles

Figure 6.10 shows the response of S_{21} over a wide bandwidth which defines the coupling between the inner and outer input ports of the two dipoles. It can be observed from the graph that the coupling between the two dipole antennas is below -70db for the most of the considered bandwidth. It should be noted that the model considered is passive thus $S_{21} = S_{12}$. This large de-coupling factor provides a clear demonstration of the theoretical motivation behind the orthogonal polarization design concept.

6.6 RADIATED FIELD PATTERNS

The field patterns of both the inner and outer dipoles have been investigated at $\theta = 90^o$, the horizontal plane is considered for Φ from 0^o to 360^o. Figures 6.11 and 6.12 show the far field radiation patterns of the inner and the outer dipoles, respectively. From the simulated results, it has been clearly shown that in case of inner dipole E_θ (see Figure

6.11) is uniform over azimuth, and was also dominant. By contrast, the outer dipole E_{Φ} (see Figure 6.12) was clearly dominant and uniform. It should be noted that the cross polar field components of the inner and outer dipoles, were found around -50 dB and -15 dB, respectively. These results are quite acceptable for practical implementations of this type of antenna geometry.

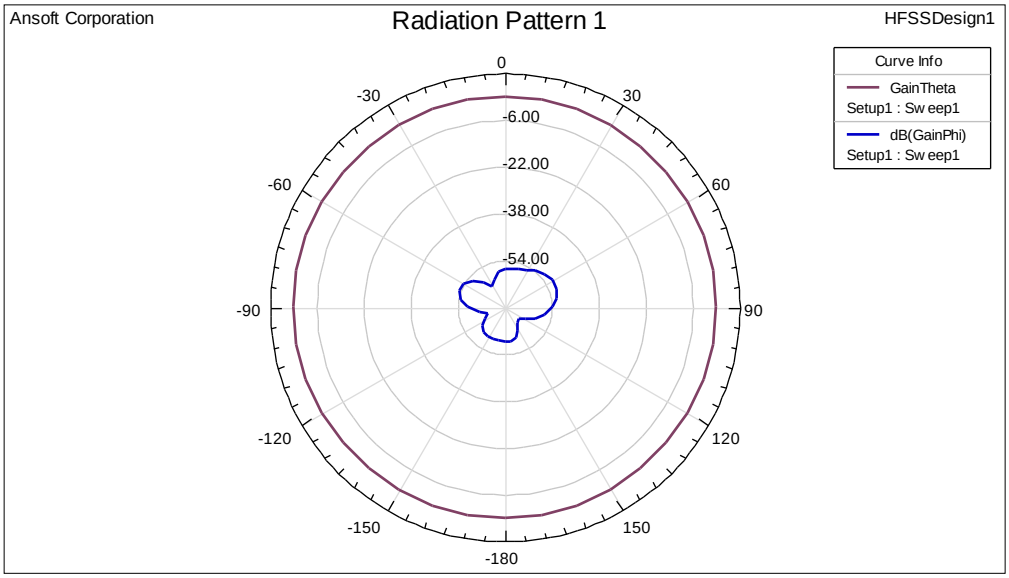

Figure 6.11: Field pattern of the inner dipole at zenith angle 90°.

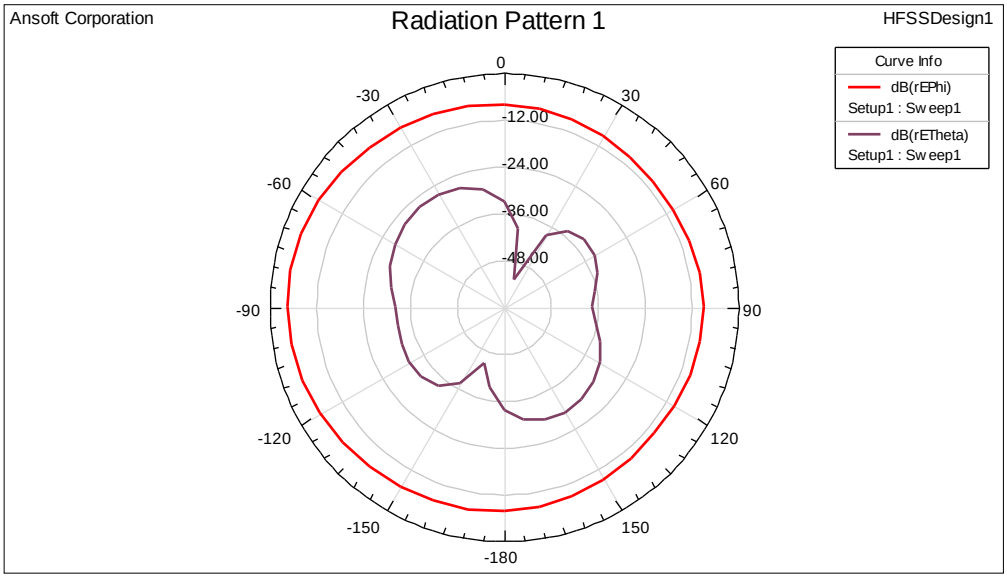

Figure 6.12: Radiated field pattern of outer dipole antenna.

The field patterns of both antennas working together are shown in Figure 6.13, for which the gain difference is stated in terms of the voltage incident fields considered at the input ports of both dipoles. These results were quite promising, and seem to prove the design concept, producing a dual-uniform cross-polarized pattern over similar azimuthal variations in the radiated fields.

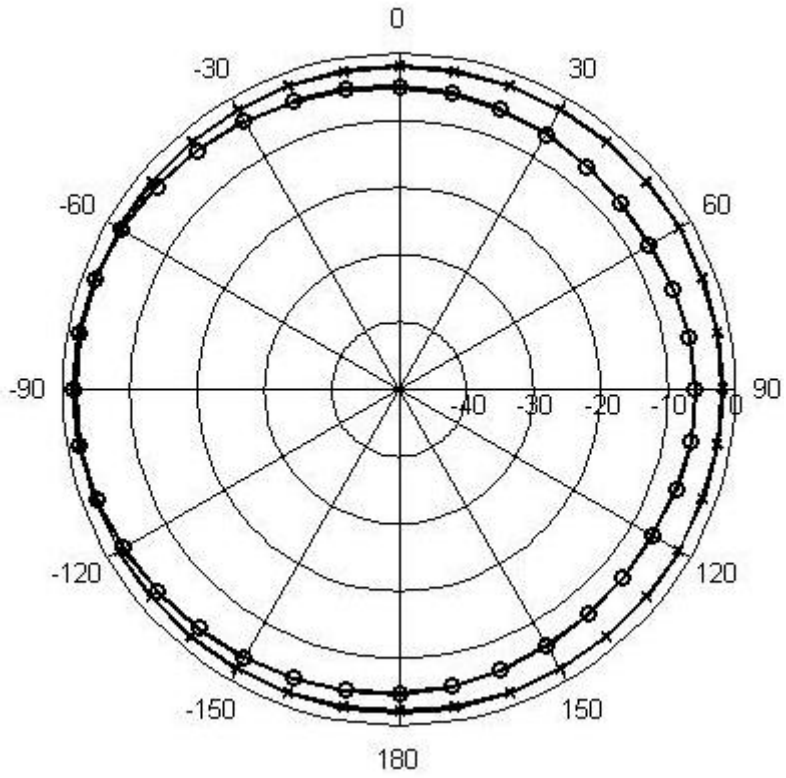

Figure 6.13: Radiated field pattern at zenith angle 90° of the antenna geometry shown in Figure 6.7 when both dipoles excited; E_θ (x-x-x), E_Φ (o-o-o).

6.7 POLARISATION DIVERSITY AND CHANNEL CAPACITY

The maximum channel capacity may be easily achieved by enforcing low mutual coupling between the radiating elements, and enhance the polarization diversity of the radiated field pattern. This is a very difficult task for these designs; however, the modelling indicates some possibilities for going forward. In this section the channel

capacity of the antenna geometry explained in previous section system is investigated over a Rayleigh fading channel having uniform, Gaussian, Laplacian and secant-squared azimuth power spectrum distributions and, uniform and raised cosine in the zenith angular distributions. This section considers the concept of a 2×2 MIMO antenna system, notionally using these antenna structures. The arrangement assumes ideal spatial polarization, considered on the transmit side, essentially as for the methodology established in Chapters 4.

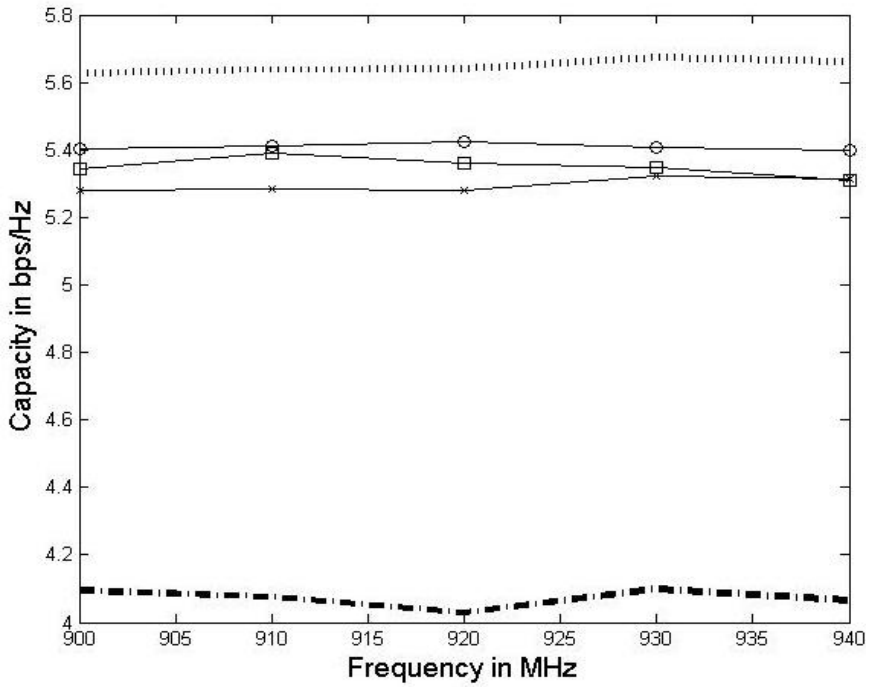

Figure 6.14: Variations of channel capacity versus operating frequency; subject to uniform PAS over 0 to 360° and uniform power spectrum over ±15° for various mean zenith angles of 40°, 70° and 90°; ('.....' upper limit of 2 × 2 MIMO), ('------'upper limit of 2 × 1 MIMO).

The channel capacities (with SNR of 10dB) vs. the operating frequency were shown in Figures 6.14 to 6.30. The variations of the channel capacity subject to uniform PAS over 0° to 360° and different power spectra over the zenith angle were presented in Figures 6.14 to 6.16. The power spectra considered along the zenith direction included:

uniform and raised cosine with different mean and raised cosine for different order. The maximum variations were found around 0.2 bps/Hz for all cases, even for the worst mean case of 90° (see Figure 6.15).

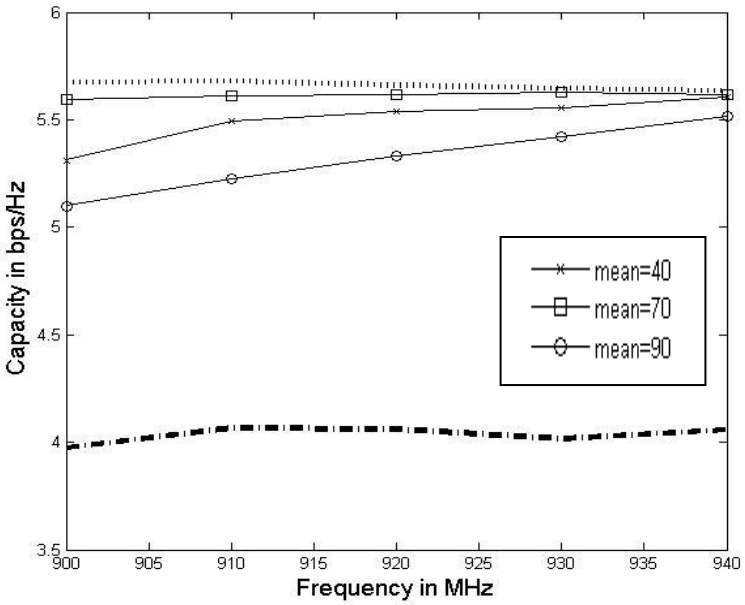

Figure 6.15: Variations of channel capacity versus operating frequency; subject to uniform PAS over 0 to 360° and raised cosine distribution power spectrum for various mean zenith angles of 40°, 70° and 90°; ('.....' upper limit of 2 × 2 MIMO), ('------ 'upper limit of 2 × 1 MIMO).

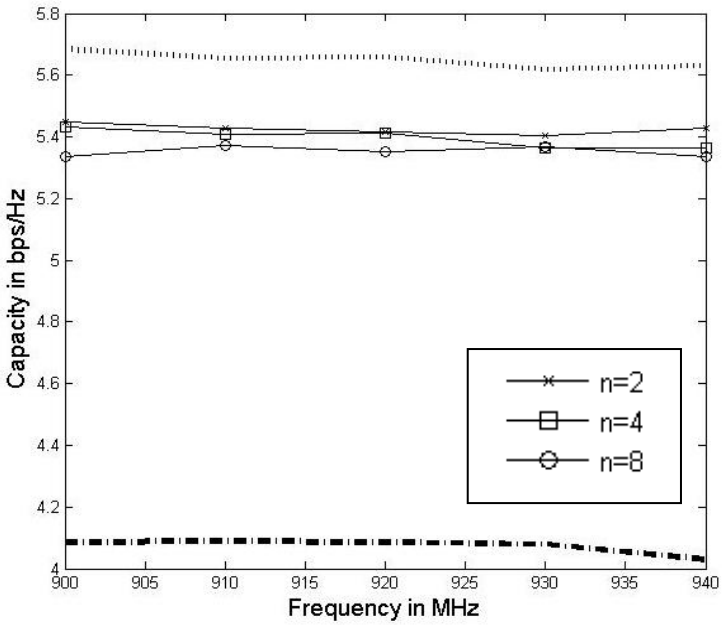

Figure 6.16: Variations of channel capacity versus operating frequency; subject to uniform PAS over 0 to 360° and n^{th} order raised cosine distribution power spectrum for mean zenith angle of 90°; ('.....' upper limit of 2 × 2 MIMO), ('------'upper limit of 2 × 1 MIMO).

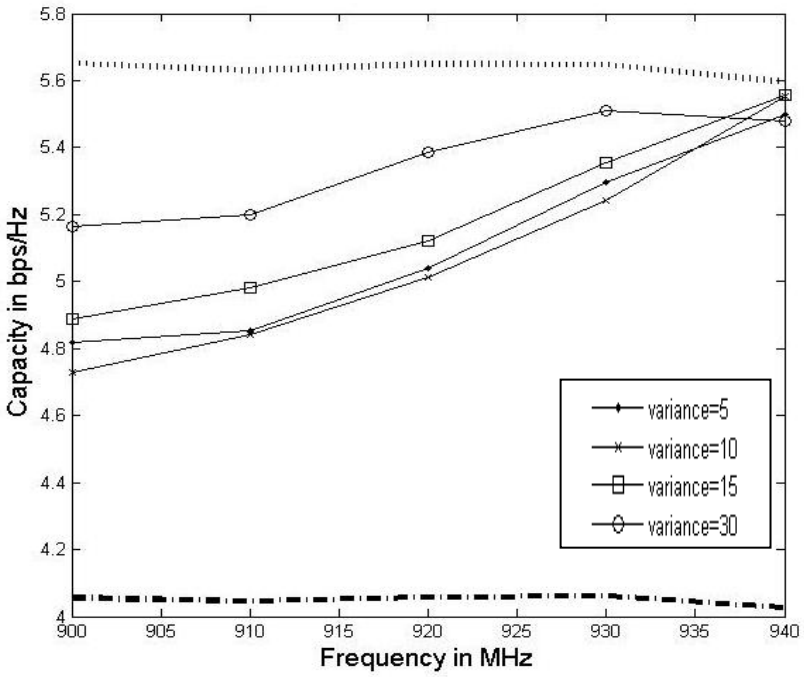

Figure 6.17: Variations of channel capacity versus operating frequency; subject to Gaussian PAS over 0 to 360° with mean 45° and different variances, and uniform power spectrum over ±15° for mean zenith angle of 90°; ('.....' upper limit of 2 × 2 MIMO), ('-----'upper limit of 2 × 1 MIMO).

Similarly, the Figures 6.17 to 6.21 demonstrate the possible variations of the channel capacities of the MIMO system for Gaussian PAS distribution over 0° to 360° for different variances, and also for various mean zenith angles and distributions. The variances used were varied between 5° and 30°, whereas the mean zenith angle was confined between 70° to 90°.

The variations in all the capacity values were acceptable, and the maximum changes appear around the worst case of smallest variance in the PAS. However, 0.6 bps/Hz is the maximum change appearing on the lowest frequency component of the capacity response. In spite of this particular case, all the capacity values were reasonable and found above 5.2 bps/Hz. It should be noted that several almost negligible changes were found when raised cosine of 2^{nd} and 4^{th} order power spectrum distributions in the zenith angular direction were considered (see Figures 6.20 and 6.21). These changes were approximately 0.1 bps/Hz, and also appear at the lowest frequency component.

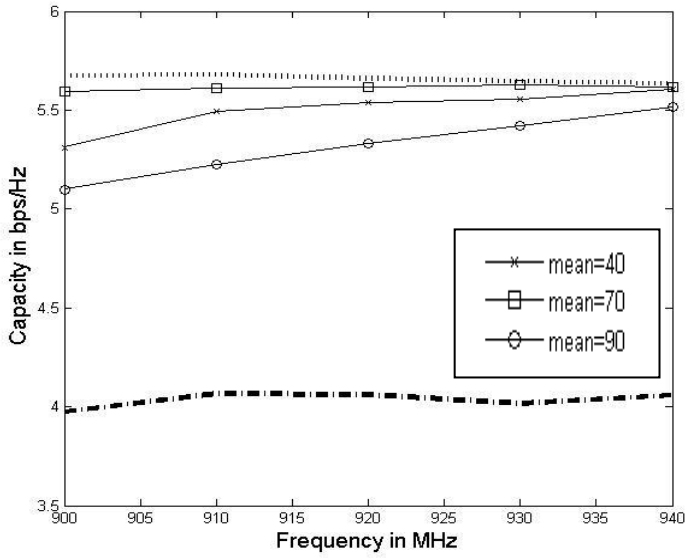

Figure 6.18: Variations of channel capacity versus operating frequency; subject to Gaussian PAS over 0 to 360° with mean 45° and variance 30°, and uniform power spectrum over ±15° for various mean zenith angles of 40°, 70° and 90°; ('.....' upper limit of 2 × 2 MIMO), ('------'upper limit of 2 × 1 MIMO).

Similarly, Figures 6.22 to 6.25 show the variations of the capacity vs. the frequency subject to Laplacian PAS distribution with various variances and different spectral power distribution in zenith angle. It is evident that there were no large variations in these distributions, except for the tiny change in the variance of the PAS. In addition, no large differences appear when changing the zenith power distribution.

Finally, the variations of the capacity vs. operating frequency using secant-squared PAS distribution were found quite similar to the Gaussian and Laplacian PAS distributions, as shown in Figures 6.26 to 6.30, for different power spectra over the zenith angle. In summary, the maximum variations are close to 0.5 bps/Hz for most of the cases studied.

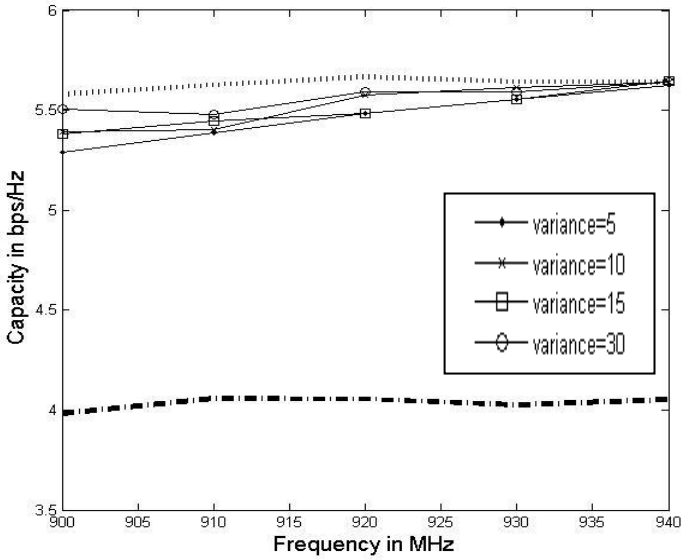

Figure 6.19: Variations of channel capacity versus operating frequency; subject to Gaussian PAS over 0 to 360° with mean 45° and different variances, and raised cosine distribution power spectrum with mean of 90°; ('.....' upper limit of 2 × 2 MIMO), ('-----'upper limit of 2 × 1 MIMO).

In general, the mean capacity values always appear located close to the ideal case of the 2×2 MIMO capacity values for all cases considered as presented in Table 6.1. These results confirm the best achievement of the proposed 2×2 MIMO system inherent in spatial polarization diversity design. The system may be extended by including one or

two more similar elements with slightly modified antenna geometry to consider the other spatial polarization components.

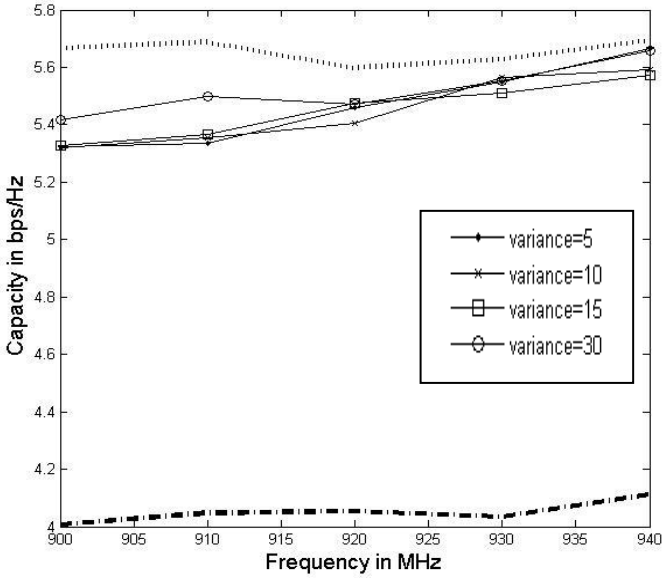

Figure 6.20: Variations of channel capacity versus operating frequency; subject to Gaussian PAS over 0 to 360° with mean 45° and different variances, and raised cosine distribution of 2nd order power spectrum with mean of 90°; ('.....' upper limit of 2 × 2 MIMO), ('------'upper limit of 2 × 1 MIMO).

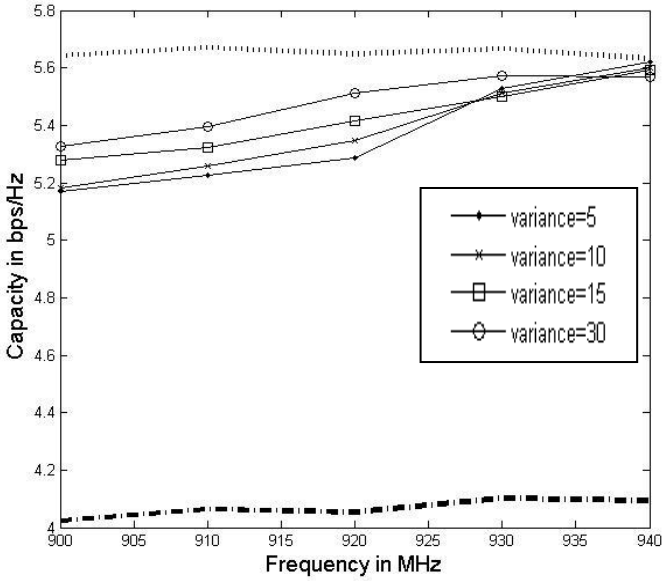

Figure 6.21: Variations of channel capacity versus operating frequency; subject to Gaussian PAS over 0 to 360° with mean 45° and different variances, and raised cosine distribution of 4th order power spectrum with mean of 90°; ('.....' upper limit of 2 × 2 MIMO), ('------'upper limit of 2 × 1 MIMO).

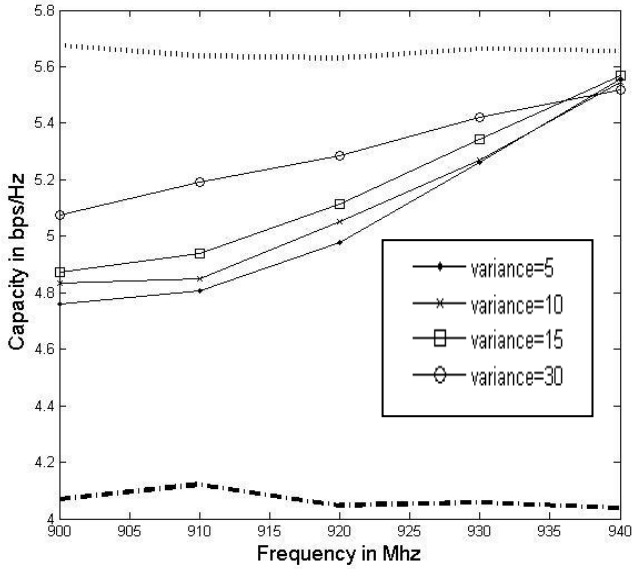

Figure 6.22: Variations of channel capacity versus operating frequency; subject to Laplacian PAS over 0 to 360° with mean 45° and different variances, and uniform distribution over ±15° power spectrum with mean of 90°; ('.....' upper limit of 2 × 2 MIMO), ('------'upper limit of 2 × 1 MIMO).

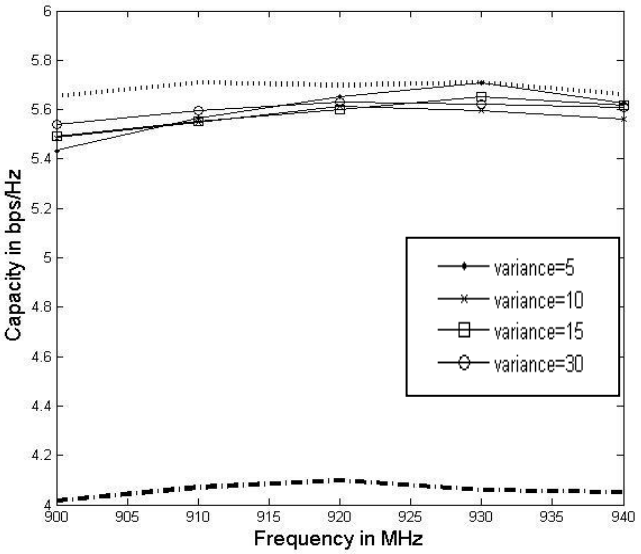

Figure 6.23: Variations of channel capacity versus operating frequency; subject to Laplacian PAS over 0 to 360° with mean 60° and different variances, and raised cosine distribution power spectrum over zenith angle with mean of 90°; ('.....' upper limit of 2 × 2 MIMO), ('------'upper limit of 2 × 1 MIMO).

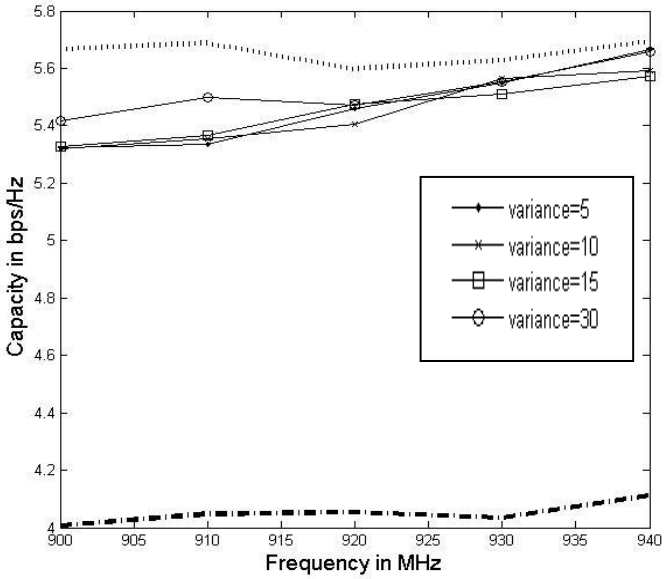

Figure 6.24: Variations of channel capacity versus operating frequency; subject to Laplacian PAS over 0 to 360° with mean 45° and different variances; and raised cosine distribution of 2nd order power spectrum with mean of 90°; ('.....' upper limit of 2 × 2 MIMO), ('------'upper limit of 2 × 1 MIMO).

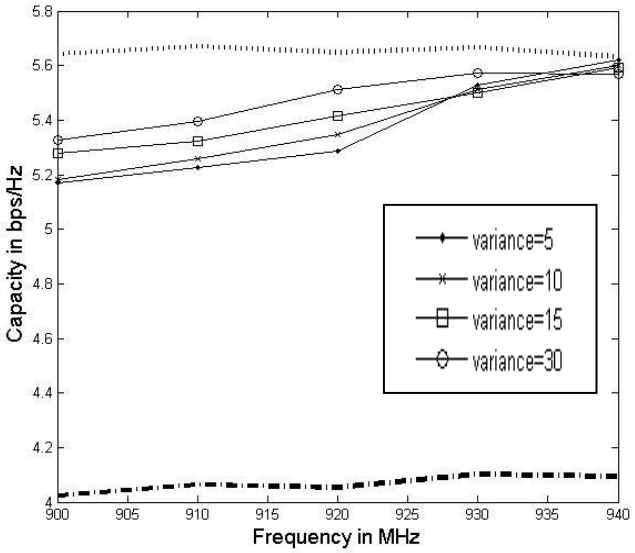

Figure 6.25: Variations of channel capacity versus operating frequency; subject to Laplacian PAS over 0 to 360° with mean 45° and different variances; and raised cosine distribution of 4th order power spectrum with mean of 90°; ('.....' upper limit of 2 × 2 MIMO), ('------'upper limit of 2 × 1 MIMO).

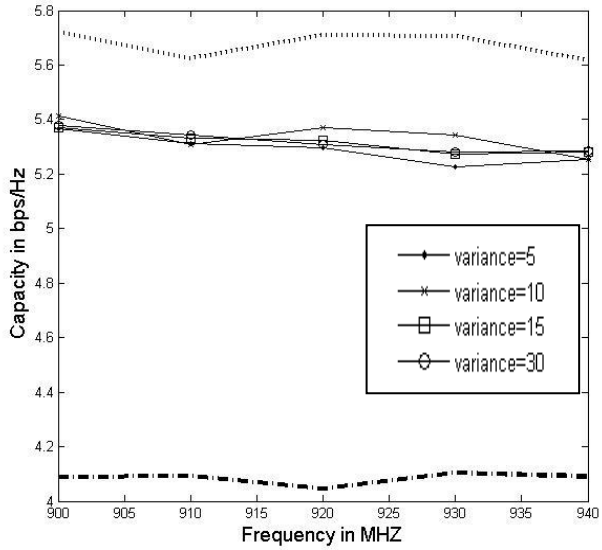

Figure 6.26: Variations of channel capacity versus operating frequency; subject to Secant Square PAS over 0 to 360° with mean 45° and different variances, and uniform distribution over ±15° power spectrum with mean of 90°; ('.....' upper limit of 2 × 2 MIMO), ('------'upper limit of 2 × 1 MIMO).

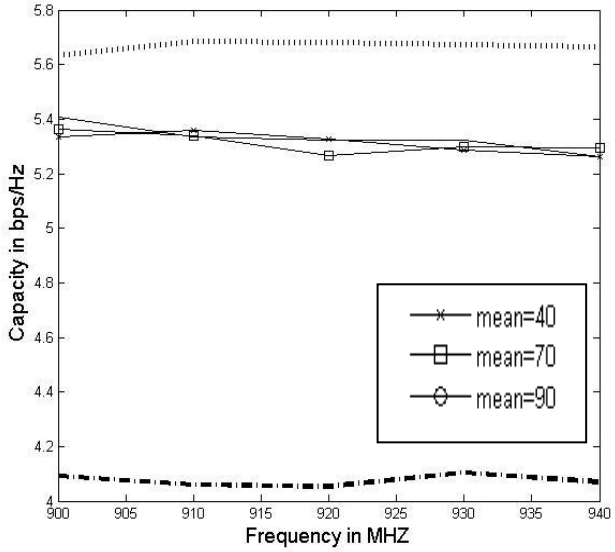

Figure 6.27: Variations of channel capacity versus operating frequency; subject to Secant Square PAS over 0 to 360° with mean 45° and variance 30°; and uniform distribution over ±15° power spectrum with various means angles of 40°, 70° and 90°;; ('.....' upper limit of 2 × 2 MIMO), ('------'upper limit of 2 × 1 MIMO).

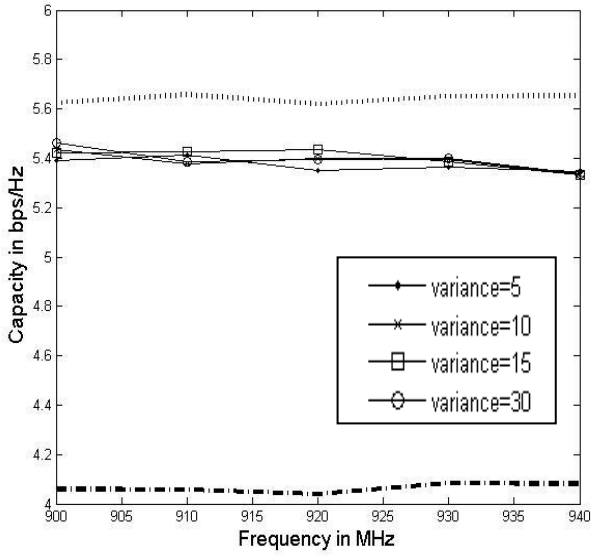

Figure 6.28: Variations of channel capacity versus operating frequency; subject to Secant Square PAS over 0 to 360° with mean 45° and different variances, and raised cosine of 2nd order distribution power spectrum over zenith angle with mean of 90°; ('.....' upper limit of 2 × 2 MIMO), ('------'upper limit of 2 × 1 MIMO).

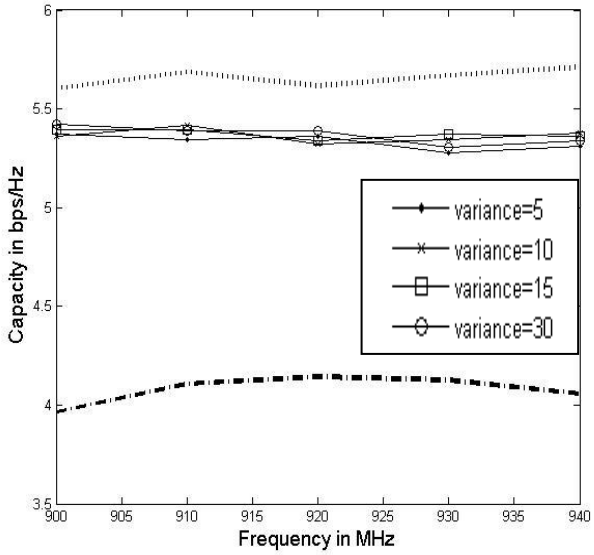

Figure 6.29: Variations of channel capacity versus operating frequency; subject to Secant Square PAS over 0 to 360° with mean 45° and different variances, and raised cosine of 4th order distribution power spectrum over zenith angle with mean of 90°; ('.....' upper limit of 2 × 2 MIMO), ('------'upper limit of 2 × 1 MIMO).

Table 6.1: Summarised channel capacity of the proposed antenna shown in Fig. 6.7.

Power Distributions		**Mean of Calculated Channel Capacity (Bps/Hz)**
Azimuth	**Elevation**	**900 to 940 MHz**
Uniform	Uniform	5.35
Uniform	Raised Cosine	5.38
Uniform	n^{th} Order raised Cosine	5.37
Gaussian	Uniform	4.81
Gaussian	Raised Cosine	5.48
Gaussian	2^{nd} Order raised Cosine	5.41
Gaussian	4^{th} Order raised Cosine	5.29
Laplacian	Uniform	5.12
Laplacian	Raised Cosine	5.53
Laplacian	2^{nd} Order raised Cosine	5.42
Laplacian	4^{th} Order raised Cosine	5.31
Secant Square	Uniform	5.33
Secant Square	Raised Cosine	5.41
Secant Square	2^{nd} Order raised Cosine	5.38
Secant Square	4^{th} Order raised Cosine	5.42

6.8 CONCLUSION

In this chapter a news style of dual polarised antenna is investigated, by simulation, for possible use in mobile MIMO terminal technologies. Two designs are proposed and optimised for GSM900 band operation, each is based on the use of over-laying an

electric and a magnetic dipole antenna ultimately into a coaxial geometry, such that their radiation patterns are nominally identical, but cross-polarised. The initial concept was developed using a FDTD code, and selectively refined through parametric optimisation using Ansoft HFSS^{TM}. The two radiators performed broadly according to expectations, i.e. as identifiable electric and magnetic dipoles with cross-polarised fields.

Channel capacity was investigated over a Rayleigh fading channel with Gaussian, Laplacian and secant-squared distributions. The analysis was for a nominal 2×2 MIMO antenna, these results clearly show the required polarisation diversity of the inner and outer dipoles, and the channel capacity is close to the ideal 2×2 maximum.

It is possible to speculate that orthogonal assemblies may be created using radiators of this type which might function as mobile array antennas, in line with the 'tripole' concept of Andrews et al [1], ultimately closing the gap between traditional line of sight transmission and the theoretical six-fold enhancement possible in a rich multi-path environments such as indoors (industrial or domestic), or from urban canyons. These simulations have illustrated some of the design challenges which need to be overcome in order to realise practical mobile multi-antenna transceivers of this type. The sleeve dipole structure proposed here for the electric dipole would enable cable feeds and physical supports to be provided, thus bringing the possibility within grasp.

6.9 REFERENCES

[1] M. R. Andrews, P. Mitra and O. Decarvalho, “Tripling the capacity of wireless communications using electromagnetic polarization”, Nature, vol. 409, no. 6818, pp. 316-318, 2001.

[2] J. B. Anderson and B. N. Getu, “The MIMO cube - a compact MIMO antenna”, 5th International Symposium on Wireless Personal Multimedia Communications, vol. 1, pp.112- 114, Oct. 2002.

[3] S. N. Marakov, “Antenna and EM Modelling with Matlab”, New York: J. Wiley, 2002.

[4] B. Vrcelj and P. P. Vaidyanathan, “MIMO Biorthogonal Partners and Applications”, IEEE Transactions on Signal Processing, vol. 50, Issue 3 , pp. 528 – 542, March 2002.

[5] Dong L.; Ling H; Heath R.W, “Multiple-input multiple-output wireless communication systems using antenna pattern diversity”, IEEE Global Telecomm. Conf., vol. 1, pp.997-1001, Nov. 2002.

[6] Usman M, Abd-Alhameed R.A. and Excell P.S, “Design Considerations of MIMO Antennas for Mobile Phones”, PIERS Online, Vol. 4, No. 1, 2008, pp.121-125.

[7] A. Hottinen, et al, “Multi-antenna Transceiver Techniques for 3G and Beyond”, Wiley, 2003.

[8] C. Oestges, B. Clerckx, M. Guillaud and M. Debbah, “Dual-polarized wireless communications: from propagation models to system performance evaluation”, IEEE Transactions on Wireless Communications, Volume 7, Issue 10, October 2008, pp. 4019 – 4031.

[9] Oestges. C, “Mutual information of non-Kronecker structured dual-polarized 2×2 channels”, IEEE Transactions on Vehicular Technology, Volume 55, Issue 1, Jan. 2006, pp. 410 – 413.

[10] A. Agmon, B. Schrenk, J. Prat, and M. Nazarathy, “Polarization beamforming MIMO-based PON: 20 Gb/s transmission over a 10 Gb/s system with dynamic power allocation and 1.8 dB improved reach”, Conference on Optical Fiber Communication OFC 2009, 22-26 March 2009, pp. 1–3.

[11] N. Prayongpun and K. Raoof, “Correlation Effects and Channel Capacities for MIMO Polarization Diversity”, International Conference on Wireless Communications, Networking and Mobile Computing, WiCOM 2006, 22-24 Sept. 2006, pp. 1–4.

[12] K. Nishimori, Y. Makise, N. Ida, R. Kudo, and K. Tsunekawa, “Channel Capacity Measurement of 8 times 2 MIMO Transmission by Antenna Configurations in an Actual Cellular Environment”, IEEE Transactions on Antennas and Propagation, Volume 54, Issue 11, Part 1, Nov. 2006, pp. 3285–3291.

[13] M. Q. Mali and D. J. Edwards, “Measured MIMO Capacity and Diversity Gain With Spatial and Polar Arrays in Ultrawideband Channels”, IEEE Transactions on Communications, Volume 55, Issue 12, Dec. 2007, pp. 2361–2370.

[14] J. F. Valenzuela-Valdes, A. M. Martinez-Gonzalez, and D. Sanchez-Hernandez, “Estimating Combined Correlation Functions for Dipoles in Rayleigh-Fading Scenarios”, IEEE Antennas and Wireless Propagation Letters, Volume 6, 2007, pp. 349 – 352.

[15] A. Dunand and J-M., Conrat, “Polarization Behaviour in Urban Macrocell Environments at 2.2 GHz”, the Second European Conference on Antennas and Propagation EuCAP 2007, 11-16 Nov. 2007, pp. 1–6.

[16] H. Ozceli and C. Oestges, “Some remarkable properties of diagonally correlated MIMO channels”, IEEE Transactions on Vehicular Technology, Volume 54, Issue 6, Nov. 2005, pp. 2143 – 2145.

[17] G. Calcev, et al, “A Wideband Spatial Channel Model for System-Wide Simulations”, IEEE Transactions on Vehicular Technology, Volume 56, Issue 2, March 2007, pp. 389 – 403.

[18] K. Shoshan, and O. Amrani, “Polarized-mimo capacity analysis in street-canyon using 3D ray-tracing model”, Electrical and Electronics Engineers in Israel, IEEEI 2008, IEEE 25th Convention of, 3-5 Dec. 2008, pp. 741-744.

[19] Yu Deng; A. Burr, and G. White, “Performance of MIMO systems with combined polarization multiplexing and transmit diversity”, Vehicular Technology Conference, VTC 2005-Spring, IEEE 61st, Volume 2, 30 May-1 June 2005, pp. 869–873.

[20] Y. Ofuji, et al, “Field Experimental Results of E-UTRA Downlink with Precoding and Non-Precoding MIMO”, Vehicular Technology Conference, VTC Spring 2009, IEEE 69th, 26-29 April 2009, pp. 1–5.

[21] M. Narayanan et al, “Multi Polarization Antenna Structures for Efficient MIMO Systems Employing Software Radio Design”, International Conference on Methodology, RF and Microwave RFM 2006, 12-14 Sept. 2006, pp. 390–392.

[22] M. Usman, R. A. Abd-Alhameed and P. S. Excell, “Dual-Band Three-Antenna Polarisation-Diverse MIMO System for Mobile Devices”, International Conferences on Internet Technologies and Applications (ITA 09), Wrexham, UK, Sept. 2009.

[23] D. G. Landon and C. M. Furse, “Recovering Handset Diversity and MIMO Capacity With Polarization-Agile Antennas”, IEEE Transactions on Antennas and Propagation, Volume 55, Issue 11, Part 2, Nov. 2007, pp. 3333–3340.

[24] J. F. Valenzuela-Valdes, M. A. Garcia-Fernandez, M. A. Martinez-Gonzalez, D. Sanchez-Hernandez, “Doubling MIMO capacity for handset MIMO using true polarization diversity”, 3rd European Conference on Antennas and Propagation, EuCAP 2009, 23-27 March 2009, pp. 1090-1092.

[25] RJ and US Imports, Australia, “Choice of Core Material”: http://users.catchnet.com.au/~rjandusimports/tut_2a.html (viewed 28/2/09).

[26] P. S. Excell and J. A. Vaul, “Evolution of a Suite of Computational Modeling Tools for Mobile Telephone Dosimetry Studies at Bradford University, U.K.”, Applied Computational Electromagnetics Society Journal, Vol. 16, No. 2, July 2001, pp. 97-105.

[27] The High Frequency Structure Simulator (HFSS^{TM} Version 11) Users’ Manual, Ansoft Corportation, Pittsburgh (USA), http://www.ansoft.com/products/hf/hfss/, (part of the ANSYS Group).

CHAPTER 7

CONCLUSIONS AND SUGGESTIONS FOR FUTURE WORK

7.1 CONCLUSIONS

The main subject of this thesis has been the study of MIMO antenna systems for terminal technology applications in the field of personal mobile communications. The necessary orientation in MIMO methodology has been reviewed, and a step by step design procedure for terminal (handset) antenna design has been proposed. MIMO 2×2 and 3×3 antenna solutions have been sought and benchmarked against the IEEE 802.11b/g (2.4GHz ISM band) and IEEE 802.11a (5GHz band) WLAN standards [1-5].

Channel capacity forecasts have been made for 2×2 and 3×3 MIMO antenna systems employing the spatial polarisation diversity approach for a variety of representative channel models. The results of this analysis show that the maximum channel capacity within a small volume of space can be achieved through the careful selection of local, spatially averaged, orthogonal field components [6,7]. These results are compared vs. a circular planar array, where it can be seen that the intrinsic antenna volume is notably larger than the proposed MIMO systems under discussion.

The results of this vigorous research showed the use of polarization concept in combination with antenna design geometry can significantly reduce the size of the MIMO antennas and practically provide the maximum level of the required channel capacity.

7.2 SUMMARY OF THE THESIS

The conclusions of this work can be summarised by Chapter as follows.

Chapter 2 presents an overview of MIMO principles taken in the context of personal mobile communications. MIMO system performance is discussed in terms of channel state information (CSI) and TDMA modelling. Some analytical solution methods are also given for comparison.

Chapter 3 is concerned with the conceptual framework, and derivation, of the channel capacity of MIMO antenna systems. Initial discussions of system models were based on Matlab simulations for a variety of common power spectra. Specifically: Gaussian, Laplacian, secant-squared and raised cosine distributions. An argument is also presented for the efficient 'space filling' of the MIMO antenna design based on the spatially averaged polarisation state geometry. The channel capacity of ideal 2×2 and 3×3 prototypes, excluding coupling, is investigated for various polarisation angles over a Rayleigh faded channel model. The utilisation of the orthogonality property in achieving maximum channel capacity is illustrated for the various power spectra alluded to above.

Chapter 4 presents different MIMO antenna designs for the proposed mobile terminal applications. These designs include 2×2 and 3×3 MIMO antennas mounted on two and three orthogonal plane surfaces respectively. The practical implementation used a copper box to emulate the chassis of the mobile. A planar inverted 'F' antenna (PIFA) in combination with an L-antenna were optimised over the given chassis volume for input return loss and element coupling over the required bandwidth. Dual band operation was considered for 2.5 GHz and 5.2 GHz WLAN operating bands. Using a design concept based on a magnetic symmetry wall, an approximately 50% reduction in the intrinsic antenna volume was achieved for the 3×3 prototype. By balancing the size and bandwidth constraints, both prototypes appear to be attractive candidates for terminal applications. In the WLAN test case, the size constraint was 30mm×15mm×8mm.

The effect of the human hand on the operation of the 3×3 prototype was investigated and discussed in terms of the input return loss and coupling effects between the elements. The results appear to be very encouraging; especially as the minimum coupling factors were observed between -12dB and -15dB.

The far field radiation characteristics of the prototypes were also investigated at the two WLAN bands, in which average gains of 3.1dB and 4.5dB were achieved for the 2.5GHz and 5.2GHz bands, respectively. Significantly, the fields show that the maximum co-polarised component appearing at the (+z) bore-sight direction for both the E and H planes. The measured field patterns indicate a satisfactory level of polarisation purity.

Channel capacity computations are presented (using Matlab codes) over various power spectra for both the azimuth and zenith directions. The M-files require the far field data for each element. Once again the effects of introducing the hand model were observed; both prototypes displayed a 0.2 to 1.2 bps/Hz reduction from the maximum achievable capacity of the freely coupled case.

Chapter 5 presents a new dual band 2×2 MIMO antenna prototype. Two planar folded dipole antennas are constructed over a 100mm×50mm copper plate ground plane. Balanced antennas are of course well known in traditional radio communications. This MIMO implementation shows notable improvements in the mutual coupling between the antenna elements and handset; this improvement was maintained when the coupling system was extended to include the hand. The prototype was antenna performance was characterised in terms of the input return loss, mutual couplings and radiation patterns, where good agreement can be observed with the computational models. There is also an enhanced channel capacity over the two WLAN bands considered in the test system.

Chapter 6 presents a new dual polarised dipole antenna design, which is intended for use as one of three orthogonally orientated collocated antennas. This system is part of the physical layer of a mobile terminal in a 'polarisation diversity MIMO' communications system. The antenna design was intended for use at 900MHz (GSM band). The proposed antenna structure comprises two overlaid dipoles, one electric, one magnetic; their radiation patterns are nominally identical, but are cross-polarised and have minimal interaction. Models were developed using a FDTD simulation code and Ansoft HFSS^{TM}. These models perform broadly according to expectation, but actual

fabrication of a physical prototype would be a serious engineering challenge. The channel capacity of this proposed system is also in line with expectations.

7.3 SUGGESTIONS FOR FURTHER WORK

The following recommendations for further study are mostly focussed on extensions to handset antenna design methodology and antenna technologies.

- Practical antenna design is often very protracted work, and the search for more efficient design strategies constitutes a large proportion of both practical design and research outputs. One possible solution for complex antenna systems such as those described in Chapters 4–6, which incorporate multiple and competing objectives, is from the implementation of Genetic Algorithms [8-10]. The abstract design space would comprise: antenna structure parameters, antenna performance parameters and coupling, biological factors relating to specific design criteria (SAR and HAC) and system/environmental metrics. Genetic algorithms offer the possibility of exploring the competition landscapes formed from these multiple criteria and seeking out more promising combinations of structural and system design parameters.

- The introduction of metamaterial solutions into practical mobile antenna design is a long term goal of many researchers. These structures are often conceptualised as periodic metallo-dielectric composites, which are characterised to work on bands of frequencies where no propagating modes exist. A particular style of metamaterial system is the EBG, a conceptual simplification of the ‘photonic crystal’ structure, suitable for substantially planar

integrated designs. In various implementations EBG properties may be used to guide, store, filter, collimate or reflect electromagnetic radiation [11-16]. The extension of metamaterial components to the subject matter of Chapters 4-6 is intriguing, and in practice may have some degree of overlap (natural, or forced) with the next three items.

- The performance of MIMO antenna systems can be investigated further by involving switchable embedded control mechanisms to the antenna assembly. The aim would be to promote multi-functionality in operations such as specific field diversity over different frequency bands [17].

- Dielectric resonator antennas (DRAs) may be considered for use in MIMO antenna systems, particularly with respect to the size reduction criteria [18].

- Fractal antennas [19] provide the possibility of multiband operation for different frequencies which are not necessarily harmonically related. Notionally, the expectation is that a specific fractal iteration may deliver the required frequency agility without the need for discrete loads.

- The use of transmit/receive (TX-RX) beam-forming is an attractive area of research which utilizes the benefit of MIMO wireless systems [20-21]. It has the potential to provide a large diversity and array gains without the need for sophisticated signal processing at the transmitter and/or receiver.

7.4 REFERENCES

[1] Gao, Y., X. Chen, Z. Ying, and C. Parini, "Design and performance investigation of a dual-element PIFA array at 2.5 GHz for MIMO terminal", IEEE Transactions on Antennas and Propogation, Vol. 55, No. 12, Dec. 2007.

[2] Manteghi, M. and Y. Rahmat-Samii, "Novel compact tri-band two-element and four-element MIMO antenna designs", Proc. IEEE Int. Symp. Antennas Propag., 4443-4446, Jul. 2006.

[3] Browne, D. W., M. Manteghi, M. P. Fitz, and Y. Rahmat-Samii, "Experiments with compact antenna arrays for MIMO radio communications", IEEE Transactions on Antennas and Propogation, Vol. 54, No. 11, Dec. 2006

[4] Gao, Y., C. C. Chiau, X. Chen, and C. G. Parini, "Modified PIFA and its array for MIMO terminals", Inst. Elect. Eng. Proc. Microw. Antennas Propag., Vol. 152, No. 4, 253-257, Aug. 2005.

[5] Gao, Y., , C. C. Chiau, X. Chen, and C. G. Parini, "A compact dual-element PIFA array for MIMO terminals", Loughborough Antennas Propag. Conf., Apr. 2005.

[6] Muhammad Usman, Raed A Abd-Alhameed and Peter S Excell “Investigation of channel capacity of MIMO system on mobile phones”, published in Informatics Workshop, University of Bradford, 2007, United Kingdom.

[7] Muhammad Usman, Raed A Abd-Alhameed and Peter S Excell , “Channel Capacity of MIMO Systems for Mobile Phones Using Polarization Diversity for

Different Power Azimuth Spectrums", by published in URSI Symposium 2-3 July 2007, University of Portsmouth, United Kingdom, paper No 6.

[8] Mirzapour. B, Hassani. H.R, "Sizareduction and bandwidth enhancement of snowflake fractal antenna", IET Microwave, Antenna & Propagation, Volume 2, Issue 2, March 2008, pp. 180-187.

[9] A Amushan, "Circular Polarization Antenna Design Using Genetic Algorithms", P.G. Dip. Report, University of Bradford, PMSC Dept., 2005.

[10] Rahmat – Samii, E. Michielssen, "Electromagnetic optimization by Genetic Algorithms", John Wiley & Sons, Canada, 1999.

[11] Arnaud. E, Chantalat. R, Koubeissi. M, Menudier. C, Monediere. T, Thevenot. M, Jecko. B, "New Process of Circulary Polarised EBG Antenna by using meander Lines", Antennas and Propagation. EuCAP, 2007. The Second European Conference on 11-16 Nov.2007, pp. 1-6.

[12] Han. T.C, Rahim. M.K.A.Masri, T, Karim.M.N.A, "Left Handed Metamaterial Design for Micro strip Antenna Application", Microwave Conference, 2007. APMC 2007. Asia-Pacific , Volume 1, 11-14 Dec. 2007, pp.1-4.

[13] A. R. Weily, K. P. Esselle, B. C. Sanders, and T. S. Bird, "High-gain 1D EBG resonator antenna", Microwave Opt. Technol Lett., vol. 47, no. 2, pp. 107-114, Oct. 2005.

[14] A. R. Weily, L. Horvath, K. P. Esselle, B. C. Sanders, and T. S. Bird, "A planar resonator antenna based on a woodpile EBG material", IEEE Trans. Antennas Propagat., vol. 53, no. 1, pp. 216–223, Jan. 2005.

[15] A.R. Weily, K.P. Esselle, B.C. Sanders and T.S. Bird, "Circularly polarized 1-D EBG resonator antenna", ANTEM 2004/URSI, Ottawa, ON, Canada, pp.405-8. July 20-23, 2004.

[16] A. R. Weily, K. P. Esselle, and B. C. Sanders, "Layer-by-layer photonic crystal horn antenna", Phys. Rev. E, vol. 70, no. 3,37602, Sept. 2004.

[17] Khaleghi. A, Kamyab. M, " Reconfigurable Single Port Antenna With Circular Polarisation Diversity", IEEE Transactions on Antennas and Propagation, Volume 57, Issue 2, Feb. 2009, pp.555-559.

[18] T. H. Lee, R.A. Abd-Alhameed and P.S. Excell, "New dielectric resonator antenna design for mobile handsets", URSI India, Oct 2005, pp.23-29.

[19] Werner.D.H, Ganguly.S, "An overview of faractal antenna engineering research", Antennas and Propagation Magazine, IEEE, Volume 45, Issue 1, Feb.2003, pp.38-57.

[20] D. J. Love, and R. W. Heath, Jr., "Grassmannian beamforming for multiple-input multiple-output wireless systems", IEEE Trans. Inform. Theroy, vol.49, no.10, pp.2735-2747, Oct. 2003.

[21] B. Modal, and R. W. Heath, Jr., "Performance analysis of quantized beamforming MIMO systems", IEEE Trans. Signal Process., vol.54, no.12, pp.4753-4766, Dec. 2006.

LIST OF AUTHOR'S PUBLICATIONS

JOURNALS

[1] **M. Usman**, R.A. Abd-Alhameed,P.S. Excell, "Design Considerations of MIMO Antennas for Mobile Phones", PIERS Online Vol. 4, No. 1, 121-125, 2008. doi:10.2529/PIER070904201511.

[2] C H See, R A Abd-Alhameed, **M Usman**, M Hragh, D Zhou and P S Excell, "Miniature Dual-Bands and Wideband Planar Inverted F-L-Antennas (PIFLAs) For WLAN and UWB Applications", IEEE Transactions on Antennas and Propagation, Sept 2009.(Under Review).

CONFERENCE AND WORKSHOP

[1] **M. Usman**, R.A. Abd-Alhameed, Peter.S.Excell, "Dual Band Three Antenna Polarisation Diverse MIMO System for Mobile Devices", Proceedings of 3rd International Conference on Internet Technologies and Applications, 8th – 11th Sep, 2009, Glyndŵr University, Wrexham, Wales, UK. ISBN: 978-0-946881-65-9.

[2] P. S. Excell, R. A. Abd-Alhameed, **M. Usman**, D. Zhou and I. E. T. Elfergani, " Compact Antenna Design for Polarisation-Diversity MIMO Communications", Proceedings of 3rd International Conference on Internet Technologies and Applications, 8th – 11th Sep, 2009, Glyndŵr University, Wrexham, Wales, UK. ISBN: 978-0-946881-65-9.

[3] S. Adnan, R.A. Abd-Alhameed, **M. Usman**, H.I. Haraga, Z. Zainal Abidain, S.M.R. Jones, " Design studies of Ultra Wide Band Microstrip Patch Antenna for Ultra Wide Band Operation", IEEE conference on Antenna and Propagation, Loughborough University, 16-17 Nov,2009.(Paper Accepted)

[4] A.G. Alhaddad, R.A. Abd-Alhameed, **M. Usman**, D. Zhou, C.H. See, Z. Zainal Abidain, P.S. Excell, " Novel Balanced Handset Antenna Design for 2.4 and 5.2GHz Band", IEEE conference on Antenna and Propagation, Loughborough University, 16-17 Nov,2009.(Paper Accepted)

[5] **M. Usman**, R.A. Abd-Alhameed, D. Zhou, "Balanced MIMO Antenna for Mobile Phones", Progress in Electromagnetics Research Symposium, Beijing, China, March 2009, pp.1277-1280.

[6] Dawei Zhou, Raed A. Abd-Alhameed, C. H. See, M. S. Alkhambashi, Z. Zainal Abidin, K. N. Ramli, Musa M. Abusitta, and **Muhammad Usman**, "Meander-line Antenna Design for UHF RFID Tag Using a Genetic Algorithm", Progress in Electromagnetics Research Symposium, Beijing, China, March 2009, pp.1253-1256.

[7] R.A. Abd-Alhameed, D. Zhou, CH See, **M. Usman** and SWJ Chung, "Current research in Electromagnetic and Antenna Desigh", IET Seminar on RF and microwave research in UK Universities, Poster Session No 2, 25 Sept 2007, Austin Court , Birmingham, UK.

[8] **M. Usman**, R.A. Abd-Alhameed,P.S. Excell, "Channel Capacity of MIMO for Mobile Phones Using Polarization Diversity for Different azimuth Spectra", URSI Symposium, University of Portsmouth, Commission C, 2-3 July 2007, UK, pp. 14.

[9] **M. Usman**, R.A. Abd-Alhameed,P.S. Excell, "Investigation of Channel Capacity of MIMO", Proceedings of the 8th Informatics workshop for research students, University of Bradford, Bradford, UK, 28 June 2007, pp.218-221.

[10] **M. Usman**, R.A. Abd-Alhameed, D.Zhou, "Balanced MIMO Antenna System for Mobile Phones", Proceedings of the 9th Informatics workshop for research students, University of Bradford, Bradford, UK, 13 June 2008, pp.227-228.

AUTHOR'S SELECTED PUBLICATIONS

Design Considerations of MIMO Antennas for Mobile Phones

M. Usman, R. A. Abd-Alhameed, and P. S. Excell

Mobile and Satellite Communications Research Centre
Richmond Road, University of Bradford, Bradford, West Yorkshire, BD7 1DP, UK

Abstract— The paper presents a new modeling and design concept of antennas using polarization diversity of 2×2 and 3×3 Multiple Input Multiple Outputs (MIMO) system that is proposed for future mobile handsets. The channel capacity is investigated and discussed over Raleigh fading channel and compared to a linear/planner antenna array MIMO channel. The capacity is also discussed over three types of power azimuth spectrums. The results are compared to the constraints capacity limits in which the maximum capacity observed.

1. INTRODUCTION

MIMO for short, which stands for Multiple Input, Multiple Output systems are theoretically able to provide increased throughput, and better error performance than traditional systems [1–5]. The particular aspect that is used by MIMO systems is called *Multi*-Path propagation [2, 5]. This effect occurs when the radio signals sent from the transmitter bounce off intermediate objects before reaching the receiver. Some of these reflected signals may travel along entirely separate paths, and even reach the receiver at different times. Currently, there are a number of MIMO applications, development platforms, and tools that are showing great promise in the quest for wireless systems with higher bandwidth and greater capabilities. The major advantage of MIMO technology is the digital beam forming, which is now making its way out of research laboratories and into real-world applications with great speed. Spatial corrrelation using polarization issues for MIMO applications has great interest since the size of the actual radiating elements can be reduced [6–12]. This study has great advantages if a MIMO system needs to be implemented on a mobile handset. This paper will consider the spatial polarization technique and how this technique can improve the capacity of the system. A MIMO system of 2×2 and 3×3 elements will be considered for implementations on mobile handsets. This will be discussed under Raleigh fading channel and the results will be compared to linear or planer array antenna MIMO system. More over different types of power azimuth spectrums will be considered for system evaluation.

2. SUMMERY OF THE METHOD

For a system having N transmitters and N receivers the channel capacity can be given by [1];

$$C = E \log_2 \left| \left(I + \frac{P_t}{n_t \sigma} H H^* \right) \right| \tag{1}$$

where I is the identity matrix of $n_r \times n_r$ dimensions. P_t is the total average transmitted power. σ is the variance of the noise power, H is the channel transfer matrix of size $n_r \times n_t$. $E()$ is the expectation average and '$*$' is the conjugate transpose operation.

If the receiver and transmitter spatial matrixes are none then the matrix HH^* can be rewritten as follows:

$$HH^* = W_r G_w W_t^* \tag{2}$$

where W_r and W_t are the spatial matrices of the receiver and transmitter respectively. G_w is the matrix that defines the channel properties. For example the elements of the G_w matrix in Raleigh fading channel are complex guassian distributed elements. Since the space availability on the transmitter side then the spatial matrix of the transmitter for maximum channel capacity can be given as an identity matrix. Therefore Eq. (2) can be reduced to the following:

$$HH^* = W_r G_w \tag{3}$$

The elements of the spatial matrix W_r can be stated as follows:

$$W_{r_{i,j}} = \frac{\oint_s (E_{ai} \cdot E_i)(E_{aj} \cdot E_i)^* d\Omega}{\sigma_1 \sigma_2} \tag{4}$$

where

$$\sigma_1 = \oint_s (E_{ai} \cdot E_i)^2 d\Omega \tag{5}$$

$$\sigma_2 = \oint_s |E_{aj} \cdot E_i|^2 d\Omega \tag{6}$$

$$\oint_s = \int_{\phi 1}^{\phi 2} \int_{\theta 1}^{\theta 2} \tag{7}$$

$$d\Omega = \sin\theta \; d_\theta d_\phi \tag{8}$$

and E_a is the electric field of the radiating element. E_i is the incident field on the receiver side.

Using polarization concept we assume that there were three dipoles collocated over the z axis and centered at origin point as shown in Figure 1. We restrict our study to three radiating elements and in which the mutual coupling are ignored and they will located with respect to the elevation angle (it is the polarization angle in our case). We reduced the complicity of the method implementation by using short diploes in which the field can be easily stated (as example for a short dipole oriented in the z axis the total field is $E_\theta = \sin\theta$).

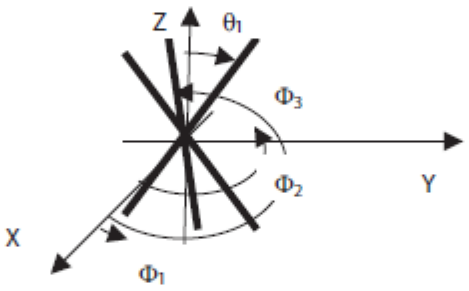

Figure 1: Basic antenna geometry.

The direction of a dipole oriented in θ_d and ϕ_d can be expressed as follows:

$$\hat{\mathbf{d}} = \sin\theta_d \cos\phi_d \hat{\mathbf{a}}_x + \sin\theta_d \sin\phi_d \hat{\mathbf{a}}_y + \cos\theta_d \hat{\mathbf{a}}_z \tag{9}$$

Then the radiated field of this dipole can be given as follows:

$$E_a = E_{\theta a} \hat{\mathbf{a}}_\theta + E_\phi \hat{\mathbf{a}}_{\phi a} \tag{10}$$

where

$$E_\theta(\theta, \phi) = \hat{\mathbf{d}} \cdot \hat{\mathbf{u}}_\theta \tag{11}$$

$$E_\phi(\theta, \phi) = \hat{\mathbf{d}} \cdot \hat{\mathbf{u}}_\phi \tag{12}$$

$$\hat{\mathbf{u}}_\theta = \cos\theta \cos\phi \hat{\mathbf{a}}_x + \cos\theta \sin\phi \hat{\mathbf{a}}_y + \sin\theta \hat{\mathbf{a}}_z \tag{13}$$

and

$$\hat{\mathbf{u}}_\phi = -\sin\phi \hat{\mathbf{a}}_x + \cos\phi \hat{\mathbf{a}}_y \tag{14}$$

3. SIMULATION AND MEASUREMENT RESULTS

If the signal to noise ratio is high then the channel capacity can be given by [5]:

$$C = \sum_{i=1}^{n} \left(I + \frac{P}{n_T \sigma} \lambda_i \right) \tag{15}$$

where λ_i for $i = 1, 2, 3$ are the eign values of the matrix given in Eq. (3). However, the channel capacity is also computed for comparison using Eq. (1). The incident fields are assumed to have uniform distribution over the range 0 to 2π for azimuth angle ϕ and 30° over the elevation angle at the horizontal plane for urban channel. For suburban channel the variation over elevation angle is similar to urban channel where as the azimuth will have laplacian spectrum distribution of various $\sigma_\phi = 5^\circ$, 10°, 15° and 20°.

The E_ϕ and E_θ of the incident fields were assumed independent over all angles of θ and ϕ, and their variations are uniform over the channel properties under considerations. It was also assumed that the phase variations are uniform over 0 to 2π.

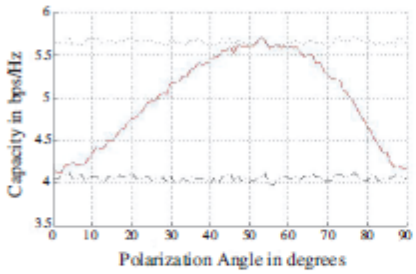

Figure 2: The channel capacity of 2×2 MIMO system as oriented in Figure 1 as a function of the polarization angle. ('. . .': upper limit of 2×2 MIMO fading channel, '.-.-.-': upper limit of 2×1 MIMO fading channel, Capacity using Eq. 1: red line, Capacity using Eq. 15: blue dots).

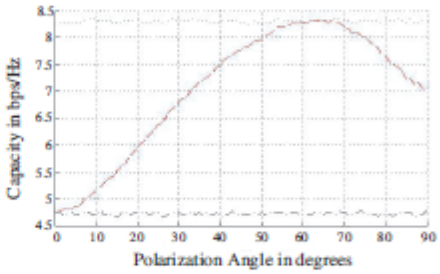

Figure 3: The channel capacity of 3×3 MIMO system as oriented in Figure 1 as a function of the polarization angle. ('. . .': upper limit of 3×3 MIMO fading channel, '.-.-.-': upper limit of 3×1 MIMO fading channel, Capacity using Eq. 1: red line, Capacity using Eq. 2: blue dots).

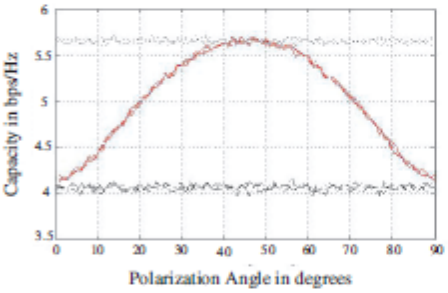

Figure 4: The channel capacity of 2×2 MIMO system as oriented in Figure 1 (the antennas are rotated by 90 degrees over azimuth angle) as a function of the polarization angle. ('. . .': upper limit of 3×3 MIMO fading channel, '.-.-.-': upper limit of 3×1 MIMO fading channel, Capacity using Eq. 1: red line, Capacity using Eq. 2: blue dots). The elevation angle is varied uniformly over 30 degrees at the horizontal plane, whereas azimuth angle varied as Laplacian spectrum of different values of σ_ϕ $(5, 10, 15, 20$ degrees for the geometry presented in Figure 1) in which the azimuth direction randomly selected between 0 and 2π.

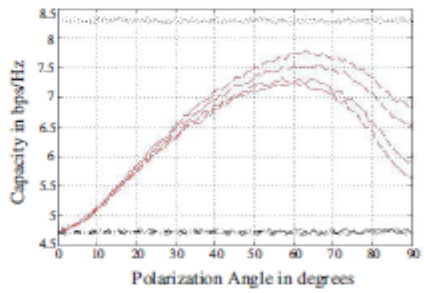

Figure 5: The channel capacity of 3×3 MIMO system as oriented in Figure 1 (the antennas are located at 90, 210 and -30 azimuth angles) as a function of the polarization angle. ('. . .': upper limit of 3×3 MIMO fading channel, '.-.-.-': upper limit of 3×1 MIMO fading channel, Capacity using Eq. 1: red line, Capacity using Eq. 2: blue dots). The elevation angle is varied uniformly over 30 at the horizontal plane, whereas azimuth angle varied as Laplacian spectrum of different values of σ_ϕ $(5, 10, 20, 30$ degrees for the geometry presented in Figure 1) in which the azimuth direction randomly selected between 0 and 2π.

Channel capacity of 2×2 MIMO and 3×3 MIMO systems for urban channel are shown in Figures 2 and 3. The antennas for 2×2 MIMO are located at $\phi = 0^\circ$ and $\phi = 180^\circ$ where as

for 3×3 MIMO at $\phi = 0°$, $120°$ and $240°$. In these figures a closed form solutions of the W_r are found and then the capacity was evaluated under Raleigh channel in which the average was taken over 1000 complex samples and in each point the transfer function was normalized to have a good prediction of the maximum variation of the spatial matrices using these types of antennas. It is simply can be noticed that the maximum capacities for 2×2 MIMO and 3×3 MIMO occur at around $55°$ and $63°$. These angles are recommended to represent the othogonalities of the spatial fields required by the antennas given in Figure 1.

Similarly, for Suburban channel the capacity of 2×2 and 3×3 MIMO system are shown in Figures 4 and 5 respectively for various values of σ_ϕ. It should be noted that the maximum capacity limits for 2×2 MIMO channel were achieved for all values presented for σ_ϕ where as for the 3×3 MIMIO were slightly reduced as σ_ϕ is increasing.

Basically, the MIMO channel capacity for different transmitted power is shown in Figure 6. In this example the variations of the elevation angle is considered between $\theta = 0$ to π where as in azimuth are similar to that presented in Figures 2 and 3. It is clearly the maximum capacities are proportional linearly with the transmitted power in which the maximum location for each transmitted power is fixed at around $63°$.

Figure 7 demonstrates the capacity variations for urban channel using ring array of three elements. The channel capacity was reached when the ring radius was about $\lambda/4$ (i.e., the separated distance between the radiating elements was around $\lambda/2$). Comparing the antenna sizes in Figures 1 and 7, it is evidence that the spatial polarization diversity has the ability to achieve the maximum capacity with certain constraints on the field orthogonalites.

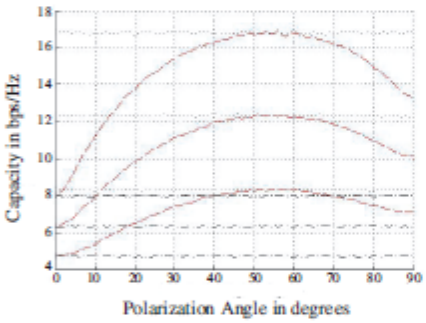

Figure 6: The channel capacity of 3×3 MIMO system as oriented in Figure 1 as a function of the polarization angle for different SNR starting from 10 dB, 15 dB and 20 dBs. ('. . .': upper limit of 3×3 MIMO fading channel, '-.-.-': upper limit of 3×1 MIMO fading channel, Capacity using Eq. 1: red line, Capacity using Eq. 2: blue dots). The elevation angle is varied uniformly over 180 degrees at the horizontal plane.

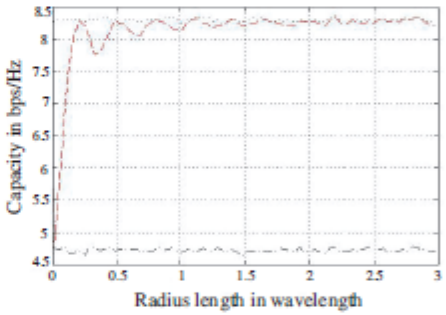

Figure 7: The channel capacity of 3×3 MIMO system as oriented on a ring (the antennas are located at $0, 120$ and -120 azimuth angles) as a function of the radius distance in wavelength (c). ('. . .': upper limit of 3×3 MIMO fading channel, '-.-.-': upper limit of 3×1 MIMO fading channel, red line, Capacity using Eq. 2: blue dots).

4. CONCLUSIONS

The channel capacity of a simple 2×2 and 3×3 MIMO systems using spatial polarization diversity was presented for different channel assumptions. The presented results show that the maximum channel capacity within small volume space can be reached with careful selection of the spatial field's orthonoalities. The results also compared to planner array MIMO system operation in which the antenna size considered was much larger to the MIMO system presented here. However, the work is still in progress to include the mutual coupling between the antennas and implementation on the mobile handset.

REFERENCES

1. Foschini, G. J. and M. J. Gans, "On limits of wireless communication in a fading environment when using multiple antennas," *Wireless Personal Commun.*, Vol. 6, No. 3, 311–335, Mar. 1998.
2. Foschini, G. J. and R. A. Valenzuela, "Initial estimation of communication efficiency of indoor wireless channel," *Wireless Networks*, Vol. 3, 141–154, 1997.
3. Wallace, J. W. and M. A. Jensen, "Modeling the indoor MIMO wireless channel," *IEEE Trans. Antennas Propag.*, Vol. 50, No. 5, 591–599, May 2002.
4. Wallace, J. W., M. A. Jensen, A. L. Swindlehurst, and B. D. Jeffs, "Experimental characterization of the MIMO wireless channel: Data acquisition and analysis," *IEEE Trans. Wireless Commun.*, Vol. 2, No. 2, 335–343, Mar. 2003.
5. Gesbert, D., H. Bölcskei, D. A. Gore, and A. Paulraj, "Outdoor MIMO wireless channels: Model and performance prediction," *IEEE Trans. Commun.*, Vol. 50, No. 12, 1926–1934, Dec. 2002.
6. Dong, L., H. Choo, R. W. Heath, and H. Ling, "Simulation of MIMO channel capacity with antenna polarization diversity," *IEEE Trans. Wireless Commun.*, Vol. 4, No. 4, 1869–1873, Jul. 2005.
7. Winters, J. H., J. Salz, and R. D. Gitlin, "The impact of antenna diversity on the capacity of wireless communication systems," *IEEE Trans. Commun.*, Vol. 42, 1740–1751, Feb. 1994.
8. Andrews, M. R., P. P. Mitra, and R. deCarvalho, "Tripling the capacity of wireless communications using electromagnetic polarization," *Nature*, Vol. 409, No. 6818, 316–318, Jan. 2001.
9. Svantesson, T., "On capacity and correlation of multi-antenna systems employing multiple polarizations," *IEEE Int. Antennas Propagation Symp. Digest*, 202–205, San Antonio, TX, Jun. 2002.
10. Stancil, D. D., A. Berson, J. P. Van't Hof, R. Negi, S. Sheth, and P. Patel, "Doubling wireless channel capacity using co-polarised, co-located electric and magnetic dipoles," *Electron. Lett.*, Vol. 38, No. 14, 746–747, Jul. 2002.
11. Andersen, J. B. and B. N. Getu, "The MIMO cube—A compact MIMO antenna," *5th Int. Symp. Wireless Personal Multimedia Communications*, 112–114, Honolulu, HI, Oct. 2002.
12. Xu, H., M. J. Gans, N. Amitay, and R. A. Valenzuela, "Experimental verification of MTMR system capacity in controlled propagation environment," *Electron. Lett.*, Vol. 37, No. 15, 936–937, Jul. 2001.

Under Review for IEEE Trans on Antennas and Propagation, Sept 2009

Miniature Dual-Bands and Wideband Planar Inverted F-L-Antennas (PIFLAs) For WLAN and UWB Applications

C H See, R A Abd-Alhameed, M Usman, M Hragh, D Zhou and P S Excell
[1]Mobile and Satellite Communications Research Centre, University of Bradford,
Bradford, West Yorkshire, BD7 1DP, UK
[2]School of Computing and Communications Technology, Glyndŵr University, Wrexham, LL11 2AW, Wales, UK
Email: r.a.a.abd@bradford.ac.uk

Abstract- *This paper presents two miniature low profile PIFLA antennas with a compact volume size of 30mm × 15mm × 8mm. By applying the magnetic wall concept a reduced size dual-band and a wideband half PIFLAs for WLAN (2.4GHz/5.2GHz) and UWB applications are achieved. The dual-band antenna shows a relative bandwidth of 12% and 10.2% at ISM2400 and IEEE802.11a frequency bands respectively for input return loss less than 10dB. By carefully tuning the geometry parameters of the dual-band proposed antenna, the two resonant frequencies can be merged to form a wide bandwidth characteristic PIFLA, to cover 3000MHz to 5400 MHz bandwidth (57%) for a similar input return loss, that is fully covering the upper band UWB (3.1-4.8GHz) spectrum. A parametric study is performed to demonstrate the influence of the geometry parameters against the impedance bandwidth of the proposed two antennas. The experimental and simulated return losses on a small finite ground plane of size 30mm × 15mm show good agreement. The computed and measured gains, radiation efficiencies far field patterns are shown to fully characterize the performance of the proposed two antennas.*

Indexing terms: Dual-frequency antenna, Wideband, PIFLA, ISM2400, IEEE802.11a, UWB

I. Introduction:

With the unprecedented growth of wireless communication technologies over last decade, this stimulates a huge demand on cableless electronic devices in the commercial market. In order to keep abreast with this tendency, the advance antenna design technology has to be coexisted to cater this unabated need. For the purpose of increasing the competiveness in sale, mobile manufacturers have to reduce their cost of production, by taking the advantage of using the licence-free ISM and UWB bands. Therefore, these bands have gained immense popularity and acceptance for most of the wireless electronic devices.

In ISM bands, the one of the most common and popular application is wireless internet (WLAN). The IEEE 802.11 is the wireless standard specification for WLAN/HyperLAN2. The IEEE 802.11b/g operates at ISM-2400 band which covers the frequency range from 2400MHz to 2485MHz, whereas the IEEE 802.11a working at ISM-5200 band that occupy the frequency band from 5150 to 5350 MHz. In term of data rates, the 802.11b/g and 802.11a devices can offer data rates up to 11 Mbps and 54 Mbps respectively. As a result, the requirement for an antenna operating at both of these two bands is increasing. PIFAs [1-3] are widely used as an internal antenna for this application. This is because its features such as high efficiency multi-frequency behavior, moderate bandwidth, low profile, low cost, less prone to breakage and reduced user power absorption compared with equivalent external antennas. Recently, dual-band antennas with one feed point have been proposed by many authors [1-6]. But, these antennas either suffer from low radiation characteristics or might not suitable for integration in some small portable devices due to limited space within the chassis.

UWB technology is invented for short range and higher data rate communication. The lower and upper UWB spectrums are 3100MHz to 4000MHz and 6000MHz to 10600MHz respectively. There are three overlapping target segments that could benefit from short-range wireless connections enabled by UWB: PC and peripheral devices, mobile devices, and consumer electronics. By implementing this technology, it is believed capable of delivering 1Gbit/s data rates over cable and wireless claims to double the exiting most of wireless terminal data-rate. This makes the constant high demand for designing smaller and lighter internal antennas, which immune to damage and low SAR. However, due to the limited volume and the influence of the plastic case, the design of internal antennas becomes a challenging issue. Planar monopole antennas [7-12] have been extensive developed for this application. This is due to low profile, ease of manufacture and simple design idea. But, this type of antenna suffers from low power gain, inconsistent radiation patterns and broadside gain direction, and high co-/cross- polarisation ratio over the operating frequency band (3100MHz to 10600MHz). In this research area, very limited published literature [13] provides a unidirectional UWB antenna with stable radiation patterns and constant gain profile.

There were several antenna size reduction techniques have been proposed over last decades, that investigate the use of high permittivity substrate, shorting pins, shorting walls and modifying the geometry of the internal antenna [14 -16]. Recently, another size reduction technique is proposed in [17-19] using the magnetic wall concept. It was interestingly found that the performances in terms of return losses, gains, radiation efficiencies, radiation patterns of half size structures of the U-slot, E-shaped [17-18] and UWB microstrip patch antennas [19] are comparable to their full structures.

By further extending authors' previous research work [20], this paper presents two 50% size reduction dual-frequency/UWB planar inverted F-L antennas (PIFLAs) with overall size of 30mm × 15mm × 8mm, mounted on a 30mm × 15mm finite ground plane. This attractive size will make these two proposed antennas can be easily integrated into laptop or mobile devices, while maintaining cost effectiveness and providing reliable performance. All of the analysis of the antenna was conducted adopting two commercial software packages [21-22]. The target frequencies were chosen to cover IEEE802.11x and UWB by using the same type of antenna [20] with different set of geometry parameters.

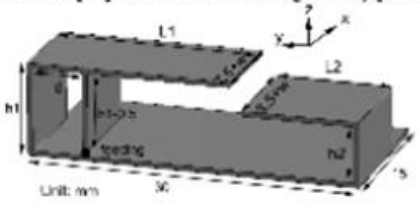

Figure1: Geometry of the proposed miniature PIFLA

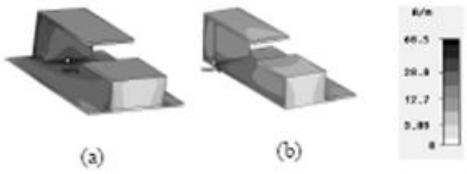

Figure 2: Current distribution of (a) full size and (b) half cut PIFLA at 2450 MHz.

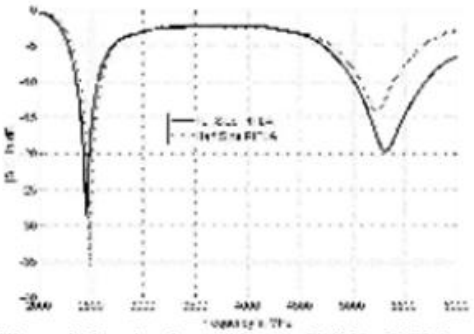

Figure 3: Simulated return Losses (Full Size PIFLA verse Half Size PIFLA (without optimized))

II. Antenna design concepts and structure

The proposed planar inverted F-L antenna (PIFLA), shown in Fig. 1, is quite similar to the antenna design of present authors previous work in [20] but the size is reduced to half using the principle of the existing magnetic wall on the antenna surface [17-19]. This antenna configuration was used as the starting point of this current research work. The initial geometry parameters of the proposed antenna are stated as follows: L1= 18.6 mm, L2=10 mm, h1=8 mm, h2= 4.5 mm, d=3.5mm and w=0 mm. It should be noted that these dimensions are the same as in [20], except the width of F-shaped, L-shaped radiator and ground plane have been cropped to half, which are 7.5 mm, 8.5 mm and 15mm respectively. The copper metal plate thickness of the proposed antenna and the gap distance for feeding are 0.5mm.

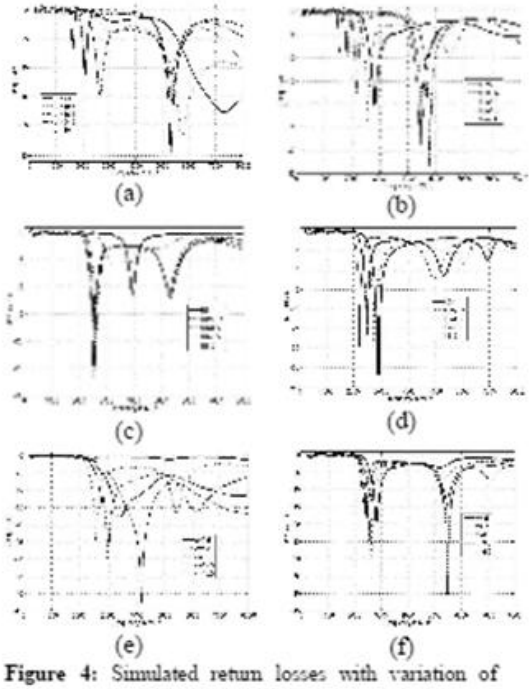

Figure 4: Simulated return losses with variation of parameters: (a) L1; (b) L2; (c) h1; (d) h2; (e) d; (f) w.

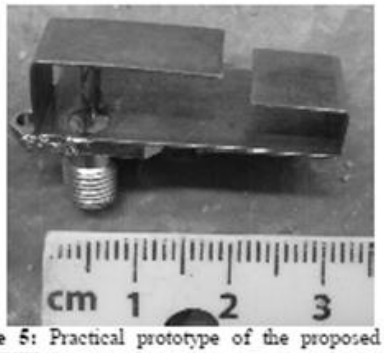

Figure 5: Practical prototype of the proposed dual-bands PIFLA

The operation mechanism of this proposed PIFLA is simple. As can be portrayed in Fig. 1, this antenna is a combination of a planar F-shaped antenna with rectangular plate feed and a planar L-shaped antenna. The F-shaped antenna which has a longer electrical length is designed to control the lower resonant mode (2450MHz), where as the L-shaped antenna is used to provide the higher resonant mode (5200MHz). Due to traditional wire feed PIFA has limited 4% to 12 % bandwidth [23-24], therefore, by changing different feed plate silhouette [23]; such as Triangular plate, Bi-

triangular plate, Rectangular plate, Rounded rectangular plate, U-shaped strip plate, the impedance bandwidth can be significantly increased from 18% to 25%. For this reason, this paper is employed the rectangular plate feed for the PIFA radiator for bandwidth enhancement purpose.

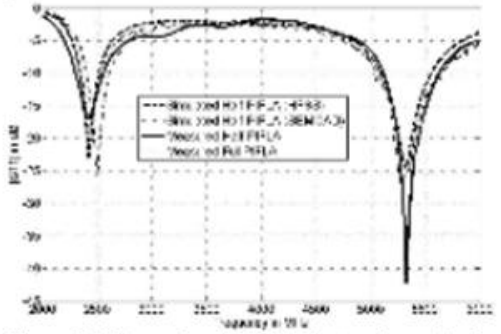

Figure 6: Measured and simulated return losses for the proposed dual-bands PIFLA

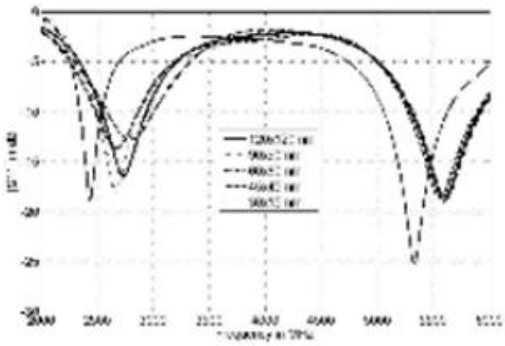

Figure 7: Simulated return losses for the proposed dual-bands PIFLA with various ground plane dimensions.

As for the antenna size miniaturisation, this paper implements the concept of removing half of the patch antenna along the line of structure symmetry, as in [17-19], hence, the volume of the patch antenna is reduced to half of the overall volume of the PIFLA antenna in [20]. So, the proposed half-size PIFLA antenna can be easily fit in small limited-space available in most wireless transceiver circuit board and casings for portable devices.

Prior to cut the full-size PIFLA to half, the current distribution of the full size PIFLA antenna [20] is investigated, as depicted in Fig. 2 (a). As can be observed, the maximum current mainly appears on the edges of the structure. Due to the minimum current appears on the centre of the structure that approximates the existing of magnetic wall. Thus, by cutting half of this full size structure, the half size structure will still hold the same properties of the same current distribution, as described in Fig. 2 (b). By keeping the same geometry parameters, the return losses for full size PIFA from previous work [20] and proposed half size PIFLA are studied. As can be seen in Fig. 3, the bandwidth for lower resonant mode remains, but, the bandwidth for higher resonant mode degrades considerably in which 12.2% (5GHz to 5.65GHz) to work in [20] and 3.8% (5.15GHz to 5.35GHz) to the half structure.

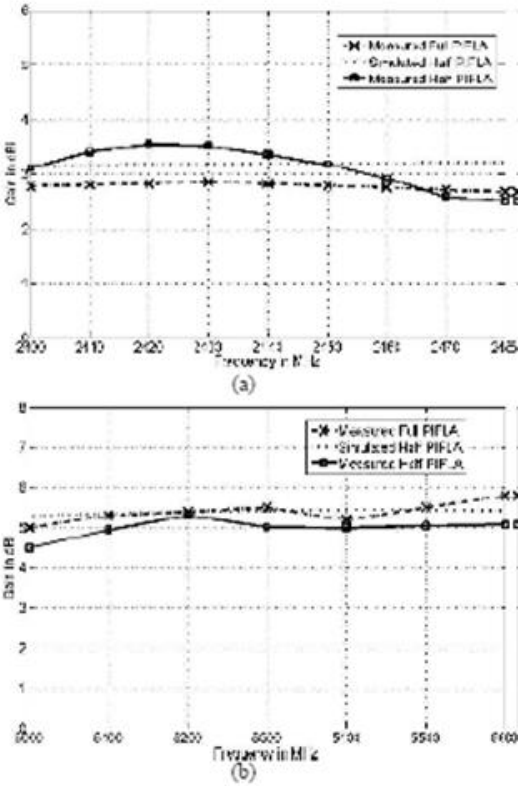

Figure 8: Measured gains for proposed dual-bands PIFLA: (a) upper band; (b) lower band

III. Parametric Study Results

The primary goal of this parametric study is to understand the impedance bandwidth variation of this proposed half-size PIFLA at lower and higher resonant modes by tuning the geometry parameters. Therefore, throughout this study, there are two outcomes are expected, i.e., (i) to optimise bandwidth of the proposed half-size dual-band PIFLA for WLAN application, so that, the proposed half size PIFLA possesses the same bandwidth at the lower and higher resonant modes as full size PIFLA [20], (ii) to establish wideband characteristic of this antenna by combining the two operating modes.

The impedance bandwidth is the main target to be optimized throughout the parametric study (defined at return loss S11 < -10dB). Each simulation is run with only one parameter varied, while other parameters stay unchanged. The fixed and variable parameters are shown in Fig. 1, where the variable parameters are considered as critical parameters in determining the lowest and highest frequency of the operating bandwidth. Due to the impedance bandwidth of the proposed antenna is heavily determined by strong mutual coupling between the two

radiating elements, simple mathematic formulas cannot found to calculate this effect analytically, so two EM simulators (HFSS [21] and SEMCAD [22]) were employed to perform this study.

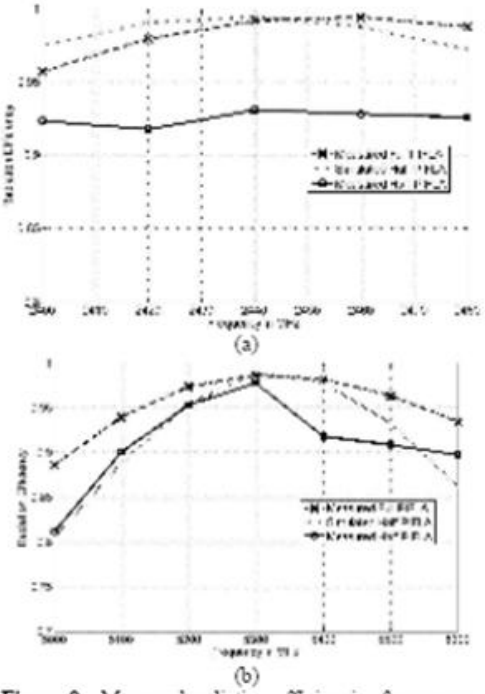

Figure 9: Measured radiation efficiencies for proposed dual-bands PIFLA: (a) upper band; (b) lower band

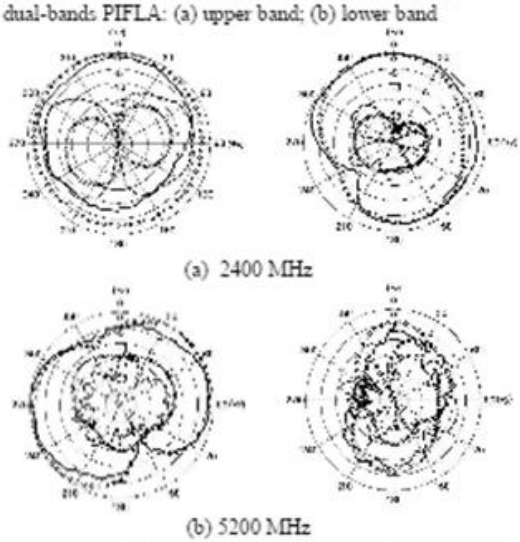

Figure 10: Simulated and measured normalised radiation patterns of the proposed dual-bands PIFLA for two planes (left: x-z plane, right: y-z plane) at (a) 2400 MHz and (b) 5200 MHz;
'xxxx' simulated cross-polarization
'oooo' simulated co-polarization
'------' measured cross-polarization
'——' measured co-polarization

A. Effect of the length of F-shaped radiator (L1)

This parameter changes the electrical length of the F-shaped radiator and it governs the lower resonant mode of this antenna. As can be noticed in Fig. 4 (a), by extending the length of the F-shaped radiator (L1) from 16.5 mm to 30 mm, the lower resonant frequency varying from 2650 MHz to 1600 MHz and the bandwidth is gradually diminished. As for the higher resonant mode, it is clearly independent of the L1. However, as the L1 becomes shorter to 10.5 mm and 4.5 mm, the lower resonant mode tends to disappear and higher resonant mode tends to shift to the upper frequency band with wider bandwidth. This is due to the both of the F_L and F_H are near to each other and good broadband impedance matching is attained.

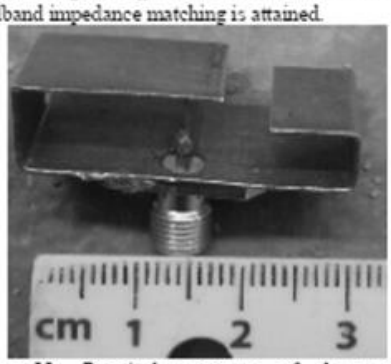

Figure 11: Practical prototype of the proposed wideband PIFLA

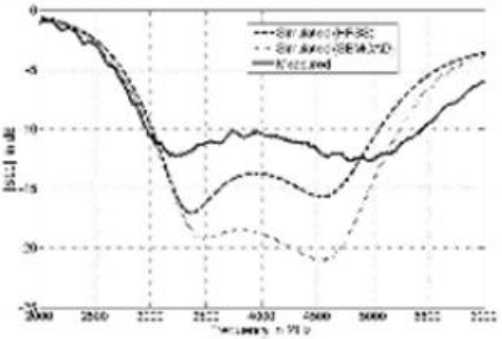

Figure 12: Measured and simulated return losses for the proposed wideband PIFLA

B. Effect of the length of L-shaped radiator (L2)

The length of L-shaped radiator determines the upper resonant mode of the proposed PIFLA. The effect of variation of L2 is elaborated in Fig. 4(b). At lower resonant mode, as the L2 is increasing from 2 mm to 24 mm, the resonant frequency seems to move from higher to lower resonant frequency (from 2900 MHz to 1500 MHz) and the impedance bandwidth is impaired accordingly. This is due to the coupling effect, as the L-shaped radiator is closer to the F-shaped radiator. Likewise, at upper resonant mode, the resonant frequency is shown to shift from higher to lower resonant frequency (from 7500MHz to 4400MHz).

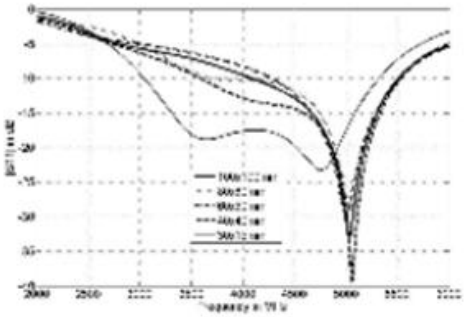

Figure 13: Simulated return losses for the proposed wideband PIFLA with various ground plane dimensions.

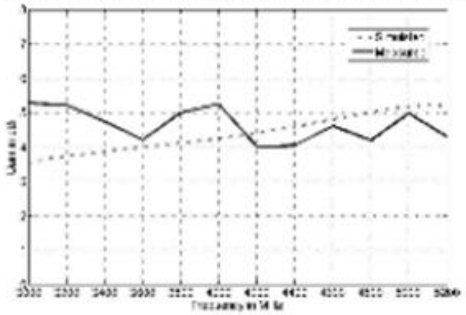

Figure 14: Measured and simulated gains for proposed wideband PIFLA.

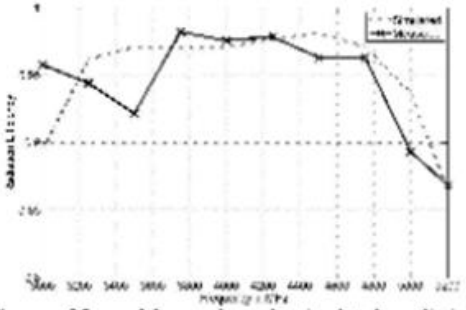

Figure 15: Measured and simulated radiation efficiencies for proposed wideband PIFLA.

C. Effect of the height of F-shaped radiator (h1)

The height of F-shaped radiator serves the same as L1 to control the fundamental resonant mode of the proposed antenna, but, it also contribute to induce capacitance from coupling with the ground plane. As can be noted from Fig. 4 (c), the smaller values of h1 as 1mm and 2.75mm, high mismatching of impedance bandwidth at both higher and lower resonant model were observed. When the h1 is stretched from 4.5mm to 8mm, it found no significant variations on the impedance bandwidth at lower and upper resonant modes. Therefore, h1 can take any value between 4.5 mm to 8 mm, without deteriorating the performance of this antenna.

D. Effect of the height of L-shaped radiator (h2)

Influences of parameter h2 are depicted in Fig. 4 (d). By varying the height of L-shaped radiator, both of the lower and upper resonant frequency seems to move the lower resonant frequency simultaneously. However, at the lower resonant mode, the degree of the impedance bandwidth remains at the same level, where as at higher resonant mode, impedance bandwidth seems to be minimised drastically when h2 below 6.5mm.

E. Effect of the position of the rectangular plate feeding (d)

The position of the rectangular plate feeding (d) is the most sensitive parameter in this study. This is because its variation can introduce different excitation mode to the proposed antenna, as described in Fig. 4(e). It is clear when d is 0.5 mm i.e., 0.5 mm away from vertical metal plate (h1) of the F-shaped radiator, the proposed PIFLA results an impedance mismatch at both modes. While positioning d to 4.5 mm, this antenna shows an obvious dual-resonant operation mode, which completely cover the bands of IEEE 802.11b/g (2400MHz to 2485 MHz, BW=3.48%) and IEEE 802.11a (5.15 MHz to 5.35 MHz, BW=3.8%) for WLAN application. As d is moved further away (d=8.5 mm), a broader impedance bandwidth can be obtained for two resonant operating modes, but, the two resonant operating band shift out of the WLAN 2400 MHz and 5200 MHz bands. However, it occupied the required operating frequency band for WLAN 5800MHz application (5725 MHz to 5825 MHz). By further increasing d to 12.5 mm and 16.5 mm, a wideband impedance response can be achieved by merging the two resonant modes into one resonant mode. This wide impedance bandwidth is suitable for uplink UWB application (3100 MHz to 5200 MHz).

F. Effect of the width of F-L shaped radiators (w)

The independent influence of width for F and L-shaped radiators has been well discussed in [20]. It was shown that prolong the width of F-shaped radiator will only affect the second resonant mode of this antenna. However, varying width of L-shaped radiator will not give any significant changing on its impedance bandwidth; so, the performance of this antenna is clearly independent of width of L-shaped radiator. In this parameter study, the width of F-L-shaped radiator (w) will be altered at the same time to examine the antenna impedance bandwidth. As can be seen in Fig. 4(f), by widening the width (w) seems to offer a better impedance matching. Inversely, if the width (w) becomes shorter, the impedance mismatch will occur at upper frequency resonate mode.

IV. Results and discussion:

Throughout the parametric study process, it was interestingly found that by identifying the right set of geometry parameters, the proposed PIFLA can be able to be manipulated to operate in dual-band WLAN or UWB application. Therefore, two distinct dimension prototype

of proposed PIFLA were fabricated for validating its experimental performance with the predicted results.

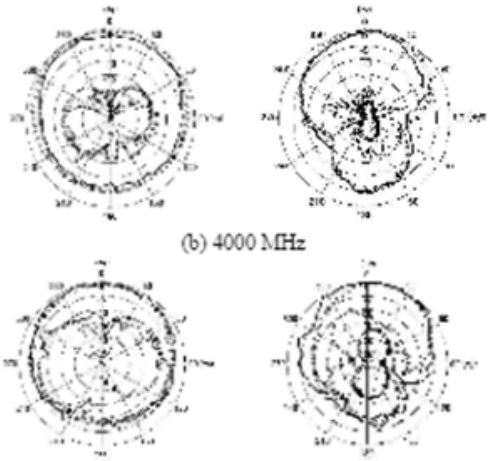

(b) 4000 MHz

(c) 5000 MHz

Figure 16: Simulated and measured normalised radiation patterns of the proposed wideband PIFLA for two planes (left: x-z plane, right: y-z plane) at (a) 3000MHz, (b) 4000MHz and (c) 5000MHz
'xxxx' simulated cross-polarization
'oooo' simulated co-polarization
'------' measured cross-polarization
'——' measured co-polarization

Two commercial packages (HFSS [21] and SEMCAD X [22]) were exploited to evaluate the proposed antennas performance, i.e. return loss, far field and gain for confirming that the simulation results are obtained with reasonable accuracy. In order to realise the practical characteristic the prototype of the proposed antennas, a HP8510C network analyser was used for return loss measurement. As for far field radiation patterns measurement, it was carried out in an anechoic chamber. In the far field measurement setup, the fixed antenna (reference antenna) was a calibrated broadband horn (EMCO type 3115) and the spacing between the test antenna and the horn was held at 4 m. Two pattern cuts (H-plane and E-plane) were taken for each designed frequency that covers the target bandwidth in paper.

A. Miniature Dual-band PIFLA

By scrutinizing the variations of the geometry parameters against the impedance bandwidth, the optimal geometry parameters can be recognised for dual-bands operation. These parameters can be given as follows: L1= 18.6 mm, L2=10 mm, h1=8 mm, h2= 5 mm, d=4.5mm and w=1.5 mm.

Fig. 5 depicts the prototypes of the first proposed miniature dual-band PIFLA antenna, where as the Fig. 6 illustrates the typical measured and computed antenna performance in term of impedance bandwidth for both full-size and half-size PIFLAs. Two adjacent resonant frequencies in the range of return loss $\leq$ -10 dB are observed, i.e., 2450 and 5350 MHz. The lower and upper mode provides 12% and 10.2% relative bandwidth from 2350 MHz to 2650 MHz and 5100 MHz to 5650 MHz, at a minimum return loss of -10 dB or less, completely satisfying the desired IEEE802.11b/g frequency band (2400-2485 MHz) and IEEE 802.11a (5.15-5.35GHz) band respectively. As can be observed, simulated and measured results for half-size PIFLA were found to be in excellent agreement. The half-size and full-size PIFLA seem to show identical measured impedance bandwidth at two resonant modes.

An investigation of the effect of the ground plane length on the antenna return loss was carried out. The size of ground plane was varied from 120 mm x 120 mm to 30 mm x 15 mm. The corresponding results are presented in Fig. 7. As can be seen, an insignificant variation in calculated return loss was observed for the cases when the sizes were 120 mm x120 mm ($\cong \lambda_o \times \lambda_o$), 90 mm x 90 mm ($\cong 0.7\lambda_o \times 0.7\lambda_o$), 60 mm x 60 mm ($\cong 0.5\lambda_o \times 0.5\lambda_o$) and 45 mm x 45 mm ($\cong 0.35\lambda_o \times 0.35\lambda_o$), where λ_o is defined at 2400MHz. However, the impedance matching for the antenna was surprisingly improved while the resonant frequency of the antenna was unchanged. This indicates that the proposed antenna also features a low degree of sensitivity to ground plane size, implying that the same antenna design can potentially be adopted for many other mobile devices with little modification, saving time for antenna customisation in industry. When the size becomes smaller than quarter wavelength, which is 30 mm x 15 mm ($\cong 0.24\lambda_o \times 0.12\lambda_o$), the return loss falls into the required dual-bands (2400MHz/5200MHz).

Figs. 8(a) and (b) illustrate the simulated and measured gain of the designed antenna in the broadside direction over the frequency ranges 2400 to 2480MHz and 5000MHz to 5600MHz respectively. At the lower band, a stable measured gain can be observed from 2.6 to 3.5 dBi. For the upper band, the range of the measured gain varies from about 4.5 to 5.2 dBi. It should be noted this measured gain for the half size PIFLA is in good agreement with the full size PIFL antenna. By analysing the gain variation over two specific operating bands, the peak antenna gain variations are found less than 1 dBi, as compared with the predictions.

By adopting the EM Simulators [21-22] and wheeler cap measurement method [26-27], the radiation efficiency of the proposed antenna is evaluated and presented in Fig. 9. At the lower frequency band (see Fig. 9 (a)), the variations of measured radiation efficiency for the Full and Half size PIFLA are 0.96 to 0.98 and 0.93 to 0.94 which corresponding to average of 97% and 93.5% over the operating frequency range. At the upper frequency band (see Fig. 9(b)), the average radiation efficiencies of 93.5% and 89% are achieved with ±9% and ±16% of radiation efficiencies fluctuation for the full size and half size proposed antenna respectively.
Figs. 10 (a) and (b) show the simulated and measured radiation patterns of both co-polar and cross-polar in the

x-z and y-z planes at 2400MHz and 5200MHz for the proposed miniature PIFLA. The simulated and measured radiation patterns of the fabricated prototype antenna are seen to be quite similar to each other at the two designated centre frequencies. In addition, by comparing the radiation patterns for Full size PIFLA [20] and half size PIFLA, both of them are indistinguishable. This leading to conclusion that using half structure techniques, the sizes of this half dual-band antenna can be reduced without appreciably impaired its performance characteristic when compared to the full-size antenna.

B. Wideband PIFLA

The optimised geometry parameters of the proposed PIFLA for UWB application are given as follows: L1= 18.45 mm, L2=8.5 mm, h1=8 mm, h2=5.5 mm, d=14.5mm and w=4.5 mm. Fig. 11 describes the experimental prototype of the PIFLA with finite ground plane of 30 ×15 mm, while Fig. 12 shows the typical measured and computed antenna performance in term of impedance bandwidth. As can be seen, the lowest and highest frequency edges i.e., 3000MHz and 5400MHz, of an input return loss ≤ -10 dB are observed. The impedance bandwidth of the proposed antenna, for -10dB return loss, is 2400 MHz or about 57% with respect to the centre frequency at 3950GHz (average of measured lower and higher frequencies with a -10dB return loss), which fully covers the frequency spectrum of uplink UWB (3100 MHz to 4800MHz). Basic agreements are achieved between the experimental and computed return loss over the desired operating frequency band.

Moreover, in order to understand the effect of the ground plane of the proposed antenna, simulations were conducted to check the variations of the return loss against the size of the ground plane, as described in Fig. 13. Considering λ_0 at 3000MHz is 100mm, from Fig. xxx, it elaborates that there are five different ground planes, which are 100mm x 100mm ($\cong \lambda_0 \times \lambda_0$), 80mm x 80mm($\cong 0.8\lambda_0 \times 0.8\lambda_0$), 60 mm x 60mm ($\cong 0.6\lambda_0 \times 0.6\lambda_0$) , 40mm x 40mm ($\cong 0.4\lambda_0 \times 0.4\lambda_0$) and 30 mm x 15 mm ($\cong 0.3\lambda_0 \times 0.3\lambda_0$), are used to this analysis. It is noticeable when the ground plane is greater or equal to $0.6\lambda_0$, the narrow impedance bandwidth characteristic was found and they do not contribute any significant bandwidth enhancement. As the ground plane becomes smaller than $0.4\lambda_0$, the impedance bandwidth becomes broader. According to [25], this is because the ground plane resonates at the operating frequency of the antenna element, so the bandwidth of the antenna-chassis combination will improve considerably. On the contrary, if the ground plane resonates far away from the operating frequency, the bandwidth will be decreased due to the insignificant contribution of the ground plane.

The simulated and measured gain of the designed antenna in the broadside direction over the frequency range from 3000 MHz to 5200 MHz, are shown in Fig. 14. An average gain of 4.5 dBi is achieved with ±1.2dBi of gain fluctuation. The simulated results relate well with measured ones. Fig. 15 elucidates the simulated and measured radiation efficiencies of the proposed antenna. As can be noticed, the maximum, minimum and average of measured radiation efficiencies are 87%, 98% and 92.5% respectively over the operating frequency range. Both simulated and measured radiation efficiencies are correlated well.

The far-field radiation characteristics of the proposed antenna were also investigated at 3000MHz, 4000MHz and 5000MHz, as depicted in Fig. 16. It is observed that the radiation patterns at different frequencies are mostly similar, which is expected from a wideband antenna. More importantly, it shows that the maximum co-polarised component appears at the direction of boresight (+z) for both E- and H-planes. At 3000 MHz and 4000 MHz, a co-pol/cross-pol ratio of better than 20dB is found at boresight in all of the measured radiation patterns. This indicates satisfactory polarization purity. While at 5000 MHz, due to the occurrences of high order mode resonances, this causes the increase in cross-polarisation levels and resulted a co-pol/cross-pol ratio of 10dB at boresight direction.

Conclusions:

A simple geometry, miniature planar inverted F-L antenna (PIFLA) has been proposed and studied experimentally and theoretically. By carefully selecting different sets of optimal geometry parameters and applying the size reduction techniques to the proposed antenna, two 50% size reduction PIFLAs have been designed and tested. By balancing the size and bandwidth constraints, these proposed antennas have a compact envelope dimension of 30mm × 15mm × 8mm and covers the required operating frequency band for WLAN and UWB applications. These features make the proposed antenna an attractive candidate for application in a range of future mobile terminals.

References:

[1] L.O.Soo, B.P.Koh, P.Song and L.Lau,"From a Simple IFA to a Dual Band PIFA" Antenna Technology: Small Antennas and Novel Metamaterials, 2008. iWAT 2008. International Workshop on 4-6 March 2008, pp.386 – 389.

[2] Y-B.Kwon, J-I.Moon, and S-O.Park, "An internal Triple-Band Planar Inverted-F Antenna," *IEEE Antennas and Wireless Propagation Letters*, vol. 2, pp. 341-344, 2003.

[3] C-T.Lee and K-L.Wong,"Uniplanar Printed Coupled-Fed PIFA With a Band-Notching Slit for WLAN/WiMAX Operation in the Laptop Computer", IEEE Trans. On Antennas and Propagation, vol.57, April 2009, pp.1252-1258

[4] D.Liu and B.Gaucher, "A new Multiband Antenna for WLAN/Cellular Applications", Vehicular Technology Conference 2004, VTC2004-Fall. 2004 IEEE 60th. Vol.1, Sept.2004, pp.243-246

[5] H-C. Tung, S-T.Fang and K-L Wong, "Printed dual-band monopole antenna for 2.4/5.2GHz WLAN access point", Microwave Optical Letters, vol.35, no.4, Nov. 2002, pp.286-288

[6] D.D. Krishna, M.Gopikrishna, C.K. Anandan, P.Mohanan and K.Vasudevan"CPW-Fed Koch Fractal Slot Antenna for

WLAN/WiMAX Applications" IEEE Trans. On Antennas and Wireless Propagation Letters, Vol.7, pp.389-392, 2008
[7] Z.N. Chen, M.Y.Chia and M. J . Ammann, "Optimization and comparison of broadband monopoles," Proc. IEE Microw. Antennas Propag., Vol.150, no.6, pp.429-435, Dec.2003
[8] A.P.Agrawall, G.Kumar, K.P.Ray, "Wide-band planar monopole antennas", IEEE Trans. Antennas Propag., vol.46, no.2, pp.294-295, Feb.1998
[9] J-C.Chun, "Wideband cylindrical monopole antenna for multiband wireless applications", Microwave and Optical Letters, Vol.51, Jan. 2009, pp.15-17
[10] P.C.Li, J.X.Liang and X.D.Chen," Study of printed elliptical/circular slot antennas for ultra wideband applications", IEEE Transactions on AP, Vol.54, pp.1670-1675, 2006
[11]A.Dastranj, A.Imani and M.N-Moghaddasi, "Printed Wide-Slot Antenna for Wideband Applications", *IEEE Antennas Propag. Mag.*, vol. 56, no. 10, pp. 3097-3102, Oct. 2008.
[12] J.Y.Sze and K.L.Wong, "Bandwidth Enhancement of a microstrip line-fed printed wide-slot antenna," IEEE Trans. Antennas Propag., vol.49, pp.1020-1024, 2001
[13] W.K.Toh, Z.N. Chen and X.Qing, "A Planar UWB antenna with a broadband feeding structure", IEEE Trans. Antennas Propag., vol.7, pp.2172-2175, 2009
[14] A.K.Skrivervik, J.-F.Zurcher, O.Staub, and J.R.Mosig, "PCS Antenna Design: The Challenge of Miniaturization," *IEEE Antennas and Propagation Magazine*, vol. 43, pp. 12-27, August 2001.
[15] C.S.Lee and K-H. Tseng, "Size reduction of microstrip antennas", Electron. Lett., Vol. 37, pp.1274-1275, 2001
[16] A. K. Shackelford, K. F. Lee, and K. M. Luk, "Design of small-size wideband width microstrip-patch antennas," *IEEE Antennas Propag. Mag.*, vol. 45, no. 1, pp. 75–83, Feb. 2003.
[17] A. A. Deshmukh and G. Kumar, "Half U-slot loaded rectangular microstrip antenna," in *IEEE AP-S Int. Symp. USNC/CNC/URSI National Radio Science Meeting*, vol. 2, 2003, pp. 876–879.
[18] R.Chair, C-L.Mak, K-F.Lee, K-M.Luk and A.A.Kishk, "Miniature Wide-Band Half U-Slot and Half E-Shaped Patch Antennas", IEEE Transactions on AP, Vol.53, No.8, pp.2645-2651 August 2008.
[19] L.Guo, S.Wang, X.Chen and C.Parini, "Miniaturised Antennas for UWB Communications", in Proceeding of Eucap2009, 23-27 March, Berlin Germany, pp-3774-3778
[20] C.H.See, R.A.Abd-Alhameed, D.Zhou and P.S.Excell, "Dual-Frequency Planar Inverted F-L-Antenna (PIFLA) for WLAN and Short Range Communication Systems", IEEE Transactions on AP, Vol.56, pp.3318-3320, Oct.2008
[21] HFSS ver.11, Ansoft. Ltd.
[22] SEMCAD X ver.14, Schmid & Partner Engineering AG, Zeughausstrasse 43, 8004, Zurich, Switzerland
[23]R. Feick, H. Carrasco, M. Olmos and H.D. Hristov, "PIFA input bandwidth enhancement by changing feed plate silhouette", Electronics Letters, vol.40, pp.921-922, July 2004.
[24] H. Nakano, N. Ikeda, Y-Y. Wu, R. Suzuki, H. Mimaka and J. Yamauchi, "Realization of Dual-Frequency and Wide-Band VSWR Performances Using Normal-Mode Helical and Inverted-F Antenna," IEEE Trans. On Antennas and Propagation, vol.46, pp.788-793, June 1998.
[25] P. Vainikainen, J. Ollikainen, O. Kivekas, and I. Kelander, "Resonator-Based Analysis of the Combination of Mobile Handset Antenna and Chassis," IEEE Transactions on Antennas and Propagation, vol. 50, pp. 1433-1444, Oct 2002.
[26] R.W. Johnston and J.G. McRory"A improved Small Antenna Radiation-Efficiency Measurement", IEEE Antenna and Propagation Magazine, Vol.40, No.5, pp. 40-48, Oct.1998
[27] H. Choo, R. Rogers and H. Ling"On the Wheeler Cap Measurement of the Efficiency of Microstrip Antennas", IEEE Trans. Antennas and Propagation, Vol.53, No.7, pp.2328-2332, July 2005

Balanced MIMO Antenna for Mobile Phones

Muhammad Usman, Raed A. Abd-Alhameed, and D. Zhou
Mobile Satellite Communications Research Centre, University of Bradford
Richmond Road, Bradford, West Yorkshire, BD7 1DP, UK

Abstract— The paper presents a new modeling and design concept of antennas using polarization diversity of 2×2 Multiple Input Multiple Outputs (MIMO) balanced antenna that is proposed for future mobile handsets. The balanced MIMO antenna is designed and its coupling has been investigated. The results are compared to the constraints capacity limits in which the maximum capacity observed.

1. INTRODUCTION

MIMO for short, which stands for Multiple Input, Multiple Output) systems are theoretically able to provide increased throughput, and better error performance than traditional systems [1–5]. The particular aspect that is used by MIMO systems is called *Multi*-Path propagation [2, 5]. This effect occurs when the radio signals sent from the transmitter bounce off intermediate objects before reaching the receiver. Some of these reflected signals may travel along entirely separate paths, and even reach the receiver at different times. Currently, there are a number of MIMO applications, development platforms, and tools that are showing great promise in the quest for wireless systems with higher bandwidth and greater capabilities. The major advantage of MIMO technology is the digital beam forming, which is now making its way out of research laboratories and into real-world applications with great speed. Spatial corrrelation using polarization issues for MIMO applications has great interest since the size of the actual radiating elements can be reduced [6–12]. This study has great advantages if a MIMO system needs to be implemented on a mobile handset. This paper will consider the implementation of balanced antennas for mobile handset the will increase the channel capacity and will reduce the coupling between the handset and body.

2. MATHEMATICAL INTERPRETATION

We start our assumption that our system under consideration consists of short dipoles and we are not taking mutual coupling between the multiples dipoles in account, then the channel capacity is given as

$$c = E\left|\log 2\left\{I + \frac{Pt}{nt\sigma}HH^*\right\}\right| \tag{1}$$

In the above equation HH^* is given as

$$[HH^*]^{1/2} = \rho_r \frac{1}{2}G$$

where as ρ_r elements is given as:

$$\rho_{i,j} = \frac{\oint\limits_s (E_{ai}.E_i)\,(E_{aj}.E_i)\,d\Omega}{\sigma_1\sigma_2} \tag{2}$$

where

$$\sigma_1 = \oint\limits_s (E_{ai}.E_i)^2 d\Omega$$

$$\sigma_2 = \oint\limits_s |E_{aj}.E_i|^2 d\Omega$$

where we have: $d\Omega = \sin\theta_\theta^d d_\phi$ and $\oint\limits_s = \int_{\phi 1}^{\phi 2}\int_{\theta 1}^{\theta 2}$.

Substituting the values of σ_1, σ_1 and $d\Omega$ into the Eq. (2) the following can be given:

$$\rho_{i,j} = \frac{\oint\limits_s (E_{ai} \cdot E_i)(E_{aj} \cdot E_i) \sin\theta_\theta^d d_\phi}{\sqrt{\oint\limits_s (E_{ai} \cdot E_i)^2 \sin\theta_\theta^d d_\phi \oint\limits_s |E_{aj} \cdot E_i|^2 \sin\theta_\theta^d d_\phi}} \tag{3}$$

The correlation coefficients will form the spatial matrix which is given as

$$\rho = \begin{bmatrix} \rho_{11} & \rho_{12} & \rho_{1n} \\ \rho_{21} & \rho_{22} & \rho_{2n} \\ \rho_{n1} & \rho_{n2} & \rho_{nn} \end{bmatrix} \tag{4}$$

The channel capacity can also be given as:

$$C = \sum_{i=1}^{n} \left(I + \frac{P}{n_T N} \lambda_i \right) \tag{5}$$

where Li is the ith eigen value of the HH^* matrix.

3. BALANCED MIMO ANTENNA AND RESULTS

The main aim of this present work was to design two elements antenna structure having a ground plane whose dimensions are compatible with a mobile phone at 5 GHz band for MIMO applications of the future wireless mobile communications. The antenna proposed here is made of two wideband balanced antenna elements and placed in parallel, as shown in Figs. 1 and 2. The proposed 2×2 MIMO balanced antenna system was designed optimized using commercial simulator HFSS (High Frequency Structure Simulator), which uses a 3D full-wave finite element Method (FEM). The antenna geometry and location on the ground plane can be found in Fig. 2. As can be seen, the antenna is fed at the centre with differential feeding which provide equal magnitude but 180 degree out of phase current for the two arms of the antenna. The input impedance of the antenna is 50 Ω.

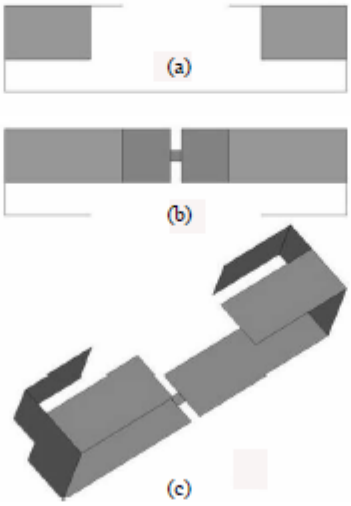

Figure 1: Antenna design. (a) Front view, (b) Top View, (c) 3D view.

The optimal configuration of the elements was chosen to minimize the coupling between elements. The two balanced antenna elements were placed inside the limits of the ground plane and the distance between them is 24 mm (see Fig. 2).

Figure 3 presents the simulated results of return loss and isolation performance of this 2×2 antenna system. As can be observed in the 5 GHz band range, the return loss is lower than 8 dB and the isolation lower than −13 dB for both elements.

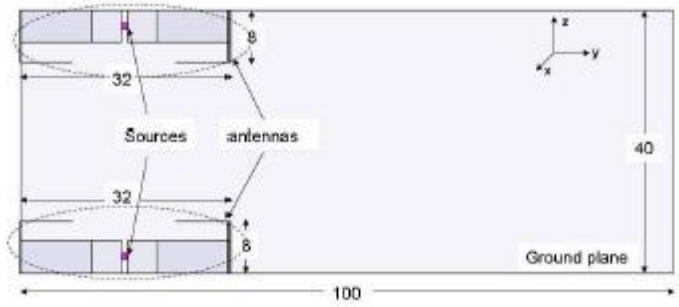

Figure 2: 2×2 Balanced MIMO antenna.

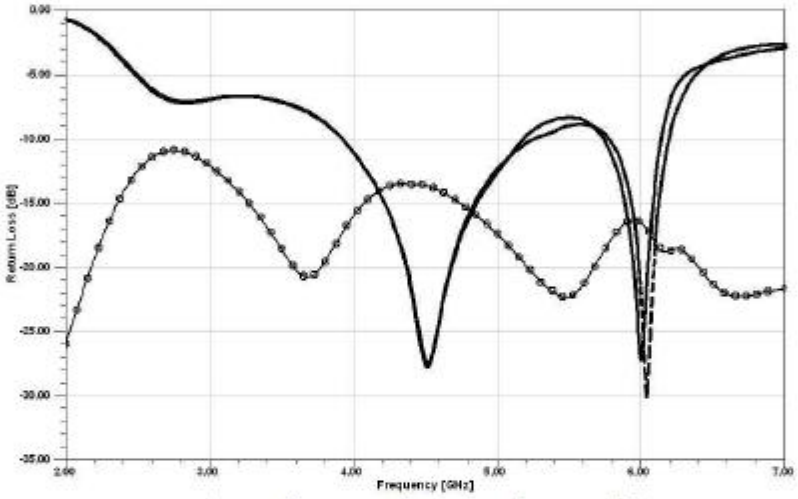

(———: S_{11}; ———: S_{22}; –□–□–: S_{21}; –○–○–: S_{12})

Figure 3: Simulated S-Parameters for 2×2 Balanced MIMO antenna.

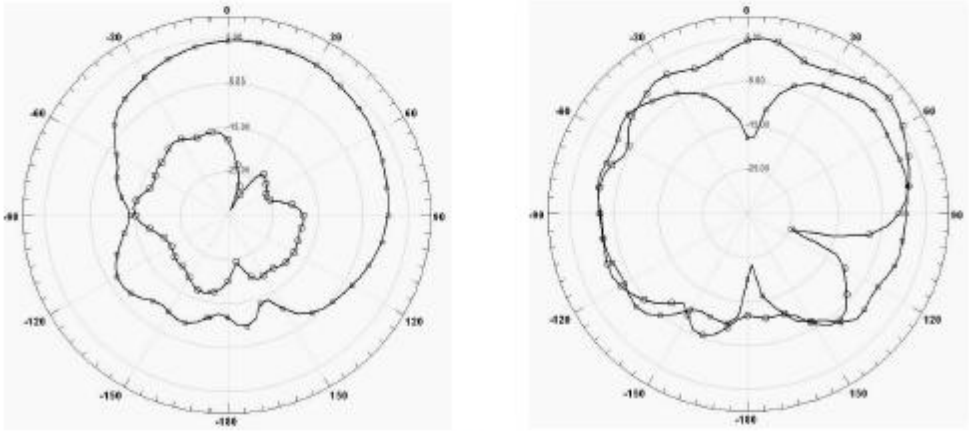

–□–□–: represents E_ϕ; –○–○–: is E_θ;

Figure 4: Radiation pattern at 5.8 GHz for xz plane (left) and yz plane (right).

The radiation property of the proposed 2×2 MIMO balanced antennas was also investigated. Two pattern cuts were taken for four selected operating frequencies that cover the designated whole bandwidth in this study. The radiation patterns in the xz plane and yz plane for the antenna systems at 5.2 GHz and 5.8 GHz were measured. The results in simulation were shown in Figs. 4 and 5, where the patterns of the prototype antenna show to be quite similar to each other for the both cases considered. The maximum power was found at around $\theta = 60°$ direction with peak gain of 5 dBi.

4. CONCLUSIONS

The simulation results using HFSS shows that the coupling between the antennas can be reduced with enhanced channel capacity. The balanced MIMO design discussed in this paper can be used for mobile handsets. The 2×2 balanced MIMO antenna systems with less volume can be incorporated efficiently into mobile phones. This design can also be used for PDAs and small handheld wireless devices.

REFERENCES

1. Foschini, G. J. and R. A. Valenzuela, "Initial estimation of communication efficiency of indoor wireless channel," *Wireless Networks*, Vol. 3, 141–154, 1997.
2. Winters, J. H., J. Salz, and R. D. Gitlin, "The impact of antenna diversity on the capacity of wireless communication systems," *IEEE Trans. Commun.*, Vol. 42, 1740–1751, Feb. 1994.
3. Andrews, M. R., P. P. Mitra, and R. deCarvalho, "Tripling the capacity of wireless communications using electromagnetic polarization," *Nature*, Vol. 409, No. 6818, 316–318, Jan. 2001.
4. Svantesson, T., "On capacity and correlation of multi-antenna systems employing mulTiple polarizations," *IEEE Int. Antennas Propagation Symp. Digest*, 202–205, San Antonio, TX, June 2002.
5. Stancil, D. D., A. Berson, J. P. Van't Hof, R. Negi, S. Sheth, and P. Patel, "Doubling wireless channel capacity using co-polarised, co-located electric and magnetic dipoles," *Electron. Lett.*, Vol. 38, No. 14, 746–747, July 2002.
6. Andersen, J. B. and B. N. Getu, "The MIMO cube — A compact MIMO antenna," *5th Int. Symp. Wireless Personal Multimedia Communications*, 112–114, Honolulu, HI, Oct. 2002.
7. Winters, J. H., J. Salz, and R. D. Gitlin, "The impact of antenna diversity on the capacity of wireless communication systems," *IEEE Trans. Commun.*, Vol. 42, 1740–1751, Feb. 1994.
8. Andrews, M. R., P. P. Mitra, and R. deCarvalho, "Tripling the capacity of wireless communications using electromagnetic polarization," *Nature*, Vol. 409, No. 6818, 316–318, Jan. 2001.
9. Svantesson, T., "On capacity and correlation of multi-antenna systems employing multiple polarizations," *IEEE Int. Antennas Propagation Symp. Digest*, 202–205, San Antonio, TX, June 2002.
10. Stancil, D. D., A. Berson, J. P. Van't Hof, R. Negi, S. Sheth, and P. Patel, "Doubling wireless channel capacity using co-polarised, co-located electric and magnetic dipoles," *Electron. Lett.*, Vol. 38, No. 14, 746–747, July 2002.
11. Andersen, J. B. and B. N. Getu, "The MIMO cube — A compact MIMO antenna," *5th Int. Symp. Wireless Personal Multimedia communications*, 112–114, Honolulu, HI, Oct. 2002.
12. Xu, H., M. J. Gans, N. Amitay, and R. A. Valenzuela, "Experimental verification of MTMR system capacity in controlled propagation environment," *Electron. Lett.*, Vol. 37, No. 15, 936–937, July 2001.

COMPACT ANTENNA DESIGN FOR POLARISATION-DIVERSITY MIMO COMMUNICATIONS

P. S. Excell[1], R. A. Abd-Alhameed[2], M. Usman[2], D. Zhou[2] and I. E. T. Elfergani[2]

[1]Centre for Applied Internet Research,
Glyndŵr University, Wrexham, LL11 2AW, Wales, UK
[2]Mobile and Satellite Communications Research Centre,
University of Bradford, Bradford, West Yorkshire, BD7 1DP, UK
p.excell@glyndwr.ac.uk, r.a.a.abd@bradford.ac.uk,
m.usman3@bradford.ac.uk, d.zhou2@bradford.ac.uk,
i.e.t.elfergani@bradford.ac.uk

ABSTRACT

A dual-polarisation dipole antenna is investigated, intended for use as one of three collocated orthogonal antennas in a polarisation-diversity Multiple-Input Multiple-Output (MIMO) communication system. The antenna actually consists of two overlaid dipoles, one electric and the other magnetic, such that their radiation patterns are nominally identical but they are cross-polarised and hence only interact minimally. Using Finite Difference Time Domain (FDTD) simulation, it was found that the antenna performed broadly as expected, although the engineering to create a physical realisation would be challenging. In principle, however, a system using two of the triplicated antennas could, in a richly scattering environment, achieve a six-fold increase in channel capacity for the same bandwidth as a traditional line-of-sight link. Unlike established MIMO systems, the antennas could be electrically small (less than a half-wavelength maximum dimension), which is essential for use in mobile terminals.

KEYWORDS

Multiple-Input Multiple-Output communications (MIMO), Polarisation diversity, Dual-polarisation antenna, Mobile communications, Finite Difference Time Domain method

1.0 INTRODUCTION

The possibility of using multiple polarisations to achieve Multiple Input-Multiple Output (MIMO) communications was announced in a landmark paper by Andrews et al [1]. In earlier MIMO realisations, having multiple antennas at each end of a communication link, co-polarised linear arrays were used. Information theory has shown that with multipath propagation, multiple antennas at both the transmitter and the receiver can establish multiple parallel channels that operate simultaneously on the same frequency band and at the same time. This gives high spectral efficiencies in a rich scattering environment such as indoors or in cityscapes. Depending on the angular spread of scattered multipath ray paths in the environment between source and receiver, substantial increases in the theoretical spectral efficiency in b/s/Hz may be obtained [2]. This system normally requires array antennas at each end which have physical dimensions of at least a half-wavelength, a size that may be unacceptable on a mobile terminal, since a half-wavelength is approximately 190 mm in the lower mobile band (around 800 MHz) and approximately 80 mm in the upper band (around 1.8 GHz).

The possibility offered by the use of multi-polarisation MIMO is that the antennas could be far smaller, since discrimination between the channels is no longer by angle of arrival alone. The use of polarisation discrimination permits antenna elements to be used which may theoretically be electrically very small (i.e. much smaller than a half-wavelength) and these elements can be

collocated at a point, rather than being required to be spaced out. Classically, radio communications have relied on one channel per frequency, although it is well understood that the two polarisation states of planar waves on a line-of-sight path allow two distinct information channels and techniques such as 'polarisation diversity' already take advantage of this [3-6]. However, by allowing for different angles of arrival discriminated by polarisation, the paper [1] showed that three independent channels can be created using electrically small arrays of orthogonal arrays of three electric dipoles.

The physics of polarisation limits the number of channels to three in this system, whereas for spatial-diversity MIMO; the link capacity grows, in principle, with the number of transmitter and receiver antennas [7]. However, by using three magnetic dipoles, a parallel system can be created and the electric and magnetic systems can then, in principle, be overlaid to create a six-channel system. To achieve this, however, sets of three superimposed electric and magnetic dipoles are required and the3 present work investigated prototype designs for one of these.

2.0 DESIGN AND MODEL CONSIDERATIONS

The most basic magnetic dipole antenna is the loop antenna, but these suffer from poor efficiency when electrically small but deviate from dipole behaviour if the electrical size approaches a half-wavelength. This dilemma can be resolved by adding a rod of high-permeability lossless material on the axis of the loop: this then becomes the well-known "ferrite rod antenna". The ferromagnetic material used (possibly ferrite but also possibly non-conducting iron powder [8]) has to be selected as having adequately low losses in the frequency range required. The key characteristics of such materials are permeability, loss performance (hysteresis models, conductivity, eddy-current models) and electrical performance (dielectric constant, capacitance models).

As a first design, a standard electric dipole antenna was located in close juxtaposition with a ferromagnetic rod antenna, as shown in Fig. 1. In principle, the electric dipole should be invisible to fields from the magnetic dipole, because its conductor is normal to the electric field from the latter. Conversely, the magnetic dipole should be relatively invisible to fields from the electric dipole, because its conductor is also normal to the electric field from the latter; however, the non-unity permittivity of the non-conducting ferromagnetic rod can be expected to cause some distortion of the electric field from the electric dipole and investigation of this was a priority.

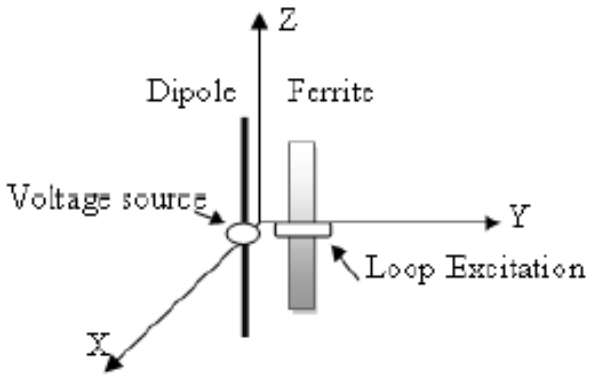

Figure 1: Electric dipole and magnetic (ferromagnetically-loaded) dipole in close juxtaposition.

A Finite Difference Time Domain (FDTD) computational model was used in the investigation [9]. Both antennas were located close to the centre of the problem space of the FDTD model, as shown in Fig. 2. An ideal ferromagnetic material with a purely real permeability and permittivity and no loss mechanisms was assumed: this was surrounded by a loop at its centre.

The operating frequency used was 900 MHz. The FDTD model used the following parameters:

FDTD increment (cell) size:	5mm
Length of the electric dipole:	170 mm (34 cells)
Length of the ferromagnetic rod:	60 mm (12 cells)
Width of the ferromagnetic rod:	20 mm (4 cells)
Relative permeability of ferromagnetic rod:	4.3

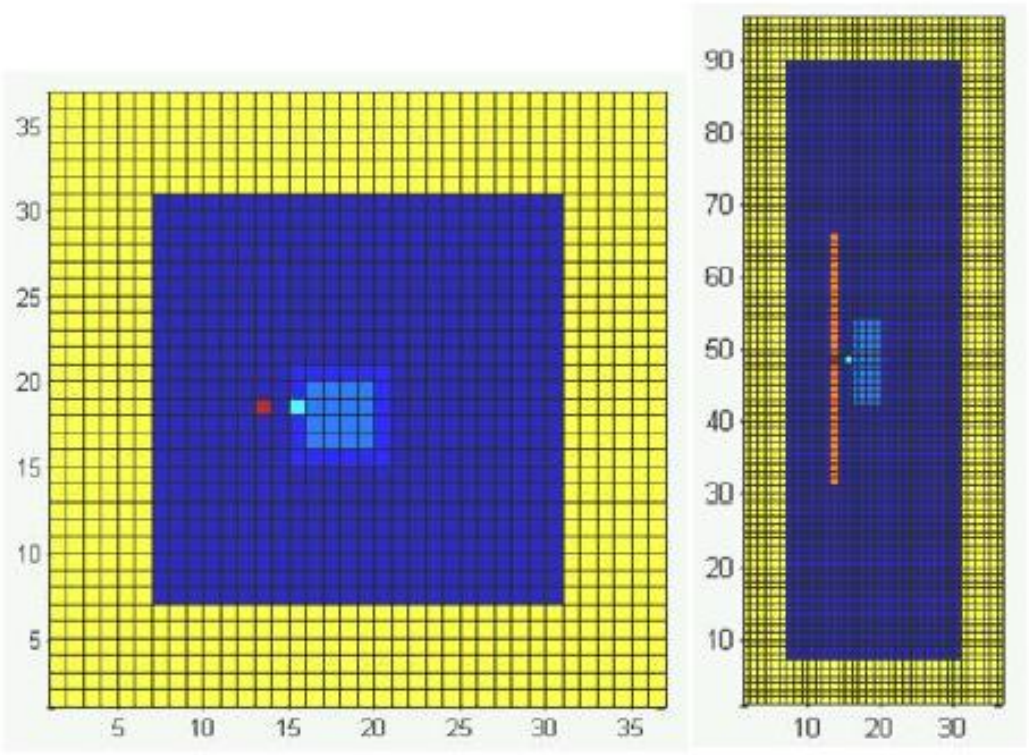

Figure 2: Conceptual FDTD model of a problem space surrounding the antennas in Figure 1. Left: cross-section; right: side view (note differing scales). Yellow: absorbing boundary condition; dark blue: air; red: electric dipole conductor; light blue: ferromagnetic rod; medium blue: loop of conductor around ferromagnetic rod; light turquoise: excitation point for conducting loop.

As a more advanced design, a configuration in which the ferromagnetic component was a hollow tube was considered, with the electric dipole threaded down its centre. This is technically feasible and it was surmised that the radiation pattern from the electric dipole would be more axisymmetric than for the first design. The second design would also offer advantages in easing collocation of three orthogonal replicas of the twin-dipole structure. The structure is shown in Fig. 3 and its conceptual FDTD model in Fig. 4.

In Figure 4, the dimensional choices were:

FDTD increment (cell) size:	3mm
Length of the electric dipole:	168 mm (56 cells)
Length of the ferromagnetic tube:	54 mm (18 cells)
Width of the ferromagnetic tube:	30 mm (10 cells)
Tube aperture width:	12 mm (4 cells)

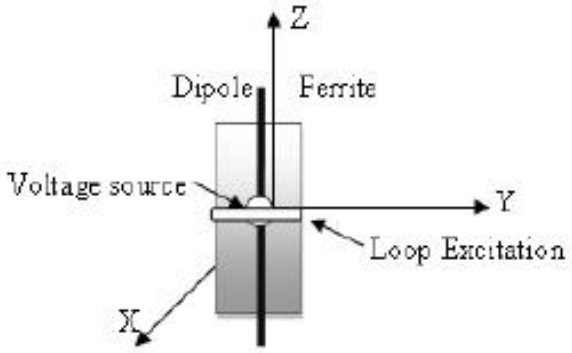

Figure 3: Coaxial electric and magnetic dipoles, using ferromagnetic tube for the latter.

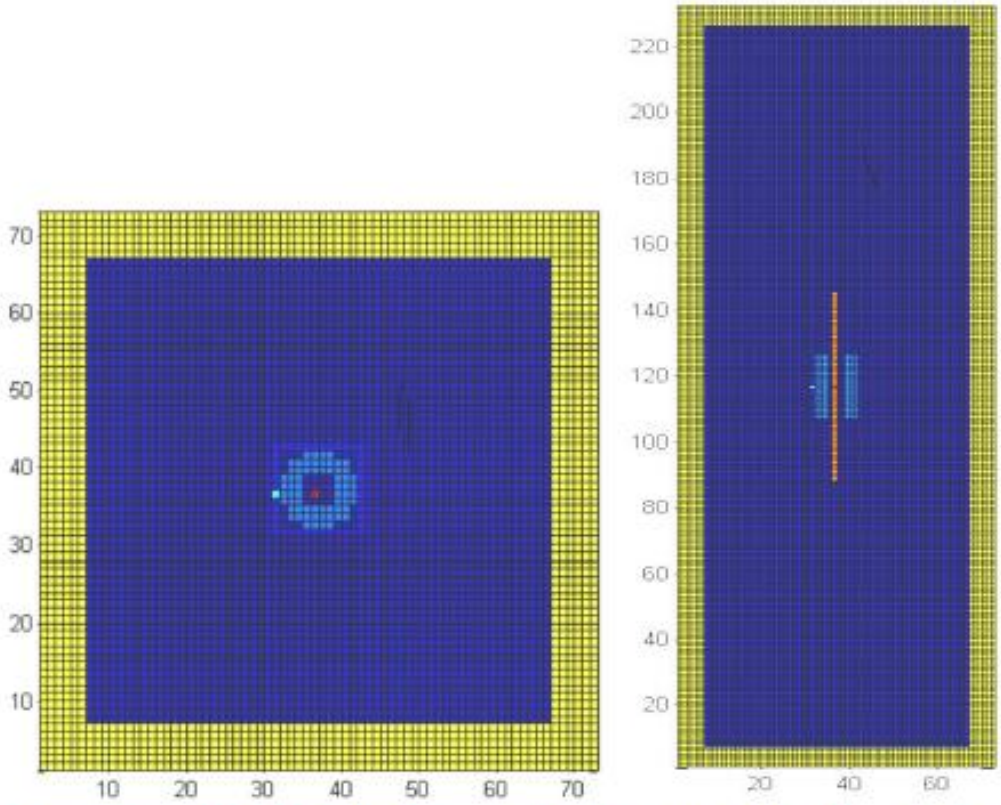

Figure 4: Geometry model of the problem space of Figure 3, using FDTD. Legend: as for Fig. 2.

3.0 Simulation and Results

The return losses for the dipole and the ferromagnetically-loaded loop were found to be -5dB and -4.6dB respectively for the simpler geometry (Fig. 2) and -3.1dB and -3.5dB respectively for the coaxial geometry (Fig. 4). These figures are close to practical values and can be improved by using external matching networks.

The radiation patterns for the two designs were computed by using the FDTD code. The patterns in the principal orthogonal planes for the antenna geometries shown in Figures 1 and 3 are shown in Figures 5 and 6 respectively. The shapes of the patterns for the electric dipole and the ferromagnetic rod are similar although not identical: the curve for the magnetic antenna being particularly skewed in the first case (the simpler design). This is probably because of the

interaction between the two antennas since they were not exactly collocated in this case the result for the coaxial antennas (the second case) are much better, the only difference being a small filling of the nulls.

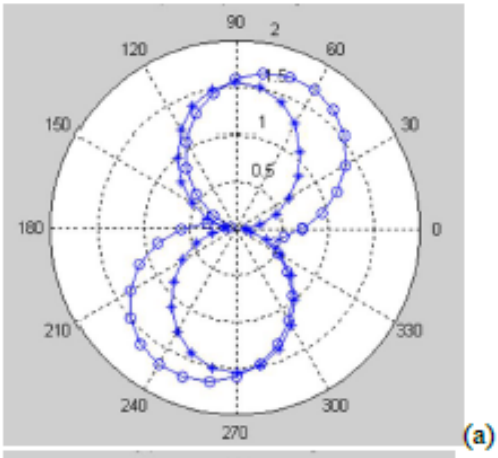

(a)

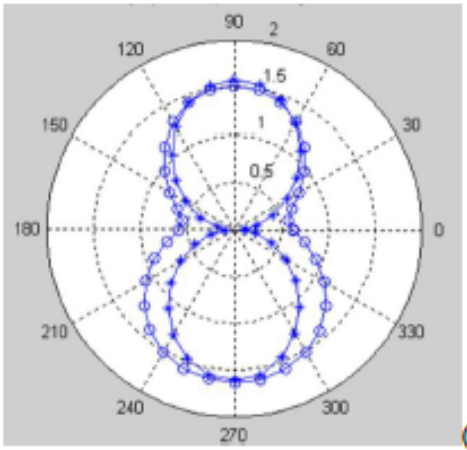

(b)

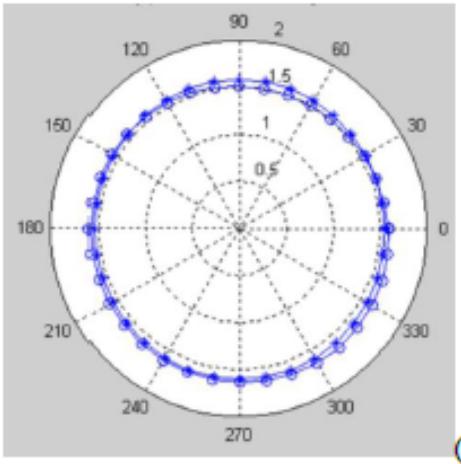

(c)

Figure 5: Radiation pattern of antenna geometry shown in Figure 1. Note that antenna is rotated to be horizontal for these plots.

(a) x-z plane i.e., $\phi = 0°$.
(b) y-z plane i.e., $\phi = 90°$
(c) x-y plane i.e., $\theta = 90°$.

"*" Electric dipole
-o- Ferromagnetically loaded loop antenna

It was noted that mismatch at the feedpoint caused some attenuation of gain for the magnetic dipole: this has been compensated out in the curves shown. In reality this can be overcome by using a multi-turn coil in place of a single-turn loop to drive the ferromagnetic rod, but the modelling of this in FDTD is significantly more involved. A matching network and a balun would also be needed for both antenna elements.

4.0 CONCLUSIONS

A dual-polarisation dipole antenna has been investigated, intended for use as one of three collocated orthogonal antennas in a polarisation-diversity Multiple-Input Multiple-Output (MIMO) communication system. The antenna consists of two overlaid dipoles, one electric and the other magnetic, such that their radiation patterns are nominally identical but they are cross-polarised. Using Finite Difference Time Domain simulation, it was found that the two antenna elements performed broadly as dipoles, but with cross-polarised fields, as expected. Three of these antennas, oriented orthogonally, could thus be assembled into an array, with their feedpoints approximately collocated, to create a six-channel diversity antenna. Applying two such arrays at each end of a MIMO link could thus, in a richly scattering environment, achieve a six-fold increase in channel capacity for the same bandwidth as a traditional line-of-sight link, while the antennas could be kept small (less than a half-wavelength maximum dimension), which is essential for use in mobile terminals. The engineering to create a physical realisation of such an array would of course be challenging, but it would appear that use of a sleeve-dipole

structure for the electric dipole would enable cable feeds and physical supports to be provided.

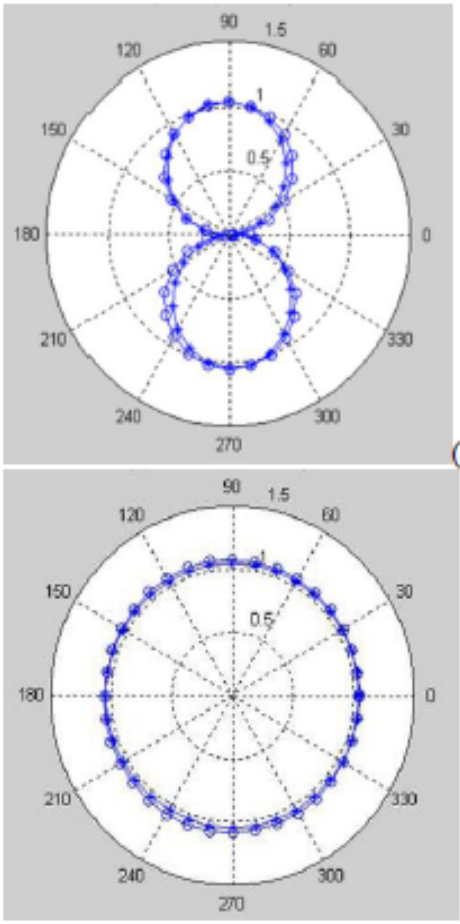

Figure 6: Radiation pattern of antenna geometry shown in Figure 3.

The legends are the same as for Figure 5.

REFERENCES

1. Andrews M.R., Mitra P. and Decarvalho O., "Tripling the capacity of wireless communications using electromagnetic polarization", Nature, vol. 409, no. 6818, pp. 316-318, 2001.
2. Andersen, J.B.; Getu, B.N, "The MIMO cube - a compact MIMO antenna", 5th International Symposium on Wireless Personal Multimedia Communications, vol. 1, pp.112- 114, Oct. 2002.
3. Makarav S.N., "Antenna and EM modelling with Matlab", New York: J. Wiley, 2002.
4. Vrcelj B. and Vaidyanathan P.P., "MIMO Biorthogonal Partners and Applications", IEEE Transactions on Signal Processing, vol. 50, Issue 3 , pp. 528 – 542, March 2002.
5. Dong L.; Ling H; Heath R.W., "Multiple-input multiple-output wireless communication systems using antenna pattern diversity", IEEE Global Telecomm. Conf., vol. 1, pp.997-1001, Nov. 2002.
6. Usman M., Abd-Alhameed R.A. and Excell P.S., "Design Considerations of MIMO Antennas for Mobile Phones", PIERS Online, Vol. 4, No. 1, 2008, pp.121-125.
7. Hottinen A., Tirkkonen O. and Wichman R., "Multi-antenna Transceiver Techniques for 3G and Beyond", Wiley, 2003.
8. RJ and US Imports, Australia, "Choice of Core Material": http://users.catchnet.com.au/~rjandusimports/tut_2a.html (viewed 28/2/09)
9. Excell P.S. and Vaul J.A., "Evolution of a Suite of Computational Modeling Tools for Mobile Telephone Dosimetry Studies at Bradford University, U.K.", Applied Computational Electromagnetics Society Journal, Vol. 16, No. 2, July 2001, pp. 97-105.

DUAL-BAND THREE-ANTENNA POLARISATION-DIVERSE MIMO SYSTEM FOR MOBILE DEVICES

Mohammed Usman[1], Raed A. Abd-Alhameed[1] and
Peter S. Excell[2]

[1]Mobile and Satellite Communications Research Centre,
University of Bradford, Bradford, West Yorkshire, BD7 1DP, UK
[2]Centre for Applied Internet Research,
Glyndŵr University, Wrexham, LL11 2AW, Wales, UK
m.usman3@bradford.ac.uk, r.a.a.abd@bradford.ac.uk,
p.excell@glyndwr.ac.uk

ABSTRACT

A triple dual-band inverted F antenna system is presented, intended for MIMO applications in mobile handsets accessing high-speed wireless local area networks (IEEE 802.11a/b/g/n standards). A comprehensive study was carried out in order to understand the enhancement of channel capacity and the effect of polarisation diversity. Means of achieving minimum coupling between the three antennas were investigated over the 2.45 GHz and 5.2 GHz bands. The antennas are placed in a geometry configuration appropriate to implement the desired field and polarisation diversities. All of the three polarised antennas in the system are resonant at 2.4 GHz and 5.2 GHz, with the return loss and coupling less than -12dB. The overall volumetric dimensions of each antenna were 30×15×8 mm. Each antenna contains two parts: a PIFA resonant at 2.4 GHz and an inverted-L behaving as a capacitive load and responsible for the resonance at 5.2 GHz.

KEYWORDS

Multiple Input Multiple Output communications (MIMO), Planar Inverted F Antenna, Channel capacity, Wireless Local Area Networks (WLAN)

1.0 INTRODUCTION

Multiple Input, Multiple Output (MIMO) communication systems are theoretically able to provide increased throughput, and better error performance than traditional systems [1-5]. The particular innovative aspect that is exploited by MIMO systems is multipath propagation [2, 5]. This effect occurs when the radio signals sent from a transmitter bounce off intermediate objects before reaching the receiver. Some of these reflected signals may travel along entirely separate paths, and even reach the receiver at different times, but being at the same frequency it has historically not been possible to use them independently: overcoming this is the breakthrough that MIMO has achieved. Currently, there are a number of MIMO applications, development platforms, and tools that are showing great promise in the quest for wireless systems with higher bandwidth and greater capabilities. The major challenge of MIMO technology is the need for agile digital beamforming, which is now making its way ino commodity applications.

Spatial correlation using polarization, rather than angle of arrival, for MIMO applications is of great interest since the size of the actual radiating elements can be reduced [6-12]. This has great advantages if a MIMO system needs to be implemented on a mobile handset.

A dual-band MIMO system can be used for mobile handsets as well as for WLAN devices. The IEEE 802.11b/g standards utilise the 2.4 GHz ISM band. This band is license-free, hence WLAN equipment will suffer interference from microwave ovens, cordless phones, Bluetooth devices and other appliances that use the same band. The IEEE 802.11a standard uses the 5 GHz band which suffers less interference; however, the frequency band used varies from one region of the world to another: typically either the 5.15-5.35 GHz band or the 5.725-5.825GHz band. A traveller with an 802.11a/b/g transceiver that can cover both 2.4 and 5.2 GHz will be able to gain access to local WLAN networks in different parts of the world and hence a dual-band MIMO antenna is an ideal choice for such an application if it can be realized with a compact design, with enhanced channel capacity and with polarisation diversity.

A planar inverted-F antenna (PIFA) is a variant of the inverted F antenna (IFA), with the wire radiating element replaced by plates in order to improve the bandwidth. PIFA antennas can be hidden in the housing of the mobile phone and has reduced backward radiation towards the user's head, minimising the electromagnetic power absorption (SAR) and enhancing the antenna performance.

2.0 ANTENNA DESIGN METHOD

The antenna geometry is adapted from the authors' earlier work [13] and modified as shown in Fig. 1. Firstly, the inverted PIFA has been designed with a resonant frequency of 2.4 GHz and then an inverted-L passive element incorporated within $\lambda/4$ of the PIFA, behaving as a capacitive load responsible for the second resonant frequency of 5.2 GHz. The widths w_1 and w_2 were selected as 13 mm and 11 mm to adjust the exact resonances required in this small antenna structure.

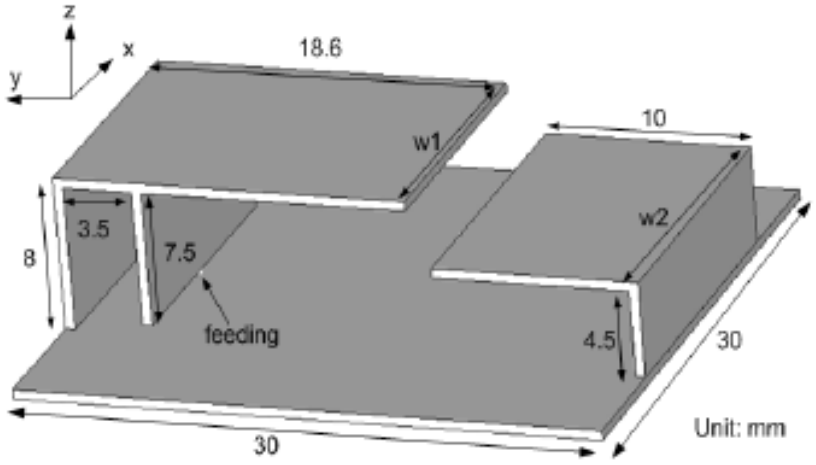

Figure 1: Dual-band antenna structure adopted.

This antenna geometry was modelled with a 50Ω matched load, using the Ansoft High Frequency Simulation Software (HFSS) package.

After individual dual-band antenna operation was achieved, the more challenging problem was addressed: to incorporate three antennas to form a 3x3 MIMO system for a mobile phone. For this, a metal box chassis was selected, with dimensions 100×50×20 mm and three of the dual-band antennas were located on three orthogonal upper surfaces of the box in order to generate three different orthogonal polarisations. Fig. 3 shows the full set of three MIMO antennas, including the box handset, the whole being modelled using HFSS.

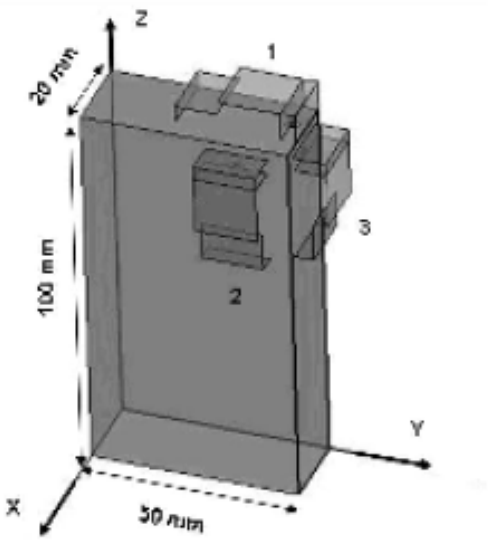

Figure 2: Three orthogonal dual-band antennas on a MIMO mobile handset.

The antenna geometry represents the polarisation-diverse MIMO system in which the position of each antenna has been carefully selected in order to have compact antenna geometry with low coupling between the three antennas. Several parameters were simulated and checked for conformance with the MIMO and dual-band responses for practical realisations.

3.0 SIMULATION AND RESULTS

The return loss, coupling, gain and radiation pattern of each antenna were checked, in the simulation, to ensure adequate performance. Fig. 3 shows the return loss of all each antenna. It is clearly noted the three antennas satisfy the requirement for dual resonance bands at 2.4 and 5.2 GHz. Within these bands, all of the antennas show a return loss ranging from -10dB to -30db, which is quite satisfactory. The relative bandwidths of each antenna were approximately 14.5% and 10% at 2.4 GHz and 5.2 GHz respectively.

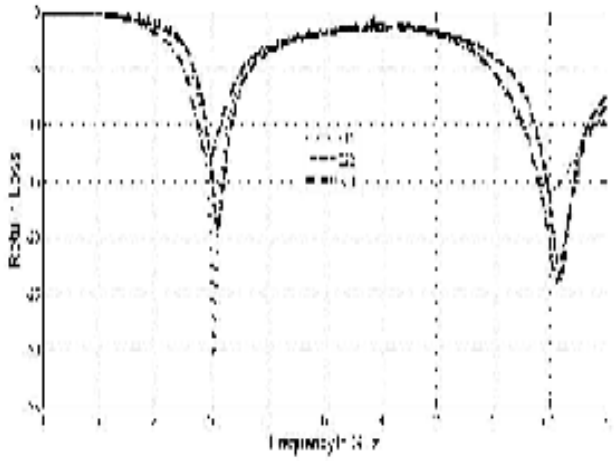

Figure 3: Return losses of orthogonal MIMO antenna system.

Figures 4 and 5 represent the coupling between the three antennas. As can be seen, the coupling variations over the bands of interest at 2.4 GHz and 5.2 GHz for the S_{12}, S_{13} and S_{23} parameters are around -12 dB or lower. These are very satisfactory results that show the feasibility of this compact geometry despite the close proximity between the three antennas and the excellent return losses for the three ports.

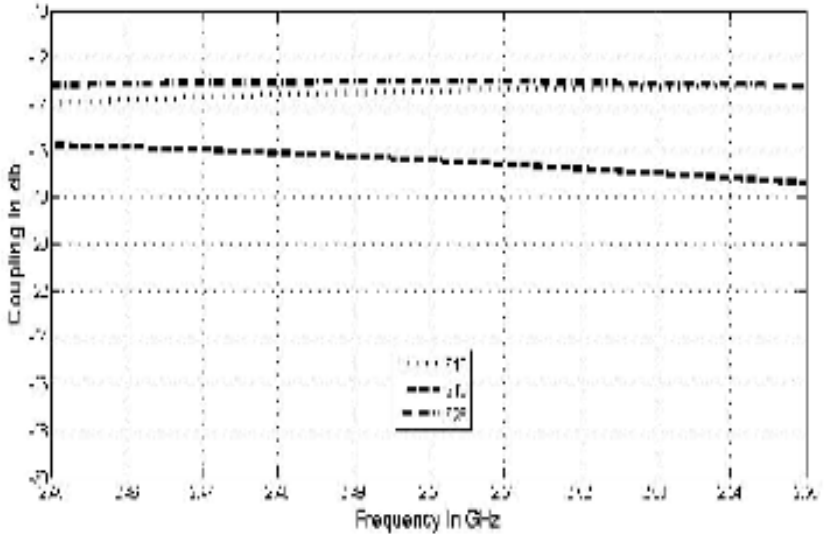

Figure 4: Coupling between Antennas around 2.5 GHz.

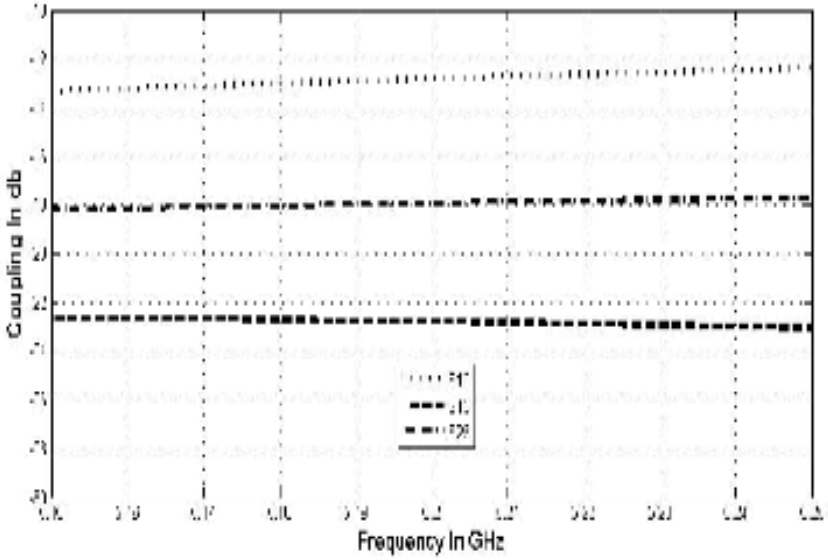

Figure 5: Coupling between Antennas around 5.2 GHz.

The channel capacity of this dual-band MIMO system was calculated using MATLAB, assuming a similar set of three antennas at the base station, giving a 3x3 structure. The results were compared with the upper limits of 3x1 and 3x3 free coupling MIMO systems (i.e. the latter exploiting angle-of-arrival, rather than polarization diversity). In order to calculate the

channel capacity, the impedance matrix was extracted from HFSS and then called by the MATLAB source file to act as input to the channel capacity algorithm.

Figures 6 and 7 show the upper limits of 3x1, 3x3 free coupling and 3x3 polarisation-diverse MIMO systems. The channel capacities were also evaluated and checked using an Eigenvalues method, which yielded results that were exactly identical and are hence not shown here. Comparing the 3x1 MIMO system and the designed polarisation-diverse 3x3 MIMO system it was noted that at the resonance frequencies 2.4 GHz and 5.2 GHz, the channel capacities of the polarisation-diverse MIMO system were close to the maximum capacity that can be obtained by the free coupling 3x3 MIMO system, although the low-band performance was better at 2.55 GHz, suggesting that a better performance could be obtained at 2.45 GHz, with some fine-tuning. The maximum degradations of the capacity at 2.5 GHz and 5.2 GHz were around 1.2 b/s/Hz and 0.5 b/s/Hz respectively.

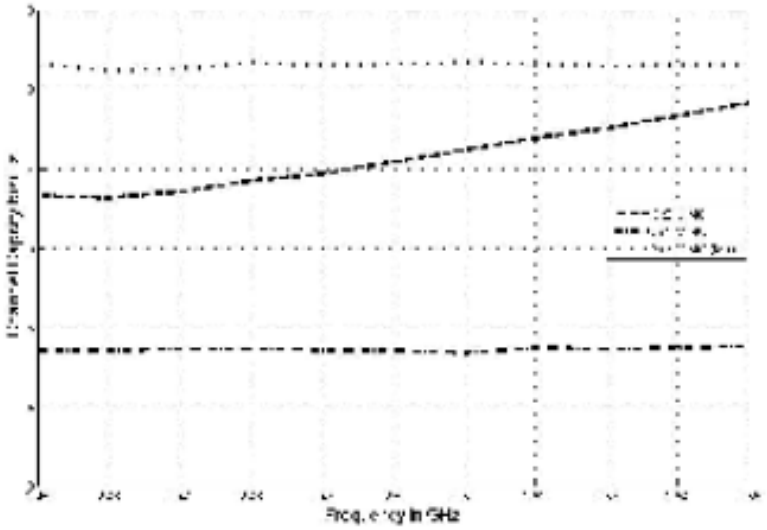

Figure 6: Channel Capacity of 3x1 and 3x3 MIMO systems around 2.5 GHz

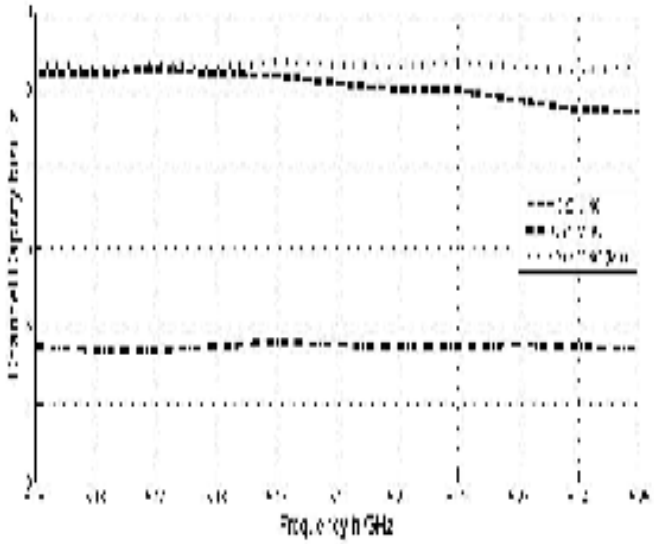

Figure 7: Channel Capacity of 3x1 and 3x3 MIMO systems at 5.2 GHz

Figures 8, 9 and 10 illustrate the simulated normalised principal-plane radiation patterns for both E_θ and E_ϕ in the x-y and x-z planes for 2.45 GHz and 5.2 GHz for each antenna of the proposed MIMO system. The simulated radiation patterns from the three radiating elements show reasonable field diversity to contribute towards good receiving/transmitting capacity, i.e. broad dipole-like patterns covering a majority of the sphere. The power gains for each radiating antenna were approximately around 2.5 dB and 4.5 dB at 2.45 GHz and 5.2 GHz respectively.

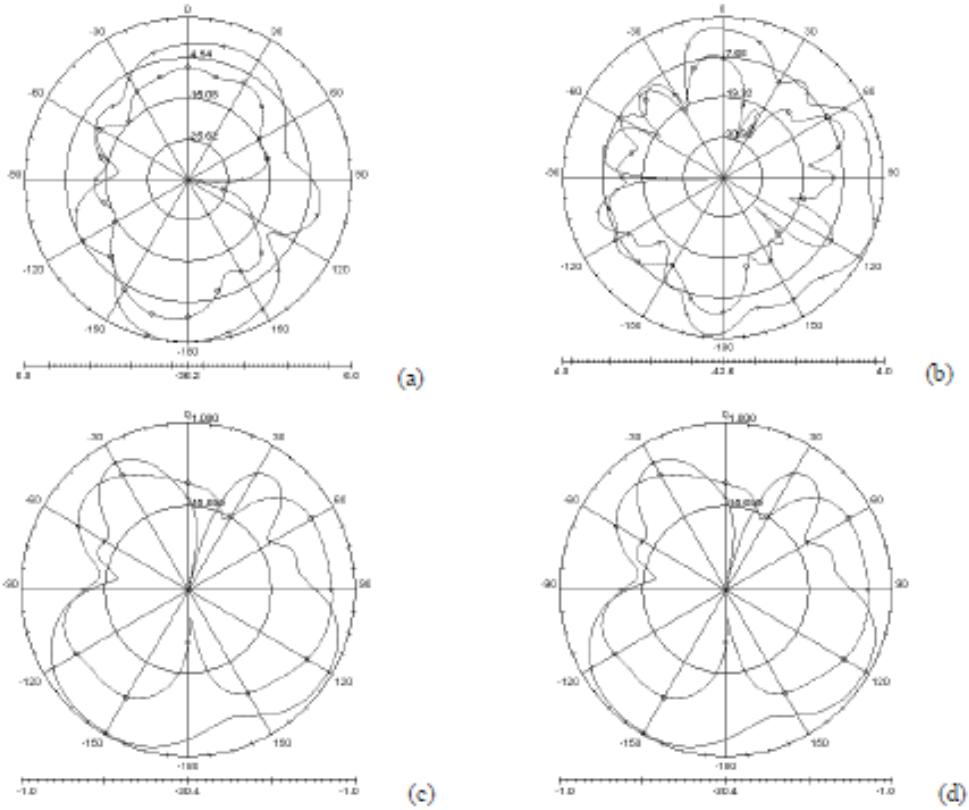

Figure 8: Radiation patterns of Antenna 1: E_θ -o- ; E_ϕ -+-
(a) $\theta = 0°$ to 360°, at $\phi = 0°$ at 2.4 GHz; (b) $\theta = 0°$ to 360°, at $\phi = 0°$ at 5.2 GHz
(c) $\phi = 0°$ to 360°, at $\theta = 90°$ at 2.4 GHz; (d) $\phi = 0$ to 360°, at $\theta = 90°$ at 5.2 GHz

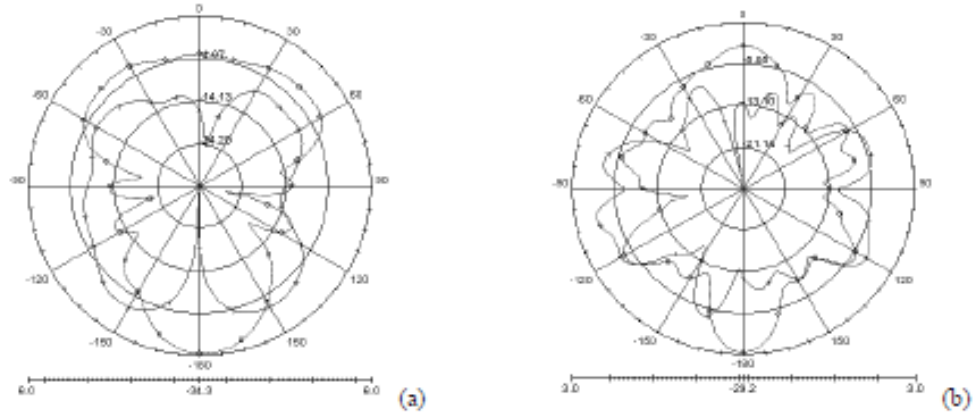

Figure 9: Radiation patterns of Antenna 2: E_θ -o- ; E_ϕ -+-. (a) and (b) legends as for Figure 8.

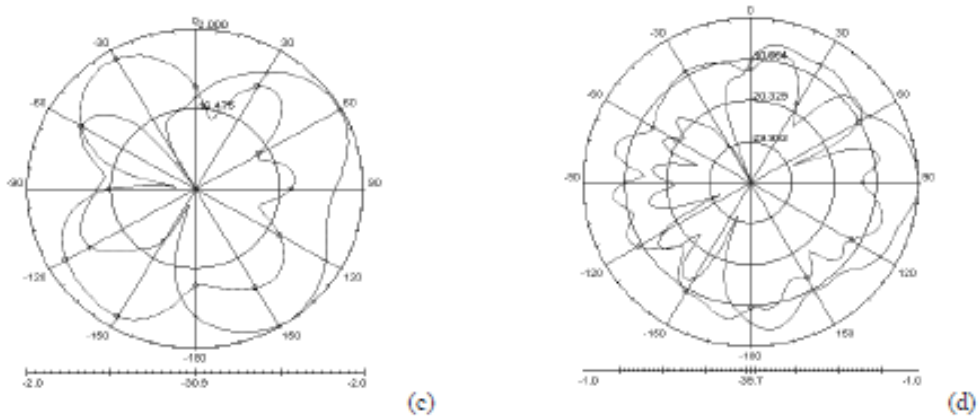

(c) (d)

Figure 9: Radiation patterns of Antenna 2: E_θ -o- ; E_ϕ -+-. (c) and (d) legends as for Figure 8.

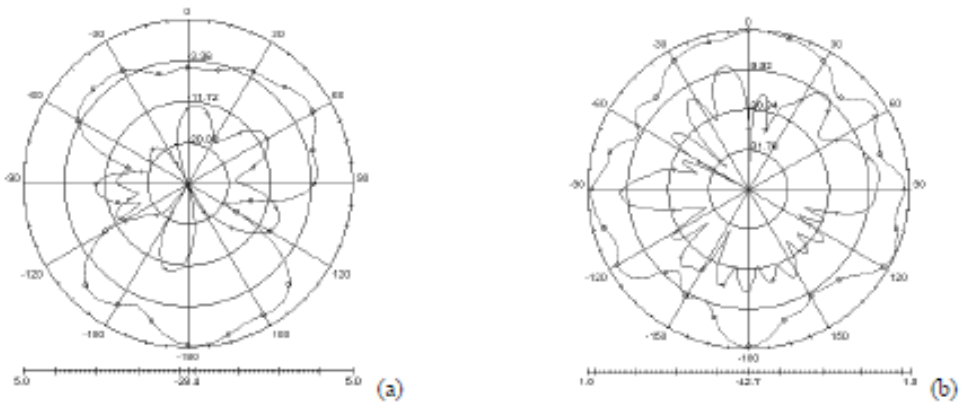

(a) (b)

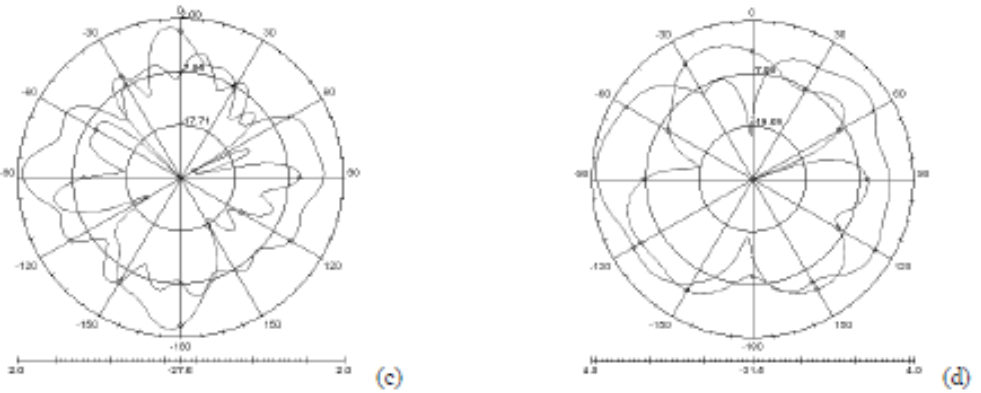

(c) (d)

Figure 10: Radiation patterns of Antenna 3: E_θ -o- ; E_Φ -+-. (a) - (d) legends as for Figure 8.

4.0 CONCLUSIONS

A system of three orthogonal dual-frequency planar inverted F-L antennas has been investigated: this was considered as mounted on mobile device (e.g. handset) to function as one end of a MIMO transmission system. By exploiting multi-polarisation diversity in MIMO, rather than the more common angle-of-arrival diversity, and by balancing the size and bandwidth constraints, the proposed set of antennas has compact dimensions that limit it to

small surface areas of the handset while still covering the required operating frequency bands for the IEEE 802.11 a/b/g/n standards. The features make the proposed antenna a well-adapted candidate for application in MIMO mobile terminals. The simulated working channel capacity in each band nearly equalled the capacity of the free coupling MIMO system (based on angle-of-arrival diversity), although this would require an unacceptably bulky mobile antenna.

REFERENCES

[1] Foschini G.J. and Gans M.J., "On limits of wireless communication in a fading environment when using multiple antennas," Wireless Personal Commun., vol. 6, no. 3, pp. 311–335, Mar. 1998.

[2] Foschini G.J. and Valenzuela R.A., "Initial estimation of communication efficiency of indoor wireless channel," Wireless Networks, vol. 3, pp. 141–154, 1997.

[3] Wallace J.W. and Jensen M.A., "Modeling the indoor MIMO wireless channel," *IEEE Trans. Antennas Propag.*, vol. 50, no. 5, pp. 591–599, May 2002

[4] Wallace J.W., Jensen M.A., Swindlehurst A.L. and Jeffs B.D., "Experimental characterization of the MIMO wireless channel: Data acquisition and analysis," *IEEE Trans. Wireless Commun.*, vol. 2, no. 2, pp. 335–343, Mar. 2003.

[5] Gesbert D., Bölcskei H., Gore D. A., and Paulraj A., "Outdoor MIMO wireless channels: Model and performance prediction," *IEEE Trans. Commun.*, vol. 50, no. 12, pp. 1926–1934, Dec. 2002.

[6] Dong L., Choo H., Heath R W. and Ling H., "Simulation of MIMO Channel Capacity with Antenna Polarization Diversity", IEEE Transactions on Wireless Communications, vol. 4, no. 4, July 2005, pp. 1869-1873.

[7] Winters J.H., Salz J., and Gitlin R.D., "The impact of antenna diversity on the capacity of wireless communication systems," IEEE Trans. Commun., vol. 42, pp. 1740–1751, Feb. 1994.

[8] Andrews M.R., Mitra P.P. and deCarvalho R., "Tripling the capacity of wireless communications using electromagnetic polarization," *Nature*, vol. 409, no. 6818, pp. 316–318, Jan. 2001.

[9] Svantesson T., "On capacity and correlation of multi-antenna systems employing multiple polarizations," in *IEEE Int. Antennas Propagation Symp. Digest*, San Antonio, TX, Jun. 2002, pp. 202–205.

[10] Stancil D.D., Berson A., Van't Hof J.P., Negi R., Sheth S. and Patel P., "Doubling wireless channel capacity using co-polarised, co-located electric and magnetic dipoles," *Electron. Lett.*, vol. 38, no. 14, pp. 746–747, Jul. 2002.

[11] Andersen J.B. and Getu B.N., "The MIMO cube—A compact MIMO antenna," in *5th Int. Symp. Wireless Personal Multimedia communications*, Honolulu, HI, Oct. 2002, pp. 112–114.

[12] Xu H., Gans M.J., Amitay N. and Valenzuela R.A., "Experimental verification of MTMR system capacity in controlled propagation environment," *Electron. Lett.*, vol. 37, no. 15, pp. 936–937, Jul. 2001.

[13] See C.H., Abd-Alhameed R.A., Zhou D. and Excell P.S., "Dual-Frequency Planar F-L Antenna (PIFLA) for WLAN and Short Range Communication Systems" IEEE Trans. On Antennas and Propag., Oct 2008, vol.56, pp.3318-3320.

Design Studies of Ultra-Wideband Microstrip Antenna for Ultra-Wideband Communication

S. Adnan, R. A. Abd-Alhameed, H. I. Hraga, Z. Zainal Abidan, M. Usman, S. M . R. Jones

Mobile and Satellite Communication Research Centre
University of Bradford
Bradford,
BD7 IDP, UK
sadnan@bradford.ac.uk
r.a.a.abd@bradford.ac.uk

Abstract: **This paper presents a circular printed monopole antenna for the Ultra-Wideband (UWB) applications. The antenna is designed and simulated using High Frequency Structure Simulator (HFSS). The antenna achieved over all bandwidth of 120%. The operating frequency of the antenna is from 3.1 to 11.5 GHz. The parameters of the antenna which affect the performance of the antenna are investigated. The paper also presents the experimental measurement of the return loss and radiation pattern, the simulated and experimental result shows that the antenna can yield an ultra-wideband with a good radiation pattern over the required band. The proposed antenna can be used in wireless ultra-wideband communication.**

Key words: *ultra-wideband; monopole antenna.*

I. Introduction

Ultra-Wideband (UWB) technology has attracted much attention and experienced considerable growth in the past few years after the allocation of the band ranging from 3.1GHz to 10.6GHz for unlicensed UWB communication applications and other purposes such as medical imaging and radar application by the FFC (Federal Communication Commission) [1]. It is very challenging to design antenna for the imaging system that satisfies all the requirements for the microwave imaging system. The antenna for the UWB required a wide bandwidth for sufficient impedance matching, good return loss, VSWR < 2 for the entire band together with reasonable gain in all directions. The microstrip antennas getting much attention in the recent years and is widely used in the UWB technology.

The concept of the Microstrip antennas (MSAs) first proposed by Deschamps in 1953. The various advantages of MSAs such as light weight, low cost, and ease of fabrication with the printed circuit technology [2]. High demand for the small and the low profile antennas make the MSAs the top priority. The MSAs in its simplest form consist of a radiating patch on one side of the substrate and ground plane on other side of the substrate. MSAs suffer some disadvantages compare to the conventional antennas i.e. Narrow BW, lower gain and low power handling capacity. Increasing the BW of the microstrip antenna is one of the major tasks in the research field. Recent studies carried out on microstrip [3-6] and monopole [7-12]. By following the research outcome of authors this paper present a printed circular monopole antenna with various techniques i.e. partial ground plane, creating slots and two step microstrip feed line to enhance the bandwidth and improve the matching. The antenna is designed using Ansoft High Frequency Structure Software (HFSS) [13]. The results show good agreement between the simulated and measured result.

The layout of the paper is as follow. Section 2 discuss the geometry and the simulation of the antenna and the parametric study of the various dimension of the antenna, section 3 discuss the comparison of the simulated and the experimental result and section 4 represent the summary and the conclusion of the study.

II. Antenna Design

Figure 1 and Table 1 show the detail geometry of the proposed circular patch antenna. The commercially available simulation software Ansoft HFSS is used to obtain the parameter of the antenna. The antenna is fabricated on the substrate FR4 with the dielectric constant (ε_r) 4.4 and tangent loss (tan δ) 0.02, the thickness of the substrate is 1.6mm the antenna is excited through 50Ω microstrip feed line

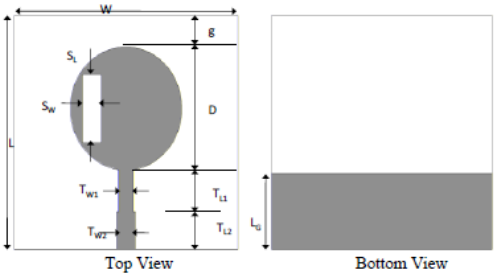

Fig 1 Geometry of the proposed antenna

Table 1. Detailed Parameter for the Proposed Antenna

Parameter	Unit (mm)
Length of the Substrate (L)	34
Width of the substrate (W)	36
Position of the antenna (g)	4.5
Diameter of the circular patch (D)	18
Width of the Transmission Line(T_{W1})	2.5
Length of the Transmission Line(T_{L1})	6
Width of the Transmission Line(T_{W2})	3
Length of the Transmission Line(T_{L2})	5.5
Length of the Ground Plane(L_G)	11
Gap Between the Ground and Antenna(h)	0.5
Width of the slot(S_W)	3
Length of the Slot(S_L)	10

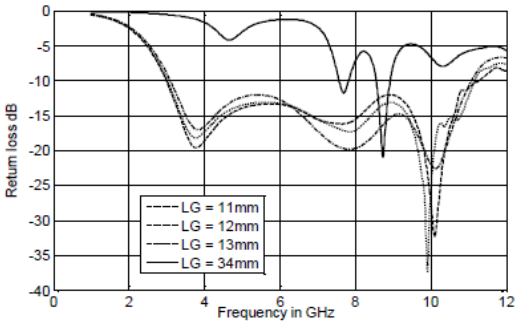

Fig: 2(a). Return loss for different size of ground plane

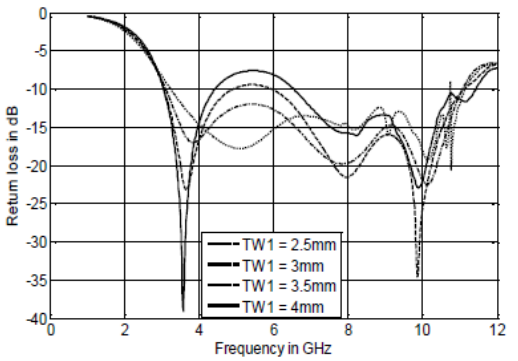

Fig: 2(b). Return loss for the different size of transmission line

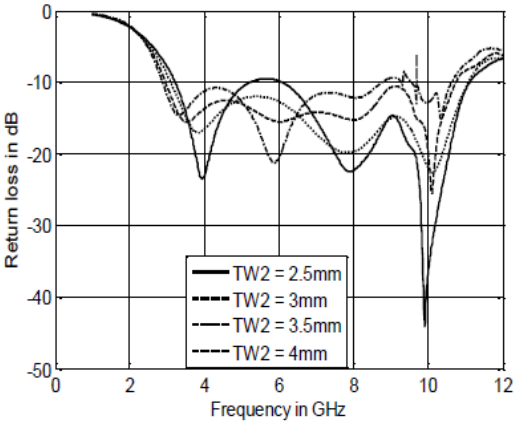

Fig: 2(c). Return loss for different size of transmission line

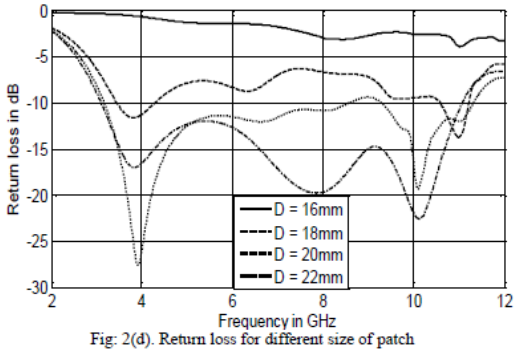

Fig: 2(d). Return loss for different size of patch

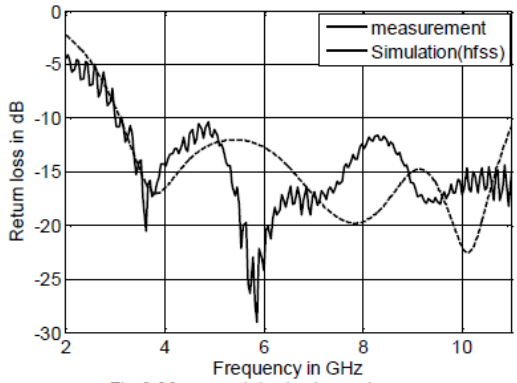

Fig: 3. Measure and simulated return loss

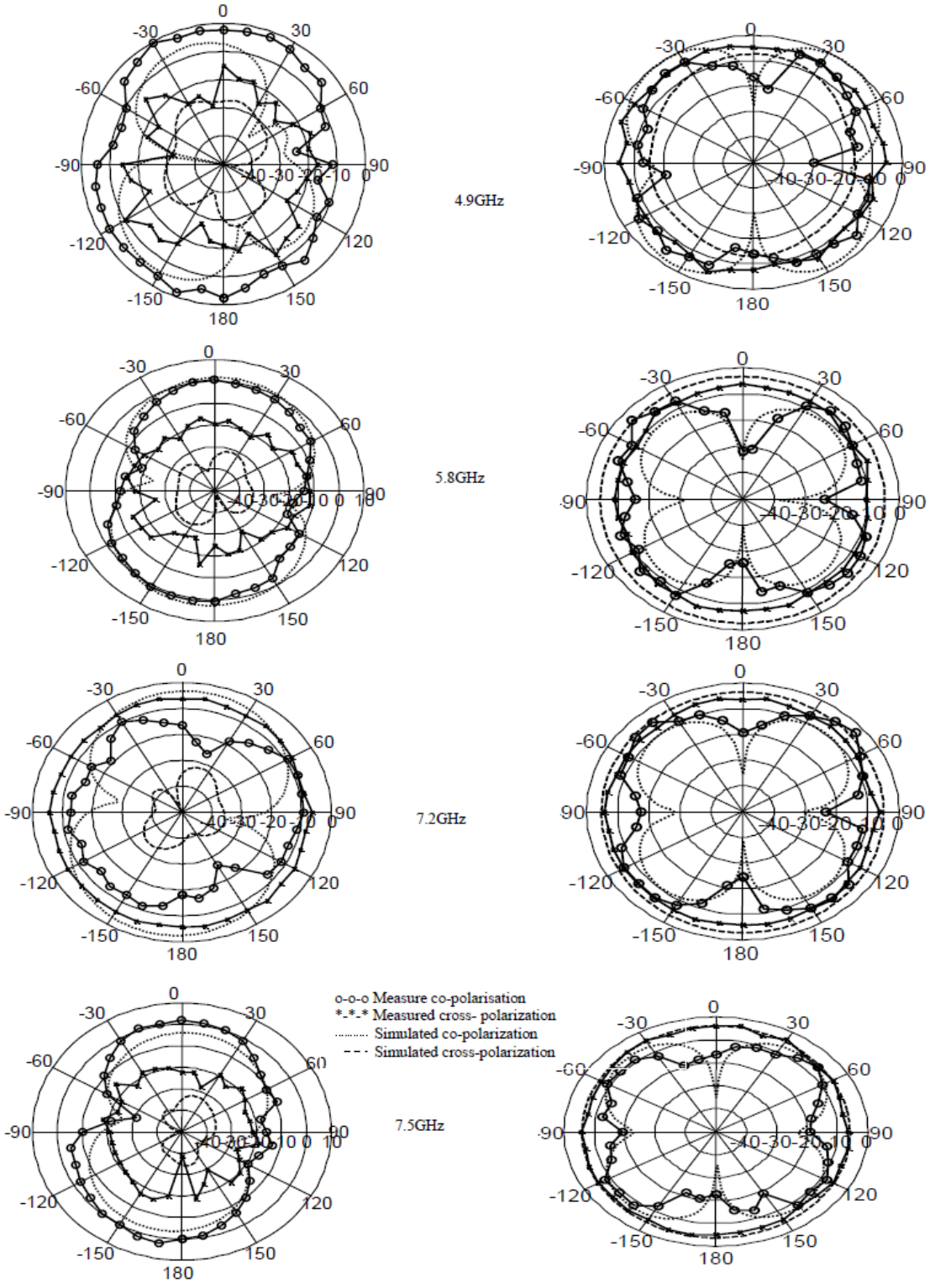

Fig 4 Simulated and measured normalized radiation pattern of the proposed antenna (left: x-z plane, right: y-z plane)

In order to optimise the design of the antenna a parametric study has been conducted. The parametric simulation is carried out with HFSS in frequency domain where the numerical analysis is based on the Finite Element Method (FEM) [13]. The parametric study help to produce the best design for experiment before the antenna is build. Different parameters of the antenna are optimised for the maximum bandwidth. To check the influence of these parameters on the Impedance bandwidth one parameter is varied and the remaining parameters remain fixed. The first parameter that undergoes the parametric study is the size of the ground plane. The antenna with full ground operate as a narrow band antenna so the length of the ground plane is decreased for the matching over wideband Fig 2(a) show the simulated return loss for different length of ground plane, from the graph it is clear the size of the ground play important role in the impedance matching. The best return loss characteristic is shown at 11mm x 36mm which cover from 3GHz up to 11.5GHz which offer bandwidth close to 120%. In order to improve the overall bandwidth other parameter that undergoes the parametric study is the width of the two stair microstrip transmission line. The first step connected to the radiating patch undergo parametric studies and different width of the transmission line is simulated for the better matching while the other parameter remain fixed. Fig 2(b) shows the simulated return loss, the simulation result shows that the width of the transmission line connected to the radiating patch has a great impact on the return loss and the best matching is obtained at the width of 2.5mm. Similarly the second step connected to the feeding is also simulated for the different width of the transmission line and the simulation result shown in Fig 2(c) which shows that at width of 3mm the antenna provide good matching and finally the size of the circular radiating patch with the rectangular slot is simulated for different sizes, the result shows that the size of the radiating patch is important for good impedance matching and the simulated result shows that at the diameter of 18mm the antenna provide the good impedance matching as shown in Fig 2(d).

III. RESULTS AND DISCUSSION

A prototype of the circular patch antenna with the rectangular slot is fabricated on FR4 substrate. The prototype of the antenna is tested for the return loss. The measurement is carried out using calibrate Network Analyzer. The antenna is tested over a bandwidth of 3GHz to 12GHz. The Experimental Result shows reasonable agreement with the simulated result. The measured and the simulate results are shown in Fig 3. The slight shift in the return loss curve can be attributed to the fabrication inaccuracies. Fig 5(a), (b), (c), and (d) show the measured and simulated normalized radiation pattern for both co and cross polarization in the x-z and y-z planes at the frequencies 4900 MHz, 5800 MHz, 7200 MHz, and 7500 MHz The results show the good agreement between the simulated and measured result.

IV. CONCLUSION

The paper presents a printed monopole antenna for Ultra Wide Band applications. A parametric study is carried out on various parameters. The antenna was fabricated and tested and achieved good results which are in good agreement with the results from simulation and the antenna can yield an ultra wide bandwidth from 4 GHz to 12 GHz The antenna show a radiation patterns with maximum gain varied between -5 to 1.3 dBs. The Result Shows that antenna is suitable for the UWB communication

ACKNOWLEDGEMENT

The authors would like to thanks Mr A Leach for his help in the fabrication and measurement of the antenna

REFERENCES

[1] New public safety applications and broadband internet access among uses envisioned by FCC authorization of ultra-wideband technology," First Report and Order (FCC 02-48), Action by the Commission February 14, 2002, February, 2002."

[2] D. H. S. David M. Pozar, *Microstrip antennas: the analysis and design of microstrip antennas and arrays*: John Wiley and Sons, 1995.

[3] C. G. Yashar Zehforoosh, and Javad Nourinia, "Antenna Design for Ultra Wideband Application Using a New Multilayer Structure," in *PIERS*, vol. 2, 2006.

[4] M. N. K. -S. Lim, and C.-P. Tan, "DESIGN AND CONSTRUCTION OF MICROSTRIP UWB ANTENNA WITH TIME DOMAIN ANALYSIS," in *Progress In Electromagnetics Research*, vol. 3, 2008, pp. 153–164.

[5] D. S. U. Veeresh G Kasabegoudar, and K. J. Vinoy, "Design Studies of Ultra Wideband Microstrip Antennas with a Small Capacitive Feed," *International Journal of Antennas and Propagation* vol. 2007, 2007.

[6] J. R.-M. N. Ghassemi, M. H. Neshati, "SLOT COUPLED MICROSTRIP ANTENNA FOR ULTRA WIDEBAND APPLICATIONS IN C AND X BAND," in *Progress In Electromagnetics Research*, vol. 3, 2008, pp. 15–25.

[7] M. A. M. Nabil Srifi, O. El Mrabet, N. Aknin, and M. Essaaidi, "UWB Compact Monopole Antennas for Breast Cancer Detection," in *OHD*. VALENCE - FRANCE, 2007.

[8] M. J. J. Ammann, M., "Some techniques to improve small groundplane printed monopole performance," in *Antennas and Propagation Society International Symposium, 2007 IEEE*, vol. 9, 2007 pp. 2825 - 2828.

[9] Y. R. Razali Ngah, Teguh Prakoso and Mohd Shukri Othman, "Printed square UWB antenna," in *International Conference on Electrical Engineering and Informatics* Institut Teknologi Bandung, Indonesia, 2007, pp. 972-975.

[10] C.-C. K. Lin, Y.-C.; Kuo, L.-C.; Chuang, H.-R.;, "A planar triangular monopole antenna for UWB communication," in *Microwave and Wireless Components Letters, IEEE*, vol. 15, 2005, pp. 624 - 626

[11] C.-L. R. X.-C. Yin, C.-Y. Ding, and J.-H. Chu, "A PLANAR U TYPE MONOPOLE ANTENNA FOR UWB APPLICATIONS," in *Progress In Electromagnetics Research Letters*, vol. 2, 2008, pp. 1–10.

[12] I. N. Hossain, S. Pistorius, S. , "A diamond shaped small planar ultra wide band (UWB) antenna for microwave Imaging Purpose " in *Antennas and Propagation Society International Symposium, 2007 IEEE*, 2007, pp. 5713-5716.

[13] Ansoft High Frequency Structure Simulator corporation, V 9.2, 2004.

Novel Balanced Handset Antenna Design for 2.4 and 5.2 GHz Bands Application

A. G. Alhaddad[#1], R. A. Abd-Alhameed[#2], D. Zhou[#3], C. H. See[#4], M. Usman[#5], Z. Zainal Abidin[#6], P. S. Excell[*7]

[#] *Mobile and Satellite Communications Research Centre*
University of Bradford, Bradford, West Yorkshire, BD7 1DP, UK
[1]A.G.Alhaddad@bradford.ac.uk
[2]r.a.a.abd@bradford.ac.uk
[3]d.zhou2@bradford.ac.uk
[4]c.h.see2@bradford.ac.uk
[5]musman3@brad.ac.uk
[6]z.b.zainalabidin@brad.ac.uk
[*] *Glyndwr University, Wrexham, LL11 2AW, Wales, UK*
[7]p.excell@glyndwr.ac.uk

Abstract— **In this paper, a balanced antenna for mobile handset applications with dual-frequency performance, covering the 2.4-GHz and the 5.2-GHz WLAN frequency bands, is investigated and discussed. The antenna is a thin-strip planar dipole with folded structure and a dual-arm on each monopole. The performance of the proposed antenna was analysed and optimised against the two targeted frequency bands. For validation, the antenna prototype was fabricated and tested. The performance of this balanced antenna was verified and characterised in terms of the antenna return loss and radiation pattern. The predicted and measured results show fairly good agreement and the results also confirm good impedance bandwidth characteristics for the proposed antenna with dual-band operation.**

I. Introduction

One of the trends observed in the mobile telephone technologies in the last ten years is to dramatically reduce the size and the weight of the handset. Antennas used for such handsets must also follow down-sizing of the handset unit. Problems considered here on the design of antenna systems for small handsets are firstly, on how to keep the antenna performance unchanged or improved, even though the antenna size becomes small, and secondly, how to reduce the degradation of antenna performance caused by the operator's adjacent effect.

An unbalanced antenna such as Planar Inverted-antenna (PIFAs) is among the most used radiating elements for mobile terminals. An advantage of PIFA is compact, low profile and easy to manufacture. However, it has a narrow bandwidth and needs a height from substrate to ground for matching [1-2]. Furthermore these antennas exhibit poor performance when held by users. This is mainly because the user holding the mobile phone largely takes the place of the ground plane since the ground plane is used as part of the radiator in these antennas therefore radiating currents are induced on both the ground plane and the antenna element resulting in currents flowing on the human body, which degrade the performance of the antenna's radiation properties and introduce losses and uncertainty in its matching [3].

The alternative strategy is to use a balanced antenna, as it has a symmetric structure and is fed by balanced lines one that has two conductors carrying currents of equal magnitude but 180 degree out of phase. These currents cancel the effect of each other and hence the current flows only on the antenna element and not on the ground plane. So if the mobile phone is held by a human, no coupling takes place between the antenna and the human body thus the performance of the antenna is not affected. A major drawback of balanced antennas is that they have a narrow bandwidth; however this bandwidth can be increased by certain techniques like using genetic algorithms. The most common encountered balanced antennas are dipole and loops. In addition, because a balanced antenna requires a balanced feed, a balun is needed. It is a device used for converting signals between an unbalanced circuit structure and a balanced circuit structure. A balun provides compatibility between systems. Through a balun an unbalanced coaxial wire is connected to a two conductor balanced lines.

Recently, many conventional balanced antennas have been successfully designed to cover dual band operation (2.4 and 5.2GHz) for mobile handsets [4, 6, and 11]. In these papers, characteristics of a built-in wideband balanced planar metal plate antenna are introduced and analyzed in order to achieve multiple-band operation.

In this paper, a newly developed dual band balanced handset antenna for 2.4 and 5.2GHz applications is presented (see Fig. 1). The antenna exhibits a balanced operation which leads to a significant reduction of current on the handset body and as a result of which the antenna's performance is not affected by the human operator's hand.

II. Antenna Design Concept

Basically, the first antenna design attempted was designed in free space and then several modifications were introduced to achieve a dual-band feature for mobile handset applications. The antenna, as shown in Fig. 1, is mounted on the top of a rectangular conductor plate (46 × 120 mm), which

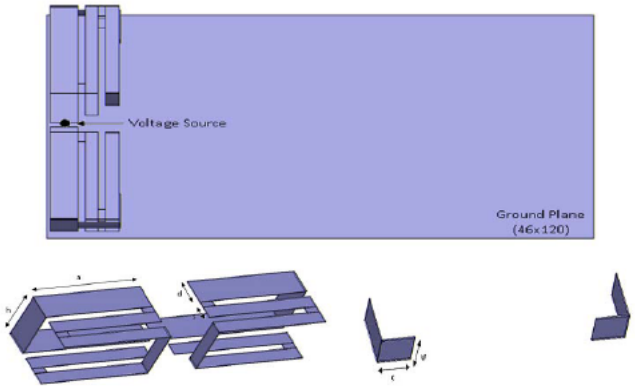

Fig. 1 Balanced mobile antenna configuration studied

can be regarded as the mobile handset chassis or ground plane of a practical mobile phone.

The design concept for producing dual-band balanced mobile antennas was applied and implemented in [12], in which a technique to generate another resonant frequency was employed by inserting an additional thin-strip arm in each arm of the planar dipole; as a result, the single resonant antenna was modified and developed as a wideband dual-resonant variant for multi-band operation.

In this study, the new proposed antenna was developed using the same design principle, but it designed for the purpose to achieve a compact small size and for different applications in WLAN and short range communication systems. Initially, a folded antenna with single arm, operating at around 2.4 GHz, was designed and optimized using the EM simulator. Subsequently, the same technique as [12] was applied by inserting an additional thin-strip arm (see Fig. 1) that is used to generate the second resonant frequency for 5.2 GHz band.

The proposed antenna design and simulation studied in terms of return loss and radiation patterns was carried out using Ansoft HFSS (High Frequency Structure Simulator), which uses a 3D full-wave finite element Method (FEM). The details of the antenna geometry are shown in Fig. 1(a = 18, d = 4, w = 3, h = 8, s = 2, c = 6; dimensions are in mm). In which there are two variable parameters h and w, which control the individual length of each one of the folded arms and improve the bandwidth impedance and subsequently have the effect on tuning the resonant frequencies for this dual-band design. From the observation of Figs 2 and 3, the optimum value of h and w were found to be 8 mm and 3 mm respectively, for the best performance of the proposed antenna at resonant frequency at 2.4 GHz and 5.2 GHz bands.

The length and location of the additional arm, including other parameters of the proposed antenna were adjusted, and further optimised to ensure that the design entirely covered the required two frequency bands (i.e. 2400-2485 MHz & 5150-5350 MHz) at suitable working return loss ≤ -10dB.

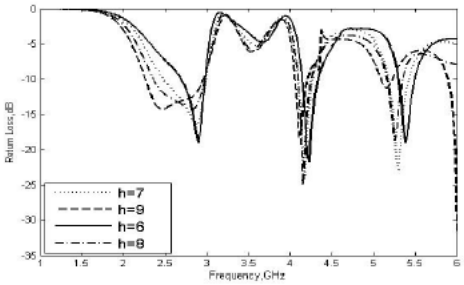

Fig. 2 Variation of the parameter h on the effect of return loss.

III. SIMULATION AND MEASUREMENT RESULTS

For the hardware realisation, copper sheet with 0.15 mm thickness was used for fabricating the proposed balanced antenna (see Fig. 4). For a balanced antenna (e.g. dipole) system, a balun is usually required as a support feeding network, to provide a balanced feed from an unbalanced source. A commercially hybrid junction from ET Industries [10] that operates from 2 to 12 GHz has been utilized in this work. Figs. 5 presents the measured return loss of the prototype antenna. As can be seen, taking into account the errors caused by manufacturing the proposed antenna, has fairly good agreement with the simulated return losses.

Moreover, an S-Parameter method for measuring input impedance for the balanced antennas [13] was also adopted in order to verify the impedance of the proposed antenna. In this case, balanced antennas are considered as two-port devices and the S-Parameters can be obtained from a well-calibrated Network Analyzer, Subsequently, a simple formula is employed to derive the differential input impedance of the balanced antenna.

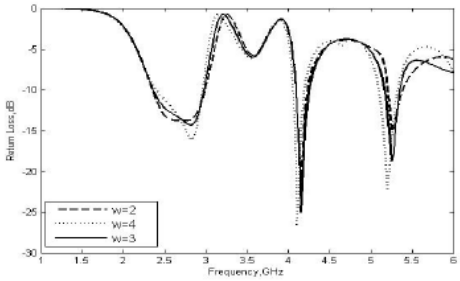

Fig. 3 Variation of the parameter w on the effect of return loss

Fig. 4 Photograph of prototype of the proposed balanced antenna design.

The measured return loss in this method was also presented in Fig. 5, in which a fairly good agreement between the two methods (i.e. measured (ant & balun) and measured (ant) was observed and both has a reasonable agreement with the simulated return loss. This result verifies the actual impedance of the proposed antenna, in addition, the effectiveness of proposed antenna system with integrated balun, confirms the validation. It also supports the evaluation of the radiation performance of the prototype antenna.

Measurements of the radiation patterns of the prototype were carried out in a far-field anechoic chamber. Two pattern cuts were taken for two WLAN operating frequencies that cover the designated whole bandwidth in this study. The radiation patterns in the xz plane and yz plane for the balanced folded dipole at 2450 MHz, 3000 MHz and 5200 MHz were measured, as presented in Fig. 6. The measured radiation patterns shown asymmetrical radiation, which is mainly due to the asymmetrical antenna structure in fabrication and imbalanced outputs from the balun device in testing.

By investigating the effect of the operator's hand and head on the antenna performance, it was found very small which explains that the antenna has a perfect balanced structure. In addition, current distribution on the mobile phone ground plane was analyzed using the EM simulator. It was observed that most of the current induced on the ground plane were high in the area beneath the antenna and minimum current distribution appeared on the rest of the ground plane, as theoretically expected. This proves the model advantage of using a balanced antenna designs for future mobile handsets.

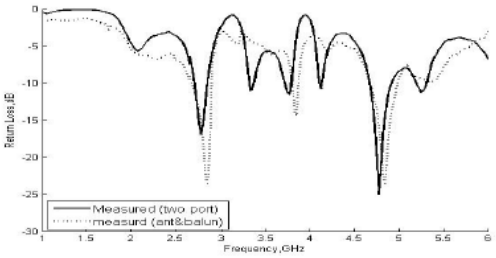

Fig. 5 Comparison of measured return loss

IV. Conclusions

A new dual-band balanced dipole antenna with novel structure for mobile devices operated over 2.4 GHz and 5.2 GHz WLAN bands has been presented. The proposed antenna model was experimentally verified in terms of antenna return loss and radiation pattern. The simulated and measured results over the two frequency bands considered show a good agreement in which it makes this proposed antenna an attractive candidate for the mobile handset applications.

References

[1] Z. Li and Y. Rahmat-Samii, "Optimization of PIFA-IFA combination in handset antenna designs", IEEE Trans. On Antennas and Propagation, Vol. 53, No. 5, pp. 1770-1778, May 2005.

[2] Y-S. Wang, M-C. Lee and S-J. Chung, "Two PIFA-related miniaturized dual-band antennas", IEEE Trans. On Antennas and Propagation, Vol. 55, No.3, pp. 805-811, March 2007.

[3] R.A. Abd-Alhameed, P.S. Excell, K. Khalil, R. Alias and J. Mustafa, "SAR and radiation performance of balanced and unbalanced mobile antennas using a hybrid formulation", Invited paper, IEE Proceedings-Science, Measurement and Technology special issue on Computational Electromagnetics, vol. 151, No. 6, pp. 440-444, November 2004.

[4] J. Janapsatya, K.P. Esselle and T.S. Bird, "A dual-band and wideband planar inverted-F antenna for WLAN applications", Microwave and Optical Technology Letters, Vol. 50, pp.138-141, January 2008.

[5] M.-C. Huynh and W. Stutzman, "Ground glane effects on planar inverted-F antenna (PIFA) performance", IEE Proc.-Microw. Antennas *Propag.*, Vol. 150, pp. 209-213, August 2003.

[6] C.H. See, R.A. Abd-Alhameed, D. Zhou and P.S. Excell, "Dual-frequency planar inverted F-L-antenna (PIFLA) for WLAN and short range communication systems", IEEE Transactions on Antennas and Propagation, Vol.56, No 10, pp.3318-3320, October 2008.

[7] D. Zhou, R.A. Abd-Alhameed and P.S. Excell, "Wideband balanced folded dipole antenna for mobile handsets", In proceedings of The European Conference on Antennas and Propagation: EuCAP 2007, Paper no. MoPA.012, Edinburgh, UK, 11-16 November 2007.

[8] H. Morishita, H. Furuuchi and K. Fujimoto, "Performance of balance-fed antenna system for handsets in vicinity of a human head or hand", IEE Proc.-Microw. Antennas Propag., Vol. 149, No, 2, pp. 85-91, April 2002.

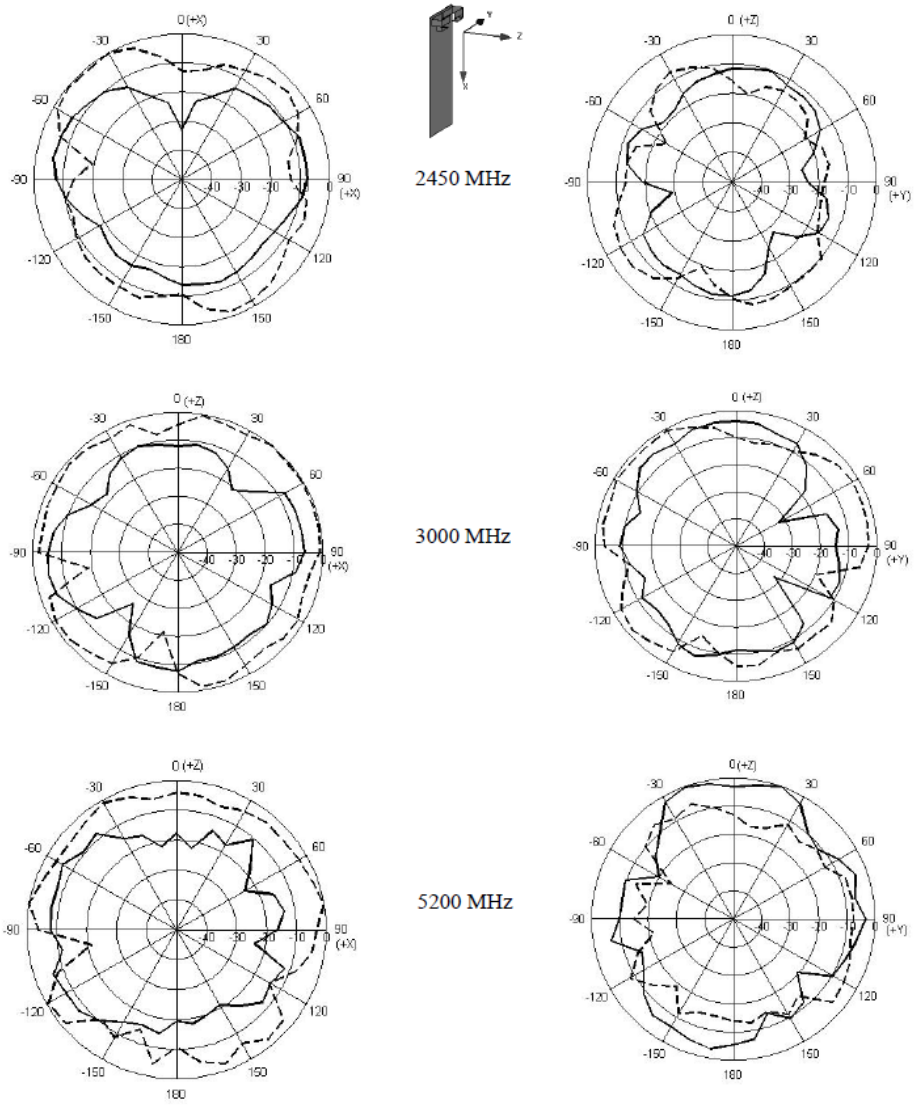

Fig. 5 Radiation patterns of the proposed antenna for 2450 MHz, 3000 MHz and 5200 MHz at: (left) xz plane; (right) yz plane, where '——' measured E_θ and '- - -' measured E_ϕ.

[9] H. Morishita, S. Hayashida, J. Ito and K. Fujimoto, "Analysis of built-in antenna for handset using human (heand,hand,finger) model", Electronics and communications in Japan, Part 1, Vol. 86, No. 9, pp. 35-45, 2003.

[10] ET Industries, USA, http://www.etiworld.com/.

[11] High Frequency StructureSimulator,Version11, Ansoft Corporation, USA

[12] D. Zhou, R.A. Abd-Alhameed, C.H. See and P.S. Excell, "Design of multiband balanced folded dipole antenna based on a dual-arm

[13] R. Meys and F. Janssens, "Measuring the impedance of balanced antennas by an S-Parameter method", IEEE antennas and propagation magazine, vol. 40, no. 6, pp. 62-65, December 1998.

APPENDIX A

Matlab Code for Calculating Channel Capacity with respect to Polarisation Angle

```
**********DEFINING ORIENTATION********

phid(1)=0.0;
phid(2)=120*pi/180;
phid(3)=240*pi/180;
n_ele=3;
segma=5*pi/180;
dist = 0.0;
for k=1:3
   rax(k) = 2*pi * dist* cos(phid(k));
   ray(k) = 2*pi * dist* sin(phid(k));
   raz(k) = 0.0;
end;
t3=pi/2-15*pi/180;
t4=pi/2+15*pi/180;
g=[1,1,1;1,1,1;1,1,1]/sqrt(1);
ntheta = 36;
nfhi   = 36;
snr=10^(10/10);
gi=[1,0,0;0,1,0;0,0,1];
m=1;
for thid=0:2:90

   thi=thid*pi/180;
      for k1=1:3
      p1=phid(k1);
      t1=thi;
      rx1=rax(k1);
      ry1=ray(k1);
      rz1=raz(k1);
     for k2=1:3
      p2=phid(k2);
      t2=thi;
      rx2=rax(k2);
      ry2=ray(k2);
      rz2=raz(k2);
         if k1 == 1
            if k2 == 2
   ur=sin(t1)*cos(p1)*sin(t1)*cos(p2);
   ur=ur+ sin(t1)*sin(p1)*sin(t2)*sin(p2);
 ur= ur + cos(t1)*cos(t2);
            end
         end

 dtheta = (t4-t3)/ntheta;
 dfhi = (2*pi-0.0)/nfhi;

*******INTEGRATION OVER THETA AND PHI*******

 sm = 0.0;
 sm1 = 0.0;
 sm2 = 0.0;
 for itheta = 1:ntheta + 1
    for ifhi=1:nfhi + 1
      t = t3 + dtheta * (itheta - 1);
      p   = 0.0 + dfhi * (ifhi - 1);

 **DEFINIG DISTRIBUTION ALONG AZIMUTH AND ZENITH**

gcon= erf(1/2*pi*2^(1/2)/segma)*pi^(1/2)*2^(1/2)*segma;
 guass=1/gcon*exp(-p^2/(2*segma^2));

et1=sin(t1)*cos(p1)*cos(t)*cos(p)+sin(t1)*sin(p1)*cos(t)*sin(p);
```

```
      et1 = et1 - cos(t1)*sin(t);
      ep1=-sin(t1)*cos(p1)*sin(p)+sin(t1)*sin(p1)*cos(p);



et2=sin(t2)*cos(p2)*cos(t)*cos(p)+sin(t2)*sin(p2)*cos(t)*sin(p);
      et2 = et2 - cos(t2)*sin(t);
      ep2=-sin(t2)*cos(p2)*sin(p)+sin(t2)*sin(p2)*cos(p);

 sm = sm + (et1 * conj(et2) + ep1 * conj(ep2)) * sin(t)   *guass;

 sm1 = sm1 + (et1 * conj(et1) + ep1 * conj(ep1)) * sin(t) *guass;

 sm2 = sm2 + (et2 * conj(et2) + ep2 * conj(ep2)) * sin(t) *guass;

       end
  end

          sm = sm   * dtheta * dfhi;
          sm1 = sm1 * dtheta * dfhi;
          sm2 = sm2 * dtheta * dfhi;



          h = sm;
          h1 = sm1;
          h2 = sm2;
s(k1,k2)=h/sqrt(h1*h2);
seig(k1,k2)=h/sqrt(h1*h2);
sno(k1,k2)=s(k1,k2);
if k1==k2
   s(k1,k2)=s(k1,k2);
end
   end
   end
hs=eig(seig);
hst=eig(s);
hsno=eig(sno);
hsmax(m)=max(hs);
hstmax(m)=max(hst);
hsnomax(m)=max(hsno);
nmat=norm(s^0.5,'fro');
xx=0;
shn=0;
shn31=0;
shn33=0;
nn=1000;
for kk=1:nn
u=(randn(3)+i*randn(3))/sqrt(2);
for ku=1:n_ele
   u31(1,ku)=u(1,ku);
end;
tu31=u31';
gg= u;
gnorm=norm(gg,'fro');
nn=sqrt(gnorm^2/(n_ele*n_ele));
hn=u*conj(u.')/gnn^2;
hn33=hn;
hn=s*hn;
ehh=eig(hn);
gnorm=norm(tu31,'fro');
gnn=sqrt(gnorm^2/(1*n_ele));
hn31=tu31*conj(tu31.')/gnn^2;
 sss=0;
for kk=1:3
```

```
 sss=sss+log10(1+snr*real(ehh(kk))/n_ele);
 end
    xx = xx + sss;
    shn=shn +log10(abs(det(gi+snr*hn/n_ele)));
    shn31=shn31+log10(abs(det(gi+snr*hn31/1.0)));
    shn33=shn33+log10(abs(det(gi+snr*hn33/n_ele)));
end
    result(m)=xx/log10(2)/nn;
    result_new(m)=shn/log10(2)/nn;
    result_new31(m)=shn31/log10(2)/nn;
    result_new33(m)=shn33/log10(2)/nn;
     tdata(m)=thid;
    urdata(m)=ur;
    m=m+1;
```

```
end
hold on
figure(1)
plot(tdata,result,'xb')
grid
hold on
plot(tdata,result_new,'or')
plot(tdata,result_new31,'xr')
plot(tdata,result_new33,'xr')

grid
xlabel('Polarization Angle in degrees')
ylabel('Capacity in bps/Hz')
```

APPENDIX B

Matlab Code for Calculating Channel Capacity Using Far Fields

```
****LOADING FAR FIELD DATA FILES****

ant1mt=xlsread('ant125gmt.xlsx');
ant1at=xlsread('ant125gat.xlsx');

ant1mp=xlsread('ant125gmp.xlsx');
ant1ap=xlsread('ant125gap.xlsx');


ant2mt=xlsread('ant225gmt.xlsx');
ant2at=xlsread('ant225gat.xlsx');

ant2mp=xlsread('ant225gmp.xlsx');
ant2ap=xlsread('ant225gap.xlsx');


ant3mt=xlsread('ant325gmt.xlsx');
ant3at=xlsread('ant325gat.xlsx');

ant3mp=xlsread('ant325gmp.xlsx');
ant3ap=xlsread('ant325gap.xlsx');


freq=[2.44 2.46 2.48 2.50 2.52];
m=1;
kadd = 0;
for kusman = 1:5

kus1= 2 + kadd;
kus2= 2+36 + kadd;


magtheta1=ant1mt(1:19,kus1:kus2);
phstheta1=ant1at(1:19,kus1:kus2);

magphi1=ant1mp(1:19,kus1:kus2);
phsphi1=ant1ap(1:19,kus1:kus2);


magtheta2=ant2mt(1:19,kus1:kus2);
phstheta2=ant2at(1:19,kus1:kus2);

magphi2=ant2mp(1:19,kus1:kus2);
phsphi2=ant2ap(1:19,kus1:kus2);


magtheta3=ant3mt(1:19,kus1:kus2);
phstheta3=ant3at(1:19,kus1:kus2);

magphi3=ant3mp(1:19,kus1:kus2);
phsphi3=ant3ap(1:19,kus1:kus2);


for k=1:19
   for  j=1:37
et_1(k,j)=magtheta1(k,j)*(cos(phstheta1(k,j)*pi/180)    +    i    *
sin(phstheta1(k,j)*pi/180));
ep_1(k,j)=magphi1(k,j)*(cos(phsphi1(k,j)*pi/180)     +     i     *
sin(phsphi1(k,j)*pi/180));

 et_2(k,j)=magtheta2(k,j)*(cos(phstheta2(k,j)*pi/180)    +    i    *
sin(phstheta2(k,j)*pi/180));
```

```
ep_2(k,j)=magphi2(k,j)*(cos(phsphi2(k,j)*pi/180)      +      i      *
sin(phsphi2(k,j)*pi/180));

 et_3(k,j)=magtheta3(k,j)*(cos(phstheta3(k,j)*pi/180)    +    i    *
sin(phstheta3(k,j)*pi/180));
 ep_3(k,j)=magphi3(k,j)*(cos(phsphi3(k,j)*pi/180)      +      i      *
sin(phsphi3(k,j)*pi/180));
   end;
end;



*****DEFINING VARIABLES*****


segma=30*pi/180;

t3=pi/2-90*pi/180;
t4=pi/2+90*pi/180;

g=[1,1,1;1,1,1;1,1,1]/sqrt(1);

ntheta = 36;
nfhi   = 36;

snr=10^(10/10);

gi=[1,0,0;0,1,0;0,0,1];
```

```
for k1=1:3

    if k1 == 1

      et1=et_1;
      ep1=ep_1;
   end
      if k1 == 2
         et1=et_2;
         ep1=ep_2;
      end
   if k1 == 3
      et1=et_3;
      ep1=ep_3;
   end



 for k2=1:3


      if k2 == 1

      et2=et_1;
      ep2=ep_1;
   end
      if k2 == 2
         et2=et_2;
         ep2=ep_2;
      end
```

```
      if k2 == 3
         et2=et_3;
         ep2=ep_3;
      end


  dtheta = (t4-t3)/18;
  dfhi = (2*pi-0.0)/36;


******INTEGRATION OVER THETA AND PHI*******

sm = 0.0;
  sm1 = 0.0;
  sm2 = 0.0;
  for itheta = 1:19
     for ifhi=1:36
       t = t3 + dtheta * (itheta - 1);
       p   = 0.0 + dfhi * (ifhi - 1);


****DEFINIG DISTRIBUTION ALONG AZIMUTH AND ZENITH******

p00=pi/4;
  gcon= erf(1/2*pi*2^(1/2)/segma)*pi^(1/2)*2^(1/2)*segma;

  guass=1/gcon*exp(-(p-p00)^2/(2*segma^2));

  usrcos=(1/(pi)*(1+cos(2*t-pi)))^4;
```

```
      sm = sm + (et1(itheta, ifhi) * conj(et2(itheta, ifhi)) +
ep1(itheta, ifhi) * conj(ep2(itheta, ifhi))) * sin(t)   *guass*usrcos;

      sm1 = sm1 + (et1(itheta, ifhi) * conj(et1(itheta, ifhi)) +
ep1(itheta, ifhi) * conj(ep1(itheta, ifhi))) * sin(t) *guass*usrcos;

      sm2 = sm2 + (et2(itheta, ifhi) * conj(et2(itheta, ifhi)) +
ep2(itheta, ifhi) * conj(ep2(itheta, ifhi))) * sin(t) *guass*usrcos;


    end
  end



        sm = sm   * dtheta * dfhi;
        sm1 = sm1 * dtheta * dfhi;
        sm2 = sm2 * dtheta * dfhi;


        h = sm;

        h1 = sm1;

        h2 = sm2;


s(k1,k2)=h/sqrt(h1*h2);
seig(k1,k2)=h/sqrt(h1*h2);
sno(k1,k2)=s(k1,k2);
```

```
if k1==k2
   s(k1,k2)=s(k1,k2);
end

     end
   end

hs=eig(seig);
hst=eig(s);
hsno=eig(sno);


hsmax(m)=max(hs);
hstmax(m)=max(hst);
hsnomax(m)=max(hsno);

nmat=norm(s^0.5,'fro');


xx=0;
shn=0;
shn31=0;
shn33=0;

nn=1000;

for kk=1:nn


u=(randn(3)+i*randn(3))/sqrt(2);

for ku=1:n_ele
   u31(1,ku)=u(1,ku);
end;

tu31=u31';

gg= u;
gnorm=norm(gg,'fro');

gnn=sqrt(gnorm^2/(n_ele*n_ele));
hn=u*conj(u.')/gnn^2;
hn33=hn;
hn=s*hn;
ehh=eig(hn);

gnorm=norm(tu31,'fro');
gnn=sqrt(gnorm^2/(1*n_ele));
hn31=tu31*conj(tu31.')/gnn^2;



 sss=0;
 for kk=1:3
 sss=sss+log10(1+snr*real(ehh(kk))/n_ele);
 end

   xx = xx + sss;
   shn=shn +log10(abs(det(gi+snr*hn/n_ele)));
   shn31=shn31+log10(abs(det(gi+snr*hn31/1.0)));
   shn33=shn33+log10(abs(det(gi+snr*hn33/n_ele)));
end

   result(m)=xx/log10(2)/nn;
```

```
    result_new(m)=shn/log10(2)/nn;
    result_new31(m)=shn31/log10(2)/nn;
    result_new33(m)=shn33/log10(2)/nn;

    tdata(m)=thid;
    urdata(m)=ur;
    m=m+1;
end

hold on
figure(1)
plot(tdata,result,'xb')
grid

hold on

plot(tdata,result_new,'or')
plot(tdata,result_new31,'xr')
plot(tdata,result_new33,'xr')

grid
xlabel('Polarization Angle in degrees')
ylabel('Capacity in bps/Hz')
```